

OligoG alginate nanomedicine mediated disruption of mucin barriers and microbial biofilms

**A thesis submitted in fulfilment of the requirements of the degree of
Doctor of Philosophy
Cardiff University**



October 2014

Manon Fflur Pritchard
Advanced Therapies Group,
School of Dentistry,
Cardiff University

Acknowledgments

I would like to express my sincere thanks to my supervisors Professor David Thomas and Dr Katja Hill for all their support, advice and encouragement throughout my Ph.D. Thanks to my colleagues and friends at the dental school for all your guidance and companionship.

I have had the privilege of working between Cardiff and Swansea University, and the welcome at both institutes has always been warm.

In Cardiff I would like to thank Dr Elaine Ferguson and Dr Saira Khan for all your help. I would also like to thank Dr Charlotte Emanuel, Dr Sarah Bamford, Dr Rachael Jordan and Mr Yuri Cavalcanti for your advice. With special thanks to Dr Iolo Doull and Mrs Allyson Lynne Smith for your reliance in collecting clinical samples during my thesis.

In Swansea I would like to express my sincere appreciation to Dr Lydia Powell, for your continuous hard work, enthusiasm and endless laughter. With special thanks to Dr Paul Lewis and Dr Karl Hawkins for your guidance and support in learning complex techniques, and to Dr Dan Curtis and Mr Aaron Lewis for your help in the laboratory.

Diolch o waelod calon i fy annwyl rieni John a Miriam, ac i fy mrawd arbennig Gwilym Sion, am eich cefnogaeth ac eich caredigrwydd cyson. Byddaf yn fythol diolchgar i chi am eich cariad i orchfygu unrhyw rwystr, a mor falch eich bod wedi rhannu y profiad yma gyda mi. Diolch i Llinos Williams, Ceryn Evans a Jonathan Cook am eich cyfeillgarwch ac am eich parodrwydd i wrando pan oedd pethau yn mynd o chwith! Mawr yw fy nyled i chi gyd.

Summary

Bacterial and fungal biofilms are an increasing clinical challenge, from non-healing wounds to chronic lung infections in cystic fibrosis (CF) patients. Escalating antimicrobial resistance has led to a need for alternative treatments. OligoG (a low MW alginate oligosaccharide), can disrupt multi-drug resistant bacterial biofilms and decrease antibiotic resistance.

This study characterised the interaction between OligoG and the most prevalent CF pathogen, *Pseudomonas aeruginosa*, using nanoscale characterisation, imaging and fluorescent conjugation. Further investigation into the effect of OligoG on CF sputum was carried out using Fourier transform infrared spectroscopy (FTIR) and rheology. The work was extended to observe changes in fungal pathogens treated with OligoG.

Electrophoretic light scattering (ELS) and dynamic light scattering revealed that the surface charge of *P. aeruginosa* became more negative when treated with OligoG ($P < 0.001$) with an increase in sizing. These interactions were not disrupted by hydrodynamic shear ($P < 0.0001$). Biofilm inhibition and disruption of a mucoid *P. aeruginosa* strain, treated with OligoG, was demonstrated using confocal laser scanning microscopy ($P < 0.05$). Fluorescent conjugation to OligoG revealed its distribution throughout the biofilm.

In vitro scanning electron microscopy (SEM), atomic force microscopy (AFM) and ELS of mucin showed disruption in aggregation when treated with OligoG ($P < 0.005$), with the surface charge becoming more negative ($P < 0.0001$). *Ex vivo* treatment of CF sputum with OligoG analysed using FTIR and rheology, demonstrated possible interaction with the sulfate moiety of mucin and a reduction in the viscous and elastic response (0.16 Hz; $P < 0.0001$).

AFM and SEM analysis of candidal biofilms treated with OligoG demonstrated a dose response in reducing biofilm formation, with a decrease in hyphal formation. An *in vitro* epithelial model demonstrated these changes at $< 2\%$ OligoG.

These studies provide insight into the role of OligoG as a treatment for CF patients. Furthermore, promising results have shown that OligoG may lower candidal pathogenicity.

Abbreviations

α	Alpha
β	Beta
AFM	Atomic force microscopy
ANOVA	Analysis of variance
AS Medium	Artificial sputum medium
ATR	Attenuated total reflectance
<i>B. cepacia</i>	<i>Burkholderia cepacia</i>
BMI	Body mass index
<i>C. albicans</i>	<i>Candida albicans</i>
<i>C. glabrata</i>	<i>Candida glabrata</i>
<i>C. tropicalis</i>	<i>Candida tropicalis</i>
CF	Cystic fibrosis
CFTR	Cystic fibrosis transmembrane conductance regulator
cfu/ml	Colony-forming units per millilitre
CLSM	Confocal laser scanning microscopy
COPD	Chronic obstructive pulmonary disease
dH ₂ O	Distilled water
DLS	Dynamic light scattering
DLVO	Derjaguin and Landau, Verwey and Overbeek
DMSO	Dimethyl sulfoxide
DNA	Deoxyribonucleic acid
EBC	Exhale breath condensate
EDC	1-Ethyl-3-(3-dimethylaminopropyl) carbodiimide
eDNA	Extracellular deoxyribonucleic acid
ELS	Electrophoretic light scattering
EPS	Extracellular polysaccharide substance
ex/em	Excitation/emission
FDA	Food and Drug Administration
FEV ₁	Forced expiratory volume in 1 second
Fig	Figure

FLC	Fluconazole
FTIR	Fourier transform infrared spectroscopy
<i>G</i>	G-force
G	α -L-guluronic acid
G'	Storage modulus (elastic response)
G''	Loss modulus (viscous response)
H	Hour(s)
HS	Hypertonic saline
IV	Intra-venous
KCl	Potassium chloride
LDH	Lactate dehydrogenase
LPS	Lipopolysaccharide
M	Molar
M-	β -D-mannuronic acid
MDR	Multi-drug resistant(ce)
MH Broth	Mueller-Hinton broth
MIC	Minimum inhibitory concentration
Mins	Minutes
mV	Millivolts
NaCl	Sodium chloride
NaOH	Sodium hydroxide
Nm	Nanometer
NP	Nanoparticles
O/N	Overnight
OD	Optical density
OM	Outer membrane
<i>P. aeruginosa</i>	<i>Pseudomonas aeruginosa</i>
<i>P. gingivalis</i>	<i>Porphyromonas gingivalis</i>
PBS	Phosphate buffered saline
PCR	Polymerase chain reaction
PD-10	Protein desalting column

PGM	Pig gastric mucin
pH	Power of hydrogen concentration
PL	Phospholipase
rhDNase I	Recombinant human deoxyribonuclease I
RHE	Reconstituted human oral epithelium
Rpm	Revolutions per minute
RPMI-1640	Roswell Park Memorial Institute medium
<i>S. aureus</i>	<i>Staphylococcus aureus</i>
<i>S. mutans</i>	<i>Streptococcus mutans</i>
SAB	Sabouraud liquid broth
SAP	Secreted aspartyl proteinases
SD	Standard deviation
SDA	Sabouraud dextrose agar
SEM	Scanning electron microscopy
Spp.	Species
sulfo-NHS	<i>N</i> -hydroxysulfosuccinimide
TSB	Tryptic soy broth
TxRd	Texas red
TxRd-G	Texas red labelled OligoG
UV	Ultraviolet
v/v	% volume in volume
w/v	% weight in volume
w/w	% weight in weight
YNB	Yeast nitrogen base

Table of Contents

Chapter 1: General introduction.....	1
1.1 Introduction	2
1.2 Alginate oligomers	2
1.2.1 Properties of alginates	2
1.2.2 Current uses of alginates.....	3
1.2.3 Alginate oligosaccharide (OligoG CF-5/20)	4
1.3 Bacterial infection	4
1.3.1 Bacterial cell wall	4
1.3.2 Clinical implications of biofilms	8
1.3.3 Stages of biofilm formation.....	8
1.3.3.1 Conditioning layer	8
1.3.3.2 Reversible adhesion	9
1.3.3.3 Irreversible adhesion.....	9
1.3.3.4 Population growth and stationary biofilm phase	10
1.3.3.5 Cell death biofilm phase	10
1.3.4 Quorum sensing.....	11
1.3.5 Extracellular polymeric substance.....	11
1.3.6 Antibiotics and resistance.....	14
1.3.7 Antibiotic resistance in biofilms.....	14
1.3.8 Developing anti-biofilm therapeutics	16
1.4 Fungal infection.....	17
1.5 Analysing bacterial and candidal biofilms	18
1.5.1 Imaging techniques.....	18
1.5.1.1 Atomic force microscopy.....	18
1.5.1.2 Scanning electron microscopy	20
1.5.1.3 Confocal Laser Scanning Microscopy	20
1.5.2 Surface charge analysis	21
1.5.2.1 Influence of bacterial surface charge and adhesion	21
1.5.2.2 The DLVO theory in relation to microbial adhesion	21
1.5.2.3 Zeta potential	22
1.6 Biofilms in human disease: cystic fibrosis.....	24

1.6.1 Cystic fibrosis	24
1.6.2 Cystic fibrosis lung environment.....	28
1.6.3 Cystic fibrosis sputum	29
1.6.4 Mucus clearance in the lung during health and disease.....	29
1.6.5 Mucin overview	31
1.6.6 Mucin production in relation to <i>Pseudomonas aeruginosa</i> colonisation ..	33
1.6.7 Mucolytic therapy.....	34
1.6.8 Developing therapies	34
1.7 Analysing sputum.....	35
1.7.1 Fourier transform infrared spectroscopy	35
1.7.2 Rheological analysis of cystic fibrosis sputum.....	35
1.7.3 Extensional rheology	36
1.7.4 Shear rheology.....	36
1.8 Aims	39

Chapter 2: Nanoscale characterisation of bacterial interactions with OligoG ..40

2.1 Introduction	41
2.1.1 Bacterial adhesion.....	41
2.1.2 Derjaguin and Landau, Verwey and Overbeek (DLVO) theory	41
2.1.3 Electrophoretic light scattering: zeta potential (surface charge)	41
2.1.4 Dynamic light scattering: cell sizing	42
2.1.5 Atomic force microscopy	43
2.1.6 Lipopolysaccharide.....	43
2.2 Aims	44
2.3 Materials and Methods	44
2.3.1 Electrophoretic and dynamic light scattering buffer (zeta potential and cell sizing measurements)	44
2.3.2 Electrophoretic and dynamic light scattering sample preparation (zeta potential and cell sizing measurements).....	45
2.3.2.1 Alginates	45
2.3.2.2 <i>Pseudomonas aeruginosa</i> treated with OligoG	45
2.3.3 Atomic force microscopy sample preparation.....	46
2.3.4 Electrophoretic light scattering (zeta potential measurements).....	46

2.3.5 Dynamic light scattering (cell sizing measurements).....	47
2.3.6 Atomic force microscopy	47
2.3.7 Hydrodynamic shear.....	47
2.3.8 Lipopolysaccharide.....	48
2.3.9 Statistical analysis.....	48
2.4 Results	48
2.4.1 Alginate oligosaccharides Protanal [®] and OligoG.....	48
2.4.2 <i>Pseudomonas aeruginosa</i> control.....	49
2.4.3 <i>Pseudomonas aeruginosa</i> and OligoG	55
2.4.4 Concentration effects of <i>Pseudomonas aeruginosa</i>	58
2.4.5 Concentration effects of OligoG.....	58
2.4.6 Atomic force microscopy	62
2.4.7 Hydrodynamic shear.....	65
2.4.8 Lipopolysaccharide.....	68
2.5 Discussion	68
2.6 Conclusion.....	75
Chapter 3: The ability of OligoG to disrupt mucoid pseudomonal biofilms.....	76
3.1 Introduction	77
3.1.1 Development of an artificial sputum medium	77
3.1.2 Use of fluorescent labelling in microbiology	78
3.1.3 Choice of fluorescence probe for OligoG labelling.....	79
3.2 Aims	80
3.3 Materials and Methods	80
3.3.1 Bacterial strains and media.....	80
3.3.2 Confocal laser scanning microscopy	81
3.3.2.1 Effect of OligoG as a treatment to inhibit biofilm formation (confocal laser scanning microscopy).....	81
3.3.2.2 Effect of OligoG as a treatment to disrupt an established biofilm.....	81
3.3.3 Effect of OligoG on biofilm development of <i>Pseudomonas aeruginosa</i> (NH 57388A; scanning electron microscopy)	82
3.3.4 Artificial sputum medium.....	82

3.3.4.1 Effect of OligoG on biofilm development of <i>Pseudomonas aeruginosa</i> (NH 57388A; scanning electron microscopy) grown in artificial sputum medium	83
3.3.5 Texas red-labelling of OligoG and conjugate characterisation	83
3.3.6 Effect of texas red-labelled OligoG as a treatment to inhibit biofilm formation	85
3.3.7 Effect of texas red-labelled OligoG on biofilm disruption.....	86
3.3.8 Image J analysis of biofilm.....	86
3.3.9 Statistical analysis.....	86
3.4 Results	87
3.4.1 The effect of OligoG as a treatment to inhibit biofilm formation	87
3.4.2 OligoG as a treatment to disrupt an established biofilm	87
3.4.3 Scanning electron microscopy of <i>Pseudomonas aeruginosa</i> (NH 57388A) biofilms.....	92
3.4.4 Texas red-labelling of OligoG and conjugate characterisation	96
3.4.5 Effect of varying concentration and pH on Texas Red cadaverine fluorescence	100
3.4.6 Effect of texas red-labelled OligoG as a treatment to inhibit biofilm formation	100
3.4.7 Effect of texas red-labelled OligoG as a treatment to disrupt an established biofilm	104
3.4.7.1 Effect of texas red-labelled OligoG as a treatment to disrupt an established biofilm: z-stack analysis.....	108
3.4.7.2 Effect of a Texas red cadaverine only control as a treatment to disrupt an established biofilm	108
3.5 Discussion	113
3.6 Conclusion.....	118
Chapter 4: Characterisation of mucin interactions with OligoG.....	119
4.1 Introduction	120
4.1.1 Mucin.....	120
4.1.2 Mucins associated with cystic fibrosis	121
4.1.3 Pig gastric mucin	123
4.1.4 Interaction of alginate oligomers with components of sputum	123
4.1.5 Fourier transform infrared spectroscopy	124

4.1.6 DNA in cystic fibrosis sputum	125
4.2 Aims	125
4.3 Materials and Methods	126
4.3.1 Extraction of pig gastric mucin	126
4.3.2 Zeta potential analysis of pig gastric mucin-OligoG interactions (surface charge)	126
4.3.3 Atomic force microscopy imaging of pig gastric mucin	126
4.3.4 Scanning electron microscopy imaging of pig gastric mucin.....	126
4.3.5 Ultra-structural analysis of cystic fibrosis sputum	127
4.3.6 ImageJ analysis and quantification.....	127
4.3.7 Fourier transform infrared spectroscopy	128
4.3.7.1 Fourier transform infrared spectroscopy of cystic fibrosis sputum ..	128
4.3.7.2 Fourier transform infrared spectroscopy data processing and analysis	128
4.3.7.3 DNA extraction from cystic fibrosis sputum samples	129
4.3.8 Statistical analysis.....	129
4.4 Results	130
4.4.1 Zeta potential analysis of pig gastric mucin-OligoG interactions (surface charge)	130
4.4.2 Atomic force microscopy imaging of pig gastric mucin	130
4.4.3 Scanning electron microscopy of pig gastric mucin.....	134
4.4.4 Ultra-structural analysis of cystic fibrosis sputum	134
4.4.5 Fourier transform infrared spectroscopy of cystic fibrosis sputum.....	138
4.5 Discussion	142
4.6 Conclusion.....	149

Chapter 5: Studies on the rheological changes induced in cystic fibrosis sputum by OligoG.....150

5.1 Introduction	151
5.1.1 Sputum.....	151
5.1.2 Mucolytics	151
5.1.2.1 rhDNase I.....	152
5.1.2.2 Mannitol.....	153
5.1.3 Rheology.....	153

5.2 Aims	154
5.3 Materials and Methods	155
5.3.1 Patients and samples	155
5.3.2 Extensional rheology	157
5.3.3 Shear rheology	158
5.3.3.1 Sample heterogeneity	159
5.3.3.2 Wall-slip testing	159
5.3.3.3 Sample incubation times	160
5.3.3.4 Longitudinal study	160
5.3.3.5 Comparative study	160
5.3.4 Statistical analyses	161
5.4 Results	161
5.4.1 Extensional rheology	161
5.4.2 Shear rheology	161
5.4.2.1 Sample heterogeneity	161
5.4.2.2 Wall slip testing	163
5.4.2.3 Incubation time	167
5.4.2.4 Longitudinal study	167
5.4.2.5 Comparative study	171
5.4.2.6 Mannitol study	171
5.5 Discussion	173
5.6 Conclusion.....	182
Chapter 6: Characterisation of the antifungal properties of OligoG.....	183
6.1 Introduction	184
6.1.1 Non-albicans <i>Candida</i> species.....	184
6.1.2 Morphology	185
6.1.3 Virulence and adherence	185
6.1.4 Models to assess candidal biofilm formation	187
6.1.5 Reconstituted human oral epithelium	187
6.1.6 Antifungal agents.....	189
6.1.7 Combination therapy	191
6.2 Aims	192

6.3 Materials and Methods	192
6.3.1 Culture media and fungal strains	192
6.3.2 LIVE/DEAD [®] staining of <i>Candida tropicalis</i> 519468 biofilms grown in OligoG	193
6.3.3 Effect of growth in OligoG on <i>Candida</i> species biofilm formation.....	194
6.3.3.1 Scanning electron microscopy imaging	194
6.3.4 Effect of OligoG and fluconazole combination therapy on growth of <i>Candida tropicalis</i> 519468 biofilms.....	194
6.3.4.1 Scanning electron microscopy imaging	194
6.3.4.2 Atomic force microscopy imaging.....	195
6.3.5 Effect of OligoG on zeta potential (surface charge) of <i>Candida</i> species	195
6.3.6 <i>In vitro</i> reconstituted human oral epithelium infection model	196
6.3.6.1 Growth curves and effect of OligoG.....	196
6.3.6.2 Preparation of <i>Candida albicans</i>	196
6.3.6.3 Preparation of RHE.....	196
6.3.6.4 Culture and imaging of infected RHE	197
6.4 Results	197
6.4.1 LIVE/DEAD [®] Staining of <i>Candida</i> species biofilms grown in OligoG .	197
6.4.2 Effect of growth in OligoG on <i>Candida</i> species biofilm formation.....	198
6.4.3 Effect of OligoG and fluconazole antifungal therapy on growth of <i>Candida tropicalis</i> biofilms.....	203
6.4.4 Effect of OligoG and fluconazole combination therapy on disruption of immature <i>Candida tropicalis</i> 519468 biofilms	206
6.4.5 Zeta potential analysis of <i>Candida</i> species.....	206
6.4.6 Reconstituted human oral epithelium	211
6.4.6.1 Growth curves.....	211
6.4.6.2 Confocal laser scanning microscopy of LIVE/DEAD [®] staining of RHE model infected with <i>Candida albicans</i> (\pm OligoG)	211
6.5 Discussion	214
6.6 Conclusion.....	220
Chapter 7: General Discussion	221
7.1 General discussion.....	222
7.2 The future	234

7.3 Conclusion.....	235
7.4 Papers published from thesis to date	236
Bibliography	237
Appendix I: Nanoscale chapter.....	271
Appendix II: FTIR patient samples	274
Appendix III: Preliminary fungal experiments	276
Appendix IV: Animal and human studies into the safety and tolerability of OligoG for inhalational delivery	284

List of Figures

Chapter 1

Fig 1.1: Structure, purification and quality control of OligoG

Fig 1.2: Schematic diagram representing the differences in cell wall content of Gram-negative and Gram-positive bacteria

Fig 1.3: Diagrammatic representation of a typical biofilm formation pattern and the *P. aeruginosa* LasI/LasR-RhlI/RhlR QS system

Fig 1.4: Diagram of the basis operation of an AFM

Fig 1.5: Derivation of the zeta potential of a colloid

Fig 1.6: Classes of CFTR mutations

Fig 1.7: Data from the UK CF Registry. Cystic Fibrosis Trust, 2013 A) Mortality age of patients; B) Lung infection rates in relation to patient's age

Fig 1.8: Schematic of the lung of a CF patient

Fig 1.9: Mucin glycoprotein illustration

Chapter 2

Fig 2.1: Typical zeta potential distributions for 10% OligoG

Fig 2.2: Effect of a wash step, pre-spin sample and post-spin sample on A) Zeta potential analysis (mV) and B) Sizing measurement (nm) distribution of OligoG control

Fig 2.3: Zeta potential (mV) measurements of Protanal[®] and OligoG

Fig 2.4: A typical sizing distribution (nm) OligoG and Protanal[®]

Fig 2.5: *P. aeruginosa* (PAO1): zeta potential analysis and sizing measurements

Fig 2.6: Untreated *P. aeruginosa* (PAO1) cells zeta potential peaks at different pHs

Fig 2.7: Untreated *P. aeruginosa* (PAO1) cells sizing analysis at different pHs

Fig 2.8: Zeta potential analysis and size distribution analysis of untreated *P. aeruginosa* (PAO1; 2% v/v) cells alone and *P. aeruginosa* (PAO1; 2% v/v) treated with 10% OligoG

Fig 2.9: Typical zeta potential distributions of *P. aeruginosa* (PAO1) cells \pm OligoG

Fig 2.10: Typical size distributions of *P. aeruginosa* (PAO1) cells \pm OligoG

Fig 2.11: AFM images of *P. aeruginosa* (PAO1) cells \pm OligoG

Fig 2.12: AFM images of *Streptococcus mutans* DSM 20523 (ATCC 25175) and *Porphyromonas gingivalis* NCTC 11834 (ATCC 33277) cells \pm OligoG

Fig 2.13: Effect of hydrodynamic shear on *P. aeruginosa* (PAO1)/OligoG binding

Fig 2.14: Effect of hydrodynamic shear on *P. aeruginosa* (PAO1)/OligoG binding with corresponding AFM amplitude images

Chapter 3

Fig 3.1: Summary of the synthetic route for OligoG and TxRd cadaverine conjugation

Fig 3.2: CLSM of LIVE/DEAD[®] staining of *P. aeruginosa* (NH 57388A) biofilms grown for 24 h in MH broth \pm OligoG

Fig 3.3: *P. aeruginosa* (NH 57388A) grown for 24 h in MH broth, followed by 1 h treatment of OligoG

Fig 3.4: *P. aeruginosa* (NH 57388A) grown for 24 h in MH broth, followed by 4 h treatment of OligoG

Fig 3.5: *P. aeruginosa* (NH 57388A) grown for 24 h in MH broth, followed by 24 h treatment of OligoG

Fig 3.6: *P. aeruginosa* (NH 57388A) grown for 24 h in MH broth \pm OligoG (2%, 6% and 10%). Imaging using SEM

Fig 3.7: AS medium only and *P. aeruginosa* (NH 57388A) grown for 48 h in AS medium \pm OligoG

Fig 3.8: *P. aeruginosa* (NH 57388A) grown for 48 h in AS medium at OligoG 6%, showing development of thin spindles

Fig 3.9: Evaluation of the effect of reaction time on reaction yield and purity of TxRd-OligoG using a PD-10 column

Fig 3.10: Evaluation of reaction yield and purity of TxRd-OligoG conjugates using a PD-10 column

Fig 3.11: A) Calibration curve for TxRd absorbance and spectrophotometric analysis of TxRd-OligoG

Fig 3.12: Effect of concentration and pH changes on the fluorescence of TxRd cadaverine

Fig 3.13: *P. aeruginosa* (NH 57388A) grown for 24 h in MH broth \pm TxRd-OligoG

Fig 3.14: *P. aeruginosa* (NH 57388A) grown for 24 h in MH broth \pm TxRd-OligoG

Fig 3.15: *P. aeruginosa* (NH 57388A) grown for 24 h in MH broth, followed by 1 h treatment of TxRd-OligoG

Fig 3.16: *P. aeruginosa* (NH 57388A) grown for 24 h in MH broth, followed by 4 h treatment of TxRd-OligoG

Fig 3.17: *P. aeruginosa* (NH 57388A) grown for 24 h in MH broth, followed by 24 h treatment of TxRd-OligoG

Fig 3.18: Quantification of TxRd-OligoG (TxRd-G) and unbound TxRd using PD-10 column analysis of supernatant from *P. aeruginosa* (NH 57388A) biofilms grown for 24 h in MH broth, followed by A) 1 h; B) 4 h and C) 24 h treatment with TxRd-OligoG

Fig 3.19: *P. aeruginosa* (NH 57388A) grown for 24 h in MH broth, followed by 4 h or 24 h treatment (MH broth control or 6% TxRd-OligoG)

Fig 3.20: *P. aeruginosa* (NH 57388A) grown for 24 h in MH broth, followed by 4 h or 24 h treatment (MH broth control or TxRd control 0.052 µg/ml [*equivalent to 6% TxRd-OligoG conjugate])

Fig 3.21: *P. aeruginosa* (NH 57388A) grown for 24 h in MH broth, followed by 4 h or 24 h treatment (MH broth control or TxRd control 0.052 µg/ml [*equivalent to 6% TxRd-OligoG conjugate]). Magnification x3.5

Chapter 4

Fig 4.1: Schematic representation of glycan oligosaccharide A) Lewis x, B) Sialyl Lewis x and C) Sulfo Lewis x

Fig 4.2: Zeta potential (surface charge) analysis (mV) of untreated PGM, OligoG treated PGM and OligoG only

Fig 4.3: AFM images of PGM only control and PGM with OligoG

Fig 4.4: Image J analysis of the percentage surface area coverage of PGM AFM images

Fig 4.5: SEM of PGM ±OligoG

Fig 4.6: SEM imaging (without gold coating) of CF sputum ±OligoG

Fig 4.7: SEM imaging (with chromium coating) of CF sputum ±OligoG

Fig 4.8: Second derivative of A) OligoG and B) CF DNA FTIR

Fig 4.9: FTIR spectral peaks of patient 6 (Table II.i)

Fig 4.10: Scatter graph of FTIR readings at 1240 cm⁻¹ representing patients 1-9 (see Table II.i)

Chapter 5

Fig. 5.1: Set up of two (1 and 2) plates (7 mm) for extensional rheology

Fig 5.2: Extensional viscosity of CF sputum showing untreated Vs 2% OligoG treated

Fig 5.3: Rheological testing of a single patient sample divided into 8 aliquots

Fig 5.4: Wall slip tests showing complex modulus (G*) values in triplicate over the frequency range 0.1- 10 Hz at set gaps 200, 400, 600 and 1000 µm (n=3)

Fig 5.5: Wall slip testing at 0.16 Hz at set gaps 200, 400, 600 and 1000 µm

Fig 5.6: Effect of incubation time on rheological testing of OligoG treated sputum

Fig 5.7: Longitudinal study of sputum samples (n=9) from a single CF patient ±OligoG

Fig 5.8: Longitudinal study for samples from a single patient collected over 9 days for various sputum treatments with/without 0.2% or 2% OligoG and/or rhDNase I (100 nM; n=9)

Fig 5.9: Changes in elastic response (G') and viscous response (G'') for 2% OligoG treatment of sputum samples compared to water treated controls

Fig 5.10: Changes in sputum rheology showing A) elastic response (G') and B) viscous response (G'') for water treated control compared to 2% mannitol and 2% OligoG treatment

Chapter 6

Fig 6.1: A) Reconstituted human oral epithelium (SkinEthic Laboratories, Nice, France); B) Oral epithelium *ex vivo* (SkinEthic Laboratories, Nice, France)

Fig 6.2: LIVE/DEAD[®] fluorescence imaging of *C. tropicalis* 519468 grown for 24 h at 37°C. Untreated control Vs 2% OligoG

Fig 6.3: SEM of *C. tropicalis* 519468 (x1200) treated with OligoG

Fig 6.4: SEM of *C. albicans* 39343 (x1200) treated with OligoG

Fig 6.5: SEM of *C. glabrata* ATCC 2001 (x1200) treated with OligoG

Fig 6.6: SEM of *C. tropicalis* 519468 (x1200) treated with 2% OligoG with/without fluconazole

Fig 6.7: AFM imaging of *C. tropicalis* 519468 grown on polystyrene with and without 2% OligoG and/or fluconazole

Fig 6.8: AFM imaging of *C. tropicalis* 519468 grown on polystyrene with and without 2% OligoG and/or fluconazole

Fig 6.9: AFM imaging of *C. tropicalis* 519468 grown on polystyrene with and without 2% OligoG and/or fluconazole

Fig 6.10: Typical zeta potential distribution for *C. albicans* 39343 and *C. tropicalis* 519468

Fig 6.11: Mean Zeta Potential (mV) values for A) *C. albicans* 39343 and B) *C. tropicalis* 519468; untreated *Candida* (pre-wash), treated *Candida* with 10% OligoG (pre-wash), untreated *Candida* (post-wash) and treated *Candida* with 10% OligoG (post-wash)

Fig 6.12: Growth curve over 24 h for *C. albicans* ATCC 90028 comparing growth in 0.2%, 2%, 6% and 10% OligoG with an untreated control

Fig 6.13: LIVE/DEAD[®] CLSM images of RHE samples infected with *C. albicans* ATCC 90028 for 12 h

List of Tables

Chapter 1

Table 1.1: Summary of rheological parameters used

Chapter 2

Table 2.1: Zeta potential (mV) and sizing (nm) analysis of the 10% OligoG control

Table 2.2: Zeta potential measurements for 0.2% OligoG, 1% LPS and combined

Chapter 3

Table 3.1: Quantification of percentage surface area under graph at elution >5.5 ml under PD-10 analysis of supernatant

Chapter 4

No table

Chapter 5

Table 5.1: Rheology study patient data, including antibiotic and rhDNase I (if applicable) regimen at time of sampling

Chapter 6

Table 6.1: *Candida* strains and source.

Table 6.2: Pre-wash mean zeta potential values of untreated *C. tropicalis* 519468 and *C. albicans* 39343 cells: control, 0.2% OligoG, 0.5% OligoG and 1% OligoG

Chapter 1:

General introduction

1.1 Introduction

A biofilm is a collection of bacterial cells within a substratum, embedded in an organic polymer matrix of microbial origin (Garrett et al., 2008). Biofilms show high resistance to antimicrobial agents via a number of different mechanisms, often causing a range of very hard to treat infections from endocarditis and ventilator-assisted pneumonia, to the chronic inflammation and infection of the cystic fibrosis (CF) lung and non-healing skin wounds (Percival et al., 2011). These recalcitrant infections therefore require novel therapeutic strategies. Since bacteria within multicellular communities form cellular aggregates, one possible anti-biofilm target is to disrupt the structure of the biofilm itself (Stewart and Costerton, 2001). Nano-sized low molecular weight (MW) oligosaccharides based on alginates have been shown to improve the efficacy of antibiotics and hence aid host defences to resolve infections and have considerable potential benefit in the treatment of biofilm infection for therapeutic use (Roberts et al., 2013).

1.2 Alginate oligomers

1.2.1 Properties of alginates

Alginates are a broad family of polysaccharides composed of blocks of various lengths and distributions (Andersen et al., 2012, Qin, 2008). Alginates are composed of copolymers, the “building blocks” of which are 1-4 linked β -D-mannuronic acid (M) and α -L-guluronic acid (G) residues (Draget and Taylor, 2011), which differ stereo-chemically due to their differences at C-5 (Qin, 2008). The most common arrangement of alginates is a block copolymer containing homo-polymeric sequences of MM-blocks and similar sequences of GG-blocks which are inter-dispersed between mixed compositions of MG-blocks. The ratio and distribution of G and M varies between species and on the growth conditions used. Alginates are highly soluble in water and form gels with cations such as Ca^{2+} , the gel-forming capacity depends on the G-block content and length (Hartmann et al., 2006). M-blocks by contrast, do not form a gel with Ca^{2+} (Andersen et al., 2012).

Alginates are currently extracted from brown seaweed, but can also be produced by microbial fermentation (Draget and Taylor, 2011). The alginate is extracted by treating raw seaweed with NaOH, to produce soluble sodium alginate.

This can be further precipitated after filtration by the addition of calcium chloride (Qin, 2008). Alginates are also produced by bacterial species belonging to the genera *Pseudomonas* and *Azotobacter* during biofilm formation (Gimmestad et al., 2003). When produced, adaptations may be enzymatically introduced by epimerisation. Pseudomonal alginates do not contain stretches of continuous G-blocks, which are commonly seen in *Azotobacter* species (Gimmestad et al., 2003). The MW of bacterial alginates (e.g. as high as 4000 kDa in a mutant strain of *Azotobacter vinelandii*) are considerably higher than alginates extracted from seaweed, ranging between 48-186 kDa (Galindo et al., 2007, Pena et al., 2002). Alginate is a polyelectrolyte containing a COOH group within its chain, giving rise to different charge-densities depending on the pH. Protonation and de-protonation of the COO⁻ will alter the hydrophobicity of the alginate (Yang et al., 2011a). pH therefore plays an important role in determining solubility of alginates in water (Hartmann et al., 2006). The G-M composition of the alginate also affects physical and mechanical properties; mannuronic acid moieties give rise to a linear flexible conformation due to their β (1-4) bonds, the guluronic acid forms a folded, rigid structural shape, due to α (1-4) bonds (Yang et al., 2011a). Interestingly alginates with a G content of >50% do not create an immune response, whilst a high M content can stimulate the innate immune system (Andersen et al., 2012).

1.2.2 Current uses of alginates

Alginates have a number of advantageous properties; being biocompatible, non-toxic and non-immunogenic. Sodium alginate is listed and defined in the European Pharmacopoeia and the US Pharmacopeia/National Formulary, in the list of materials Affirmed Generally Recognized as Safe by the U.S. Food and Drug Administration (Yang et al., 2011a). No known alginate degrading enzymes exist in humans. Alginates applied as biomaterials *in vivo* will therefore depolymerise only via spontaneous β -elimination. At sites of infection, alginate breakdown by alginate lyases in bacteria (which catalyse the β -elimination of bacterial alginates) and degradation by reactive oxygen species (free-radical de-polymerisation) may occur (Andersen et al., 2012). Alginate chains are relatively stable under physiological conditions (pH 7.4). However, glycosidic linkages of alginates are susceptible to

acid hydrolysis and alkaline β -elimination. Since the optimum stability for alginate is around pH 6, this implies that degradation at pH 7.4 is dominated by β -elimination (Andersen et al., 2012). Initially, alginates were developed for industrial applications in the food and pharmaceutical industries. The alginate Protanal[®] has several applications such as gelling and stabilizing certain foods, for example bakery creams and yogurt (BioPolymer, 2014). Alginates have several other applications, and can be formed into macro- and micro-scale fibres for biomedical applications such as wound dressing and tissue engineering (Andersen et al., 2012, Qin, 2008, Boateng et al., 2008, Attwood, 1989). Alginates are widely used in medicine e.g. in dental impression materials and in reducing gastric reflux (Gaviscon[®]; Draget and Taylor, 2011).

1.2.3 Alginate oligosaccharide (OligoG CF-5/20)

OligoG is a G-block oligosaccharide with a very narrow MW range and a specific chemical structure following purification and fractionation (**Fig 1.1A**; Khan et al., 2012). As with most alginates, it too is produced from the stem of brown seaweed (*Laminaria hyperbora*), which has a low variability in G content. Purification employing charcoal filters is followed by spray-drying, and results in OligoG powder. Purified OligoG is characterised by hydrogen-1 nuclear magnetic resonance and high-performance anion-exchange chromatography with pulsed amperometric detection (**Fig 1.1B&C**). OligoG is composed of 90-95% guluronic acid with a MW of approximately 2600 g/mol. OligoG is composed of 5-20 monomer units. OligoG is a soluble anionic compound, with its solubility limited by viscosity when at >15% (Khan et al., 2012). Each batch produced is tested for viable counts, endotoxins, heavy metal counts and ions. Initial tests were compared to oligomers of similar MW, but altered M content, via epimerisation technology.

1.3 Bacterial infection

1.3.1 Bacterial cell wall

Bacteria are single-celled prokaryotes, bound by a thin elastic, semi-permeable phospholipid bilayer plasma membrane (5-10 nm thick). The membrane is

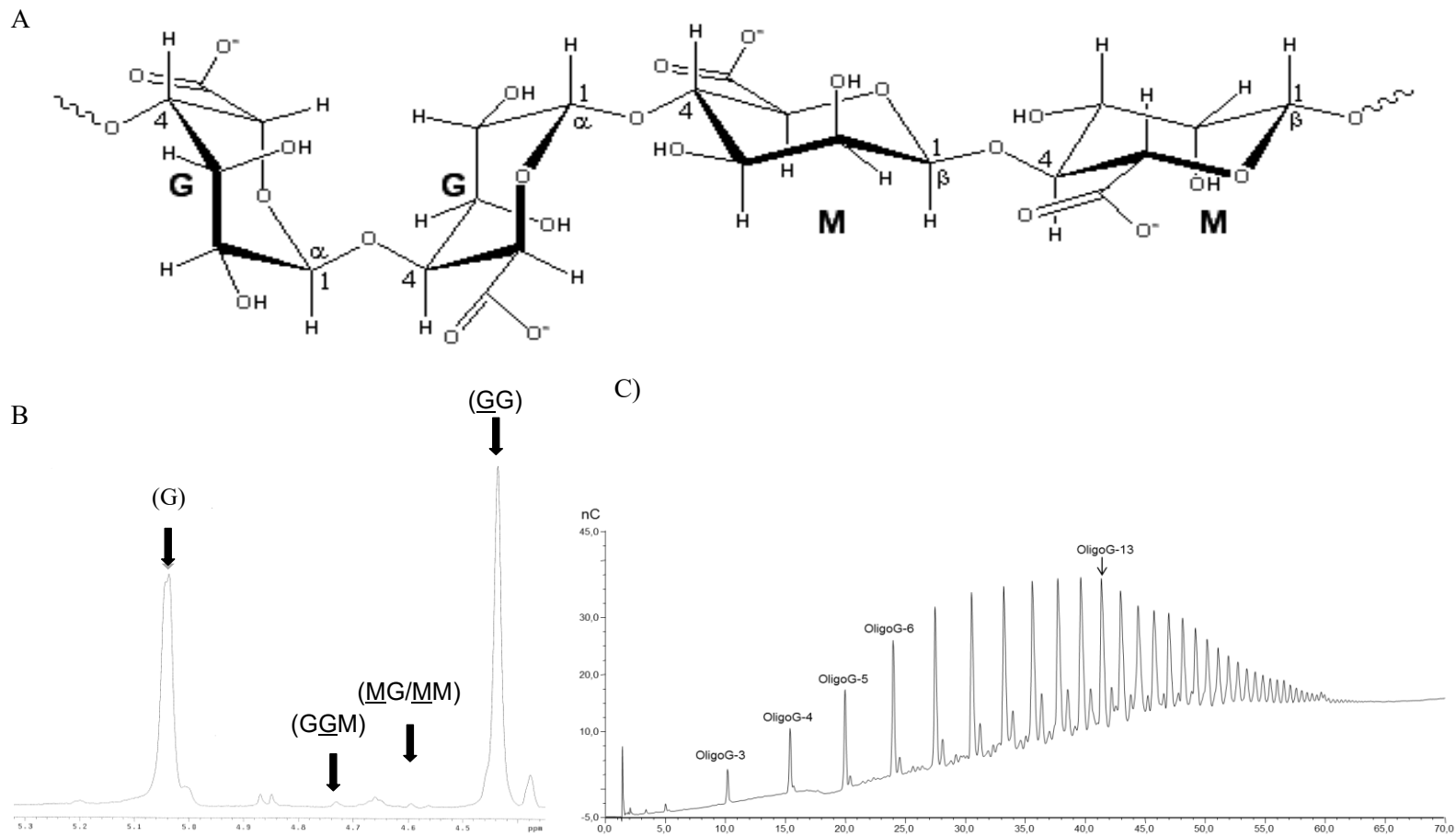


Fig 1.1: Structure, purification and quality control of OligoG. A) Structure of α -L-gulonate (G) and β -D-manuronate (M); OligoG has at least 90-95% of the monomer residues as G residues. B) NMR spectrum of OligoG containing 96% G. C) Characterisation of OligoG with high performance anion exchange chromatography with pulsed amperometric detection (HPAEC-PAD). Image courtesy of Khan et al. (2012).

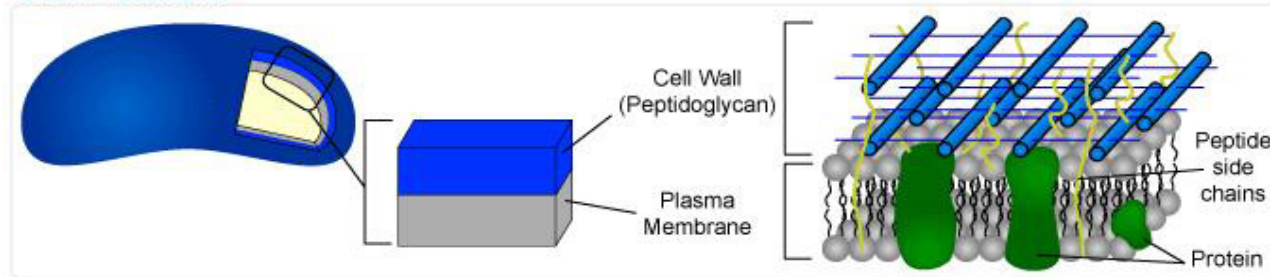
surrounded by a porous, semi-permeable cell wall. The cell wall lies immediately external to the phospholipid layer (10-25 nm thick). The wall provides strength and rigidity and opens freely to molecules <1 nm. The main cell wall component is peptidoglycan, which is made up from *N*-acetylglucosamine (NAG) and *N*-acetylmuramic (NAMA) acid molecules (Greenwood et al., 2007).

Gram-positive and Gram-negative bacteria differ in their outer cell envelope (**Fig 1.2**), which will contribute to the net electronegativity of the cell surface. The peptidoglycan cell wall of Gram-positive bacteria is very thick and tightly cross-linked by inter-peptide bridges and has a phosphoryl group located in the substituent teichoic and teichuronic acid residues, and un-substituted carboxylate groups. The peptidoglycan found in Gram-negative bacteria is very thin, loosely cross-linked and sequestered within the periplasmic space; phosphoryl and 2-keto-3-deoxyoxonate carboxylated groups of lipopolysaccharide (LPS) are found in the outer leaflet of the outer membrane (OM) resulting in the observed negative electrostatic surface charge (Wilson et al., 2001).

Gram-negative bacteria are resistant to a large number of noxious agents due to the effective permeability barrier function of the OM, which is impermeable to macromolecules. The OM protects the bacteria from complement and antibody binding, and hence phagocytosis. The molecular basis of the integrity of OM is due to the LPS, which is highly polyanionic. The adjacent polyanionic LPS molecules are linked electrostatically by divalent cations such as Mg^{2+} and Ca^{2+} (Vaara, 1992) and LPS also plays a role in bacterial adhesion (Kipnis et al., 2006).

Pseudomonas aeruginosa is an opportunistic pathogen and colonises the respiratory epithelium of CF patients (Kipnis et al., 2006). *P. aeruginosa* (PAO1) has two distinct LPS *O*-polysaccharide species (A and B band) and their expression is under environmental control (Makin and Beveridge, 1996). CF patients colonised with *P. aeruginosa* were found to synthesise LPS with specific lipid A structures, which indicates the unique recognition of the CF airway environment (Ernst et al., 1999). *P. aeruginosa* in CF adapts to select mutants with specific lipid A modifications, which allow resistance to host antimicrobial peptides, and increased Toll-like receptor 4 activation (Kipnis et al., 2006), resistance to cationic antimicrobial peptides and, therefore, promoting an increased inflammatory response (Ernst et al., 1999). *P. aeruginosa* is capable of twitching, swimming and swarming

Gram⁺ Bacteria



Gram⁻ Bacteria

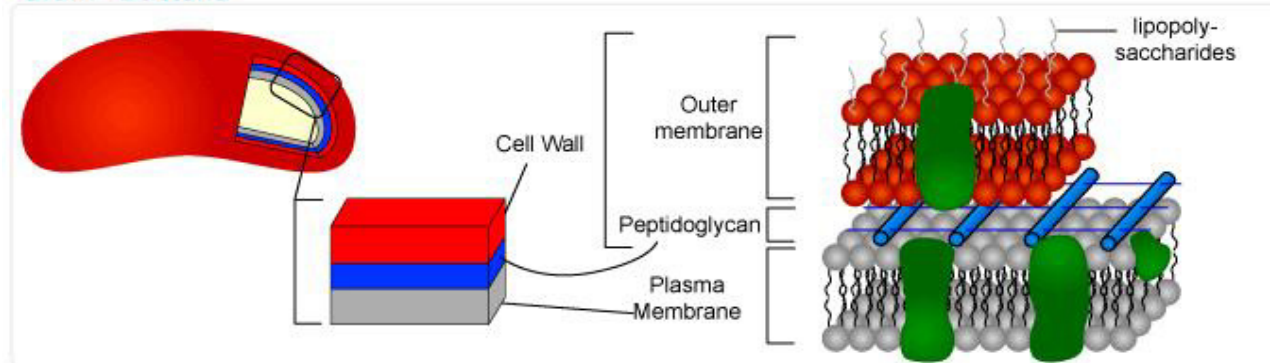


Fig 1.2: Schematic diagram representing the differences in cell wall content of Gram-negative and Gram-positive bacteria (Accessed 15/09/2014; <http://www.expertsmind.com/topic/microbiology/bacterial-cell-wall-92313.aspx>).

motility (Caiazza et al., 2005, Harshey, 1994). These phenotypes play an important role in irreversible adhesion to epithelial cells and are a critical step in colonisation of the respiratory epithelium. Flagella is a motile appendage often found in Gram-negative bacteria and are complex proteic structures, which form a filamentous polar appendage at the cell surface. Flagella can also be very immunogenic, becoming a disadvantage to colonisation. To overcome this, *P. aeruginosa* can adapt to become aflagellar mutants once initial colonisation has occurred and thereby avoid the host response (Kipnis et al., 2006). Pili or fimbriae are filamentous surface appendages and are smaller than flagella, but are also important for motility and adhesion (Greenwood et al., 2007).

1.3.2 Clinical implications of biofilms

An estimated 99% of the world's bacteria are found in biofilm structures. The advantages for a bacteria cell existing as a biofilm includes higher concentrations of nutrients close to the biofilm surface, increased genetic exchange, as well as better protection from the host's immune system (Palmer et al., 2007a).

The human body is home to a diverse and large number of microbes known as the indigenous microbiota or normal micro-flora (Bruinsma et al., 2001). However, more than half of all infectious diseases that affect mildly compromised patients are commensal species of the human body or are common environmental organisms (Costerton et al., 1999). Biofilms can be found on inert surfaces (e.g. medical devices), dead tissue, or on living tissue (e.g. endocarditis or in the CF lung). Immune response occurs due to the stimulation of antibodies, but is frequently ineffective against biofilms. Even the host defence system in a healthy individual can rarely completely eradicate a biofilm (Alavi et al., 2012).

1.3.3 Stages of biofilm formation

1.3.3.1 Conditioning layer

The conditioning layer is composed of many organic and inorganic particles and becomes the "foundation" on which biofilms grow. Interaction between the conditioning layer and substrate can alter surface charge, surface potential and surface tension, all of which may favour bacterial adhesion and act as anchorage sites

and/or nutrients for bacterial growth (Garrett et al., 2008, Donlan, 2002). Attachment and loss of bacterial mobility may initially be transient (Alavi et al., 2012).

The content of the aqueous medium can affect bacterial attachment. The variability can depend on pH, nutrient availability, ionic strength and temperature. The cell itself also affects the bacterial attachment via a presence of fimbriae/flagella and surface hydrophobicity (Donlan, 2002, Alavi et al., 2012).

1.3.3.2 Reversible adhesion

Physical forces or bacterial appendages (e.g. flagella), can lead to planktonic cells contacting the conditioning surface. Reversible adhesion occurs in a fraction of the cells at the surface, depending on the available energy, surface functionality, bacterial orientation and temperature. For adhesion to occur, attractive forces need to exceed repulsive forces (Garrett et al., 2008). The weakness of the bonds initially formed is evident in the low activation energy for desorption of bacteria (van Merode et al., 2006). The physical forces involved include van der Waals forces and electrostatic interactions. These forces are known as the Derjaguin, Verwey, Landau and Overbeek (DLVO) theory which is described further in section 1.5.2.2. Bacterial adhesion is driven by these interactions between the bacteria and substratum. These interactions occur between the entire cell body and more-specific localised adhesion sites, such as proteins on the cell surfaces. In nature, nearly all bacterial surfaces carry a net negative charge in physiological conditions (van Merode et al., 2006).

1.3.3.3 Irreversible adhesion

A number of absorbed bacterial cells will remain immobilised. A number of factors are thought to be involved in irreversible absorption including short-range forces (covalent and hydrogen bonding) as well as hydrophobic-hydrophilic interactions at the surface (Palmer et al., 2007a). In this immobilisation, the physical repulsive force of the bacteria surface is overcome by bacterial appendages, e.g. flagella, fimbriae and pili which interact with the conditioning layer and strengthens the binding of the bacteria to the surface (Garrett et al., 2008, Hall-Stoodley and Stoodley, 2002). Cell surface proteins can lead to attachment, e.g. the *O*-antigen

component of LPS in Gram-negative bacteria (Donlan, 2002). Co-aggregation is also of particular importance clinically since a multi-species biofilm may develop as certain species may bind to other species rather than to the substrate (Alavi et al., 2012).

1.3.3.4 Population growth and stationary biofilm phase

The immobilised cells divide by binary division to form clusters, as the daughter cells spread outwards and upwards from the point of attachment. An exponential growth phase follows with a rapid increase in population. As nutrients from the surrounding bulk fluid and substrate are required, the exponential growth rate is dependent on the physical and chemical nature of the environment. Stronger bonds are then formed between cells due to interaction with divalent cations and excretion of extracellular polymeric substances; EPS (Dunne, 2002). As the cells change from planktonic to an adherent biofilm population, gene expression alters and the production of bacterial appendages is inhibited in immobile sessile cells (Hall-Stoodley and Stoodley, 2002), whilst the expression of genes for the production of cell surface proteins and excretion products increases (Hancock et al., 1990). In the initial lag phase of biofilm formation, the interaction and growth lead to the development of a mushroom-like structure.

At high cell densities, a series of cell signalling mechanisms are employed by the biofilm and this is termed quorum sensing (QS). In QS, chemical and peptide signals at high concentrations regulate the genetic expression of a number of important processes including both mechanical and enzymatic processors of bacterial alginates (Singh et al., 2000). Eventually cell division will equal cell death in the established biofilm.

1.3.3.5 Cell death biofilm phase

Eventually enzymes produced by the biofilm community start to breakdown the EPS matrix of the biofilm. The breakdown of the biofilm structure will allow release of surface-associated bacteria. Gene expression for flagella becomes up-regulated to facilitate bacterial motility to “shed” bacterial cells. These planktonic bacteria are available for the colonisation of new surfaces, where the process of

biofilm formation begins again (Perni et al., 2014). A schematic summary of biofilm formation can be seen in **Fig 1.3A**.

1.3.4 Quorum sensing

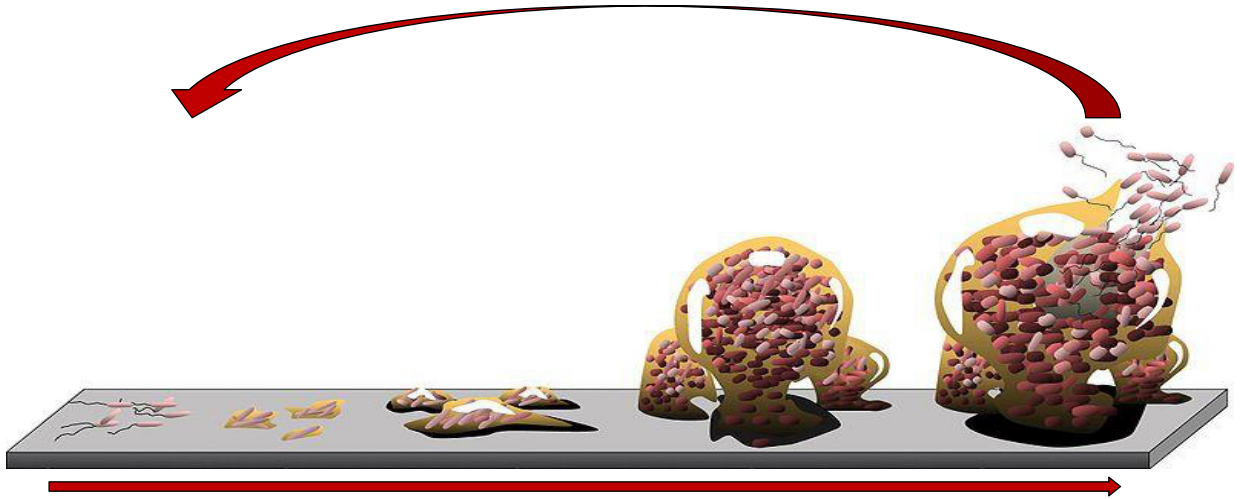
QS was first described by Greenberg in (1994). QS allows bacterial and fungal communities to function as a “multicellular organism” by collectively responding to signalling processes (Waters and Bassler, 2005) in relation to population density. In bacterial communities this is facilitated by the release of chemical signals, known as “autoinducers”. The extracellular concentration of these autoinducers increases with greater cell population density and will alter gene expression and protein production in bacterial community (Waters and Bassler, 2005). QS in Gram-negative bacteria occurs via small signalling molecules known as acyl homoserine lactones (AHL) which are co-factors of transcriptional regulators and diffuse freely across bacterial membranes (Kipnis et al., 2006). In *P. aeruginosa* the QS is regulated by LuxI/LuxR circuit, specifically by the homologues LasI/LasR and RhlI/RhlR (**Fig 1.3B**). LasI and RhlI are autoinducer synthases. These regulatory circuits work in tandem to control the expression of several virulence factors (Miller and Bassler, 2001).

Bacteria constantly interact with their surrounding environment and exchange information with other cells. Signalling between cells allows for optimal growth, as they are able to adapt to their changing environment.

1.3.5 Extracellular polymeric substance

Bacteria within biofilms are encased in a matrix composed of EPS (Monroe, 2007) which are biopolymers of microbial origin such as glycoproteins, glycolipids and eDNA (Flemming et al., 2007). The proportion of cells present in a biofilm is species-dependent and can range from 10-25% cells in a 75-90% EPS matrix (Garrett et al., 2008). The EPS of Gram-negative bacteria includes uronic acid (e.g. D-guluronic, D-galacturonic and mannuronic acid) or ketal-linked pyruvates, which all have anionic properties. EPS allows association of divalent cations, e.g. Ca^{2+} and Mg^{2+} and facilitates cross-linking within biofilms. The EPS of Gram-positive bacteria, such as *Staphylococcus* species is mainly cationic (Donlan, 2002).

A



B

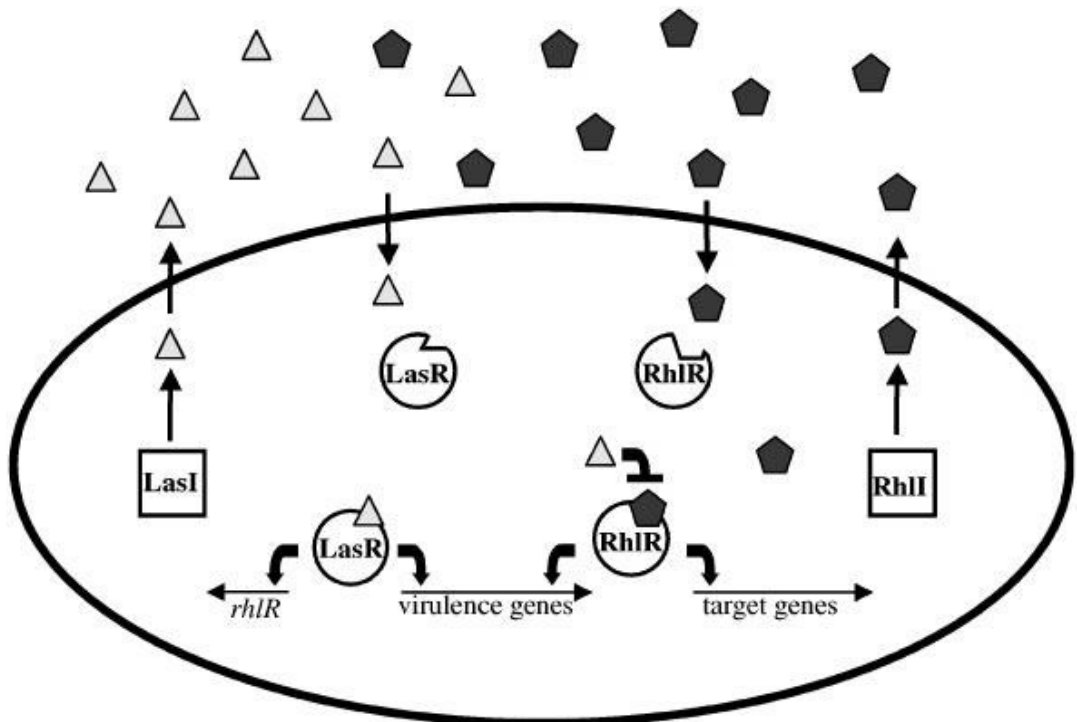


Fig 1.3: Diagrammatic representation of a A) typical biofilm formation pattern (image courtesy of Monroe 2007), B) *P. aeruginosa* LasI/LasR-RhlI/RhIR QS system (image courtesy of Miller and Bassler 2001).

EPS has many functions, which are constructive (structural components), sorptive (for ion exchange and sorption), active (due to extracellular enzyme polymer degradation) or surface active via membrane vesicles (Flemming et al., 2007), and provide a barrier to chemicals (Alavi et al., 2012). Other functions of the EPS are specificity and recognition through lectins, providing genetic information and structure via nucleic acids, as well as aiding resistance to antimicrobial agents via deactivation. EPS is redox active from bacterial refractory polymers which are thought to act as electron donors or acceptors, as well as having nutritive roles, with various polymers being a source of carbon, nitrogen and phosphate (Flemming et al., 2007).

Within the CF lung environment, *P. aeruginosa* frequently converts to a mucoid phenotype (Kipnis et al., 2006), which produces high MW alginates. The degree of acetylation varies widely between the mucoid exopolysaccharide purified from different *P. aeruginosa* isolates. It may only mutate to a mucoid form when iron, phosphate or nutrients are limited (Boyce and Miller, 1982, Terry et al., 1992). The mucoid phenotype is controlled by transcriptional regulation of the GDP-mannose dehydrogenase encoded by the *algD* gene, which is the first gene of the alginate biosynthetic operon. The *algD* gene is regulated under a complex multi-tier regulation mechanism, by both constitutive and inducible gene products (Lyczak et al., 2000). The alginate anchors *P. aeruginosa* to the respiratory epithelium, protects *P. aeruginosa* from phagocytosis and antibiotics, and attenuates the host response, as well as being a structural component in the biofilm (Kipnis et al., 2006).

Exchange of genetic material occurs within biofilms where there is access to a large gene pool (Alavi et al., 2012) and horizontal gene transfer can also occur. In addition, extracellular deoxyribonucleic acid (eDNA) is found in abundance within biofilms and is thought to be derived from lysed dead cells. It has postulated that eDNA within biofilms of *P. aeruginosa* may also have a structural role (Allesen-Holm et al., 2006). In *P. aeruginosa* biofilms eDNA is under the control of QS (Flemming et al., 2007).

1.3.6 Antibiotics and resistance

Development of antibiotic resistance is a worldwide problem (Pruden et al., 2013). An increase in antibiotic resistance has led to an increase in the dosage and duration of antibiotic therapies required to induce a clinical response (Maragakis et al., 2008). It is, however, recognised that the need for new antibiotics targeting multi-drug resistant (MDR) Gram-negative infections remains largely unmet (Mossialos et al., 2010). Antibiotics target structures or processes which are vital for bacterial growth or survival, but must do so without harming the infected eukaryotic host. They work either bacteriocidally or impeding growth via a bacteriostatic effect (Walsh, 2000).

Various vehicles for transfer of resistance for genetic adaptation and development of antibiotic resistance exist including gene transfer, genetic recombination/transposition (DNA rearrangements, gene duplications, transposition and insertional activation) as well as point mutations (Stewart and Costerton, 2001). For example, mutants may facilitate spread of resistance to its near neighbours, ultimately leading to dominance within the population. This spread may be facilitated by mobile genetic elements, e.g. plasmids or transposons which replicate independently and pass easily between bacterial cells and even species (Luis Martinez et al., 2009). The presence of bacterial membrane protein pumps (efflux pumps) can export the drug resulting in an ineffective intracellular concentration to affect bacterial protein synthesis (Paulsen et al., 1996). Other modes of bacterial resistance include destruction of the antibiotic, e.g. the hydrolytic deactivation of the β -lactam ring by the hydrolytic enzyme β -lactamase (Bradford, 2001, Poole, 2004). Another method of antibiotic resistance is the reprogramming or “camouflaging” of the target. For example, resistance to erythromycin can be gained by methylation of the 23S rRNA component found in the 50S subunit of the bacterial ribosomes which inhibits bacterial protein synthesis by altering ribosome function (Bussiere et al., 1998).

1.3.7 Antibiotic resistance in biofilms

When planktonic cells form biofilms they may be up to 1000 times more resistant to antimicrobial agents. Distinct phenotypic/genotypic differences can be

found between identical cells grown planktonically compared to when they are grown in a biofilm (Mah and O'Toole, 2001). There are several hypothesis related to antimicrobial resistance and biofilms (Brooun et al., 2000). Penetration will be greatly retarded in a biofilm and the antibiotic may never reach its target at a high enough concentration to be effective (Normark and Normark, 2002). This theory however has flaws in that there is no barrier to the size of antibiotics which can penetrate through a biofilm and they are often found to readily permeate biofilms (Stewart and Costerton, 2001). However, positively charged agents e.g. aminoglycosides (Jana and Deb, 2006) will bind to the biofilm EPS components which, therefore, limits transport of the compound (Mah and O'Toole, 2001). Antibiotics may be sequestered by binding to multi-layered thick cell wall, e.g. periplasmic glucans on *P. aeruginosa* cell wall interacts physically with tobramycin (Mah et al., 2003).

Within the CF lung, oxygen deprivation and anaerobic growth has been linked to antimicrobial resistance of *P. aeruginosa*, where it is estimated that oxygen only penetrates to around 5% of the depth of the lung biofilm (Smith, 2005). The metabolic waste products can lead to local accumulation of acidic waste which can antagonise the activity of antibiotics. Cells within a biofilm may also be metabolically inactive due to depletion of substrates or accumulation of inhibitive waste products, causing them to enter a non-growing state (being viable but not cultivable). As a number of antibiotics target cell wall synthesis (Normark and Normark, 2002), these will be unaffected by antibiotic therapies when in a dormant state (Mah and O'Toole, 2001).

Another hypothesis for increased resistance of biofilms to antibiotics explores the possible formation of a sub-population of micro-organisms which are a phenotypically distinct (Stewart and Costerton, 2001). Persister cells are dormant variants of regular cells which form stochastically in microbial populations (Lewis, 2010). *P. aeruginosa* persister cells are common isolates found in human airway infections (Mulcahy et al., 2010). The osmotic environment within a biofilm differs and may lead to an osmotic stress response in the cell wall. This may eventually lead to a change in the relative proportions of porins, which reduces cell envelope permeability to antibiotics (Stewart and Costerton, 2001). Elevated antibiotic resistance is reported in swarming populations of bacteria such as *P. aeruginosa*.

Swarming bacteria move in multicellular groups and this genotype is an effective strategy for prevailing against antimicrobials (Butler et al., 2010). Swarm cells exhibit an elevated resistance to a variety of antibiotics, including those which target protein translation, cell envelope, DNA replication and transcription (Kim et al., 2003).

1.3.8 Developing anti-biofilm therapeutics

Novel alternative anti-biofilm strategies are clearly required to attack different stages in the biofilm life cycle, from inhibition of cell attachment, disruption of cell-cell communication (QS), degrading the biofilm matrix and physical removal/disruption of the disseminating biofilm (Alavi et al., 2012). Several mechanisms to prevent biofilm attachment have been reported including coating surfaces with antibiotic compounds, but the persistent low concentration of antibiotics may increase resistance (Francolini et al., 2004). Other novel compounds have been tried such as natural cationic peptides. Natural cationic peptides are 12-50 amino acids in length and are amphiphilic. A natural human cathelicidin peptide LL-37 was shown to block *P. aeruginosa* biofilm growth and accelerate biofilm breakdown (de la Fuente-Nunez et al., 2012). Not only was LL-37 found to decrease attachment of bacterial cells, but also stimulated twitching motility and down-regulated genes essential for biofilm formation by influencing the QS systems *Las* and *Rhl* (Overhage et al., 2008). A small cationic peptide 1037 (9-amino acid) was found to inhibit biofilms by reducing swimming and swarming motility, stimulating twitching motility and suppressing a variety of genes found in biofilm formation (de la Fuente-Nunez et al., 2012). Alternative anti-biofilm mechanisms have included electrical enhancement via a bioelectric effect and ultrasound enhancement of antimicrobial transport. Further approaches include photodynamic therapies as photosensitising drugs to induce local production of reactive oxygen species which are difficult for the microorganism to defend against (Smith, 2005). Liposomes have also been postulated as a drug delivery/targeting vehicle to concentrate agents at the biofilm interfaces, to be taken up into cells harbouring intracellular pathogens (Smith, 2005, Pinto-Alphandary et al., 2000).

Recently other workers have purified components from the marine environment to disrupt biofilms. A bacterial EPS (A101) derived from a marine bacterium (*Vibrio* sp. QY101) and an enzyme (NucB) derived from *Bacillus licheniformis*, both exhibit significant anti-biofilm properties *in vitro* (Jiang et al., 2011, Nithya et al., 2010, Shakir et al., 2012, Nijland et al., 2010). The EPS of *Oceanobacillus iheyensis* BK6 derived from marine natural biofilms exhibited anti-biofilm activity against a pathogenic strain of *Staphylococcus aureus*. It has high viscosity, emulsifying properties and has the potential for pharmaceutical and industrial application (Kavita et al., 2014). Interestingly, the properties of A101 appear to be very similar to those initially reported of the algal-derived OligoG, particularly with regard to antibiotic potentiation specificity and biofilm disruption properties (Khan et al., 2012, Jiang et al., 2011).

1.4 Fungal infection

In recent years there has been an increased incidence of invasive fungal infections. These lead to an increase in morbidity and mortality, making them a serious public health concern (da Silva et al., 2013). *Candida* species co-exist as harmless commensals but the source of most cases are endogenous, (Lass-Floerl, 2009) and they become opportunistic pathogens in immune-compromised (Silva et al., 2011b) and debilitated patients. When fungal infections become systemic they are associated with significant mortality (Lass-Floerl, 2009). Candidal infections can be superficial, as well as being systemic, leading to complications in major body organs. The rise in fungal infections is thought to be mainly due to an increase use of medical practices such as invasive surgical procedures, immunosuppressive therapies (Ene et al., 2012, Silva et al., 2012), cytotoxic drugs (Silva et al., 2011b) and broad-spectrum antibiotics (Ramage et al., 2006, Silva et al., 2012). The increased use of anti-neoplastic agents, prosthetic devices and grafts have also contributed to the rise in fungal infections (Lass-Floerl, 2009).

The epidemiology of fungal diseases is changing due to the increase in antifungal prophylaxis (Lass-Floerl, 2009). Once a candidal biofilm is formed *in vivo*, the only mechanism to eliminate the infection is often removal of the substratum that supports the biofilm. The removal of medical devices is often

impossible, due to the patient's condition, the anatomic location of the infection/disease and/or underlying disease processes (Ramage et al., 2006).

1.5 Analysing bacterial and candidal biofilms

1.5.1 Imaging techniques

1.5.1.1 Atomic force microscopy

Atomic force microscopy (AFM) was invented by Binnig et al. (1986) and has revolutionised the techniques for exploring the microbial surface (Sheu et al., 2010, Dorobantu and Gray, 2010). In microbiology, AFM has provided three-dimensional imaging of surface ultrastructure under physiological conditions with minimal preparation and has been used to study the effect of antimicrobial agents on planktonic and sessile bacterial cells (Johansen et al., 1996, Powell et al., 2014, Kasas et al., 1994, Braga and Ricci, 1998, Bekir et al., 2014). AFM has also been used to study the interactions of bacterial biofilms with different materials and biological surfaces (Beech et al., 2002). AFM has been used to study the nanoscale interaction of antimicrobial agents e.g. colistin, and antimicrobial peptides with a range of MDR Gram-negative organisms including *P. aeruginosa*, *Acinetobacter baumannii* and *E. coli* (Li et al., 2007, Rossetto et al., 2007, Soon et al., 2009).

Tapping mode has great potential for imaging surface topography with minimal applied force (Dufrene, 2002, Moller et al., 1999). AFM consists of an AFM tip, a piezoelectrical scanner, an optical deflection system made up of a laser diode and a photodetector and an electrical feedback system (**Fig 1.4**). The AFM tip is mounted at the end of a flexible cantilever (Dorobantu and Gray, 2010) and senses the force between a very sharp probe and the sample surface. This is generated by recording the force change as the probe is scanned in the x and y directions (Dufrene, 2002). Small forces of interaction deflecting the cantilever give rise to images which can be viewed three-dimensionally by topographic and phase images (Dorobantu and Gray, 2010; Sheu et al., 2010).

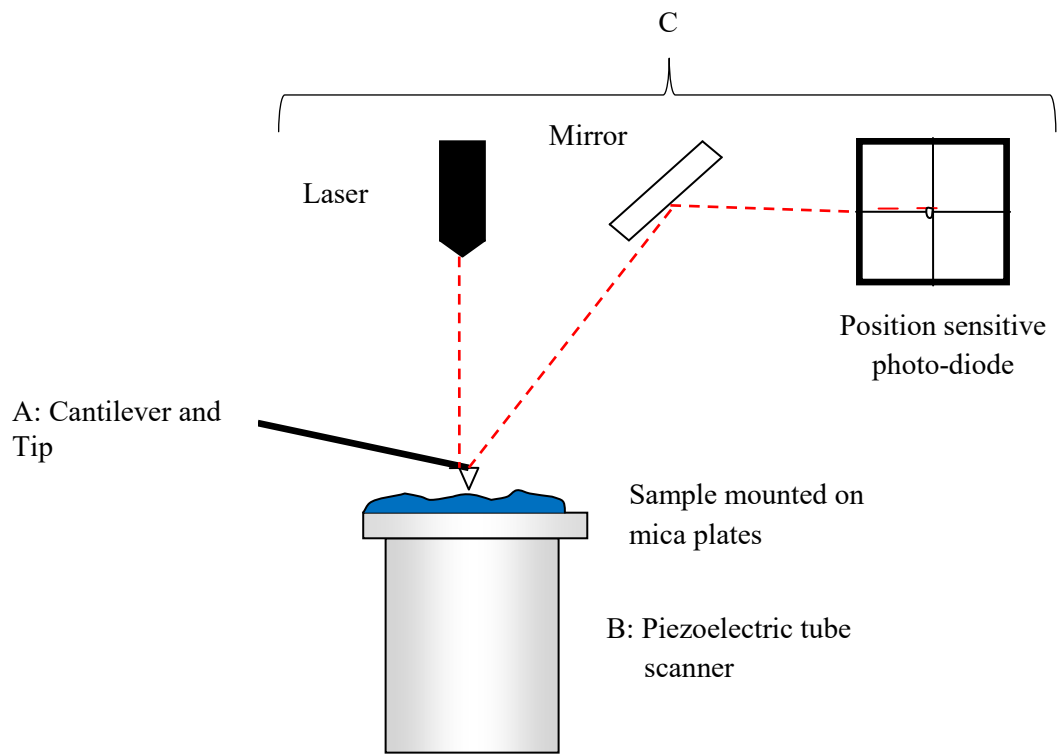


Fig 1.4: Diagram of the basic operation of an AFM; A) cantilever and AFM tip, B) piezoelectrical scanner, C) an optical deflection system made up of a laser diode and a photodetector and an electrical feedback system.

1.5.1.2 Scanning electron microscopy

In scanning electron microscopy (SEM) a de-magnified electron beam scans the sample surface. Emissions are formed when the electron probe interacts with the sample and are captured by detectors. SEM for planktonic and biofilm imaging of *P. aeruginosa* has been described extensively in the literature (Luca et al., 2013, Khan et al., 2012, Jesaitis et al., 2003, van Gennip et al., 2012) and combination of dehydration and fixation techniques are widely used and aim to preserve the delicate organic structures of bacterial samples through minimal destructive surface tension forces during drying (Fratesi et al., 2004). However, care should be taken when analysing SEM *in vitro* biofilms compared to those *in situ*, since changes in the number of bacteria, texture of biofilm and structural differences are reported (Wimpenny et al., 2000).

Different SEM preparation techniques have been shown to enhance different components of a heterogeneous sample (Fratesi et al., 2004). For example, ethanol dehydration with hexamethyldisilazane preserves both bacteria and EPS layer well, but may dissolve certain polysaccharides. Fixation can also be used prior to dehydration to increase resistance to deformation.

1.5.1.3 Confocal laser scanning microscopy

In confocal laser scanning microscopy (CLSM), a laser-light-beam is directed through the head of the microscope which passes via the objective into the microscope slide. The fluorescent dye-stained specimen on the microscope slide excites, and the fluorescent image is captured by the objective. A module on the head of the microscope receives the fluorescent image, and transfers it to the computer screen (Rowland and Nickless, 2000). CLSM has the advantage of imaging the full thickness of the specimen by imaging serial sections. This is accomplished due to its ability to focus on planes within opaque objects and acquire a series of sections (“Z” stack) to produce three-dimensional images (Sharp, 2014). The ability to use a narrow range of excitation wavelengths will reduce auto-fluorescence and improve image quality. Details on CLSM uses in microbiology, choice of fluorescent probes and its limitations are discussed further in **Chapter 3**.

1.5.2 Surface charge analysis

1.5.2.1 Influence of bacterial surface charge and adhesion

The ability of bacteria to attach to a surface and the subsequent resistance of a biofilm to physical disruption relies on their physical and mechanical properties when formed in physiological environments (Aggarwal and Hozalski, 2010). The development of a new anti-biofilm therapy treatment requires an understanding of the bacterial surface charge (Palmer et al., 2007a). A previous study found that alteration of the bacterial repulsive electrostatic charge led to a reduced biofilm formation (Gross et al., 2001). Bacteria are described as being ion-impenetrable, with the charge located on the outer cell surface only (Poortinga et al., 2002). The cell surface charge of bacteria is caused by the dissociation or protonation of carboxyl, phosphate and amino groups. At physiological pH between 5 and 7, bacterial strains are mainly negatively-charged due to the number of carboxyl and phosphate groups exceeding the number of amino acid groups present (Poortinga et al., 2002, Wilson et al., 2001, Palmer et al., 2007a). The negative surface charge may reflect the presence of COO^- groups in the LPS of Gram-negative bacterial cell wall (Shephard et al., 2008). This is further influenced by local hydrophobicity, electrical potential and the adsorption of specific ions, e.g. Ca^{2+} (Poortinga et al., 2002).

1.5.2.2 The DLVO theory in relation to microbial adhesion

The Derjaguin, Verwey, Landau and Overbeek (DLVO) theory is a quantitative simplistic model to describe the interaction between non-biological lyophobic colloids (e.g. polystyrene particles), but has been used to for biological materials and bacterial cell samples. In contrast, characterising bacterial cell surfaces is more complex since they are chemically and structurally heterogeneous (Perni et al., 2014), however researchers have used the extended DLVO theory to include non-classical DLVO. The extended DLVO theory also takes account of the hydrophobic, hydrophilic, steric and osmotic interactions involved (Perni et al., 2014) which better quantitatively predicts bacterial adhesion. The DLVO theory was first used to describe the effects of electrolyte concentration on the initial, reversible phase of

biofilm formation (Marshall et al., 1971) and has since been used to describe bacterial adhesion (Hermansson, 1999, Perni et al., 2014).

The DLVO theory explains how particle adhesion is determined by long range interactions between adhering particles and macroscopic substratum surfaces (Poortinga et al., 2002). It therefore describes the net interaction between a cell and a flat surface (substratum) which is a balance between two main factors; the attractive interactions from the Lifshitz-van der Waal forces and repulsive interactions from overlapping electrical double layers (Hermansson, 1999). The electrical double layers are made up of the counter-ions around the charged cell and bind to the surface which forms the inner Stern plane (**Fig 1.5A**). The boundary is set when the ions outside this layer are not fully neutralised, resulting in an area of accumulated counter-ions and depleted co-ions. The further from this boundary the ions get, the closer the value gets to the ion concentration of the bulk solution. This outer layer is known as the diffuse layer, and the ions here are in rapid thermal motion (Hermansson, 1999). The diffuse layer contains a notional boundary known as the shear plane, where ions on the inner surface are a part of the stable entity, whilst those on the outer surface of the layer stay within the bulk solution, and the potential at the theoretical boundary is known as the zeta potential; **Fig 1.5B** (Wilson et al., 2001). Since no direct method exists for determining surface charge, instead measurement of the zeta potential can be used as an indirect method (Palmer et al., 2007a) and will therefore, estimate the electrical potential of bacteria.

1.5.2.3 Zeta potential

Zeta potential is defined as the electrical potential of the interfacial region between the bacterial surface and the aqueous environment (Cowan et al., 1992). Zeta potential is calculated from the mobility of the bacteria in the presence of an electrical field under a defined salt concentration and pH (Palmer et al., 2007a, Wilson et al., 2001) using electrophoretic light scattering (ELS; described further in **2.1.3**). ELS offers distinct advantages regarding accuracy of measurement and measurement time (Wilson et al., 2001) in comparison to techniques such as microelectrophoresis and electrostatic interaction chromatography. Since a large number of individual cells are examined during the course of each ELS test, zeta

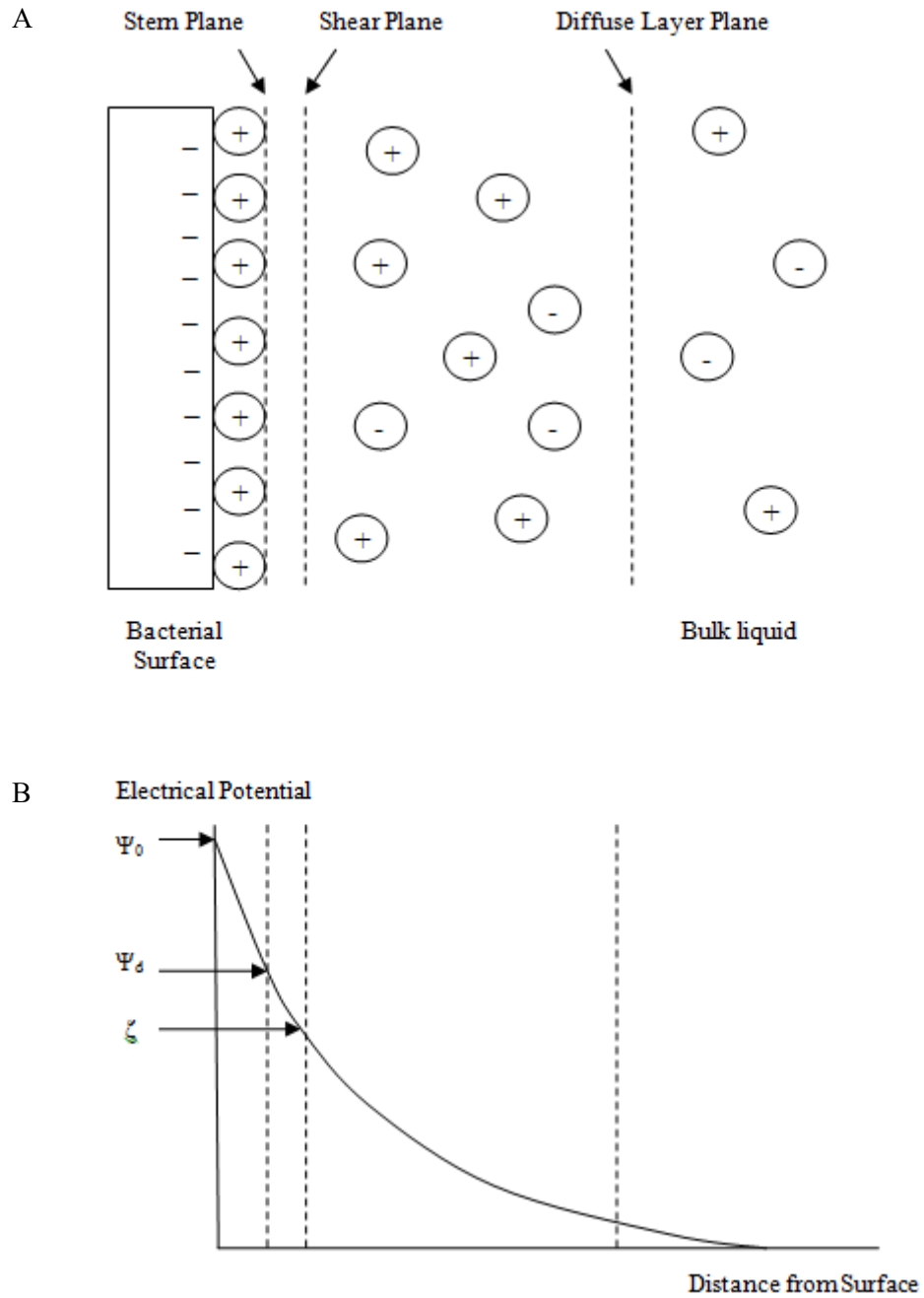


Fig 1.5: Derivation of the zeta potential of a colloid. A) The electric double layer surrounding a bacterial cell. B) Electrical potential from the bacterial surface, where Ψ_0 is the surface potential, Ψ_s is the potential at the stem plane and ζ is known as the zeta potential.

potential measurements also have the advantage of being sensitive to variation within cell populations (Cowan et al., 1992).

ELS has become an established tool for the determination of the zeta potential measurements for many types of bacteria (Bayer and Sloyer, 1990, Vandermei et al., 1988) and is often employed to “unravel” the mechanisms of bacterial adhesion and aggregation to biophysical host tissues and biomaterial substrates (Alves et al., 2010, Bowen et al., 2002, Roosjen et al., 2006, Shephard et al., 2008). Zeta potential has been extensively used in studies to detect charge on different bacteria in both planktonic and sessile (sonicated biofilm cells) states (Guiot et al., 2002). Studies on the surface charge of *P. aeruginosa* strains have previously been carried out under various growth conditions and electrolytic environments (Bruinsma et al., 2006, Horst et al., 2010). ELS has been expanded to detect physical changes in bacteria as well as being developed into a diagnostic tool to aid determination of phenotypic features (Klodzinska et al., 2010). Hence, surface charge can be used as a function of the viability and nutrient state of cells (Soni et al., 2008). More recently ELS has been used to characterise the effects of antimicrobial peptides on the surface charge of *E. coli*, in an attempt to correlate biological and biophysical data, and understand their antimicrobial activity (Alves et al., 2010).

1.6 Biofilms in human disease: cystic fibrosis

1.6.1 Cystic fibrosis

CF is a heterogeneous recessive genetic disorder. Its pathological features arise from mutations in the CF transmembrane conductance regulator (CFTR) gene affecting Cl⁻ and Na⁺ transport across all epithelial membranes. This results in a range of chronic problems which include bacterial infection of the airway/sinuses, malabsorption of fat and nutrients due to pancreatic insufficiency and infertility (Knowles and Durie, 2002).

The 2010 CF annual review reported that 95.2% of CF patients were genotyped (Bilton and Osmond, 2010) with 91.3% diagnosed with DF508 mutations (52.6% homozygous and 38.7% heterozygous). This mutation leads to disruption of the quantity of functional CFTR on the cell surface. The second most commonly occurring mutation is G551D (in 5.7% of patients), which affects the function of

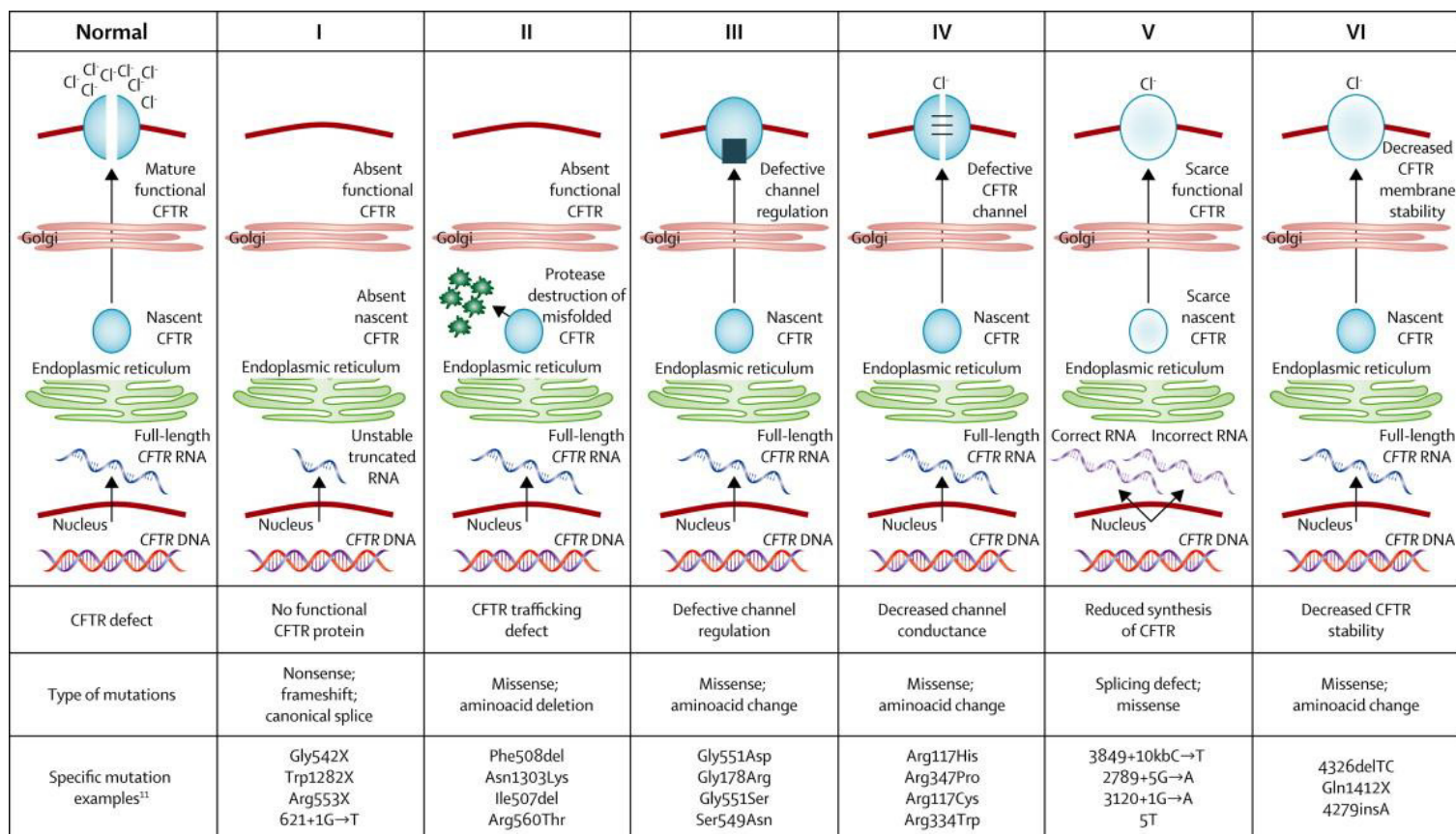


Fig 1.6: Classes of CFTR mutations: grouped into six classes based on their effect on CFTR protein production, trafficking and function or stability. Illustration courtesy of Boyle and De Boeck (2013).

CFTR with defective opening of the CFTR Cl⁻ channel (Bilton and Osmond, 2010). The six classes of CFTR mutations, with their corresponding effect on function, are described in **Fig 1.6** (Boyle and De Boeck, 2013). Screening of newborns for CF is becoming universally accepted, but there are several methods used (Vernooij-van Langen et al., 2012) and the current median age of diagnosis is 3 months; 65.5% (Bilton and Osmond, 2010).

Progressive lung disease represents a major cause of morbidity and mortality in CF patients, and leads to premature deaths in 90% of sufferers (Lambiase et al., 2006). The absent or deficient CFTR protein at the apical surface of airway epithelium leads to abnormal salt and water transport. This causes the airway surface liquid (ASL) height to be insufficient for mucociliary transport, and biochemically alters the mucus, being much thicker (Konstan, 2008). The pulmonary infections become chronic with a progressive influx of neutrophils, which remain once the acute phase has subsided. As well as the increase in numbers seen, these neutrophils do not undergo normal apoptosis. Larger eDNA volumes in sputum have been reported at a young age within asymptomatic patients (Konstan, 2008). Treatment of CF patients aims to improve quality of life by alleviating these symptoms and slowing down the decline in lung function. This is accomplished by attempts to improve airway clearance and decreasing bacterial growth and infection which leads to airway inflammation (Gibson et al., 2003). Recent figures have shown an increase in the median predicted survival rate from 34.4 years seen in 2009, to 36.6 in the 2013 Annual Cystic Fibrosis review; **Fig 1.7A** (Bilton and Osmond, 2010).

P. aeruginosa is the most common pathogen in the lower airway of CF sufferers leading to chronic infection, with periodic cycles of inflammation (Lambiase et al., 2006). The prevalence of *P. aeruginosa* increases from 54.2% at age 6-12 to 78.8% in the 18+ years (Navarro et al., 2001). The younger CF patient age group (6-10 and 11-15) has a higher incidence of *Haemophilus influenzae* and *S. aureus*. Within the second and third decade, prevalence of these bacterial species tends to decrease as the colonisation rate of *P. aeruginosa* increases; **Fig 1.7 B** (Valenza et al., 2008).

The mucoid *P. aeruginosa* strains typically found within samples from CF patients are non-favourable prognostic factors due to their excessive production of EPS and alginate which may alter the immunological response of the host (Valenza et al., 2008). The mucoid strain of *P. aeruginosa* was found in 12% of patients,

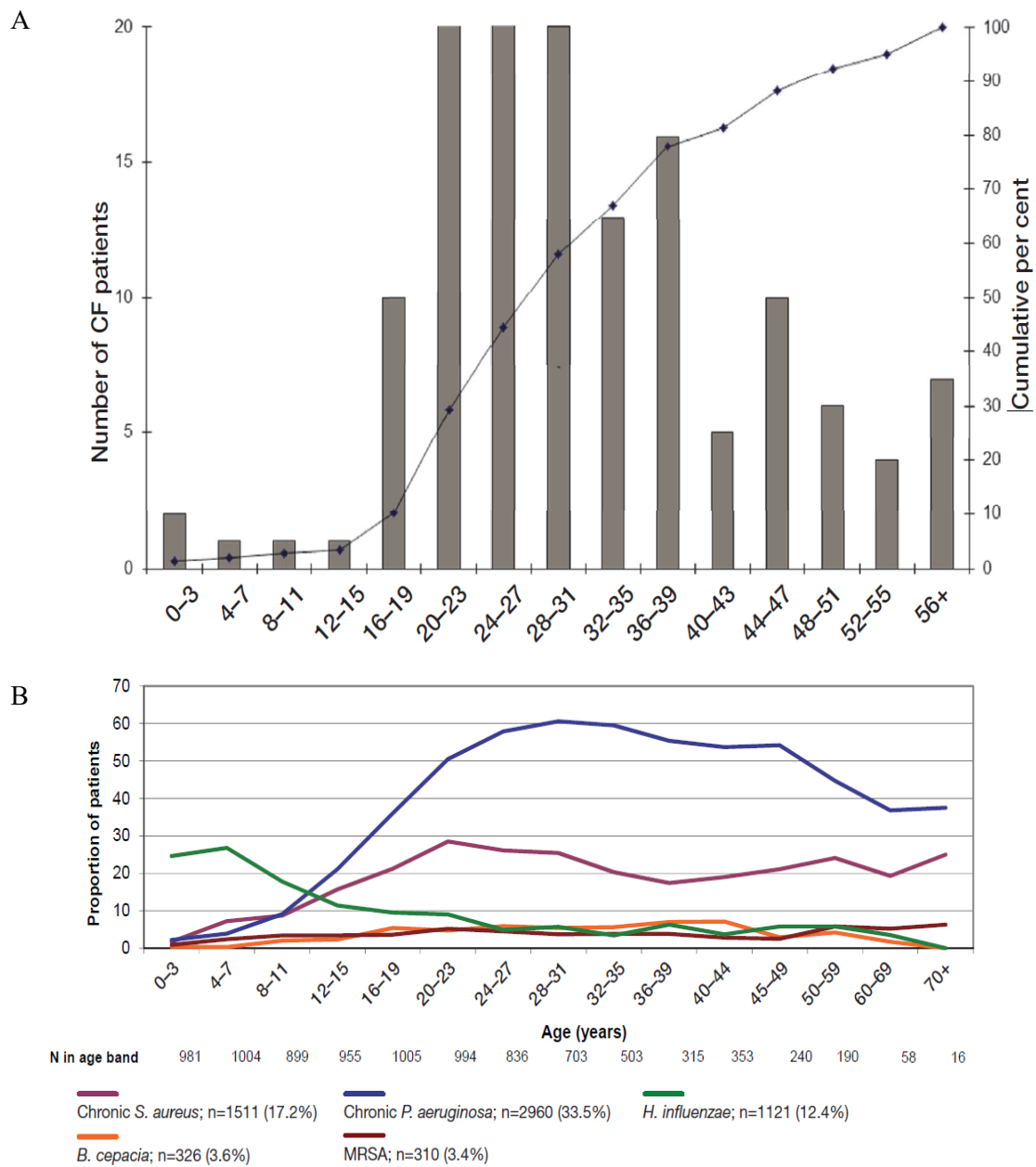


Fig 1.7: Clinical features of UK cystic fibrosis population, A) mortality B) lung infection rates. Data from the UK CF Registry. Cystic Fibrosis Trust, 2013.

being more prevalent in those over 17 years old (Paixao et al., 2010). A large proportion of patients have been found to be colonised with fungal strains. *C. albicans* (78.3%) was most prevalent in the age group 11-15, with a high incidence of *Aspergillus fumigatus* (58.3%) and *Penicillium* species (18.3%) found as well. It is not clear whether their presence in the pathogenesis of respiratory infections led to a worsening of clinical parameters (Valenza et al., 2008).

1.6.2 Cystic fibrosis lung environment

Respiratory epithelium is covered by a 5-40 μm film of liquid known as the ASL which is composed of two layers; a watery solution between the cilia, and an upper-layer of mucus which covers the tips. The depth of the ASL is similar to the length of the cilia and allows them to beat effectively below the mucus and remove foreign particles. pH has an important effect on ASL, causing changes in ion conductance, which leads to different salt and water movements (Fischer and Widdicombe, 2006). The median pH of the infected CF lung at the onset of pulmonary exacerbation (estimated using exhaled breath condensate; EBC) is 6.61 Vs 8.14 in healthy controls (Tate et al., 2002). These results were higher than those of an earlier study (Newport et al., 2009) giving EBC pH values of 5.88 in stable CF patients, 5.32 in CF patients undergoing exacerbation, 5.71 following antibiotic treatment and 6.15 in healthy controls.

Samples from older patients and those with more severe disease was more acidic which may reflect oxidative stress within the CF lung (Newport et al., 2009). The CFTR has permeability to HCO_3^- and plays a role in buffering the acidity within the lung (Fischer and Widdicombe, 2006), but in CF patients luminal HCO_3^- conductance cannot be maintained, with reduced buffering capacity during inflammation (Tate et al., 2002). An *in vivo* study found that there is no statistically significant difference between the pH of a CF patient and a non-CF patient in the nasal or lower airway (McShane et al., 2003). This suggests that the CFTR may only be a minor component of pH homeostasis of the airway surface (McShane et al., 2003).

The Cl^- concentration of the CF lung is abnormal due to the defective CFTR function (with altered trans-epithelial electrolyte and fluid transport) and secondarily

due to chronic pulmonary inflammation. The Cl^- concentration of bronchial ASL varies greatly within the literature from 140 mM up to 182 mM (Gilljam et al., 1989, Joris et al., 1993, Jayaraman et al., 2001, Song et al., 2003, Smith et al., 1996) compared to 85 mM to 132 mM in healthy controls subjects (Gilljam et al., 1989, Smith et al., 1996). Studies have reported the Cl^- concentration in CF being higher than in healthy control (Kozlova et al., 2006), whilst others report no differences (Tarran et al., 2001). A study comparing the function of polymorphonuclear neutrophils at higher Cl^- concentrations demonstrated how increased Cl^- concentration may significantly affect local immune function (Wills et al., 1997). In relation to this, it was also noted that apoptosis and cell lysis accelerated in media with a high Cl^- concentration (Tager et al., 1998). The ionic and inflammatory changes seen in the CF lung are summarised in **Fig 1.8**.

1.6.3 Cystic fibrosis sputum

Mucus is a protective semi-permeable secretion that coats several mucosal epithelia throughout the body (Xabi et al., 2014) and plays an important physiological role in epithelial homeostasis. Mucus acts as a physical barrier to pathogens and environmental particulates and maintains hydration of the respiratory epithelia (Rubin, 2007). Mucus is secreted by goblet and mucous cells of the sub-mucosal glands; it is highly adhesive and heterogeneous, and composed principally of water, ~93-95% (King and Rubin, 2002). Mucus production is increased in inflamed airways. Sputum is a collection of airway mucous mixed with bacteria and cellular debris (Henke et al., 2011) being composed of a complex assembly of glycosylated mucins, EPS, inflammatory and epithelial cells and high MW eDNA, and is poorly transported by the ciliated respiratory epithelium (Wills et al., 1997). Within sputum, eDNA, mucin and alginate are all anionic polymers (Wills et al., 1997) and inter-connect via cross-linking, non-covalent interactions e.g. electrostatic, hydrogen and hydrophobic bonding (Sanders et al., 2000).

1.6.4 Mucus clearance in the lung during health and disease

For secreted mucus to spread across the airway epithelium, a liquid-like deformation must occur alongside a low surface tension. Conversely, continuous

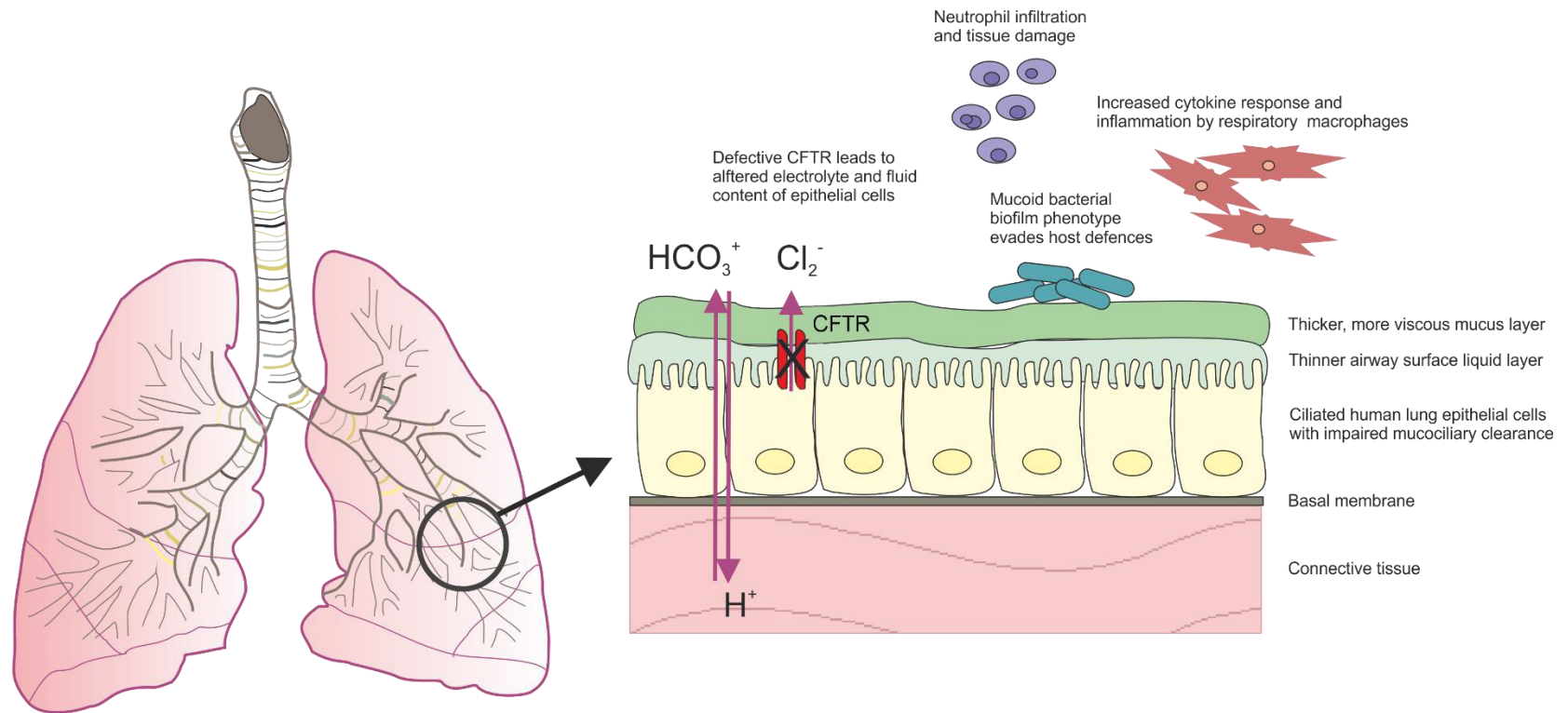


Fig 1.8: Schematic of the lung of a CF patient representing key ions across the epithelial layer, inflammatory and bacterial changes as well as its effect on the mucus layer.

propulsion by the cilia requires stored energy, which is translated into motion of the mucus sheet upon recoil thereby preventing mucus movement into the lung due to gravity (Rubin, 2007). Two main mechanisms of “clearing” the airway exist; firstly via mucociliary transport and secondly by coughing (Raff and Levitzky, 2011). Mucociliary transport removes particles trapped in the mucus lining, which is estimated to have a total surface area of 0.5 m². Cilia beat (at frequencies between 600 and 900 beats/min) facilitates continuous movement of the mucus up the airway (opposing the effects of gravity) towards the pharynx and away from the alveoli (Raff and Levitzky, 2011).

The removal of foreign matter by coughing is not an important clearance mechanism under normal physiological conditions (King, 1987), with the mucociliary mechanism being the only operative mechanism if there is no hyper-secretion (King et al., 1989). However, the mechanism of fluid clearance alters when the mucociliary system is damaged or insufficient (King et al., 1985). A cough occurs by stimulating multimodal nerve receptors within the trachea, responding to a variety of chemical mediators and mechanical stimuli (Servera et al., 2003). In CF patients, mucus hyper-secretion occurs, making the cough mechanism a significant mode of mucus clearance (King, 1987). The energy of expired air couples with the adherent mucus layer within the airway walls, and hence, transfers a portion of the stored energy as momentum. The shear-force produced leads to acceleration of the fluid layer, causing high airflow rates to carry the sputum (King, 1987).

1.6.5 Mucin overview

Mucins are high MW poly-disperse, naturally occurring biopolymer (2-2000 kDa; Rose and Voynow, 2006) glycol-conjugates with a heavily glycosylated protein core (Potapenko et al., 2010b). Human mucins are encoded by the *MUC* gene localised on chromosome 1, 3, 4, 7, 11, 12 and 19 (Rose and Voynow, 2006) and may be either secreted or membrane-bound (Potapenko et al., 2010b). In the lower respiratory tract, 12 mucin genes have been identified (*MUC1*, *MUC 2*, *MUC 4*, *MUC 5AC*, *MUC 5B*, *MUC 7*, *MUC 8*, *MUC 11*, *MUC 13*, *MUC 15*, *MUC 19*, *MUC 20*). Typically *MUC5AC* is expressed in the goblet cells and *MUC5B* in the glandular mucosal cells (Rose and Voynow, 2006). Mucins are heterogeneous, the

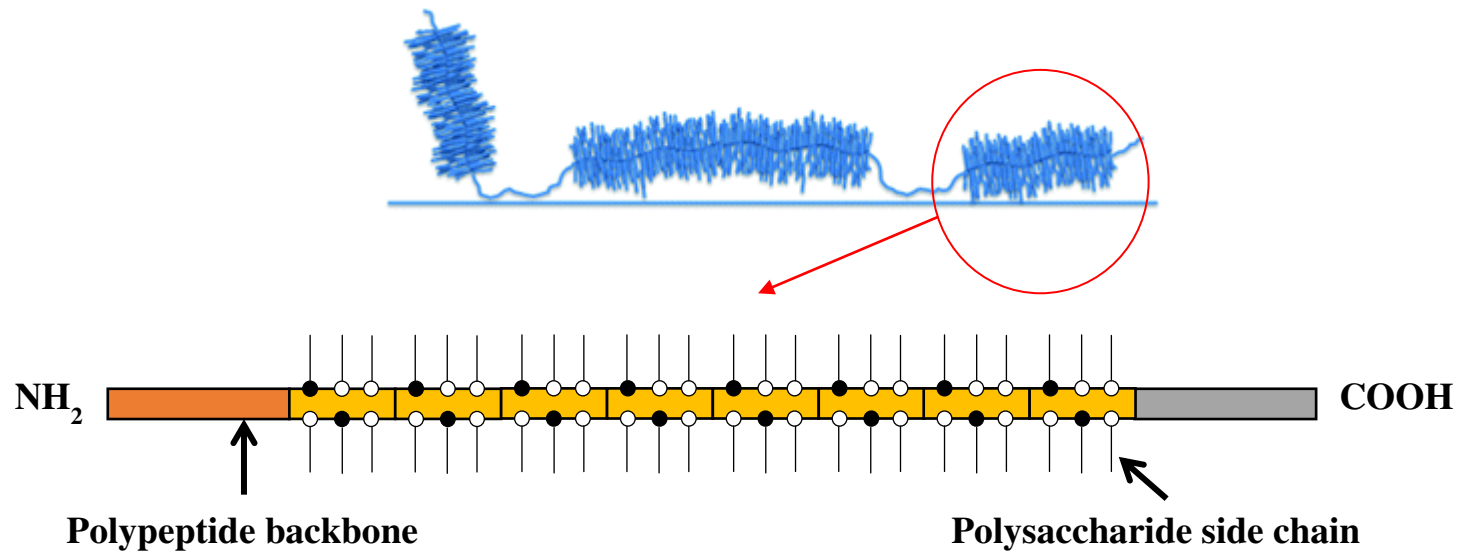


Fig 1.9: Mucin glycoprotein comprising of MUC polypeptide backbone (yellow) with NH₂-terminal domain (red) and a COOH-terminal domain (green). Several O-glycans are attached to the tandem repeat domains (threonine, black circles and serine, white circles). Image courtesy of Dedinaite (2012).

majority of the molecular mass made from oligosaccharide sugars being 70-80% per dry weight of mucin which link to hydroxylated amino acids, serine and threonine-rich proteins cores; see **Fig 1.9** (King and Rubin, 2002).

1.6.6 Mucin production in relation to *Pseudomonas aeruginosa* colonisation

P. aeruginosa is a versatile opportunistic human pathogen often presenting in a range of chronic human diseases and is the 3rd most common pathogen associated with nosocomial acquired infections (Moreau-Marquis et al., 2008). *P. aeruginosa* has a physical/genetic “pliability” that enables it to colonise and proliferate in a diverse range of habitats. *P. aeruginosa* is of particular importance in the CF biofilm as the dominant, persistent pathogen (Yang et al., 2011b), representing a formidable challenge to conventional antibiotic therapy (Høiby et al., 2010), inducing chronic inflammation and reducing lung function (Hassett et al., 2010). When a CF patient is diagnosed with *P. aeruginosa* lung infections there is a strong association with declining clinical status and worsened prognosis. The lack of successful treatment is associated with the formation of antibiotic-resistant biofilms in the lung. The anaerobic environment created by the viscous mucus layer of the CF airway also facilitates its growth. Attachment of *P. aeruginosa* to host mucin appears to be related to the acquisition of the MDR phenotype in biofilms (Moreau-Marquis et al., 2008).

Mucin interactions are important for protection of the underlying mucosa (Lamblin et al., 2001), but it has been postulated that products from *P. aeruginosa* may induce mucin MUC5AC production in human airway epithelial cells. This may be due to expression and activation of epidermal growth factor receptor (Kohri et al., 2002), which is induced by tumour necrosis factor- α (Takeyama et al., 1999). The expression of mucin genes, particularly such as *MUC5AC*, can be induced by several other internal factors such as neurogenic regulation, bacterial products and certain cytokines (Lamblin et al., 2001, King and Rubin, 2002).

1.6.7 Mucolytic therapy

In CF, agents that alter the hydrophobicity or electrostatic charge of sputum are therapeutically efficacious (Bansil et al., 1995). There are a large number of medications available to change the properties of airway secretions, collectively termed “mucoactive”. Of all the “mucoactive” agents, the mucolytics are the most commonly used (King and Rubin, 2002). The aim of mucolytic agents is to improve pulmonary function, and hence gas exchange, as well as prevent recurrent infections which lead to pulmonary damage (**Fig 1.8**). Mucolytic agents were developed to break down the structure of sputum and have been shown to affect both elastic and viscous properties (Visick and Fuqua, 2005). Rheology has shown to be a sensitive method in evaluating changes in viscoelasticity which correlates with CF sputum clearance (Dasgupta et al., 1998).

1.6.8 Developing therapies

Several other possible therapies to improve lung function have been described in the literature. Agents such as low MW dextrin have been shown to alter the viscoelasticity and improve mucociliary clearance of CF sputum (Feng et al., 1998, Feng et al., 1999), this research does not appear to have progressed to human clinical trials. More recently, nanomedicine approaches based on carbon nanoparticles have been demonstrated, *in vitro*, to disrupt the structure of mucus and sputum (Chen et al., 2012) and to facilitate drug delivery (Cartiera et al., 2010, Tang et al., 2009).

High MW alginates increase the elasticity and viscosity of mucus, but conversely the low MW alginates reduces the elasticity and viscosity of mucus (Sletmoen et al., 2012). The ability to engineer alginate oligomers of defined guluronic/mannuronic acid composition, size, or degree of polymerization (DP_n) has allowed development for distinct biological applications (Gimmestad et al., 2003). In a previous study, treatment with a prototype low MW alginate oligomer (DP_n 10) was shown to alter the rheology of mucin/alginate gels, mucin/DNA gels and sputum from a CF patient (Nordgard and Draget, 2011). *In vitro* studies have shown that low MW alginate oligosaccharides are able to displace mucin-alginate interactions, as might be expected to occur in the chronically-infected lung (Sletmoen et al., 2012).

1.7 Analysing sputum

1.7.1 Fourier transform infrared spectroscopy

Fourier transform infrared spectroscopy (FTIR) is a highly sensitive technique which can detect changes in the functional groups of molecules (e.g. tissue or cells) in a non-invasive manner (Lewis et al., 2010). FTIR is a cost-effective, high-throughput screening tool which studies the interaction between matter and radiated energy (Lewis et al., 2010). It is a sensitive analytical method to identify and measure chemical bond vibrations found in functional groups within complex biological mixtures by producing an infrared absorption spectrum, which records a “fingerprint” of a sample based on the principle that different chemical bonds absorb at different wavelengths of electromagnetic radiation (Whiteman et al., 2008). FTIR measures the intensity of the infrared beam after it has been absorbed by the sample and compares it with the intensity of the infrared beam from reference samples. The absorbance reference is then calculated by: $-\log_{10}(IS/IR)$, where IS is the intensity of the infrared beam after it has been absorbed by the sample and IR is the intensity of the infrared beam from the reference. Repeating identical tests on a sample multiple times, as well as on different days, has been found to give highly reproducible FTIR results. For biological application the spectrum of wavelengths is often taken from the mid infrared range; 4000 to 400 cm^{-1} (Lewis et al., 2010).

1.7.2 Rheological analysis of cystic fibrosis sputum

Mucus is a pseudoplastic gel and has a non-Newtonian behaviour (King and Rubin, 2002). The extent of its elasticity is determined by its capacity to store energy when the material is deformed (King, 1998). Operating alongside these elastic forces are viscous forces due to dissipation. These are proportionate to the rate, but not to the extent of deformation, and together they produce viscoelastic effects (Barnes, 2000). It has been shown that a reduction in sputum viscosity and elasticity may benefit CF patients (Shah et al., 1995). There are two basic types of flow with relative movement of adjacent particles of liquid, namely, extensional and shear flows (Barnes, 2000).

1.7.3 Extensional rheology

Extensional rheology is usually quantified as extensional viscosity, which is a function of extensional strain rate/time. In extensional rheology, the velocity gradient is in the flow direction (whereas in shear flow it is at right angles to the flow direction). Extensional rheology measures extensional stress σ_e (also called tension) and the extension rate $\dot{\epsilon}$ (elongation or stretching). The ratio of stress to rate provides a uniaxial extensional viscosity:

$$\eta_e = \sigma_e / \dot{\epsilon}$$

Liquid threads have a natural tendency to break-up due to surface tension forces. This break-up is governed by the extensional viscosity of the liquid threads under the stretching conditions. At high extensional viscosities, it opposes local thinning tendencies, as the thread is stretched (Barnes, 2000).

Alterations of the rheological properties of many complex polymeric biological fluids can lead to disease. Understanding the extensional rheology of healthy, as well as unhealthy fluids, is therefore an important aspect of developing novel treatments, therapies and potential diagnostic applications (Haward et al., 2011). Fluids of biological relevance previously studied include saliva (Zussman et al., 2007), synovial fluid (Bingoel et al., 2010) and blood (Sousa et al., 2011).

1.7.4 Shear rheology

In shear rheology, a shear stress or strain is applied to the test material and the resulting stress or strain measured (Barnes, 2000). The force placed on a sample leads to stress σ (force/area) and strain γ (which is the relative deformation). A pure elastic system stores all the energy applied during deformation. This is known as Hooke's law, where σ is the stress, G is the elastic modulus or elastic response (material constant) and γ is the strain (Nielsen et al., 2004).

$$\sigma = G\gamma$$

In an ideal Newtonian liquid, the stress is directly proportional to the shear rate. Shear rate is a time derivative of strain, and can be calculated by:

$$\sigma = \eta \dot{\gamma}$$

where η is the shear viscosity, which is independent of time and shear rate ($\dot{\gamma}$) in an ideal Newtonian liquid.

The viscoelastic properties of sputum can be measured by applying oscillatory shear strain or oscillatory shear stress deformations to the sample. Within a sinusoidal shear deformation, the stress and strain oscillates in time (Nielsen et al., 2004). This provides a repetitive sinusoidal straining motion over a certain time/cycle, at a frequency that is inversely proportional to time. The viscoelastic properties are analysed by assessing the input/output wave. The parameters measured are listed in **Table 1.1**. An ideal solid produces an output wave ‘in phase’, whilst a pure Newtonian response produces an output wave in quadrature with the input (i.e. out of phase by 90°). The elastic (solid-like) properties are assessed by measuring the *storage modulus* (G') or elastic response, whilst the viscous (liquid-like) response is given as the *loss modulus* (G'') or viscous response. Both these values will vary with the applied frequency ω (rad/s), which can be defined as $2\pi f$, f being frequency in Hz (Barnes, 2000). The complex modulus (G^*) takes into account both the elastic and viscous properties of the sputum, regardless if it is recoverable or non-recoverable (Shah et al., 1996). The ratio of viscous to elastic response (G''/G') is known as the $\tan \delta$, or *loss tangent*. This is the recoil factor of the material, and determines how mucus behaves when subjected to external forces (King, 1998). Sputum is a predominantly elastic biomaterial that exhibits an elastic response that is larger than the viscous response over a wide range of frequency (Sanders et al., 2000).

Cough clearance index (CCI) has been computed from *in vitro* relationships (King, 1987) to predict sputum clearance by cough mechanism and is based on measured rheological properties and observations of clearance from *ex vivo* animal model studies (King et al., 1997). CCI modelling has been used in several other studies using a magnetic microrheometer technique (King, 1987). The CCI measurements were performed at 1 and 100 rad/s, to analyse both the complex modulus (G^*) and loss tangent ($\tan \delta$). A material with a high $\tan \delta$ deforms permanently under stress, whilst at low $\tan \delta$, recoil after stress is removed. This method has also been employed for rheological analysis of sputum from smokers (Zayas et al., 1990).

Table 1.1: Summary of rheological parameters used.

Parameter		Definition
Elastic response	G'	Elastic component of oscillatory flow
Viscous response	G''	Viscous component of oscillatory flow
Complex modulus	G^*	Measure of materials overall resistance to deformation
Loss tangent	$G'' : G'$	Ratio of viscous response to elastic response (quantifying the extent of elasticity in a sample)
Phase angle	δ	Presence and extent of elastic behaviour in a fluid

Limitations of rheology testing need to be overcome before testing can be successfully accomplished. Since sputum acts as a colloid it is composed of two phases: the internal phase is known as the *dispersed phase*, which is within the dispersion medium known as the *continuous phase*. In a colloidal system undergoing a multi-phase system, the disperse phase may undergo a slip, which needs to be taken into account (Barnes, 2000). Static effects lead to constraints acting on the particles in the disperse phase adjacent to the walls, and steric, hydrodynamic, viscoelastic and chemical forces arise in the suspension flowing near the smooth walls. This leads to the continuous phase being present at the boundary of the smooth wall, which is usually of low viscosity. This may lead to the easier flow of the colloid near the boundary due to a lubrication effect known as “wall slip” which can introduce errors into the bulk viscoelastic measurement (Barnes, 2000). Hence, the effects of “wall slip” need to be tested and accounted for prior to rheological analysis.

1.8 Aims

The aims of this study were to investigate the role of the alginate oligomer, OligoG, in disrupting bacterial and fungal biofilms. These studies aimed to further our understanding into the mechanism by which this low MW alginate oligomer interacts with microorganisms, as well as with mucin and CF sputum.

The specific aims of this study were to:

- Analyse changes in bacterial surface charge and sizing when treated with OligoG.
- Assess the ability of OligoG to inhibit or disrupt a mucoid bacterial isolate and to study the disruption of OligoG within the biofilm.
- Investigate the interaction of OligoG with mucin and CF sputum.
- Quantify the rheological changes in CF sputum treated with OligoG.
- Characterise the interaction of OligoG with fungal pathogens.

Chapter 2:
**Nanoscale characterisation of bacterial
interactions with OligoG**

2.1 Introduction

2.1.1 Bacterial adhesion

Bacterial adhesion is influenced by properties of the bacterium, substratum, as well as the surrounding environmental conditions. For example, bacterial adhesion is known to be influenced by cell hydrophobicity, motility, release of extracellular substances (e.g. polysaccharides), proteins, bio-surfactants and surface charge (Roosjen et al., 2006). In addition, there are many substratum factors also involved in cell surface attachment including; surface conditioning, mass transport, bulk surface roughness and surface micro-topography (Palmer et al., 2007a). Initial cell attachment as a prelude to bacterial biofilm formation (described in section 1.3.3) is of vital importance as all other cells rely on these interactions between the surface and bacterial cell for their own attachment and survival.

2.1.2 Derjaguin and Landau, Verwey and Overbeek (DLVO) theory

Both ionic strength and pH are important variables to examine when considering the Derjaguin and Landau, Verwey and Overbeek (DLVO) theory (see section 1.5.2.2-1.5.2.3) for adhesion analysis of Gram-negative bacteria (Shephard et al., 2010). The charged groups on the lipopolysaccharide (LPS) of the Gram-negative cell wall can associate and dissociate under these variables, including when they approach another charged surface, be it another bacterium or a substratum (Poortinga et al., 2002). This can then drive changes in cell surface appendages, not included in the DLVO theory, e.g. fibrils, flagella or fimbriae (Hermansson, 1999).

2.1.3 Electrophoretic light scattering (ELS): zeta potential (surface charge)

The zeta potential is deduced from electrophoretic mobility measurements (U_E) from within an electric field. Since the zeta potential can be calculated from the electrophoretic mobility measurements (Poortinga et al., 2002), the model used for large particles is that of Smoluchowski. The Smoluchowski equation is derived from Henry's equation, which is:

$$U_E = \frac{2\varepsilon_o\varepsilon_r\zeta}{3\eta} f(\kappa a)$$

where ϵ_0 is the Relative Dielectric Constant, ϵ_r is the Electrical Permittivity of a Vacuum, ζ is the Zeta Potential, η is the Solution Viscosity, $f(\kappa a)$ is the Henry's function (which is the ratio of particle radius to double layer thickness), κ is the unit of reciprocal length (where $1/\kappa$ is equal to the "thickness" of the electrical double layer known as the Debye length) and 'a' is the particle radius.

The Smoluchowski approximation can be applied when particles are larger in size and dispersed within an aqueous moderate electrolyte concentration, where $f(\kappa a) = 1.5$. Therefore the Smoluchowski equation is:

$$U_E = \frac{\epsilon_0 \epsilon_r \zeta}{\eta}$$

The Smoluchowski approximation is valid for the sizes of most bacteria and viruses (Wilson et al., 2001).

2.1.4 Dynamic light scattering (DLS): cell sizing

Dynamic light scattering (DLS) is based around Brownian motion which is the random motion of particles in a solution (Malvern, 2014a). When monochromatic light hits small particles, the light scatters in all directions (Berne and Pecora, 2000, Schatzel, 1991). Light scattering from a suspension of particles undergoing Brownian motion fluctuates with time. Random fluctuations around a mean are seen over long time periods. However for shorter time scales, the particles have insufficient time to move far from their initial position and the intensity of the signals can therefore be correlated across small time spans. Distribution of diffusion coefficients can be recorded, from which particle size distribution can be calculated (Malvern, 2014a).

Refractive index differences of solutions affect light scattering (i.e. fluctuations) caused by random thermal motion, but can also be influenced by other confounding factors (Schatzel, 1991) such as viscosity and virial effects. The virial effect occurs due to attractive or repulsive electrostatic interactions between particles. Modern DLS can provide diffusion coefficient measurements for samples of high concentrations. At higher concentrations there is an increased possibility that a scattered photon will interact with another macromolecule, increasing re-scattering, (known as multiple scattering). Viscous drag can add to resistance in Brownian motion. Hence the Stokes-Einstein equation takes viscosity into account to calculate

the hydrodynamic size from the measured diffusion coefficient. Fortunately, no change in DLS distribution up to a relative concentration of about 10% has been noted (Malvern, 2014b). The new Zeta Sizer Nano takes these interactions into account during analysis.

2.1.5 Atomic force microscopy

Analysis of the microbial cell surface is recognised as being increasingly important since it separates the cell from its immediate environment. The cell wall has many functions, including providing shape to the organism, protecting the cytoplasm and its contents, supporting the internal turgor pressure of the cell, providing a molecular sieve and controlling the interactions of cell adhesion and aggregation (Ahimou et al., 2002). Atomic Force Microscopy (AFM) is an essential tool to visualise and analyse microbial systems and gives a unique insight into their behaviour and relationship with the environment (Wright et al., 2010, Dufrene, 2002). AFM also has the ability to image nanostructures and surface components on the exterior of bacterial cell surfaces (Dorobantu and Gray, 2010, Sheu et al., 2010).

Bacterial samples for AFM are routinely immobilised on to an anatomically flat surface, e.g. mica or gold (Parot et al., 2007). Mica is often chosen due to its extremely even surface, as well as its ability to be cleaved and hence allow removal of contamination. Other studies have also previously used poly-L-lysine (0.01%) as a surface coating to facilitate bacterial attachment (Hwang et al., 2012).

During imaging, it is important to be aware of possible artefacts arising on resulting images. The size and shape of an AFM probe is an important component in determining image contrast as it may lead to a broadening of surface features because of the finite size of the AFM probe in comparison to surface features. The sample can interact with the sides of the probe, leading to the resulting image being a combination of real sample topography and the probe geometry (Dufrene, 2002).

2.1.6 Lipopolysaccharide

Gram-negative bacteria have charged surface LPS molecules which may be influenced by ionic strength, and in turn may affect cell surface charge properties and hydrophobicity. *P. aeruginosa* has the ability to alter the function of its LPS in

conjunction with environmental changes, as described in section **1.3.1** (Shephard et al., 2010). *P. aeruginosa* has an extremely diverse physical/genetic variability which enables it to colonise and proliferate in a diverse range of habitats and is an important opportunistic human pathogen in a range of chronic human disease. These studies have focused on *P. aeruginosa* which is of particular importance in cystic fibrosis (CF) where it represents the dominant, persistent pathogen (Yang et al., 2011b).

2.2 Aims

The hypothesis of this study was that OligoG interacts with the cell surface of planktonic bacteria to disrupt bacterial attachment and subsequent biofilm formation. Interactions between OligoG and planktonic bacteria were investigated at the nanoscale level.

The specific aims of these studies were:

- To quantify changes in bacterial cell surface charge and size induced by OligoG using zeta potential (using ELS) and sizing analysis (using DLS).
- To study the resistance of the interactions of OligoG and the bacterial surface to hydrodynamic shear.
- To study the interaction between OligoG and the surface structure of *P. aeruginosa* using AFM.
- To quantify any interactions between OligoG and LPS using zeta potential analysis through ELS and sizing analysis through DLS respectively.

2.3 Materials and Methods

2.3.1 Electrophoretic and dynamic light scattering buffer (zeta potential and cell sizing measurements)

CF patients have a deficiency in their CF transmembrane conductance regulator gene (CFTR) which is important for channelling chloride ions across cell membranes. Both ELS and DLS measurements of *P. aeruginosa* were, therefore, performed at three ionic strengths (0.1 M, 0.01 M and 0.001 M NaCl). The buffer pH (5-9) was also varied to correspond to the range of pHs observed within the CF lung (Fischer and Widdicombe, 2006).

2.3.2 Electrophoretic and dynamic light scattering sample preparation (zeta potential and cell sizing measurements)

2.3.2.1 Alginates

Zeta potential (ELS) and sizing analyses (DLS) were performed using two alginates, OligoG (CF-5/20) and Protanal[®] (LF-10/60). Protanal[®] has a high MW (100 kDa) with a higher M:G ratio (%G: 65-67%) compared to OligoG (%G: 90-95%; 2600 Da; 5-20 repeating monomers). Protanal[®] (10% w/v) and OligoG (10% w/v) were dissolved in each electrolytic solution (0.1 M, 0.01 M and 0.001 M NaCl at pH 5, 7 and 9) prior to loading 1 ml into the folded capillary cell for analysis. For accurate analysis of planned hydrodynamic shear experiments, ELS and DLS measurements of centrifuged OligoG was required, therefore, 10% OligoG (w/v) was also dissolved in buffer and centrifuged for 3 mins at 5,500 g for analysis.

2.3.2.2 *Pseudomonas aeruginosa* treated with OligoG

Cells were prepared for ELS and DLS as previously described by Klodzinska et al. (2010). Briefly, single colonies of *P. aeruginosa* (PAO1) were inoculated into sterile Mueller-Hinton (MH) broth (Oxoid; Basingstoke, Hampshire), incubated at 37°C O/N, (shaking at 60 rpm) and 1 ml of the medium was centrifuged at 5,500 g for 3 mins. The supernatant was removed and the pellet washed (x2) in 1 ml of dH₂O and the pellet re-suspended in 100 µl of appropriate buffer. A cell concentration of 20% (v/v) was used as well as additional tests carried out using 2% (v/v) *P. aeruginosa* (PAO1) in 0.01 M NaCl, at pH 5 with appropriate controls. Initial experiments showed that the use of high salt concentrations (>0.1 M NaCl) corroded the electrodes of the folded capillary cell (DTS1061 Malvern Instruments), with subsequent large increases in the variability of results (see **Appendix I**) so this buffer was not used further.

For the *P. aeruginosa* (PAO1)-only control, 20 µl of the bacterial stock suspension in 100 µl of test buffer was re-suspended in 1 ml of test buffer defined prior to being left to stand for 20 mins. It was then centrifuged (2,500 g; 6 mins), the supernatant was removed and cells re-suspended in 1 ml of buffer. The sample was loaded into the folded capillary cell, using a syringe for ELS and DLS analysis.

For the OligoG-treated *P. aeruginosa* (PAO1) samples, 20 µl of the bacterial suspension in 100 µl of test buffer were re-suspended in 1 ml of buffer containing OligoG (0.2, 2 and 10%) and left to stand for 20 mins. Samples were then centrifuged (2,500 g; 6 mins), the supernatant removed, and then re-suspended in 1 ml of test buffer. Analysis of the effect of OligoG involved use of both OligoG-treated cell samples and supernatants using ELS and DLS analysis.

2.3.3 Atomic force microscopy sample preparation

Preparation for AFM imaging of *P. aeruginosa* (PAO1) followed the protocol described in section 2.3.2.2, but the buffer was replaced with dH₂O to prevent crystal formation which could damage the AFM tip. Five 7 µl samples were placed onto 0.01% poly-L-lysine coated mica plates (Agar Scientific) and allowed to air-dry for 40 mins in a sterile hood.

Streptococcus mutans DSM 20523 (ATCC 25175) was grown in Tryptone Soy Broth (TSB; LabM, Heywood, Lancashire) and incubated in a CO₂ cabinet for 72 h. *Porphyromonas gingivalis* NCTC 11834 (ATCC 33277) was grown in Fastidious anaerobe broth (FAB) in an anaerobic cabinet for 48 h. Both bacteria were then washed as described for *P. aeruginosa* (PAO1) in section 2.3.2.2.

The optimal concentration for OligoG imaging varied for the bacterial strains used. Treated samples were, therefore, re-suspended in OligoG (0.2 and 0.5% w/v for *P. aeruginosa* (PAO1); 0.5 and 0.7% w/v for *S. mutans* and 0.1 and 0.3% w/v for *P. gingivalis*).

2.3.4 Electrophoretic light scattering (zeta potential measurements)

A Zetasizer Nano ZS (Malvern Instruments) with disposable capillary cells (DTS1061 Malvern Instruments) was used for zeta potential analysis (ELS). The zeta potential of *P. aeruginosa* (PAO1) was calculated by applying the Smoluchowski model (Wilson et al., 2001). Prior to each experiment, the folded capillary cell was thoroughly cleaned by washing with 70% ethanol (v/v), followed by a thorough rinse protocol in dH₂O. Then, 1 ml of the sample was loaded into the cell, ensuring no air bubbles were incorporated. Ten measurements were taken for each test condition and the mean and standard deviations calculated.

2.3.5 Dynamic light scattering (cell sizing measurements)

Tests for size (DLS) were performed on *P. aeruginosa* (PAO1) cells to detect any possible changes in size in the presence of OligoG. The refractive index value and absorption options on the software were selected (1.39 and 0.001 respectively). A previous study had reported bacteria having a similar refractive index at 1.42 (Foladori et al., 2008). The temperature used was 25°C for all experiments as for previous studies on *P. aeruginosa* (Bruinsma et al., 2001, Nagant et al., 2011) with an equilibrium time of 2 mins to allow stabilisation of the test vessel between runs. Ten measurements were taken for each test condition; and the mean and standard deviations calculated.

2.3.6 Atomic force microscopy

AFM was carried out on *P. aeruginosa* (PAO1), *S. mutans* and *P. gingivalis* cells to detect any possible changes in cell morphology in the presence of OligoG. A Dimension 3100 AFM (Bruker) was used to achieve AFM images in an air environment. The experiment was carried out under tapping mode operation (Soon et al., 2009) with OTESPA tips (Bruker). The images were collected at a frequency of 0.8 Hz and image resolutions of 1024 x 1024. A 10 μm^2 area was initially scanned, followed by more detailed imaging over a 5 μm^2 area.

2.3.7 Hydrodynamic shear

To analyse the strength of any bacterial-OligoG interactions, test samples were exposed to hydrodynamic shear. For this, *P. aeruginosa* (PAO1) cultures were grown O/N in MH broth \pm 10% OligoG (24 h, shaking 60 rpm, 37°C). Triplicate 1 ml samples were taken from the O/N culture. The first sample was analysed with no wash step. The second sample was centrifuged at 5,500 g; 3 mins, and re-suspended in buffer prior to analysis. The third sample underwent 2 wash steps by centrifugation at (5,500 g; 3 mins) and the pellet was re-suspended in 1 ml buffer (0.01 M NaCl, pH 5) prior to ELS and DLS analysis.

To determine the effect of hydrodynamic shear, AFM imaging was carried out following each wash stage. For this, a sample was dried onto 0.01% poly-L-lysine coated mica plates (Agar Scientific) as previously described.

2.3.8 Lipopolysaccharide

Due to anomalies of the results with the buffer at 0.1 M NaCl, the closest clinically relevant buffer solution of 0.01 M NaCl, pH 5 was chosen for analysis of the interactions between OligoG and LPS. The LPS used (source strain ATCC 27316, Sigma L 9143) was from *P. aeruginosa* serotype 10 (Muraschi et al., 1966). Initial experiments were carried out at 1% LPS (w/v) \pm 2% OligoG (w/v). LPS and OligoG were mixed and placed in a water bath at 37°C for 4 h before ELS and DLS analysis on the Zetasizer nano ZS (Malvern instruments) following the same parameters described in sections 2.3.4 and 2.3.5. Following this experiment, the concentration of OligoG was lowered to 0.2% due excess OligoG interference with the results, whilst maintaining LPS at 1%. This was also incubated for 4 h prior to ELS and DLS analysis.

2.3.9 Statistical analysis

Graph Pad Prism[®] was used for statistical analysis. Group wise comparisons were analysed by the nonparametric Kruskal-Wallis one-way analysis of variance followed by the Mann-Whitney test. To account for multiple testing, the Bonferroni-Holm correction was applied to adjust P values.

2.4 Results

2.4.1 Alginate oligosaccharides Protanal[®] and OligoG

Overall, OligoG was found to have a wide distribution of charge at the applied salt concentration, which slightly extended into being positive (**Fig 2.1**). The mean zeta potential of the OligoG control was negative in value and did not differ greatly across all the salt concentrations used (0.01 M and 0.001 M NaCl) nor for the different pHs (5, 7 and 9) tested, with the peak values ranging between -18.6 mV \pm 1.2 to -22.4 mV \pm 1.0 (**Table 2.1**). Sizing measurements for OligoG were also similar across all buffer solutions ranging between 1.32 nm \pm 0.29 in 0.01 M NaCl; pH 9 and 1.62 nm \pm 0.33 in 0.001 M NaCl; pH 5 (**Table 2.1**).

The effect of a wash step on the OligoG control (in 0.01 M NaCl, pH 5) showed little difference between the pre- and post-spin samples for both zeta

potential analysis ($-17.60 \text{ mV} \pm 1.55$ and $-18.64 \text{ mV} \pm 1.15$ respectively; **Fig 2.2A**) and sizing experiments ($1.40 \text{ nm} \pm 0.31$ and $1.57 \text{ nm} \pm 0.38$ respectively; **Fig 2.2B**) and no pellet was obtained from the suspension.

Due to the highly viscous nature of 10% Protanal[®] (w/v), it was not possible to carry out zeta potential measurements at this concentration, so all subsequent experiments were carried out at 2% Protanal[®] instead, whilst maintaining the concentration of OligoG at 10%. Protanal[®] was found to be far more negatively-charged than OligoG in all the buffer combinations tested (**Fig 2.3**). Changes in pH had little effect on zeta potential values for either alginate; however Protanal[®] demonstrated a wider range of zeta potential values than OligoG at the different salt concentrations used. There was an observable greater negative-charge with decreasing NaCl concentration at all pH values for Protanal[®], a trend not consistently shown by OligoG (**Fig 2.3**). Sizing was very uniform and constant for OligoG whilst Protanal[®] showed single, double or triple peaks forming at all pHs tested. Protanal[®] showed a wider base of the peaks and resulted in a large amount of clumping (**Fig 2.4**).

2.4.2 *Pseudomonas aeruginosa* control

The zeta potential values obtained for the *P. aeruginosa* (PAO1) control did not appear to be affected by pH, not varying greatly between pH values of 5, 7 and 9 ($-30.9 \text{ mV} \pm 0.80$ to $-30.0 \text{ mV} \pm 0.97$, at 0.01 M NaCl; **Fig 2.5A**). Distinct differences were seen in both salt buffers tested, with a more negative-charge observed with a decrease in NaCl concentration. A uni-modal peak was seen for *P. aeruginosa* (PAO1) alone at all buffer concentrations (**Fig 2.5B**). The mean size of *P. aeruginosa* (PAO1) cells was $914 \text{ nm} \pm 284$ in 0.01 M NaCl, pH 5 (**Fig 2.5C**).

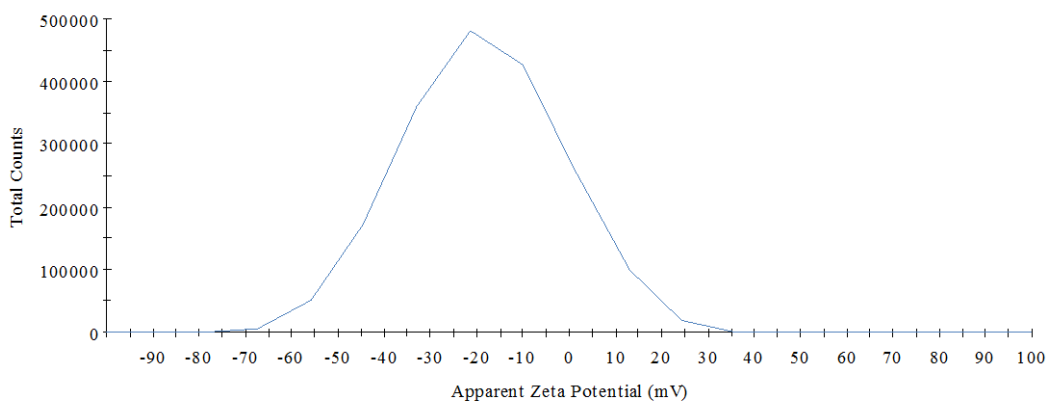


Fig 2.1: Typical zeta potential distributions for 10% OligoG control in 0.01 M NaCl, pH 5.

Table 2.1: Zeta potential (mV) and sizing (nm) analysis of the 10% OligoG control in a range of buffer solutions (n=10 \pm standard deviation).

Buffers	Mean Zeta potential (mV)	Mean Sizing (nm)
0.01 M NaCl, pH 5	-18.6 \pm 1.2	1.58 \pm 0.44
0.01 M NaCl, pH 7	-22.0 \pm 1.5	1.50 \pm 0.37
0.01 M NaCl, pH 9	-20.0 \pm 1.7	1.32 \pm 0.29
0.001 M NaCl, pH 5	-22.4 \pm 1.0	1.62 \pm 0.33
0.001 M NaCl, pH 7	-21.2 \pm 0.9	1.49 \pm 0.32
0.001 M NaCl, pH 9	-21.6 \pm 0.9	1.51 \pm 0.35

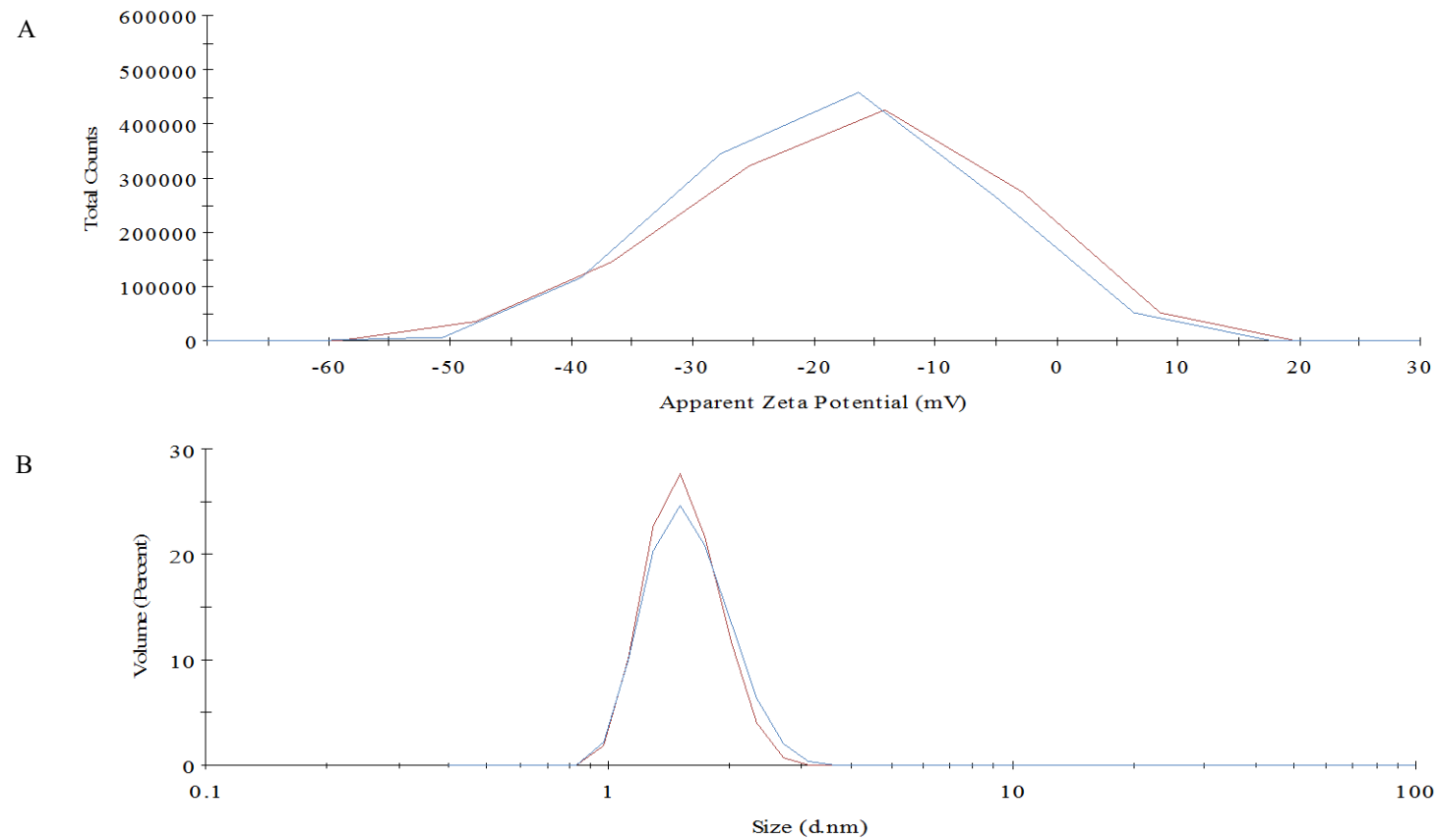


Fig 2.2: Effect of a wash step, pre-spin sample (blue solid line) and post-spin sample (red solid line) on A) Zeta potential analysis (mV) and B) Sizing measurement (nm) distribution of OligoG control in 0.01 M NaCl, pH 5 buffer.

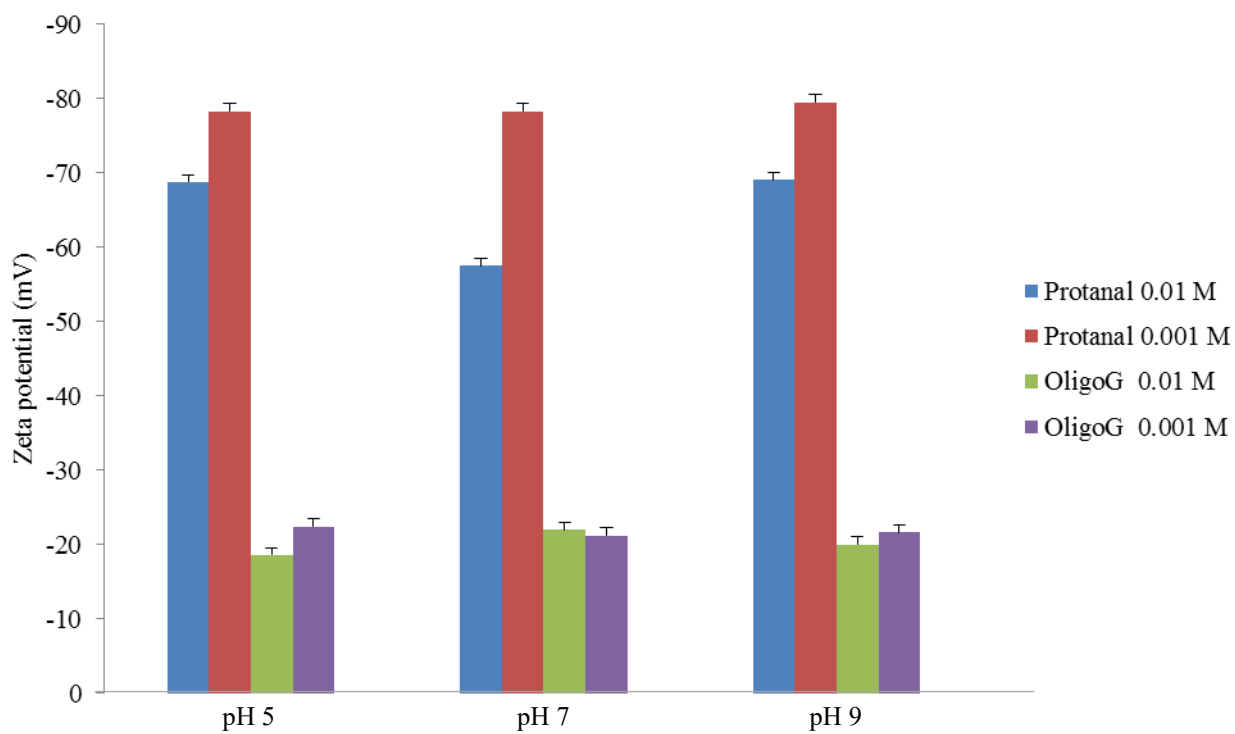


Fig 2.3: Zeta potential (mV) measurements of Protanal[®] (2%) and OligoG (10%) in 0.01 M and 0.001 M NaCl, pH 5, 7 and 9. Mean value (n=10) \pm standard deviation.

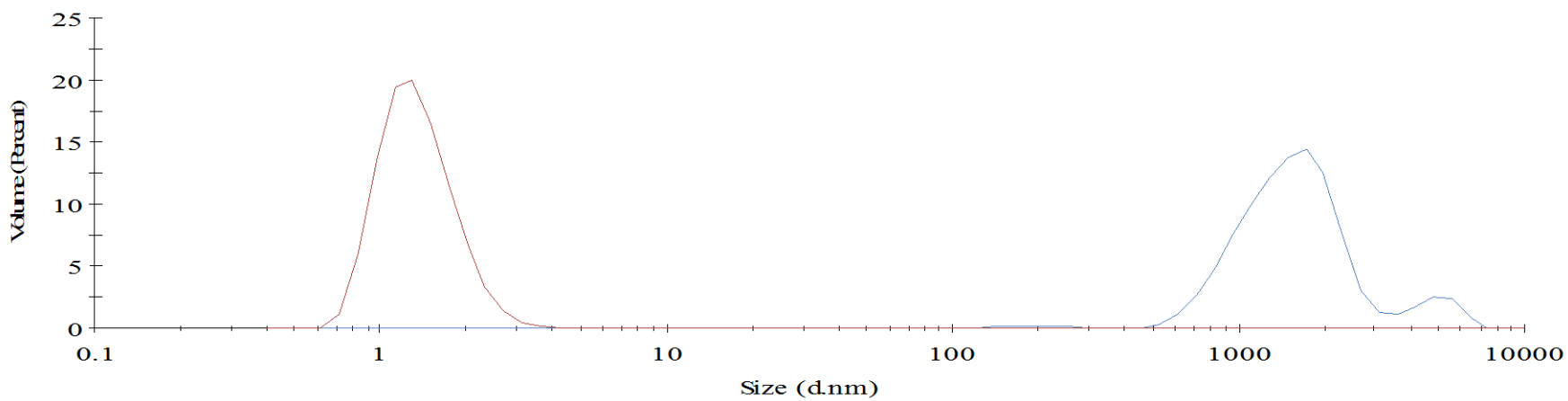


Fig 2.4: A typical sizing distribution (nm) A) OligoG 10% (red solid line) and B) Protanal[®] 2% (blue solid line) in 0.01 M NaCl, pH 5 buffer.

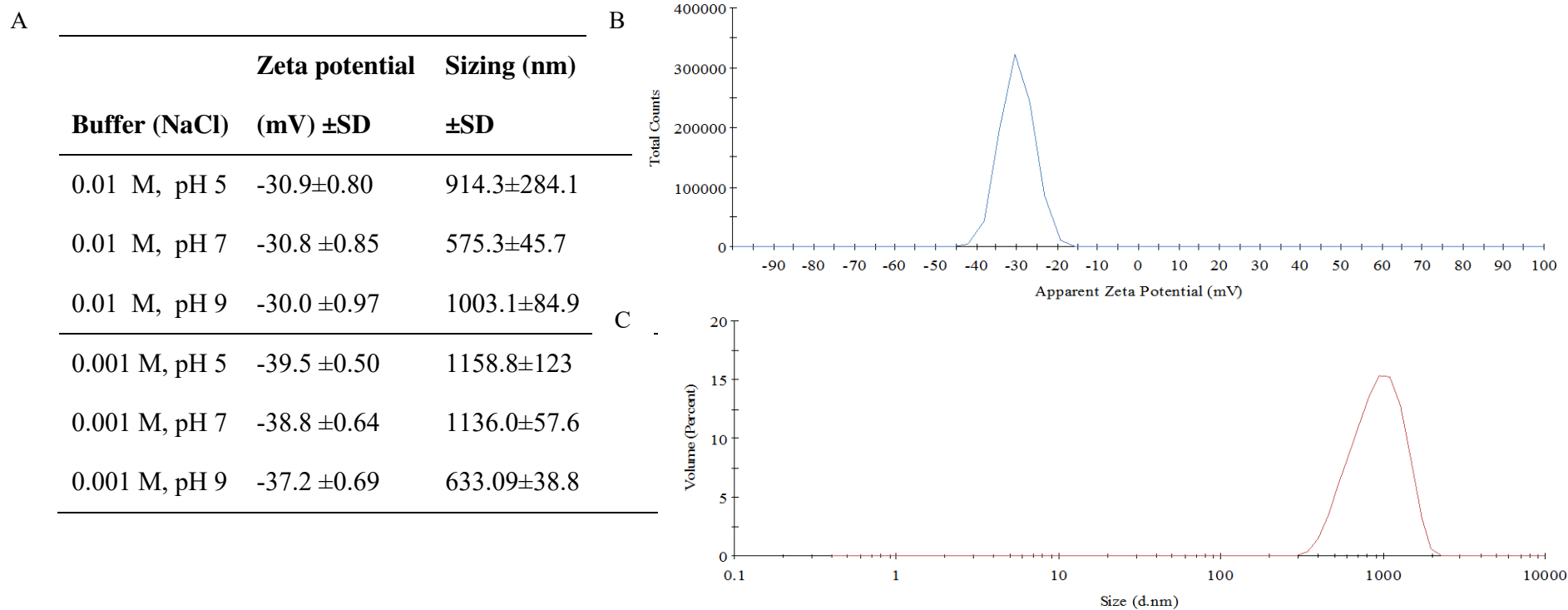


Fig 2.5: *P. aeruginosa* (PAO1) only control. A) Zeta potential and sizing analysis at a range of buffer concentrations, B) Zeta potential (mV) distribution in 0.01 M NaCl, pH 5 buffer (n=10) and C) Sizing measurements (nm) in 0.01 M NaCl, pH 5 buffer.

2.4.3 *Pseudomonas aeruginosa* and OligoG

As already stated above, the *P. aeruginosa* (PAO1) control produced a unimodal zeta potential peak in buffer 0.01 M NaCl, pH 5 (**Fig 2.6A**). When *P. aeruginosa* (PAO1) was combined with OligoG (after 20 min), zeta potential measurements using ELS were initially masked by the excess of OligoG in the solution as noted by the wide bell-shaped curve obtained (-75 mV to +48 mV; **Fig 2.6A**). After the washing step it became evident that OligoG treatment induced a significant alteration in the surface charge (zeta potential) of the bacteria. OligoG treatment increased the overall mean negative bacterial surface charge from -30.9 mV \pm 0.8 to -47.0 mV \pm 2.3 in 0.01 M NaCl, pH 5 buffer. This change was evident at all pH values used (pH 5–9; $P < 0.001$) and at salt concentrations of 0.001 M and 0.01 M NaCl. In the case of *P. aeruginosa* (PAO1) cells that had been treated with OligoG and then washed, a secondary and more negative peak occurred (**Fig 2.6A**), (-57.8 mV \pm 2.7; 0.01 M NaCl, pH 5). Although the mean zeta potential became more negative (**Fig 2.6B** and **2.6C** respectively), when analysing the individual peaks it became evident that this effect occurred due to a secondary more negative peak forming at both 0.01 M and 0.001 M NaCl.

To further analyse these findings, sizing measurements (DLS) were carried out using the same buffers. *P. aeruginosa* (PAO1) was found to be much larger in size than OligoG and showed a greater variability in size between pHs (**Fig 2.5A** and **Table 2.1** respectively). For example, in 0.001 M NaCl buffer at pH 9, the values were lower at 632.89 nm compared to 1191.30 nm at pH 5. Interestingly at 0.01 M NaCl, the size was lowest and considerably smaller at neutral pH (pH 7) compared to pH 5 and 9; this effect was not evident in 0.001M NaCl. When *P. aeruginosa* (PAO1) was tested in combination with OligoG, it was evident that aggregation had occurred, which was maintained even after washing. Sizing analysis using DLS showed a 2-3 fold increase in the measured size for 10% OligoG-treated cells pre-wash (e.g. 914 nm \pm 284 to 2599 nm \pm 472; in 0.01 M NaCl, pH 5; **Fig 2.7A**) at all pH values (pH 5-9; $P < 0.001$) and at salt concentrations of 0.001 M and 0.01 M NaCl (**Fig 2.7B** and **2.7C** respectively).

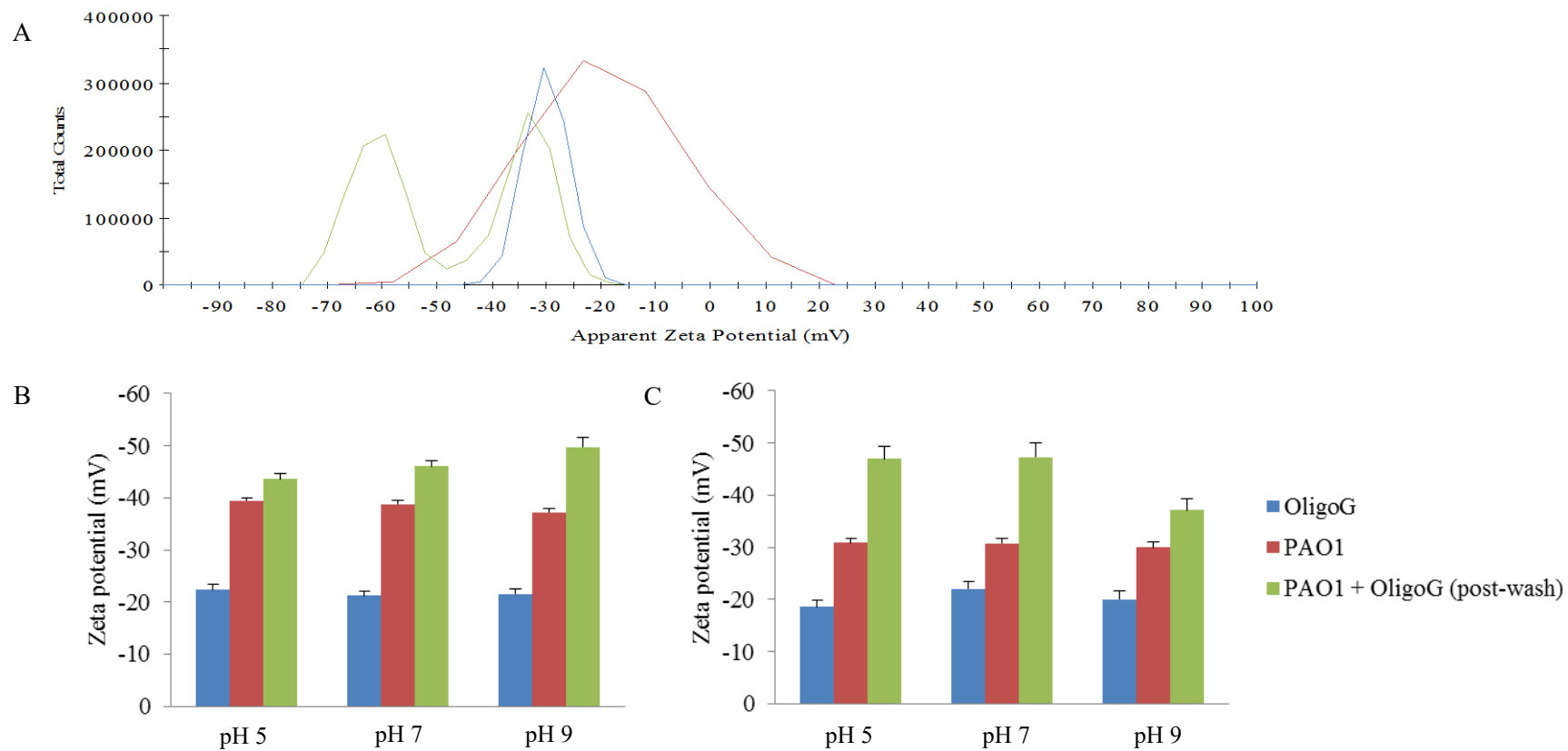


Fig 2.6: A) Untreated *P. aeruginosa* (PAO1) cells only (blue solid line); *P. aeruginosa* (PAO1) treated with 10% OligoG (pre-wash; red solid line) and *P. aeruginosa* (PAO1) treated with 10% OligoG (post-wash; green solid line) in 0.01 M NaCl, pH 5 buffer. B) Zeta potential peaks at pH 5-9 in 0.01 M NaCl. C) Zeta potential peaks in pH 5-9 at 0.001 M NaCl.

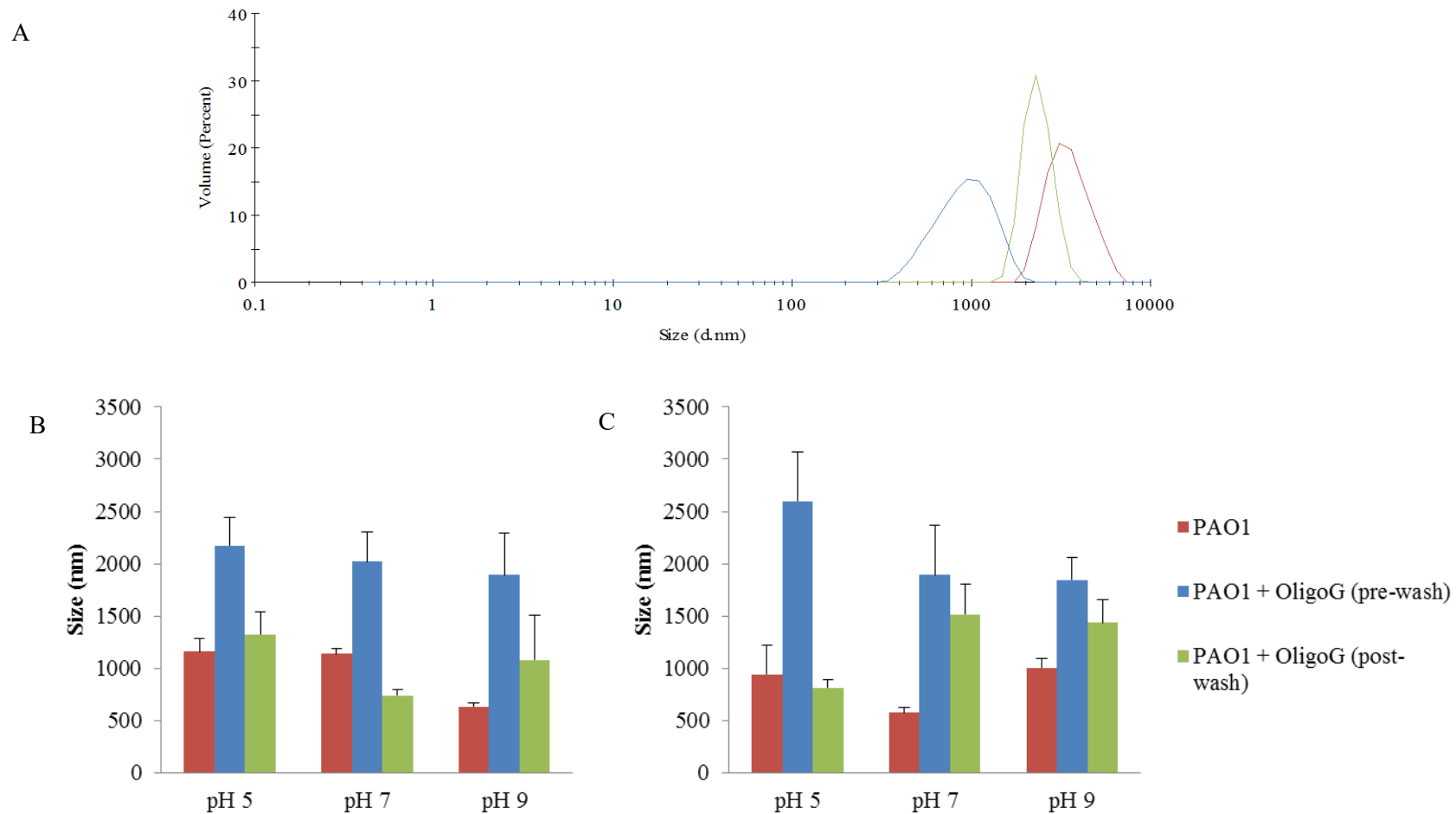


Fig 2.7: Sizing analysis of A) Untreated *P. aeruginosa* (PAO1) control cells (blue solid line); *P. aeruginosa* (PAO1) treated with 10% OligoG, pre-wash (red solid line); *P. aeruginosa* (PAO1) treated with 10% OligoG, post-wash (green solid line) in 0.01 M NaCl, pH 5 buffer. Sizing values for untreated *P. aeruginosa* (PAO1) control cells (red), pre- (blue) and post- (green) wash at B) 0.001 M NaCl and C) 0.01 M NaCl at pH 5-9.

2.4.4 Concentration effects of *Pseudomonas aeruginosa*

Using *P. aeruginosa* (PAO1) at a lower concentration (2% instead of 20% v/v) resulted in zeta potential measurements for *P. aeruginosa* (PAO1) which were maintained at both buffer concentrations (-30.0 mV \pm 0.77 Vs -30.9 mV \pm 0.80 respectively). When combined with OligoG, a secondary, more negative peak was formed, showing the interaction of OligoG with the surface of the *P. aeruginosa* (PAO1) cells, which was maintained over both *P. aeruginosa* (PAO1) concentrations tested ($P < 0.05$). **Fig 2.8A** shows the uni-modal peak produced by 2% (v/v) *P. aeruginosa* (PAO1) and how this became more negative after OligoG treatment in 0.01 M NaCl, at pH 5. It had been previously shown that *P. aeruginosa* (PAO1) sizing was affected by OligoG treatment (**Fig 2.7**) and the use of the lower *P. aeruginosa* (PAO1) concentration again showed that aggregation of the cells had occurred, as seen by the increase in peak size and the wider base of the peak (**Fig 2.8B**). The initial sizing of *P. aeruginosa* (PAO1) (2%) was 598.7 nm \pm 97, with an increase to 1761.0 nm \pm 469 when treated with OligoG ($P = 0.0015$).

2.4.5 Concentration effects of OligoG

Zeta potential and sizing analyses was used to examine the effect of reduced, more clinically-relevant, concentrations of OligoG (0.2% and 2%) on *P. aeruginosa* (PAO1) cells. OligoG treatment resulted in an increase in the overall negative bacterial surface charge (**Fig 2.9A**) in both 0.2% and 2% OligoG (**Fig 2.9B**; $P < 0.001$). The effects of 0.2% and 2% OligoG treatment on size were less marked (**Fig 2.10**). The wider base distribution indicates possible aggregation of *P. aeruginosa* (PAO1) with 0.2% OligoG post-wash.

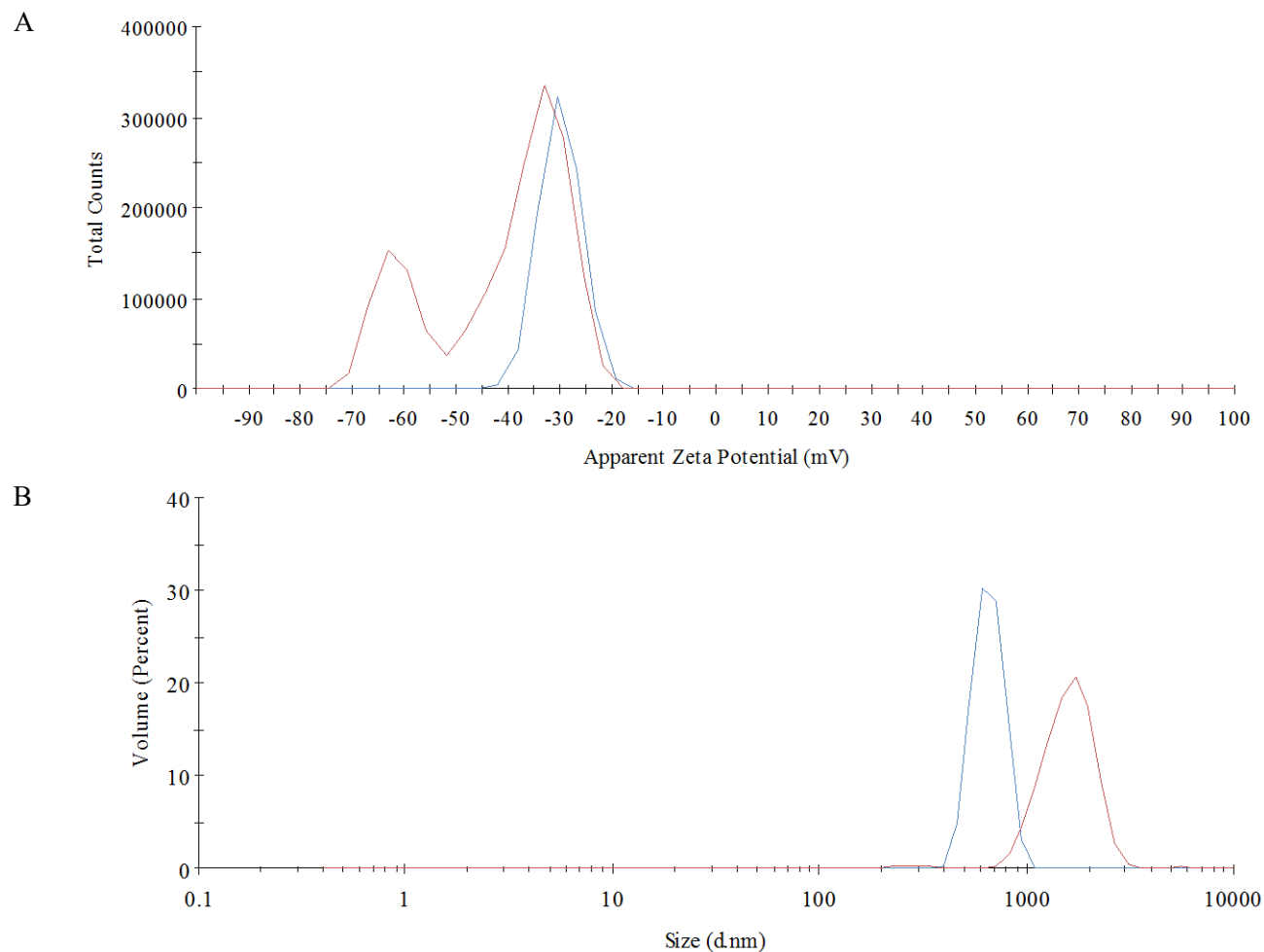
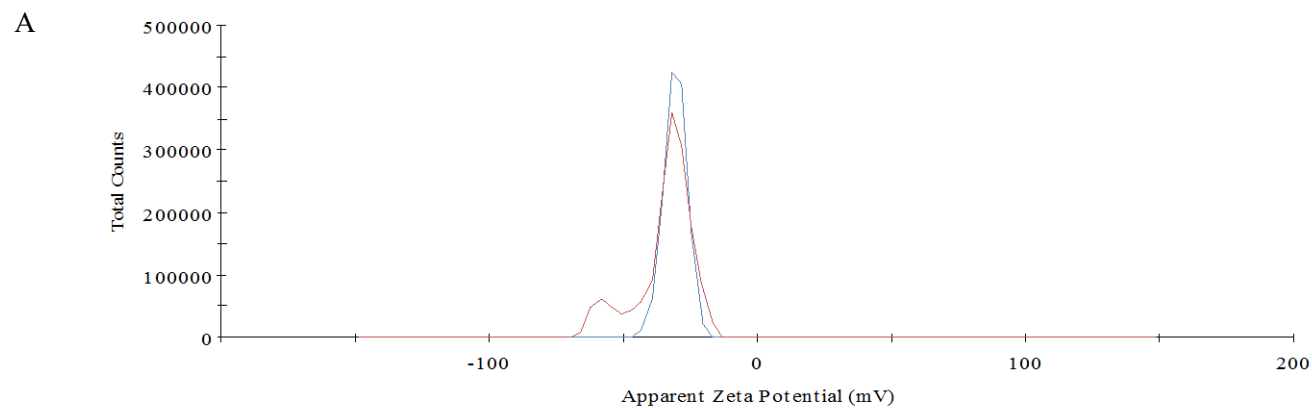


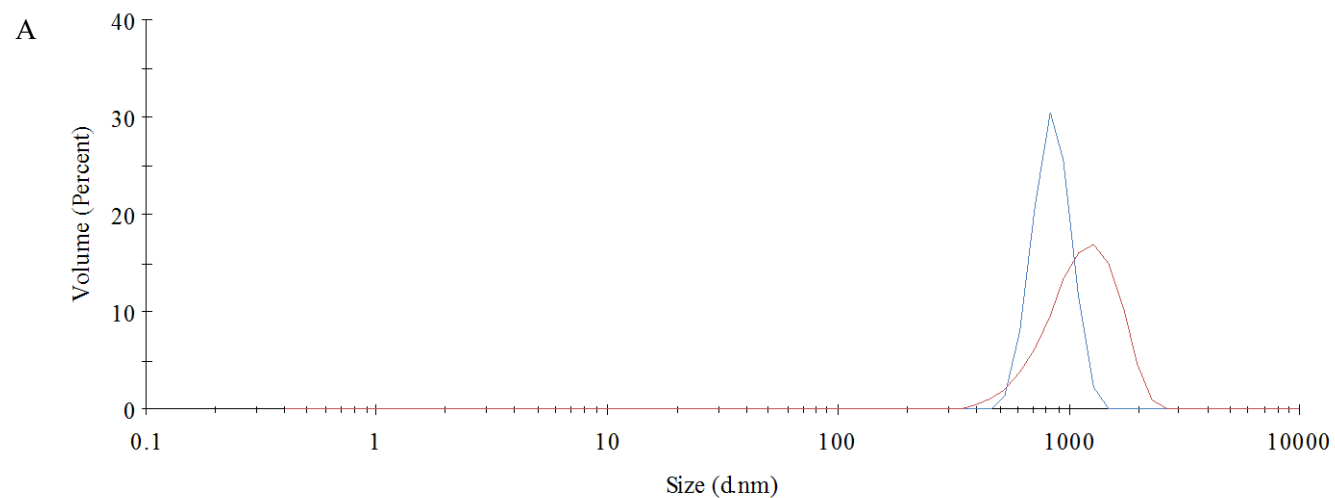
Fig 2.8: A) Zeta potential analysis (mV) and B) Size distribution analysis (nm) of untreated *P. aeruginosa* (PAO1) (2% v/v) cells alone (blue solid line) and *P. aeruginosa* (PAO1) (2% v/v) treated with 10% OligoG (red solid line). Both sets of data analysed in 0.01 M NaCl, pH 5.



B

	Mean Zeta Potential (mV)		
	<i>P. aeruginosa</i> (PAO1)	<i>P. aeruginosa</i> (PAO1) & OligoG (pre-wash)	<i>P. aeruginosa</i> (PAO1) & OligoG (post-wash)
0.2% OligoG	-31.5 ±0.6	-36.0 ±0.9	-34.4 ±0.6
2% OligoG	-30.9 ±0.8	*	-33.3 ±0.9

Fig 2.9: Typical zeta potential distributions in 0.01 M NaCl, pH 5 of A) Untreated *P. aeruginosa* (PAO1) cells only (blue solid line); *P. aeruginosa* (PAO1) treated with 0.2% OligoG (post-wash; red solid line) and B) Mean zeta potential values (mV) of *P. aeruginosa* (PAO1) after OligoG (0.2% and 2%) treatment (2%; P<0.001). *Not determined as OligoG masked this measurement.



B

	Mean Sizing (nm)		
	<i>P. aeruginosa</i> (PAO1)	<i>P. aeruginosa</i> (PAO1) + OligoG (pre-wash)	<i>P. aeruginosa</i> (PAO1) + OligoG (post-wash)
0.2% OligoG	837.0 ±74.8	872.9 ±61.3	1131.9 ±137.5
2% OligoG	900.1 ±49.4	970.9 ±96.3	905.9 ±71.6

Fig 2.10: A) Typical size distribution by volume in 0.01 M NaCl, at pH 5 of *P. aeruginosa* (PAO1) (blue solid line); *P. aeruginosa* (PAO1) treated with 0.2% OligoG (post-wash; red solid line) and B) Corresponding mean sizing values (nm) for *P.aeruginosa* (PAO1) with and without 0.2-2% OligoG.

2.4.6 Atomic force microscopy

The interaction of OligoG with *P. aeruginosa* (PAO1) was studied using AFM to visualise the effect of OligoG on the morphology of the *P. aeruginosa* (PAO1) cells. **Fig 2.11A** shows the untreated *P. aeruginosa* (PAO1) control cells in comparison to the treated samples (0.2-0.5% OligoG; **Figs 2.11B-C**) where AFM clearly demonstrated the binding of OligoG to the cell surface of *P. aeruginosa* (PAO1). Furthermore, **Fig 2.11B** shows OligoG not only binding to the cell wall, but demonstrates its interaction with the bacterial flagella. There were no apparent changes in cell morphology observed, but aggregation was evident with the aggregated cells surrounded by OligoG (**Fig 2.11C**). In contrast, AFM of other bacterial species such as oral bacteria treated with OligoG showed distinct changes in cell morphology after OligoG treatment (**Fig 2.12**). In this case, the effect on planktonic cells varied depending on the species being studied. Whilst untreated *S. mutans* produced distinct chains with altered cellular morphology, on exposure to OligoG, obvious cellular aggregation and ‘clumping’ was observed. Interestingly, AFM showed that OligoG caused a complete collapse or flattening of *P. gingivalis* cells. The cells appear to be lysed and have undergone a complete loss of cellular structure.

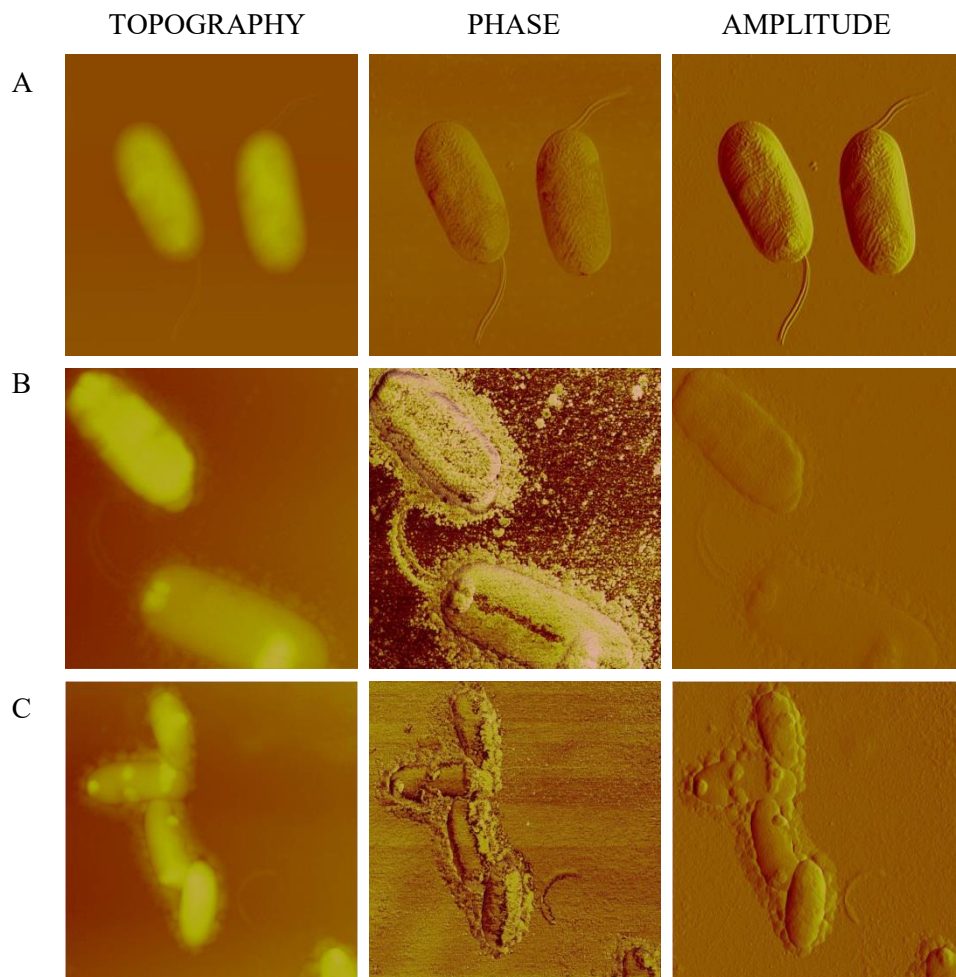


Fig 2.11: AFM images (4 μm) of A) *P. aeruginosa* (PAO1) cells, B) *P. aeruginosa* (PAO1) treated with 0.2% OligoG (post-wash), z scale of 800 nm and C) image (7 μm) of *P. aeruginosa* (PAO1) treated with 0.5% OligoG (post-wash), z scale of 700 nm.

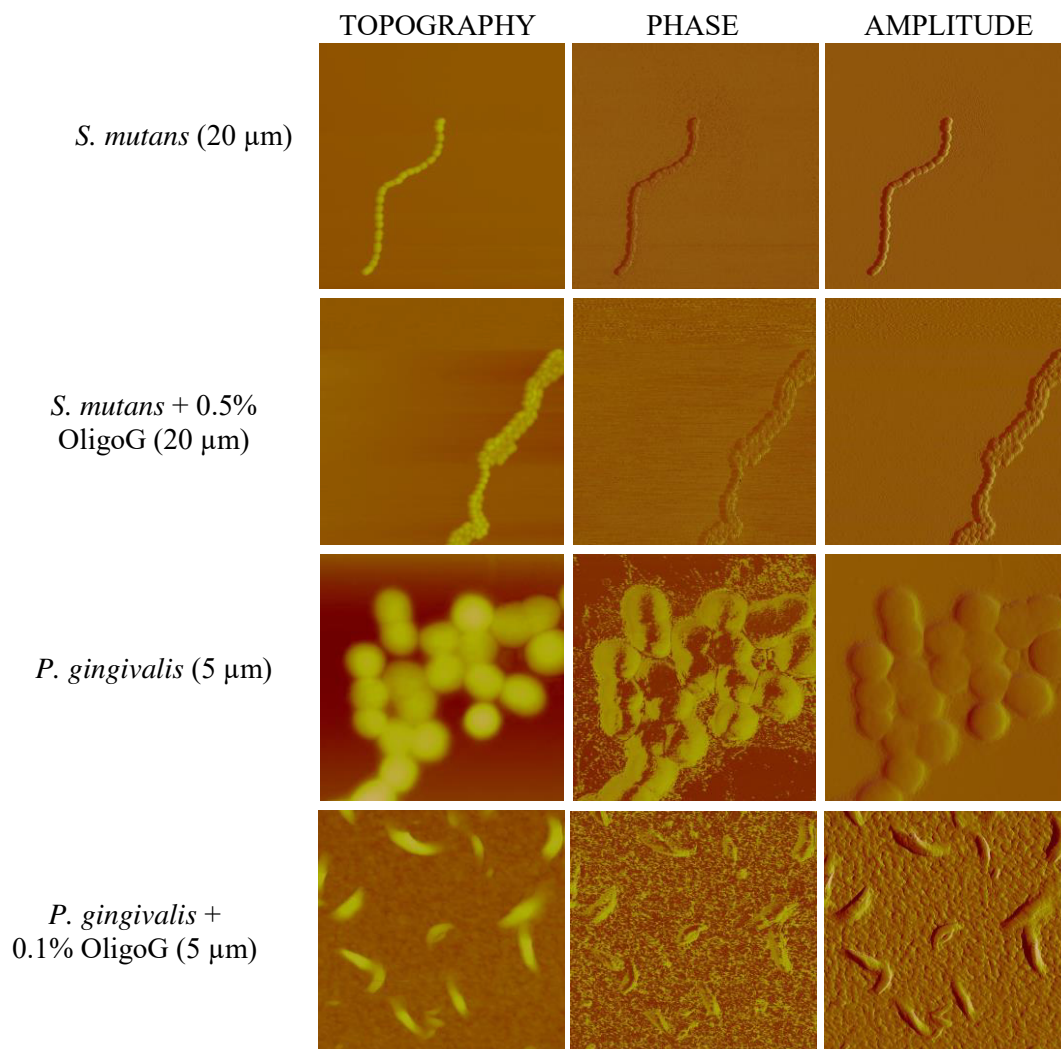


Fig 2.12: AFM images of *Streptococcus mutans* DSM 20523 (ATCC 25175) and *Porphyromonas gingivalis* NCTC 11834 (ATCC 33277) cells \pm OligoG.

2.4.7 Hydrodynamic shear

The interaction between *P. aeruginosa* (PAO1) and OligoG was further demonstrated by *P. aeruginosa* (PAO1) cells grown in the presence of OligoG being subjected to hydrodynamic shear. This involved repeated washing in dH₂O, followed by centrifugation and analysis at each different wash step (n=2), to detect the strength of interaction between *P. aeruginosa* (PAO1) and OligoG. The buffer solution chosen for this series of tests was 0.01 M NaCl, pH 5. Zeta potential and sizing measurements were then compared to an untreated *P. aeruginosa* (PAO1) control washed in the same way.

The zeta potential values revealed that *P. aeruginosa* (PAO1) cells grown in OligoG exhibited an overall more negative bacterial surface charge which was significantly different for each of the hydrodynamic shear tests (washes) when compared to *P. aeruginosa* (PAO1) alone (30.0 mV \pm 0.9 to -33.1 mV \pm 1.1; 0.01 M NaCl, pH 5; 2nd wash; P<0.005). The zeta potential distributions revealed that the secondary, more negative zeta potential peak remained after application of hydrodynamic shear, although the secondary peak size reduced in magnitude by approximately half after the 1st wash (P<0.0001; **Fig 2.13A**).

P. aeruginosa (PAO1) sizing increased after OligoG treatment, with **Fig 2.13B** showing the increase in size from 869 nm \pm 74 for *P. aeruginosa* (PAO1) to 1423 nm \pm 145 when grown in OligoG and washed twice (P<0.0001), as seen by the wider base of the peak (**Fig 2.13B**).

AFM analysis confirmed the results obtained from the zeta potential and sizing analyses, showing OligoG bound to the cell surface. Although the majority of the cell surface associated OligoG was removed by the initial exposure to hydrodynamic shear (i.e. the wash steps), OligoG remained bound to the cell surface, and this was evident after two wash steps and was associated with cellular aggregation (**Fig 2.14**).

Reducing the centrifugation step from 5,500 g to 3,300 g produced very similar results. The zeta potential maintained its more negative peak until the 2nd wash step (P=0.0001) and the bimodal peak again was maintained after two washes (P=0.0039; see **Appendix I**). Sizing again demonstrated the clumping that occurred in the presence of OligoG.

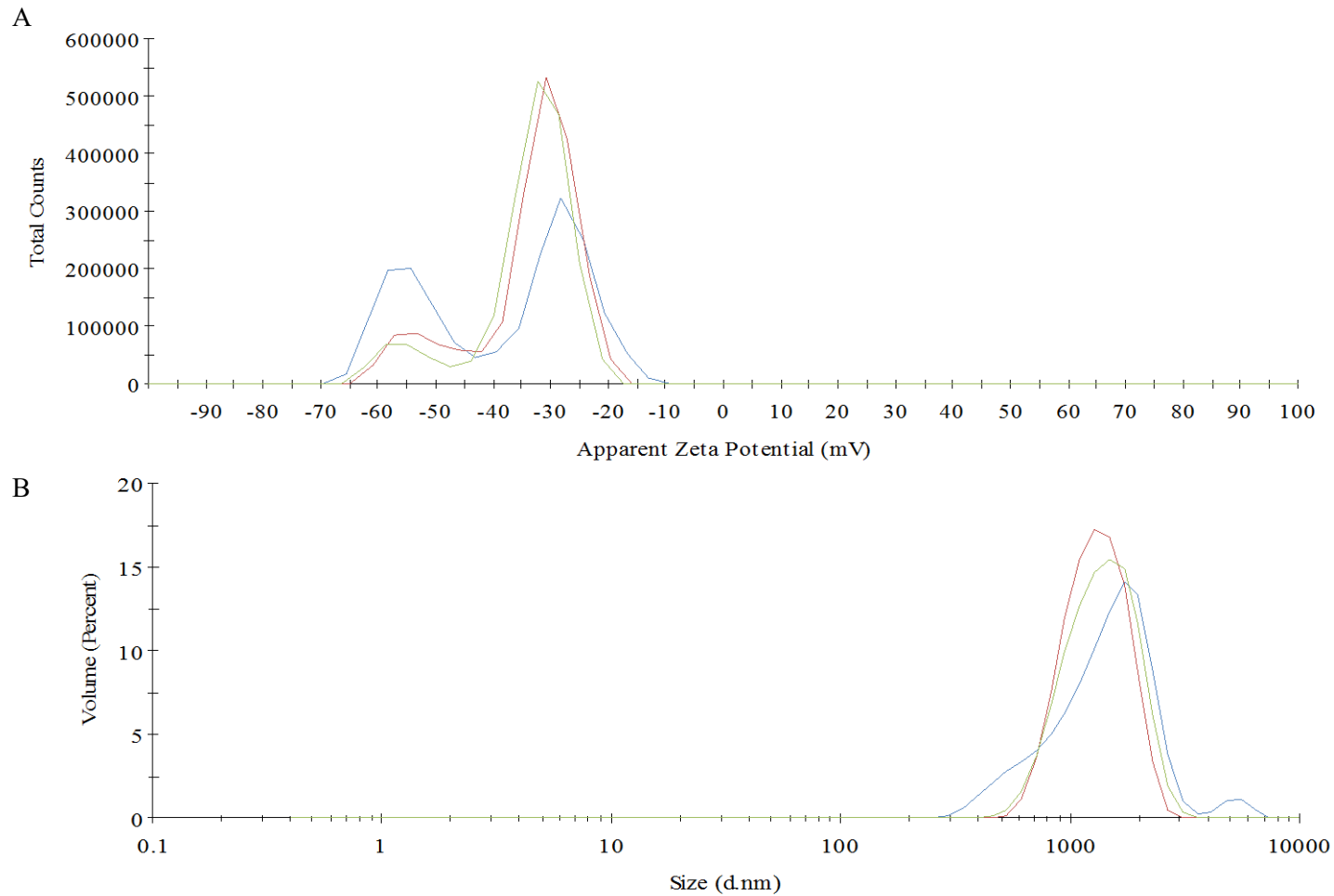


Fig 2.13: Effect of hydrodynamic shear on A) Zeta potential (surface charge) and B) Cell sizing measurements of *P. aeruginosa* (PAO1)/OligoG binding. No wash (blue solid line), 1st wash (red solid line) and 2nd wash (green solid line).

A

	No wash	1 st wash	2 nd wash
Mean Zeta Potential (mV)			
<i>P. aeruginosa</i> (PAO1)	-29.9 ±0.6	-29.3 ±0.5	-30.0 ±0.9
<i>P. aeruginosa</i> (PAO1) + OligoG	-35.9 ±1.6	-32.5 ±1.1	-33.1 ±1.1
Mean Sizing (nm)			
<i>P. aeruginosa</i> (PAO1)	902 ±123	728 ±36	869 ±74
<i>P. aeruginosa</i> (PAO1) + OligoG	2085 ±952	1346 ±128	1423 ±145

B

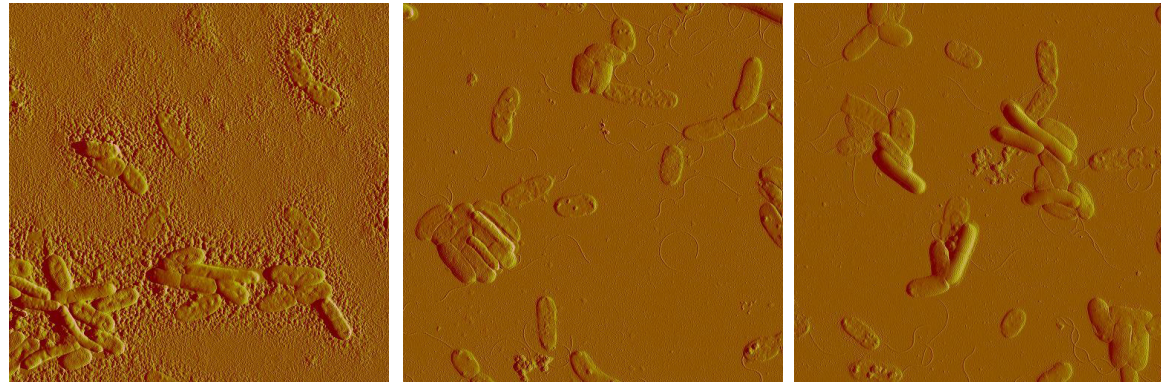


Fig 2.14: Effect of a hydrodynamic shear test at 5,500 g for 3 mins on OligoG treated cells tested in 0.01 M NaCl, pH 5 A) Mean zeta potential values (mV) and mean sizing values (nm). B) Corresponding AFM amplitude images of *P. aeruginosa* (PAO1) grown in 10% OligoG after each of three hydrodynamic shear tests.

2.4.8 Lipopolysaccharide

The effect of 2% OligoG on the zeta potential (surface charge) of LPS was tested. The test samples at this concentration were found to be dominated by the OligoG so could not be measured. The OligoG concentration was therefore lowered to 0.2%. There was no significant difference in the zeta potential value when 1% LPS was combined with 0.2% OligoG at all pH values measured using 0.01 M NaCl buffer (**Table 2.2**).

Table 2.2: Zeta potential measurements for 0.2% OligoG, 1% LPS and combined in 0.01 M NaCl buffer at pH 5, 7 and 9.

Zeta Potential (mV)			
	0.2% OligoG	1% LPS	1% LPS and 0.2% OligoG
pH 5	-28.6 ±9.71	-40.4 ±2.82	-37.7 ±2.40
pH 7	-41.7 ±3.96	-36.0 ±1.81	-36.5 ±2.63
pH 9	-40.0 ±4.10	-36.3 ±3.66	-37.7 ±2.47

In contrast to the surface charge data, sizing of the LPS only control produced a large standard deviation (99.77 nm ±51.17). When LPS was combined with 0.2% OligoG, no change in size occurred, producing a similar result of 95.73 nm ±46.25 in 0.01 M NaCl, pH 5.

2.5 Discussion

Biofilm growth is governed by a number of physical, chemical and biological processes. The initial stages of bacterial adhesion involve the transport of cells to a surface. Bacteria readily attach to surfaces when in contact with liquid present in bulk flow, carrying organic and inorganic substances. This can ultimately lead to a higher concentration of nutrients on the surface than in the liquid phase. Adsorption of organic molecules like proteins may condition the surface and alter its physical-chemical properties. Factors involved in bacteria adhesion to surfaces include electrostatic charges, surface free energy, hydrophobicity (Stover et al., 2000), physical interactions, such as hydrodynamic forces, Brownian motion and bacterial appendages e.g. flagella-mediated locomotion. Initial (reversible) adhesion is

governed by “long range forces” including: electrostatic (double-layer) interactions (usually repulsive due to negative-charges of the cells and surface), steric interactions and van der Waals forces (attractive) (Garrett et al., 2008, Jenkins et al., 2005). These cell-surface interactions are altered by bacterial surface charge, ionic strength of the suspending medium and pH (Soni et al., 2008). Determination of the surface charge properties of *P. aeruginosa* (PAO1) in the presence of OligoG in an aqueous environment may facilitate our understanding of potential cell-surface interactions in these early stages of bacterial attachment and subsequent biofilm growth. Since we cannot measure the cell surface charge directly *per se*, it is characterised by its zeta potential (Soni et al., 2008).

OligoG is negatively-charged, which greatly improves its chance of penetration through bacterial extracellular polymeric substance (EPS). Fluorescence correlation spectroscopy has previously found limitations in diffusion of latex beads in the biofilm matrix due to EPS (Guiot et al., 2002), where cationic latex beads within biofilms showed no fluorescence correlation signals in comparison to the anionic particles of the same size containing the same fluorophore, demonstrating the role of electrostatic interactions within biofilms. It was suggested that the cationic charge of the latex beads and the negative-charge of *Lactococcus lactis* and *Stenotrophomonas maltophilia* bacteria or EPS interact and inhibit possible diffusion of beads through the biofilms and thus, biofilms act as a barrier to diffusion of positively-charged particles. In the absence of such attractive electrostatic interactions, negatively-charged foreign entities could more easily penetrate and diffuse the biofilm EPS (Guiot et al., 2002). Inhibition of diffusion of positively charged particles within a globally negatively-charged biofilm may, therefore, explain how the net negative-charge of OligoG could promote penetration of the biofilm.

The zeta potential for *P. aeruginosa* (PAO1) was found to be negative in value (Powell et al., 2014), which was as expected as this is reported for nearly all bacteria in physiological conditions. Gram-negative bacteria are negatively-charged at most pH values due to a large number of phosphate and carboxyl groups present on bacterial LPS (Cowan et al., 1992). The zeta potential was not greatly affected between pH 5 and 9, as seen in other studies (Soon et al., 2011). Instead, the greatest effect was seen by the change in the NaCl concentration of the test solution, where the zeta potential values became more negative as the salt concentration was

lowered. In the current study, the data at 0.1 M NaCl was excluded as the high salt concentration obscured results due to “ion shielding” (see **Appendix I**). This has previously been noted in a study comparing colistin-susceptible and resistant *Acinetobacter baumannii*. The increase in zeta potential towards neutral at higher ionic strengths noted by the authors was due to the “shielding” of the true surface-charge, because of the large amount of cations present around the negatively-charged bacterial surface. These data suggested that at ionic strengths below 0.1 mM, the zeta potential became independent of the ionic strength (Soon et al., 2011).

Interestingly, all *P. aeruginosa* (PAO1) samples showed a uni-modal peak regarding zeta potential, but became bimodal following OligoG treatment. Other studies have reported the bimodal nature of some *P. aeruginosa* strains (Nagant et al., 2011). When the zeta potential of multiple strains of *P. aeruginosa* was investigated in 10 mMol/l phosphate buffer, pH 7 (Nagant et al., 2011), a great variation in zeta potential was observed with four exhibiting clear bimodal heterogeneity and two being narrow and uni-modal (Nagant et al., 2011). These investigations also showed a wide distribution of zeta potential in *Pseudomonas* strains, but there was no statistically significant difference between the mucoid and a non-mucoid strains tested. In these experiments, *P. aeruginosa* (PAO1) alone showed only a uni-modal peak at all buffer concentrations. Once treated with OligoG, the bimodal peak was evident in all buffers tested.

Several strains of sub-gingival bacteria have also been found to be bimodal (Cowan et al., 1992), as well as *Enterococcus faecalis* strains which usually comprise of subpopulations with different surface charges, typified by the bimodal zeta potential distribution observed here for OligoG-treated *P. aeruginosa* (PAO1) (van Merode et al., 2006). It should be noted however, that bacterial strains can display distinct sub-populations that differ in flagellation, natural competence and cell surface charge. In a heterogeneous culture, the zeta potential may show a wide Gaussian distribution, or even more than one distinct Gaussian distribution. It can be speculated that when bacteria approach the negatively-charged surface, the electrostatic repulsion is higher for bacteria with a negative zeta potential (van Merode et al., 2006). This may, in part, explain the mode of action of OligoG, which produces an overall more negative zeta potential, inhibiting long-range bacterial adhesion to surfaces and disrupting normal biofilm formation.

The CF lung is typically more acidic and has a higher salt concentration (section 1.6.2) than the healthy lung (Tate et al., 2002, Newport et al., 2009), so the experiments in this study focused on 0.01 M NaCl, pH 5 buffer. Under these conditions, the main zeta potential peak for *P. aeruginosa* (PAO1) was bimodal once treated with OligoG. From AFM images, OligoG clearly interacted with the surface of *P. aeruginosa* (PAO1), with OligoG also seen to coat the flagella. This physical interaction may be a possible explanation for the observed change in surface charge as surface appendages, such as fibrils, are thought to contribute heavily to the charge properties of a bacterium (Cowan et al., 1992). AFM studies not only showed OligoG binding to the flagella, but also inducing cellular aggregation of the bacteria at high OligoG concentrations. This may reflect one of the direct mechanisms of action for OligoG in the inhibition of bacterial cell motility (Powell et al., 2014).

It has been previously stated that the more negative the zeta potential value, the greater the effect of a drug. For example, CSA-13 is a cationic steroid, previously shown to be more effective (i.e. with greater correlation between sensitivity to the drug and electrostatic interaction) when the zeta potential was below -50 mV (Nagant et al., 2011). Bruinsma et al. (2006) concluded that the more negative the surface charge (zeta potential), the more susceptible a bacterium was to an antimicrobial (Bruinsma et al., 2006). Teichoic acid is a highly charged cell wall polymer which plays a key role in the initiation of biofilm formation in *Staphylococcus aureus*. Gross et al., (2001) showed that negatively-charged materials were of particular relevance in reducing colonisation, with repulsive electrostatic forces leading to reduced staphylococcal biofilm formation. The large negative zeta potential observed in this study when *P. aeruginosa* (PAO1) and OligoG were combined supports the theory that OligoG may behave in a similar way to reduce bacterial adhesion and hence biofilm formation.

Increased repulsion due to the more negative-charge on *P. aeruginosa* (PAO1) may create a more open porous biofilm. This altered structural assembly of OligoG-treated pseudomonal biofilms may explain how OligoG treatment was able to potentiate a range of antibiotics/antimicrobials against Gram-negative multi-drug resistant (MDR) organisms (Khan et al., 2012) and oral pathogens (Roberts et al., 2013), *in vitro* by allowing easier access into the biofilm.

Alteration of the bacterial surface-charge was evident following OligoG treatment, and initially this could have been thought to have arisen due to binding directly to LPS on the bacterial cell outer membrane. The zeta potential value for LPS with 2% OligoG was masked by the high OligoG concentration, but once lowered to 0.2% OligoG, the zeta potential observed was unchanged at all pH values. This suggests a different mechanistic interaction between OligoG and *P. aeruginosa*.

Electrostatic interactions play an important role in the mechanical stability of biofilms (Chen et al., 2012, Guiot et al., 2002, Mayer et al., 1999). Alterations in electrostatic repulsion between negatively-charged moieties within a biofilm (in the presence of a negatively-charged bioelectric field) may effectively modulate the resultant mechanical structure and thickness (Stoodley et al., 1997). In addition to mediating alterations in bacterial adhesion, this observed change in charge following OligoG treatment may, therefore, result in the altered structural assembly of *Pseudomonas* biofilms. The altered structural assembly of OligoG-treated biofilms has been previously quantified through AFM force measurements and rheometry (Powell et al., 2013). In these studies, AFM force measurements revealed a significantly lower Young's modulus for OligoG treated biofilms, and rheometry revealed an observed increase in phase angle (the difference between stress and strain in an oscillatory test), which reflected a decreased ability of the OligoG-treated biofilm to resist structural rearrangement under stress (Powell et al., 2013).

Applying a specific electric current to a developing biofilm has a significant effect on biofilm thickness (Stoodley et al., 1997). This study involved growing a mixed species (3 day) biofilm under flow. By fitting wire electrodes to the flow cell, the developing biofilm expanded by 4% when the applied charge was cationic and reduced by 74% when the applied charge was anionic. Alteration of pH, (without electric current) was also shown to have a significant effect. At pH 10, the biofilm was unaltered, whilst at pH 3 became compacted to 69% of its original thickness. This may be due to molecular interactions between the biofilm EPS and bacterial cell walls under acidic conditions. Contraction under acidic conditions may be due to the elimination of electrostatic repulsion from neutralisation of negatively charged carboxylate groups, through protonation, as well as due to hydrogen bonding between carboxylic acids and oxygen atoms in the sugars. The electrostatic interaction between the negatively-charged groups of the biofilm and the charged

wire may explain the biofilm contraction under anionic charge and expansion under cationic charge (Stoodley et al., 1997). This current study emphasised the importance of the net negative-charge of OligoG in biofilm inhibition and disruption.

Size estimation for *P. aeruginosa* is problematic due to its rod (or bacillus-like) shape, and so will be dependent upon the angle of the cell when the measurement is made. This may explain the variability observed in the *P. aeruginosa* (PAO1) a size measurement across different pHs, however these values remain within size distributions expected for *P. aeruginosa* (PAO1). Interestingly, when *P. aeruginosa* (PAO1) and OligoG were combined, the peak value for sizing increased, suggesting they were bound together or aggregated. DLS demonstrated clear differences in the size of OligoG-treated *P. aeruginosa* (PAO1). DLS however, assumes Brownian motion of the cells and *Pseudomonas* species are motile. To ensure that the observed increase in size did not simply reflect decreased motility, direct cell measurements were performed using AFM. This confirmed that cellular aggregation following OligoG treatment was directly responsible for the size changes observed (Powell et al., 2014).

The strength of the relationship between OligoG and *P. aeruginosa* (PAO1) appeared (in part) to be disrupted following use of the hydrodynamic shear washes and therefore may explain why some decrease in size occurred. As size values remained much higher than for *P. aeruginosa* (PAO1) or OligoG alone, it must be assumed that the interaction between them was strong enough to withstand the hydrodynamic shear. The strength of the bond was maintained during AFM imaging, which confirmed cell “clumping” in the presence of OligoG (Powell et al., 2014).

The epithelial cells of the CF patient have a significantly reduced (more negative) surface charge compared to those of the non-CF patient. This may be important in the increased adherence of microorganisms in the CF lung (Thethi and Duszyk, 1997). In the lung, epithelial surfaces are coated with mucin, which is negatively-charged due to the presence of *N*-acetylneuraminic acid and sulfated sugars (Lai et al., 2009a, Thornton et al., 1991). The importance of electrostatic charge in surface adhesion has been highlighted by the failure of a *S. aureus* mutant, (with increased negative-charge due to the lack of D-alanine esters in its teichoic acids) to colonise material surfaces (Gross et al., 2001, Smith, 2005). The greater

negative-charge on *P. aeruginosa* surface induced by OligoG, may effectively increase electrostatic repulsion between OligoG-treated *P. aeruginosa* (PAO1) and mucin/ epithelial cells in the CF lung (van Merode et al., 2006), thereby reducing bacterial adherence, and subsequent biofilm formation.

Alterations in cell surface charge may not only affect biofilm development, but may also modify EPS production. Three main weak interactions are of interest when studying bacterial EPS. The first of these are dispersion forces which are active over the entire molecule and therefore not localised into functional groups. These are produced by spontaneous formation of transient dipoles due to fluctuations in the electron distribution within the molecule. The temporary dipoles polarise neighbouring molecules leading to dipolar attraction forces, to produce what is known as an oscillating induced-dipole-induced-dipole interaction, which reflects the main cohesive forces between hydrocarbon chains. The second force is electrostatic interaction which is active between ions, as well as permanent and induced dipoles. These are quite strong and mainly involve divalent cations, especially Ca^{2+} , accounting for a considerable proportion of the overall binding energy. Lastly, hydrogen bonding is mainly due to the active bonds between hydroxyl groups frequently found in polysaccharides and water molecules. These also support the tertiary structure in proteins. Electrostatic interactions and hydrogen bonds were found to be the predominant forces among EPS macromolecules within the biofilm of a mucoid strain of *P. aeruginosa* (Mayer et al., 1999). OligoG could potentially further disrupt these bonds during biofilm formation and EPS production, and competitively bind to divalent cations such as Ca^{2+} (Khan et al., 2012).

P. aeruginosa (PAO1) used in this study was isolated from a wound many years ago. There are limitations involved in looking at the zeta potential of laboratory cultured organisms. Following successive subculture and perhaps many years 'in laboratory' since original isolation, they may not truly represent what is seen in the clinical situation, and may have unwittingly been exposed to different chemicals or physical impacts in that time (Bruinsma et al., 2001). *P. aeruginosa* (PAO1) therefore represents simply a model organism for these studies. For the zeta potential experiments, *P. aeruginosa* (PAO1) was grown planktonically in suspension. Although shaken whilst growing to facilitate planktonic growth, higher cell concentrations (i.e. at stationary phase) may lead to increased likelihood of

aggregation occurring. Klodzinska et al. (2010) highlighted the importance of lowering cell concentrations to detect possible anomalies and assess the validity of the results obtained for zeta potential analysis. The study of Klodzinska et al. (2010) showed that whilst the value of the zeta potential remained the same, the distribution could change. Reducing the concentration of both *P. aeruginosa* (PAO1) cell and OligoG in this study confirmed the results obtained at higher concentrations. An important finding was that the observed changes in surface charge and cell aggregation in *P. aeruginosa* were evident regardless of whether the bacteria were grown in the presence of OligoG, or were established cultures which were subsequently exposed to OligoG. This was unsurprising, as previous studies had shown effects on *Pseudomonas* species in planktonic minimum inhibitory concentration (MIC) assays, CLSM LIVE/DEAD[®] imaging and SEM studies of OligoG treated, established pseudomonal biofilms (Khan et al., 2012). Hence, OligoG may have potential application in both preventing biofilm development (on host or material surfaces) following debridement and bacterial decolonisation (Percival et al., 2011) and also as a treatment for established biofilms.

2.6 Conclusion

The physical, surface-charge and structural effects on *P. aeruginosa* described here may partly explain the observed action of OligoG on bacterial attachment, biofilm formation and antibiotic potentiation that have previously been described (Khan et al., 2012, Powell et al., 2013). The benefits of using a combination of nanoscale technologies to characterise interactions between bacteria and antibacterial compounds, was also evident.

The study utilised ELS, DLS and AFM to investigate the mechanisms by which OligoG modifies the Gram-negative bacterial cell-surface, structure, charge and function. OligoG was demonstrated to bind to the surface of *P. aeruginosa* (PAO1) thereby inducing a more negative cell-surface charge and increased cellular aggregation. The results revealed that OligoG had a similar effect on *P. aeruginosa* (PAO1) populations, whether it was present during or after the growth phase. In addition, the application of hydrodynamic shear showed that this binding was strong, and not readily physically reversible (Powell et al., 2014).

Chapter 3:
**The ability of OligoG to disrupt mucoid
pseudomonas biofilms**

3.1 Introduction

Bacteria gain several advantages from forming biofilms including protection from antibiotics, disinfectants and stresses arising from dynamic environments. By using intercellular communication, bacteria are able to adapt to changing environments such as nutrient deficiency, by modifying gene expression to allow phenotypic variation (Garrett et al., 2008). Biofilms are known to cause up to 80% of all infections and show significantly higher levels of antibiotic resistance (up to 1000 fold) compared to their planktonic counterparts (Davies, 2003).

Most cystic fibrosis (CF) patients will become chronically colonised by mucoid variants of *Pseudomonas aeruginosa* by early adulthood (Govan and Deretic, 1996). Thereafter, as it is rarely then eradicated, anti-pseudomonal therapy, for the most part, is largely palliative. Chronic lung infections in CF patients cause an accumulation of *P. aeruginosa* mutations, leading to strains with both genotypic and phenotypic variations. This diversification process leads to multiple pseudomonal sub-types co-existing within the same infected lung population (Wright et al., 2013).

Fluorescent labelling has previously been used to assess the localisation of therapeutics. Previous studies have looked into the use of phospholipase A2 (PLA2) crotoxin, (an anti-tumour protein) conjugated to dextrin as a polymer therapeutic, with the ultimate aim to decrease its toxicity. Fluorescence labelling with Oregon Green (OG) was used to detect phospholipase A2 presence in human breast carcinoma cell lines (Ferguson and Duncan, 2009). The synthesis and characterisation of OG labelled probes has been described and confocal laser scanning microscopy (CLSM) used to define the fate of the dextrin-OG in cells (Ferguson et al., 2010). Fluorescent microscopy techniques have also been used to confirm localisation of water-soluble polymeric carriers in late endocytic intracellular compartments (Richardson et al., 2008).

3.1.1 Development of an artificial sputum medium

Due to changes in its consistency during sterilisation, intra- and inter-patient variability, its limited availability, and the prolific antibiotic use of CF patients, CF sputum itself is a less than ideal material to use for research purposes (Fung et al., 2010). To improve our understanding of *P. aeruginosa* infection in the CF lung,

artificial sputum (AS) medium was therefore developed to mimic the nutritional environment in the sputum of CF patients. In contrast to CF sputum, the artificial sputum is a defined medium. AS medium employed in previous studies has lacked mucin and DNA, both of which are important constituents of the extracellular polymeric matrix which characterises *P. aeruginosa* biofilm growth in the human lung (Palmer et al., 2007b). Subsequent studies have incorporated both DNA and mucin in an attempt to aid understanding of the biology and microbiology of the CF lung (Kirchner et al., 2012).

Previous studies reported difficulties in the preparation of AS medium, including sterilisation, which required filtration rather than autoclaving to avoid damage to the complex 3-dimensional structure of the mucin component of the medium (Fung et al., 2010). The AS medium, whilst not ideal, does provide a model for the *in vivo* situation.

3.1.2 Use of fluorescent labelling in microbiology

Fluorescence occurs in some molecules when the absorption of a photon leads to emission of a light with a longer wavelength and lower energy. This emission is known as fluorescence, and there are environmental factors that affect this spectrum such as temperature and pH (Sun et al., 2010). Several factors need to be optimised prior to fluorescent imaging, including selection of an appropriate fluorophore (Pearson, 2007). Fluorescence of macromolecules can provide information on binding sites, solvent interactions, degree of flexibility, inter-molecular distances and rotational diffusion coefficients. For molecules with no intrinsic fluorescence, a fluorescent probe can be attached to the polymer by “chemical coupling”. Prior to conjugation, it is essential to select an appropriate probe. There are several important factors to consider when incorporating a fluorescent probe into a molecule including the need for the fluorescent probe to be tightly bound at a unique location, the fluorescence should not be sensitive to environmental conditions (e.g. pH) and should not affect the features of the macromolecule being investigated (Freifelder, 1982). For example, attachment of a hydrophobic probe would promote non-specific cell binding or alter the conformation of an oligosaccharide such as OligoG, and therefore possibly alter potential anti-biofilm effects.

The use of fluorescent probes to analyse the structure of cell membranes is well documented (Loh et al., 1984, Gomperts et al., 1970, Helgerson and Cramer, 1977, Madeira and Antunesm-Madeira, 1973, Uratani, 1982), and have been used to study the interaction of aminoglycosides (gentamicin) with *P. aeruginosa* (Loh et al., 1984). The mechanism by which aminoglycosides interact with the *P. aeruginosa* cell surface has been shown to involve an “initial step” comprising rapid ionic binding that neutralises the cells’ net negative-charge (Loh et al., 1984). In this case, the charge on the probe can be a limiting factor when analysing membrane studies, as evident with commonly used negatively-charged probe, 1,8-anilino-1-naphthalenesulfonic acid. This could not be used to analyse polycationic gentamicin uptake in *P. aeruginosa* due to charge neutralisation, since it would complicate the kinetic analysis of diffusion. Therefore, a neutral probe, 1-*N*-phenylnaphthylamine, was employed instead (Loh et al., 1984).

3.1.3 Choice of fluorescence probe for OligoG labelling

OligoG has been shown to bind to the cell surface of *P. aeruginosa* (PAO1; Powell et al., 2014, Roberts et al., 2013). In these studies, OligoG binding was demonstrated to modify the surface charge of the bacteria and physical interaction of the oligomers with the cell surface was clearly demonstrated (Powell et al., 2014). The location of OligoG within the biofilm was however unknown.

Texas Red (TxRd) cadaverine was selected as the fluorescent probe of choice in these studies since it is biologically inert, and has previously been conjugated to various polysaccharides, drugs and macromolecules in studies of cellular localisation (Anees, 1996, Chvatal et al., 2008). TxRd cadaverine contains a primary aliphatic amine that enables conjugation to OligoG, via its COO⁻ groups in aqueous solution using water-soluble carbodiimides, resulting in a stable amide bond (Ferguson and Duncan, 2009).

TxRd has previously been conjugated to pentosan polysulphate, a highly negatively charged polysaccharide (Anees, 1996) and is also commonly employed to label dextran, a biologically inert hydrophilic polysaccharide (Sinai et al., 1995). TxRd-labelled dextran is widely used for neuronal tracing, intercellular communication and endocytosis (Hollenbeck, 1993, Oparka et al., 1997, Roberts et

al., 1997). TxRd has also been used as a fluorescent probe for lectins (wheat germ agglutinin) to visualise their binding to *Sphingomonas* biofilms made from commercially available extracellular polymeric substance (EPS; Johansen et al., 1996), and *Staphylococcus epidermis* biofilms (Sanford et al., 1996).

Methylprednisolone (MP) has been conjugated to TxRd cadaverine and placed in biodegradable poly(lactic-co-glycolic acid) based nanoparticles (NP) to analyse a minimally invasive drug delivery system for contusion injury of the spine (Chvatal et al., 2008). TxRd cadaverine was used as a fluorescent probe in these previous studies because of its low molecular weight (MW), which would less likely impede on diffusion. By analysing the difference in nitric oxide production by cells treated with MP-NP or TxRd-MP-NP, Chvatal et al. (2008) also showed that conjugation of TxRd did not affect the anti-inflammatory function of MP-NP.

3.2 Aims

The hypothesis of these studies was that the interaction of OligoG with the cell surface of a mucoid strain of *P. aeruginosa* would inhibit biofilm development and this could be studied using fluorescently labelled OligoG. Specific aims were:

- To perform LIVE/DEAD[®] imaging on developing and established biofilms treated with OligoG.
- To investigate biofilm growth with OligoG in a more clinically relevant *in vitro* environment.
- To develop a fluorescent-labelled OligoG to allow detection of OligoG location in bacterial cell populations and biofilms.

3.3 Materials and Methods

3.3.1 Bacterial strains and media

A stable mucoid strain of *Pseudomonas aeruginosa* (NH 57388A) isolated from the sputum of a chronically colonised CF patient attending the Danish CF Centre, Rigshospitalet, Copenhagen, Denmark (from N. Høiby, Copenhagen) was employed. Fresh overnight (O/N) growth of *P. aeruginosa* (NH 57388A) isolated on blood agar plates was employed to inoculate tryptone soy broth (TSB; LabM, Heywood, Lancashire) which was “roller mixed” at 37°C to produce an O/N broth

culture of the organism. These experiments employed sterile Mueller Hinton (MH) broth or an Artificial Sputum (AS) medium control (section 3.3.4). The AS medium reproduced several components found in the CF sputum and created a less nutritious environment for bacterial growth.

3.3.2 Confocal laser scanning microscopy

Whatman glass-bottomed optical 96-well plates were used for all CLSM experiments. For LIVE/DEAD[®] (BacLight[™] Bacterial Viability Kit, Invitrogen, Paisley, UK) experiments, the green fluorescing nucleic acid dye, SYTO[®] 9 was used to visualise cells with intact cell membranes (live cells), and the red dye, propidium iodide those with compromised membranes (dead or dying cells). Images were scanned using appropriate settings for sequential fluorescence recordings of SYTO[®] 9 (Ex/Em max: 480/500_{nm}) and propidium iodide (Ex/Em max: 490/635_{nm}). SYTO[®] 9 was used without propidium iodide for experiments in which TxRd-labelled OligoG was studied.

CLSM was performed using an Olympus FV1000 confocal microscope with images at x400 or x600 magnification under oil. CLSM data was processed using Imaris software.

3.3.2.1 Effect of OligoG as a treatment to inhibit biofilm formation (confocal laser scanning microscopy)

MH broth \pm 0.2%, 0.5%, 2%, 6% and 10% OligoG w/v (90 μ l) was inoculated with 10 μ l of *P. aeruginosa* (NH 57388A) culture and the developing biofilms were incubated for 24 h on a rocker. The supernatant was removed and 6% LIVE/DEAD[®] (v/v) stain in phosphate buffered saline (PBS) was placed on the biofilms for 10 mins in the dark prior to imaging.

3.3.2.2 Effect of OligoG as a treatment to disrupt an established biofilm

Experiments were established in triplicate so that the biofilms could be visualised at the three different incubation/growth times points used (1 h, 4 h and 24 h). The *P. aeruginosa* (NH 57388A) culture was standardised to 10⁷ cfu/ml (Russo

2013; OD₆₀₀ 0.05) and 10 µl of the standardised O/N culture was placed in 90 µl MH broth. Biofilms were incubated at 37°C for 24 h with gentle rocking prior to treatment. Half the supernatant was then gently removed and replaced with 50 µl fresh MH broth ± OligoG. The final concentrations of OligoG were 0.5%, 2% and 6% (v/v). The samples were then incubated for 1 h, 4 h and 24 h. At the selected time points, the supernatant was gently removed and 6% LIVE/DEAD[®] (v/v) stain in PBS was placed on the biofilms for 10 mins prior to imaging.

3.3.3 Effect of OligoG on biofilm development of *Pseudomonas aeruginosa* (NH 57388A; scanning electron microscopy)

MH broth ± 2 ml OligoG 0.2%, 2%, 6% and 10% (w/v) was prepared in a 12-well plate (Greiner Bio-One, Stonehouse, UK) containing thermanox glass slides (Agar Scientific), followed by a 20 µl inoculum of the *P. aeruginosa* (NH 57388A) culture, prior to incubation with rocking for 24 h. The supernatant was then removed and biofilms fixed with 2.5% (v/v) glutaraldehyde for 1.5 h. Following vigorous washing (x4) with dH₂O, the fixed biofilms were covered with 1 ml dH₂O and freeze-dried. Imaging was performed using Hitachi S4800 scanning electron microscope (SEM) and no sputter coating was used.

3.3.4 Artificial sputum medium

Briefly, AS medium comprised of: 4.0 g of deoxyribonucleic acid (DNA) from salmon fish sperm (Sigma Aldrich) and 5.0 g of porcine stomach (type II) mucin (Sigma Aldrich) dissolved O/N at 4°C in sterile dH₂O. Twenty ml of RPMI 1640 amino acids solution (Sigma Aldrich), 5.9 mg of diethylenetriaminepentaacetic acid (DTPA; Sigma Aldrich), 5 ml of egg-yolk emulsion (Sigma Aldrich), 5.0 g NaCl and 2.2 g of KCl were then added. Following mixing, the pH was adjusted to 7.0 ± 0.1 by the addition of 0.5 M NaOH, and made up to 1 L. The AS medium was then filter-sterilised using a (0.22 µm pore) barrel filter (Millipore) and stored at 4°C (up to a month) in the dark.

3.3.4.1 Effect of OligoG on biofilm development of *Pseudomonas aeruginosa* (NH 57388A; scanning electron microscopy) grown in artificial sputum medium

The *P. aeruginosa* (NH 57388A) culture was adjusted to OD₆₀₀ 0.05 for 10⁷ cfu/ml. The resultant bacteria were centrifuged (5,500 g; 6 mins) and then washed with PBS (x2), and re-suspended in 1 ml PBS. Ten µl of the resultant bacterial suspension was then added to 1 ml of AS medium containing OligoG 0.2% 2% and 6% (w/v), in a 12-well plate on thermanox glass slides. The biofilms were then incubated at 37°C for 48 h under gentle rocking. The biofilms were prepared for SEM imaging as described in section 3.3.3.

3.3.5 Texas red-labelling of OligoG and conjugate characterisation

To localise OligoG both within the biofilm model and during biofilm disruption, CLSM was employed. OligoG was labelled with TxRd cadaverine (MW 690.87 g/mol) using EDC and sulfo-NHS as zero-length crosslinking agents. EDC aids conjugation by activating carboxyl groups for spontaneous reaction with primary amines, while sulfo-NHS increases the efficiency of the EDC-mediated coupling (**Fig 3.1**).

OligoG (100 mg) was dissolved in 1 ml PBS buffer (pH 7.4) in a 10 ml round-bottomed flask. To this, EDC (10 molar eq.) and sulfo-NHS (10 molar eq.) were added, and the mixture stirred for 15 mins. Subsequently, TxRd cadaverine (dissolved in dimethyl sulfoxide, DMSO; 5 mg/ml and stored at -20 °C until use) was added (2 molar eq.). The pH was adjusted to 8.0 via “drop-wise” addition of NaOH (0.5 M) and the reaction mixture was left stirring in the dark (5 h). The resultant conjugate was then purified by size exclusion chromatography (SEC) using a disposable PD-10 desalting column containing Sephadex G25 equilibrated with dH₂O (25 ml added in total). The entire reaction mixture was added to the column and 5.5 ml of the eluted dH₂O was collected, lyophilised and stored at -20°C.

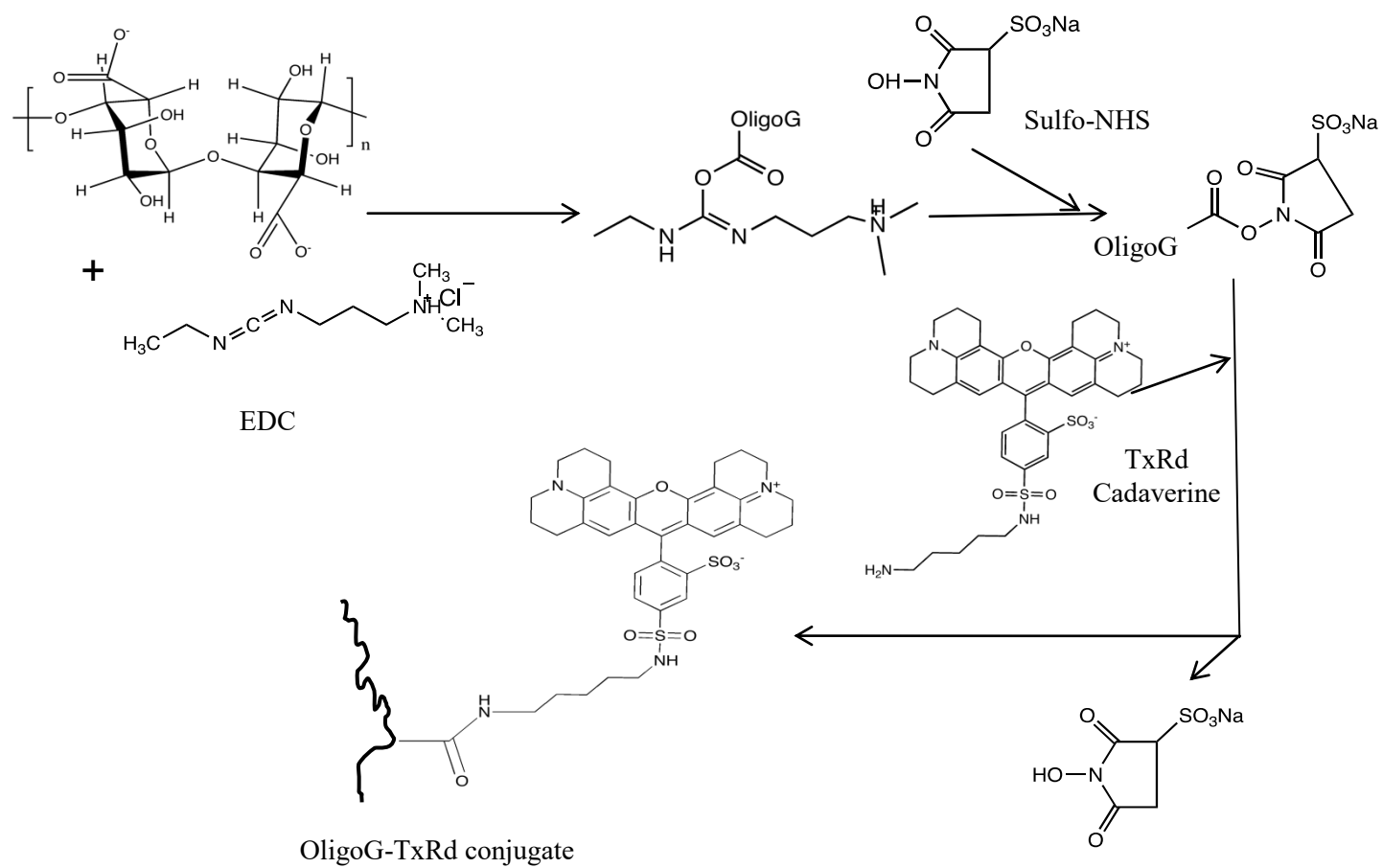


Fig 3.1: Summary of the synthetic route for OligoG and TxRd cadaverine conjugation.

UV spectroscopy was used to determine the total TxRd content of the TxRd-OligoG conjugate. The TxRd-loading was determined by analysing a 5 mg/ml solution in PBS and relating this to a TxRd calibration curve (1-10 µg/ml). The values were then plotted against fraction volume and bound TxRd was expressed as percentage of total fluorescence measured for all fractions. Specific activity (µg TxRd/mg TxRd-labelled conjugate) was calculated using the following equation:

$$\text{Specific activity } (\mu\text{g TxRd/mg TxRd conjugate}) = \frac{(\mu\text{g TxRd from UV}) \times \% \text{ TxRd bound}}{100 \times \text{mg TxRd-labelled conjugate}}$$

The reaction mixture was characterised by SEC prior to, and after purification, by analysis of SEC fractions for fluorescence (free TxRd: TxRd-OligoG; 5 mg/ml solution in PBS). Fractions (0.5 ml) were collected in 1.5 ml microcentrifuge tubes. A sample of each fraction (100 µl) was placed in duplicate into a black 96-well microtitre plate and fluorescence measured using a fluorescent plate reader ($\lambda_{\text{ex}} = 591 \text{ nm}$, $\lambda_{\text{em}} = 612 \text{ nm}$, gain 1000). To analyse the pH and concentration dependence of TxRd cadaverine, the fluorescence was measured at concentrations 1-10 µg/ml in PBS at pH 5, 7 and 9 using a fluorescent plate reader

3.3.6 Effect of texas red-labelled OligoG as a treatment to inhibit biofilm formation

An inoculum of 10 µl of *P. aeruginosa* (NH 57388A) culture was placed in 90 µl MH broth ± TxRd-labelled OligoG (TxRd-OligoG), alongside an MH broth only control. The concentrations of TxRd-OligoG conjugate used were 0.5%, 2% and 6% (there was insufficient yield of product to carry out the test using 10% TxRd-OligoG). Biofilms were incubated for 24 h on a rocker. The supernatant was then removed and 8% SYTO[®] 9 (v/v) stain in PBS was placed on the biofilms prior to imaging by CLSM.

3.3.7 Effect of texas red-labelled OligoG on biofilm disruption

Conjugate concentrations were prepared in triplicate so that the biofilms could be visualised at the three different time points. The *P. aeruginosa* (NH 57388A) culture was standardised to 10^7 cfu/ml (OD₆₀₀ 0.05) and 10 µl of the standardised O/N culture placed in 90 µl MH broth. Biofilms were incubated at 37°C for 24 h with rocking prior to treatment. Half of the supernatant volume was gently removed and replaced with 50 µl fresh MH broth ± TxRd-OligoG. The final concentration of TxRd-OligoG used was 0.5%, 2% or 6% and the samples were incubated. At the appropriate time points (1 h, 4 h and 24 h), the supernatant was gently removed and 8% SYTO[®] 9 (v/v) in PBS added to the biofilms before imaging. To confirm that the TxRd-OligoG had not dissociated to release free TxRd, the supernatant was analysed using a PD-10 column to quantify bound/unbound TxRd after incubation with biofilms. Control experiments also included addition of the equivalent concentrations of “free” TxRd cadaverine (0.052 µg/ml, equivalent to 6% TxRd-OligoG conjugate).

3.3.8 Image J analysis of biofilm

Images were processed using Image J (1.47v) to quantify biofilm area of coverage. During CLSM, the strength of the laser was maintained throughout the series of experiments, making them directly comparable. The images were processed to be smoothed, followed by a standardised adjustment of the brightness threshold. The images were then made binary and the percentage area coverage calculated.

3.3.9 Statistical analysis

Graph Pad Prism[®] statistical software were used to calculate any statistical change in biofilm coverage after treatment with OligoG. In these analyses, the Tukey-Kramer multiple comparisons test was employed based on a one-way ANOVA test.

3.4 Results

3.4.1 OligoG as a treatment to inhibit biofilm formation

OligoG was found to inhibit *P. aeruginosa* (NH 57388A) biofilm growth in a dose-dependent manner (0-6% OligoG) with an increase in bacterial “clumping” and a more disorganised structure of the biofilm seen at 6% OligoG. Interestingly, whilst biofilm development was markedly impaired by the addition of OligoG at the commencement, there were few dead cells present in these biofilms (**Fig 3.2**).

3.4.2 OligoG as a treatment to disrupt an established biofilm

Established 24 h biofilms of *P. aeruginosa* (NH 57388A) in which a well-structured biofilm had formed were treated with OligoG. Following 1 h of OligoG treatment, no apparent effect was seen on biofilm development (**Fig 3.3**). Following 4 h of treatment, very few changes in both the thickness of the biofilm and the number of dead cells was seen (**Fig 3.4**). Following 24 h of OligoG treatment, however, a clear effect was observed, with marked disruption and reduced biofilm thickness with increasing OligoG concentration (0-6%). In these studies there were no differences in non-vital bacterial cells observed in the treated biofilms (**Fig 3.5**).

Image J analysis of the surface area demonstrated a dose-dependent reduction in biofilm coverage with increasing concentration of OligoG (0-6%). The aerial view images showed a significant reduction from 32.73% (control) to 8.07% coverage for the 6% OligoG-treated biofilm ($P < 0.05$; **Fig 3.5B**). Similar observations from the side view images (biofilm depth) showed the percentage area coverage dropped from 22.07% (control) to 4.75% coverage for the 6% OligoG treated biofilm ($P < 0.05$).

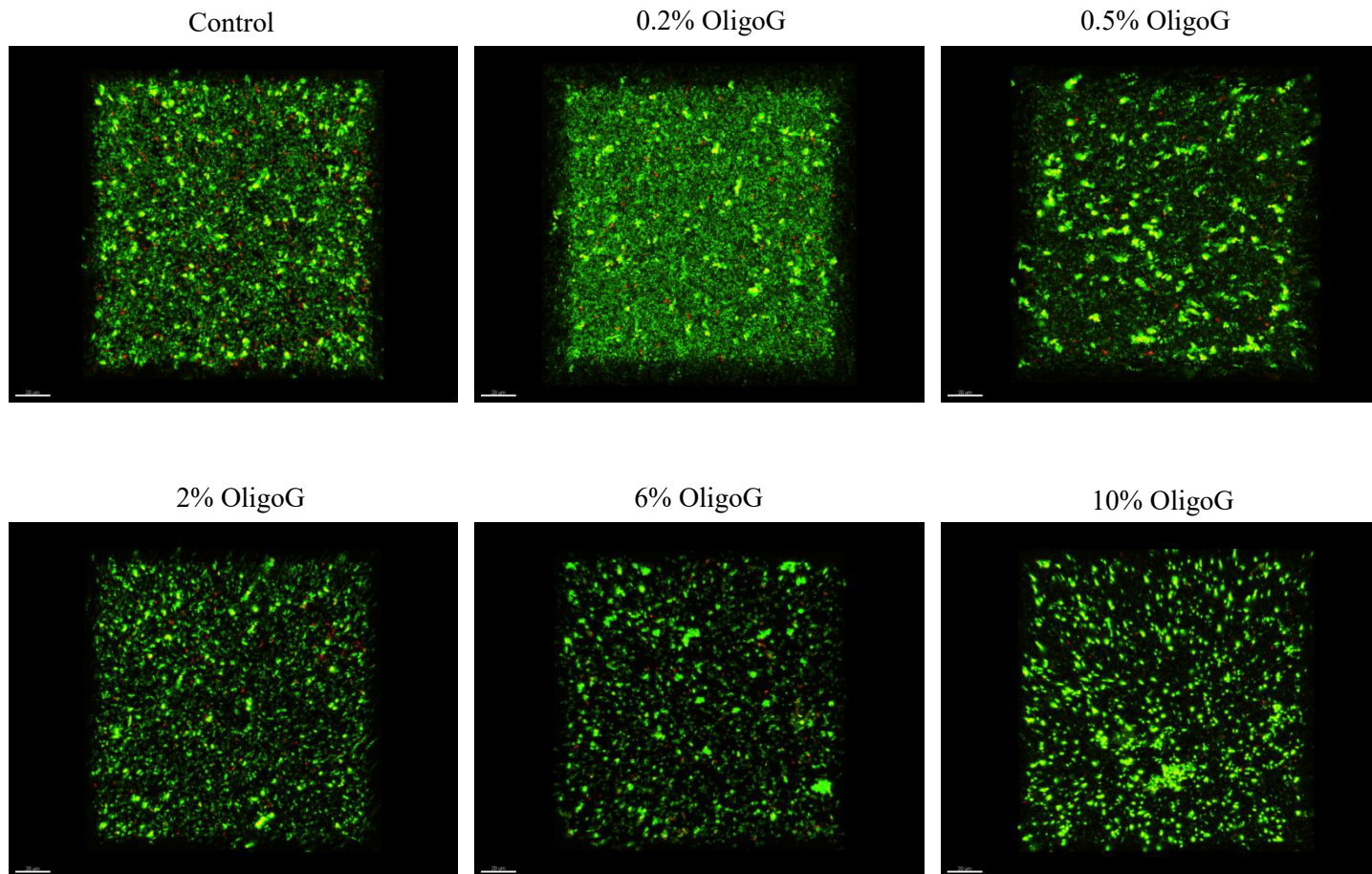


Fig 3.2: CLSM of LIVE/DEAD[®] staining of *P. aeruginosa* (NH 57388A) biofilms grown for 24 h in MH broth \pm OligoG (0.2%, 0.5%, 2%, 6% or 10%). x400 magnification.

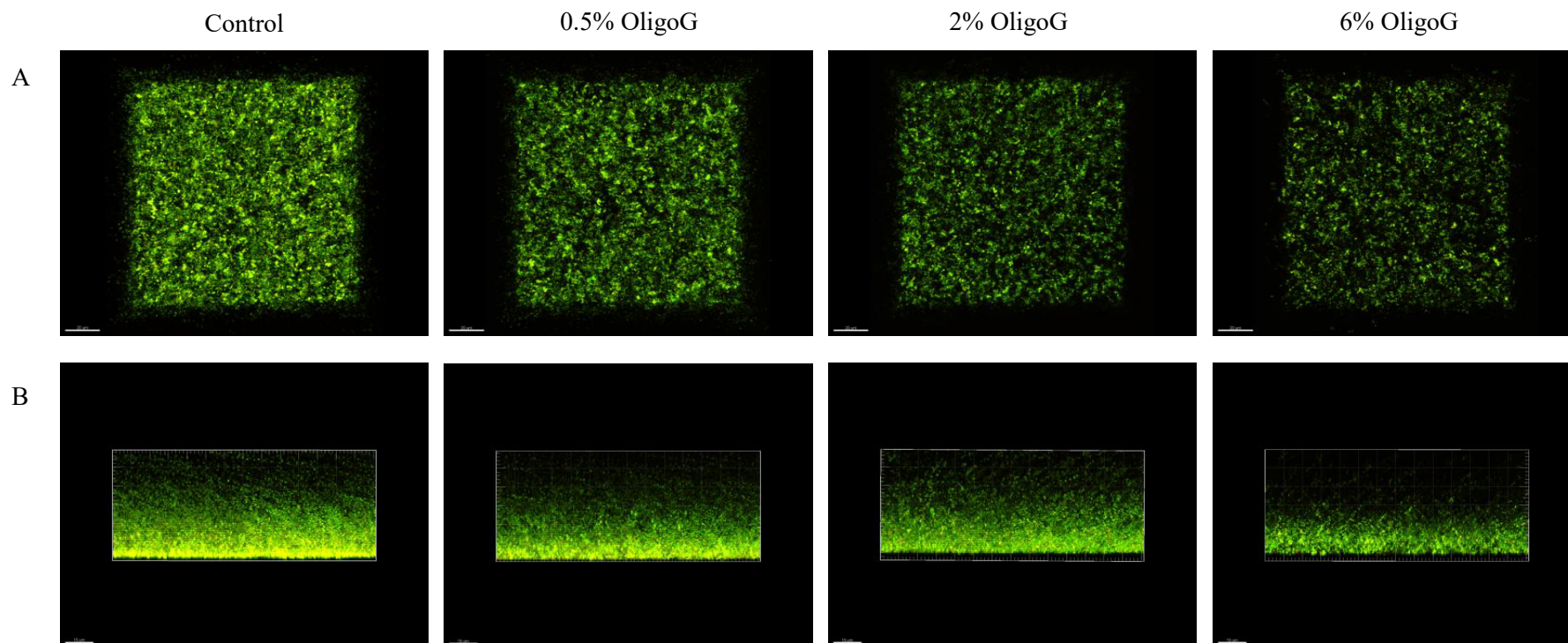


Fig 3.3: *P. aeruginosa* (NH 57388A) grown for 24 h in MH broth, followed by 1 h treatment of OligoG (0.5%, 2% and 6%). Imaged with LIVE/DEAD[®] staining using CLSM (x400 magnification). A) Aerial view; B) Side view (biofilm depth).

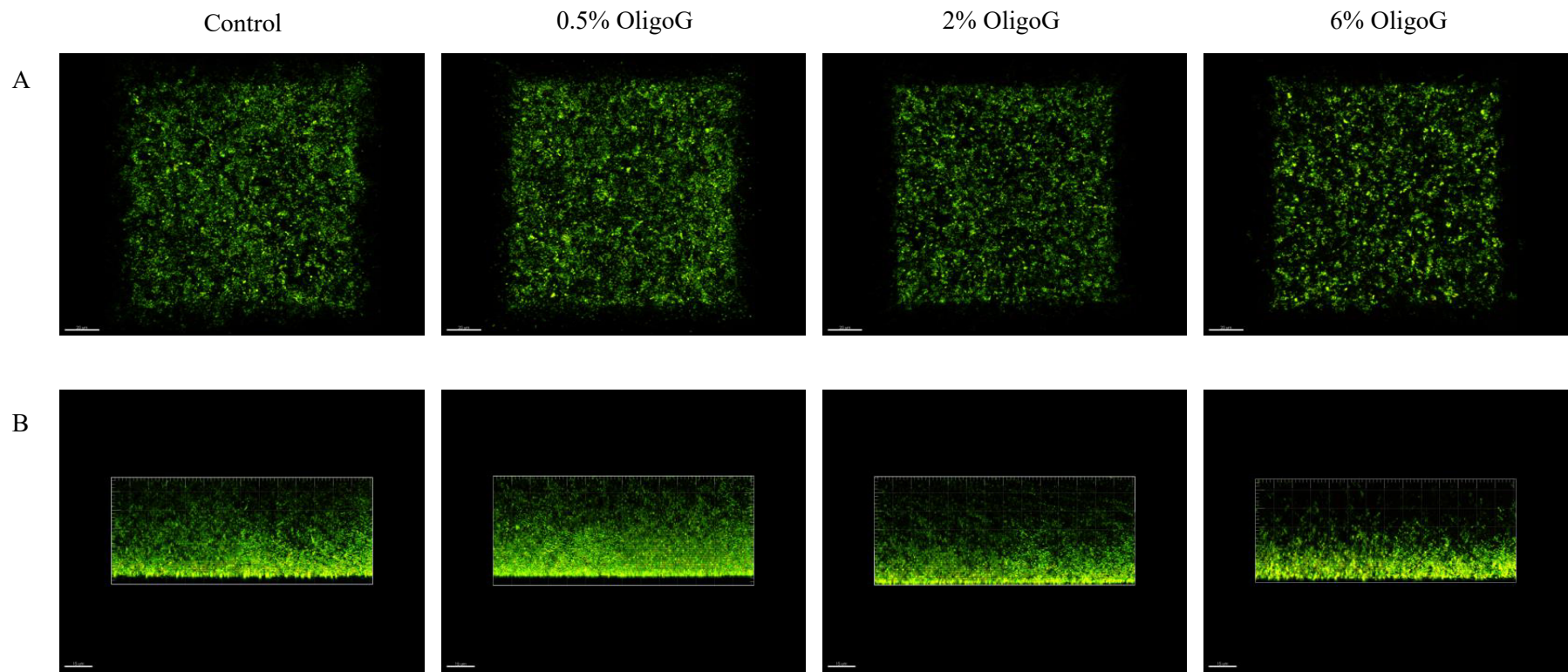


Fig 3.4: *P. aeruginosa* (NH 57388A) grown for 24 h in MH broth, followed by 4 h treatment of OligoG (0.5%, 2% and 6%). Imaged with LIVE/DEAD[®] staining using CLSM (x400 magnification). A) Aerial view; B) Side view (biofilm depth).

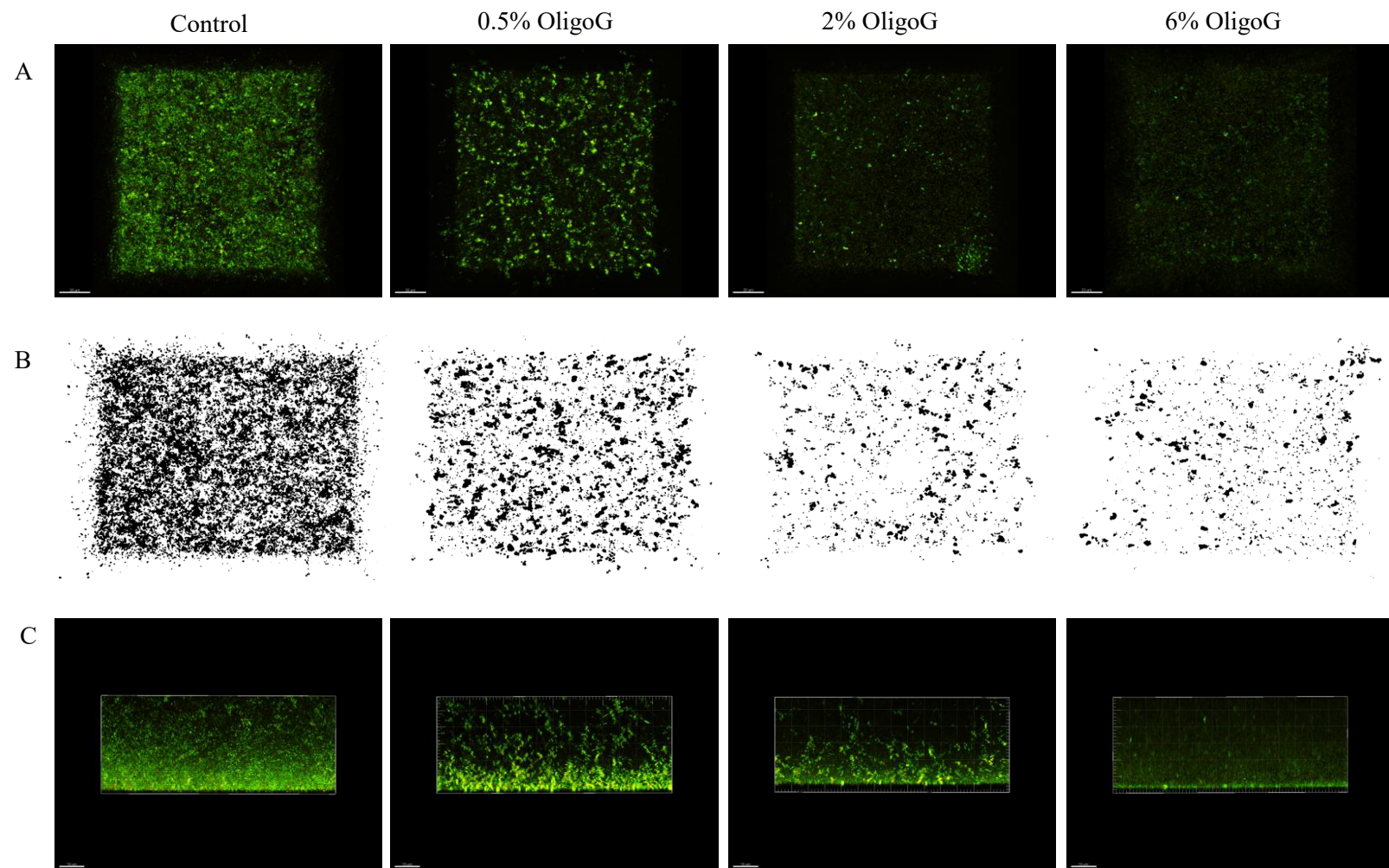


Fig 3.5: *P. aeruginosa* (NH 57388A) grown for 24 h in MH broth, followed by 24 h treatment of OligoG (0.5%, 2% and 6%). Imaged with LIVE/DEAD[®] staining using CLSM (x400 magnification). A) Aerial view; B) Aerial (binary) view from Image J analysis; C) Side view (biofilm depth).

3.4.3 Scanning electron microscopy of *Pseudomonas aeruginosa* (NH 57388A) biofilms

Initial studies of *P. aeruginosa* (NH 57388A) biofilm formation in MH broth \pm OligoG showed a substantial reduction of cells and poor growth as the concentration of OligoG increased. There was also a corresponding reduction in the EPS formed, with very few cells found to be embedded in matrix at the highest OligoG concentration (10%). In addition, at this concentration, OligoG seemed to cluster around the cells forming a distinctive granular pattern (**Fig 3.6**).

Sterile AS medium only showed the formation of non-uniform open structures (**Fig 3.7**). Due to the low nutrient content of AS medium compared to MH broth, biofilms were grown for longer (48 h Vs 24 h respectively). Interestingly *P. aeruginosa* (NH 57388A) formed microcolonies of perfectly round spheres. The images clearly show individual bacterial cells embedded on the surface of these microcolonies, surrounded by EPS (**Fig 3.7**). Also evident (at all concentrations) were linear formations of the cells prior to microcolony formation (**Fig 3.7**). Increased concentrations of OligoG (6%) were associated with increasing cellular debris visible. Budding colonies were also seen to form extensively but not exclusively at the higher OligoG concentrations, with several images showing smaller microcolonies adjacent to the larger ones (**Fig 3.7A**, 6% OligoG). An additional distinctive morphological feature was also noted at higher OligoG concentrations namely, thin spindles jutting out at right angles to the microcolonies (**Fig 3.8**, 6% OligoG).

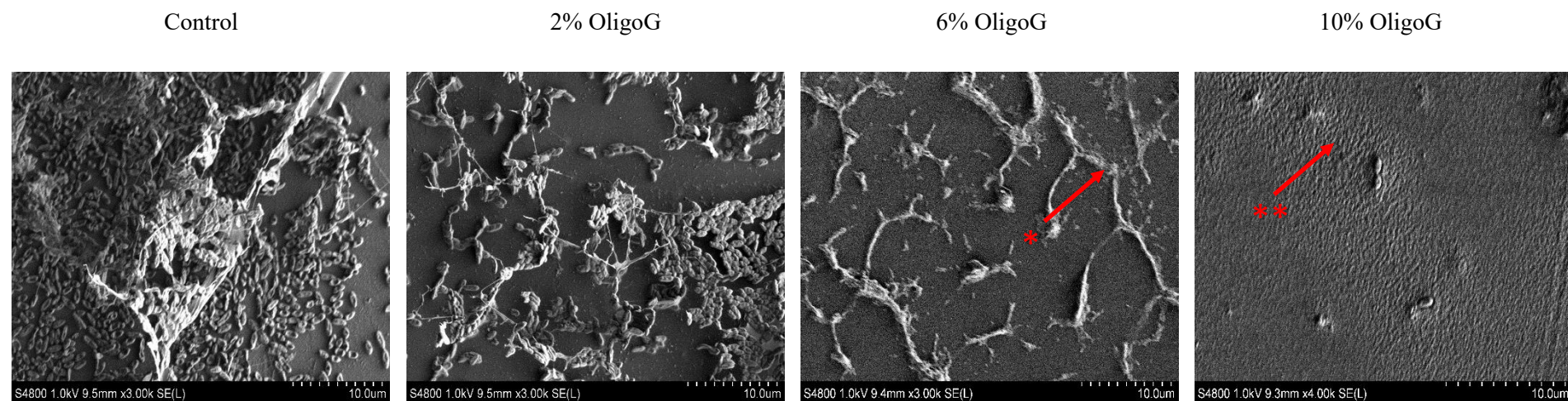


Fig 3.6: *P. aeruginosa* (NH 57388A) grown for 24 h in MH broth \pm OligoG (2%, 6% and 10%). Imaging using SEM (no gold coating). Scale bar 10 μ m. Red arrow denotes; * EPS and ** OligoG surrounding the cells.

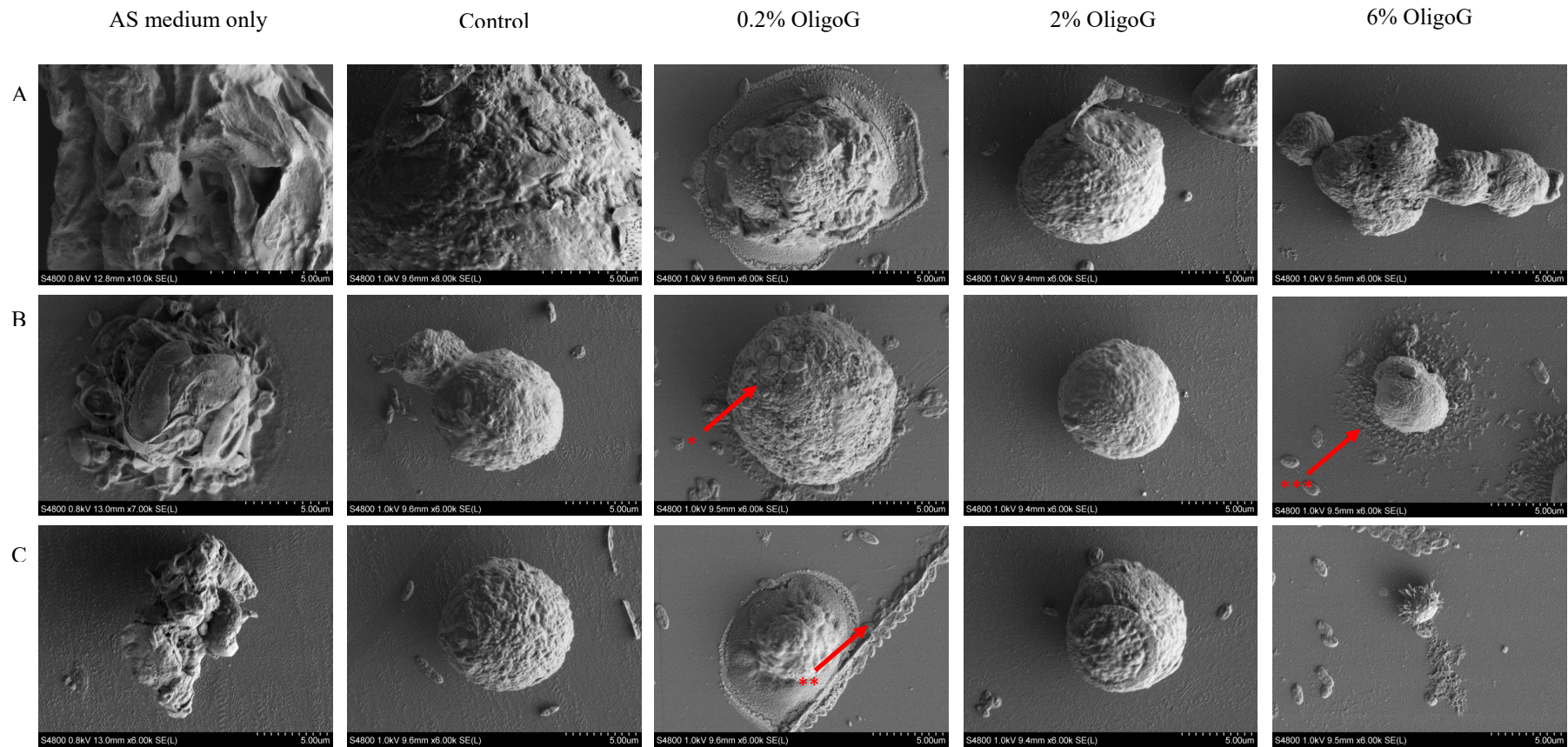


Fig 3.7: AS medium only and *P. aeruginosa* (NH 57388A) grown for 48 h in AS medium ± OligoG (0.2%, 2% and 6%), replicates A-C. Imaging using SEM (no gold coating). Scale bar 5 μ m. Red arrow denotes; * cells embedded in microcolony, ** linear cell formation and *** cellular debris.

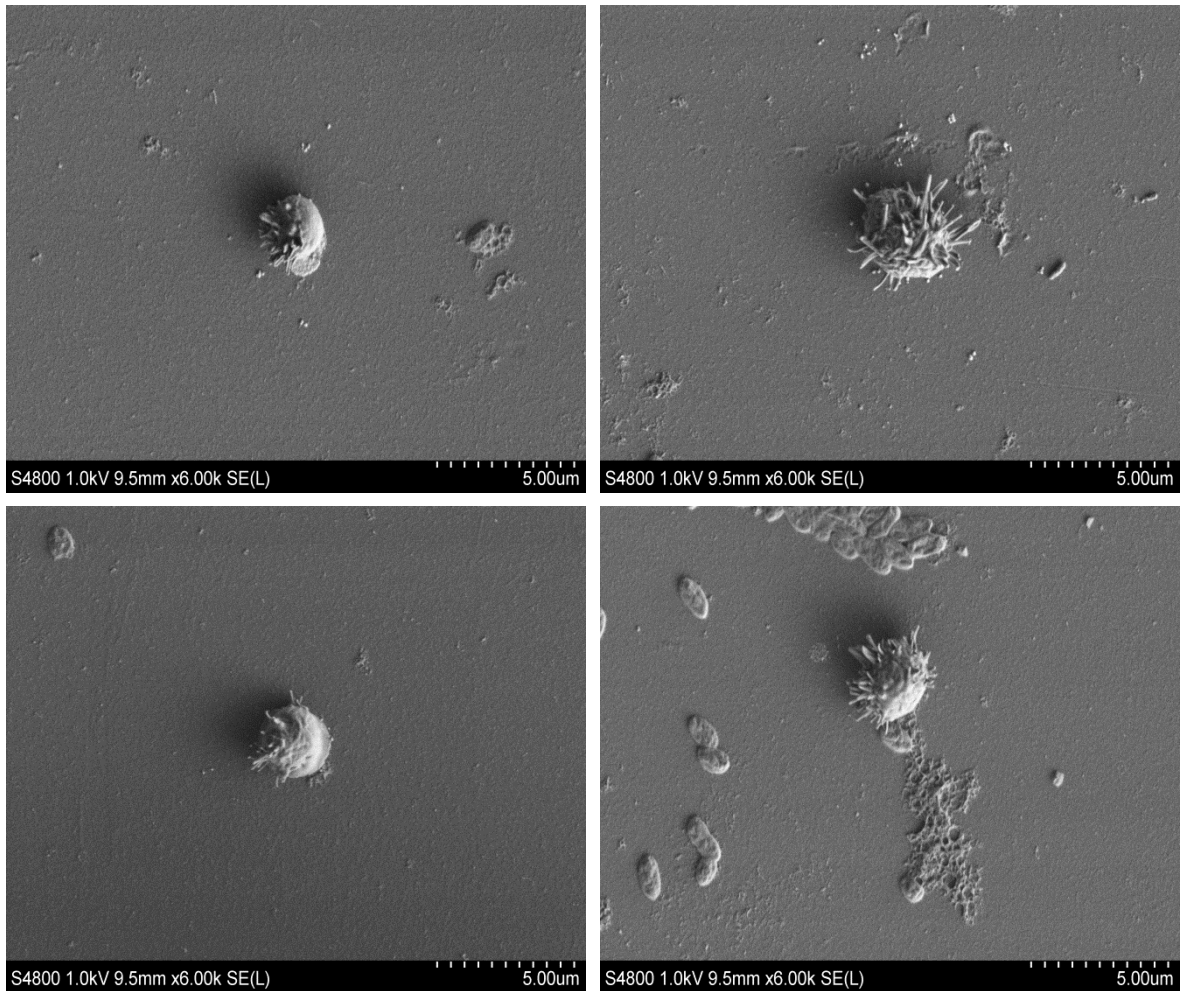


Fig 3.8: *P. aeruginosa* (NH 57388A) grown for 48 h in AS medium at OligoG 6%, showing development of thin spindles. Imaging using SEM (no gold coating). Scale bar 5 μ m.

3.4.4 Texas red-labelling of OligoG and conjugate characterisation

Optimisation of the TxRd-OligoG conjugation was performed to determine the optimum time required for reaction with EDC and sulfo-NHS. A maximum stirring time of 5 h was found to be optimal, providing the highest fluorescent output for the greatest yield. TxRd-OligoG was eluted from the PD-10 columns in a 5.5 ml volume of PBS (**Fig 3.9**). Unbound TxRd cadaverine and TxRd-OligoG was eluted through the PD-10 column at 5 mg/ml in PBS (**Fig 3.10**). To detect the percentage of free TxRd and yield of OligoG bound to TxRd, a calibration curve of TxRd cadaverine absorbance was produced using UV spectrophotometry (**Fig 3.11A**). UV spectrophotometric analysis of the TxRd-OligoG (5 mg/ml in PBS) showed peak absorbance at 589 nm, which was equivalent to 0.5145 A.U. (**Fig 3.11B**).

It could therefore be concluded that the purified TxRd-OligoG produced in these experiments contained < 1% free TxRd and 0.86 μg TxRd/ mg TxRd-OligoG (1 TxRd: 306.5 OligoG molecules). The yield of TxRd-OligoG was low, and this therefore limited the range of concentrations that could be used in subsequent experiments.

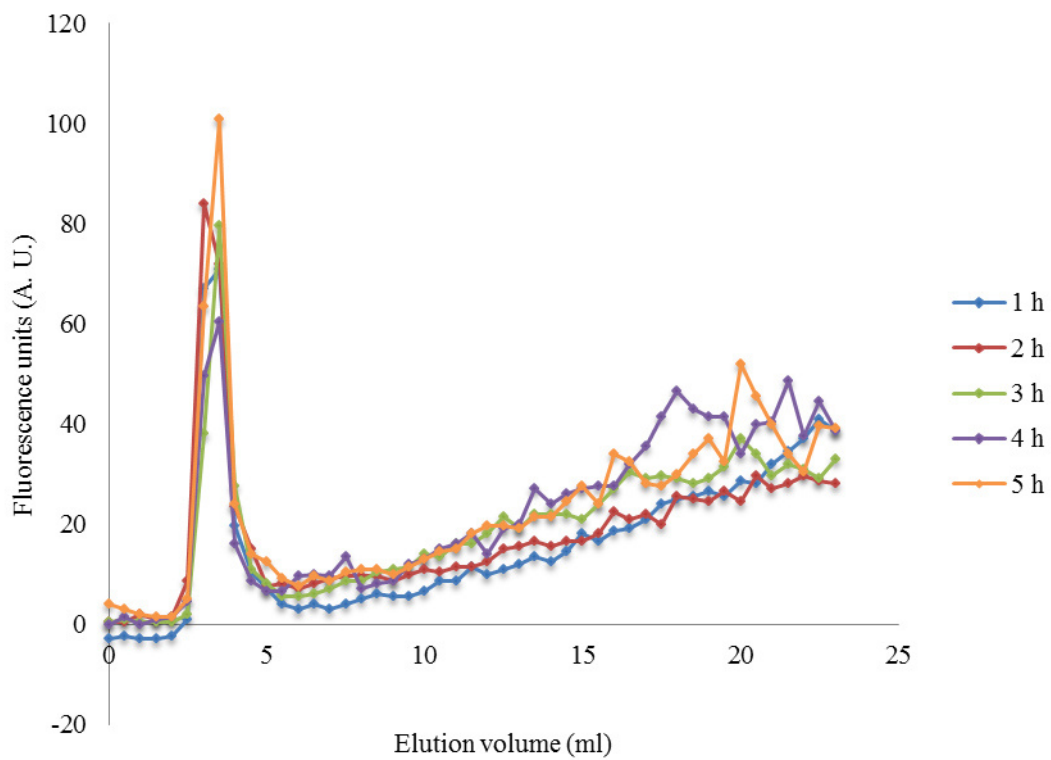


Fig 3.9: Evaluation of the effect of reaction time on reaction yield and purity of TxRd-OligoG using a PD-10 column.

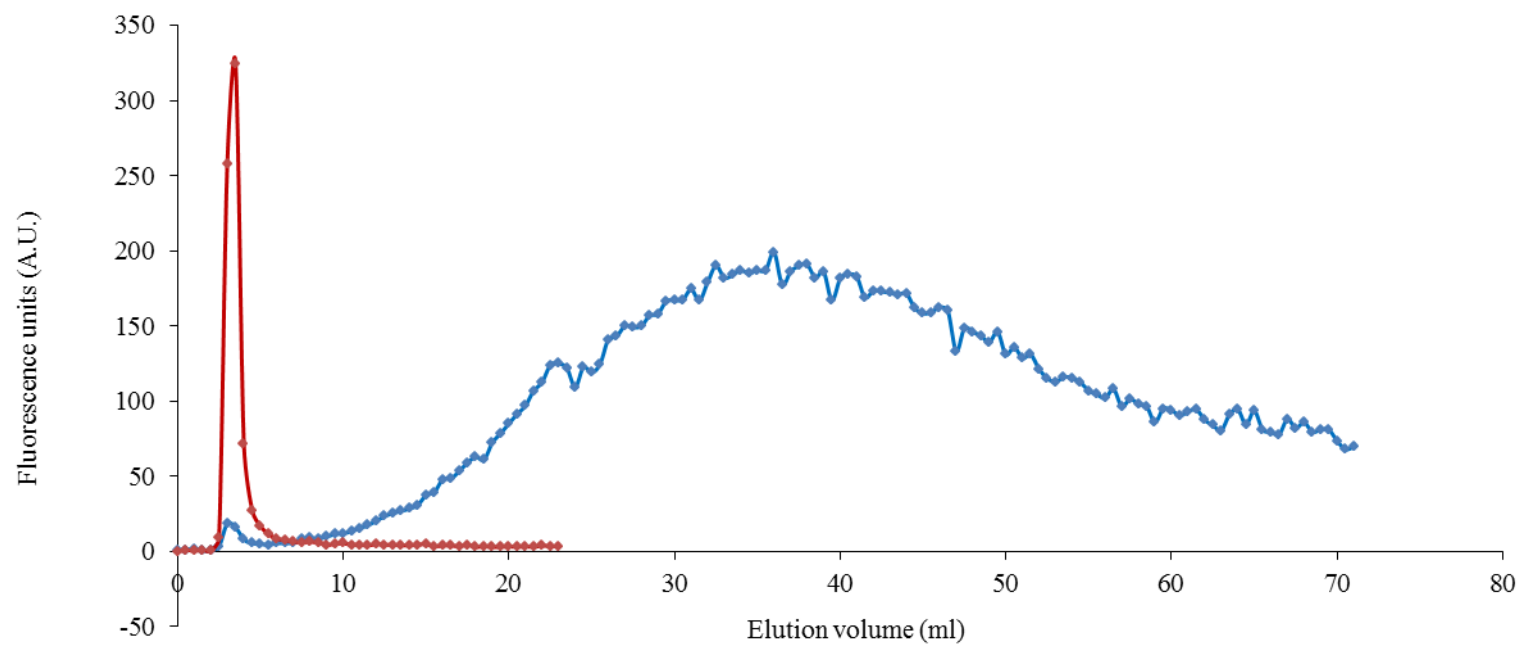


Fig 3.10: Evaluation of reaction yield and purity of TxRd-OligoG conjugates using a PD-10 column. Elution profile of free TxRd (blue solid line; 5 mg/ml in PBS) and TxRd-OligoG (red solid line; 5 mg/ml in PBS).

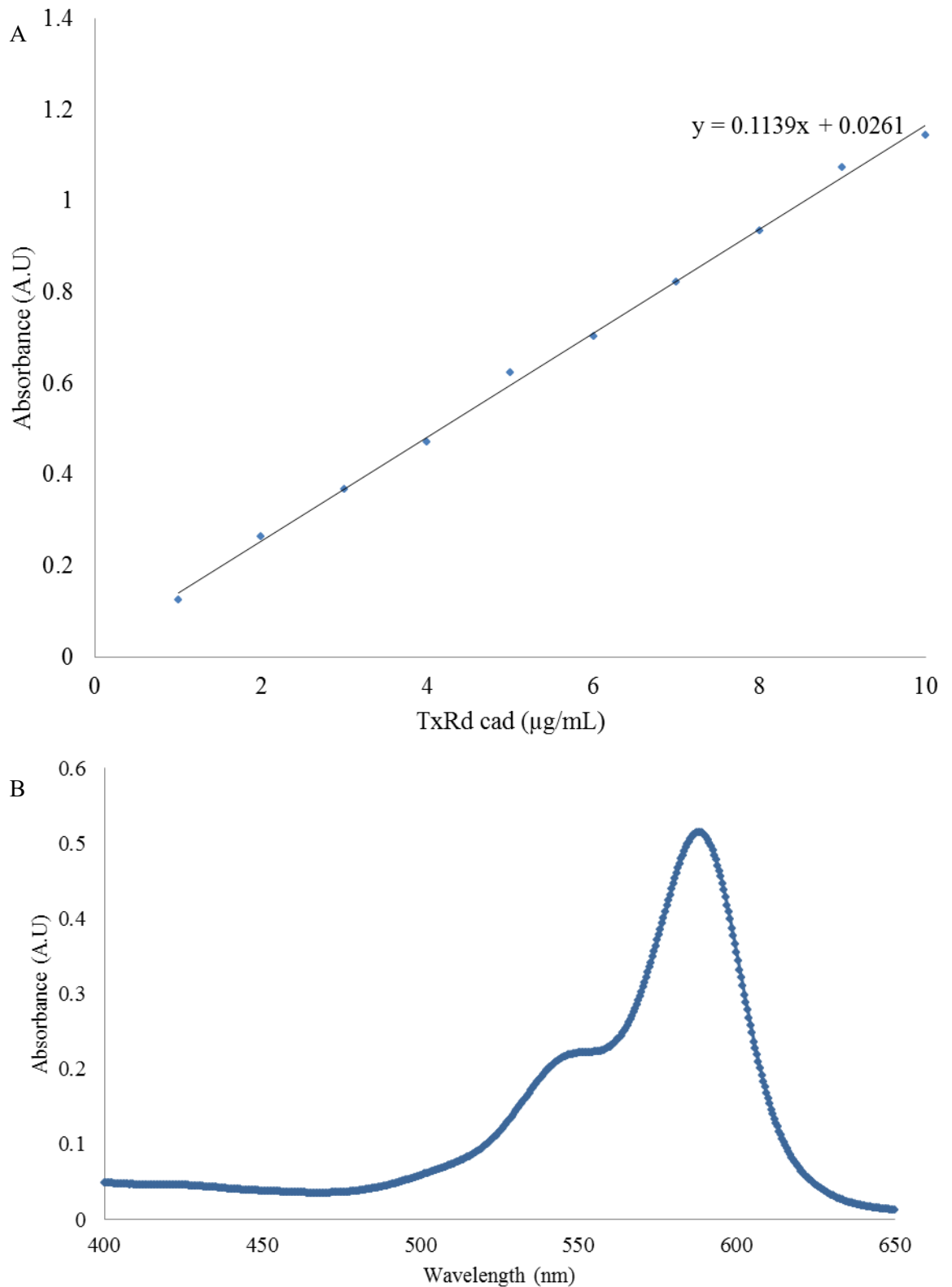


Fig 3.11: A) Calibration curve for TxRd absorbance (1-10 $\mu\text{g}/\text{ml}$) at wavelength 589 nm; B) Spectrophotometric analysis of TxRd-OligoG (5 mg/ml in PBS).

3.4.5 Effect of varying concentration and pH on Texas Red cadaverine fluorescence

The fluorescence had a linear relationship in relation to the concentration of TxRd, which was seen at all pHs. The fluorescence did not vary between pH 5 and pH 7, but there was a slight decrease in fluorescence as the pH increased to pH 9 (**Fig 3.12**).

3.4.6 Effect of texas red-labelled OligoG as a treatment to inhibit biofilm formation

CLSM images (x400 magnification) showed that the biofilm inhibition properties of TxRd-OligoG were comparable to those of the un-labelled OligoG. In both cases, the biofilm was less well formed at higher TxRd-OligoG concentrations with a significant decrease in biofilm depth (**Fig 3.13**). Furthermore, at higher magnification (x600), areas of red fluorescence (TxRd-OligoG) were evident and these increased with higher TxRd-OligoG concentrations (**Fig 3.14**). From the side view images showing biofilm depth, the TxRd-OligoG was visible throughout the entire depth of the biofilm, even at concentrations as low as 0.5% TxRd-OligoG.

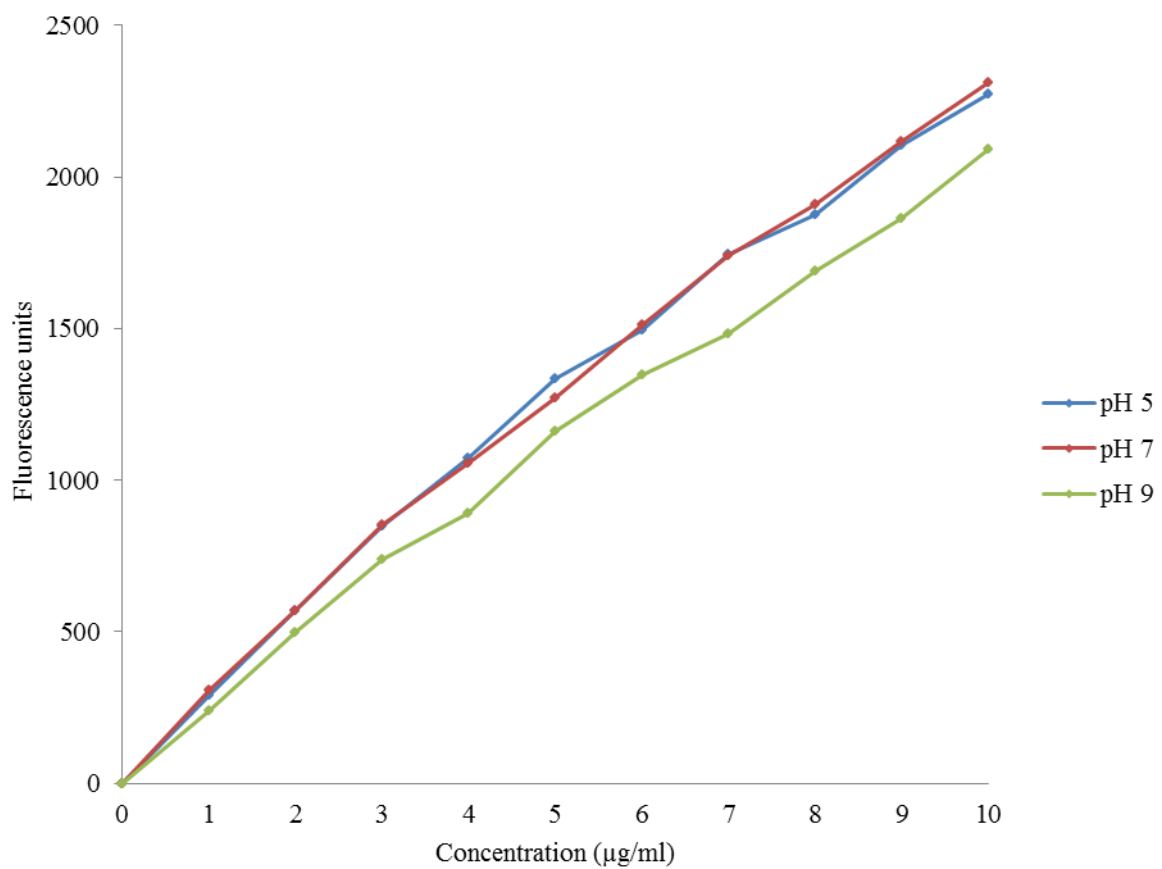


Fig 3.12: Effect of concentration and pH changes on the fluorescence of TxRd cadaverine.

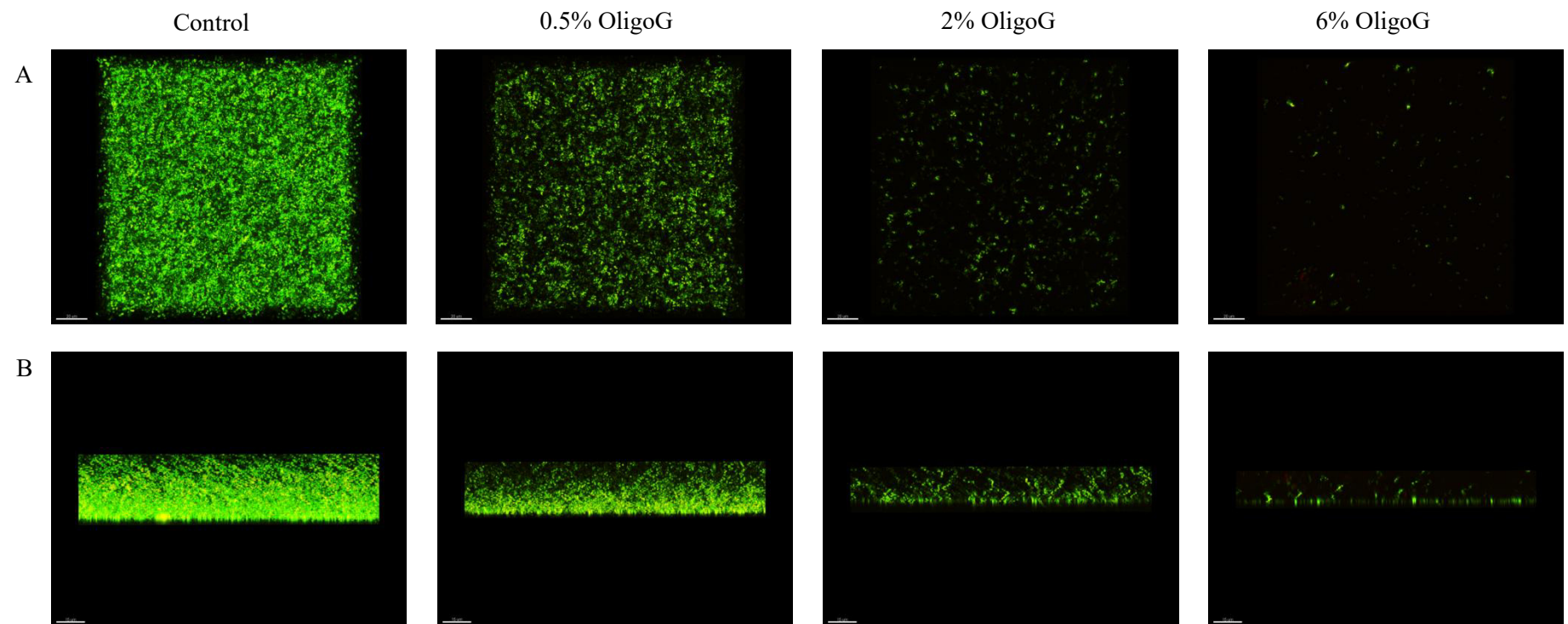


Fig 3.13: *P. aeruginosa* (NH 57388A) grown for 24 h in MH broth \pm TxRd-OligoG (0.5%, 2% and 6%). Imaged with SYTO[®] 9 stain using CLSM (x400 magnification). A) Aerial view; B) side view (biofilm depth).

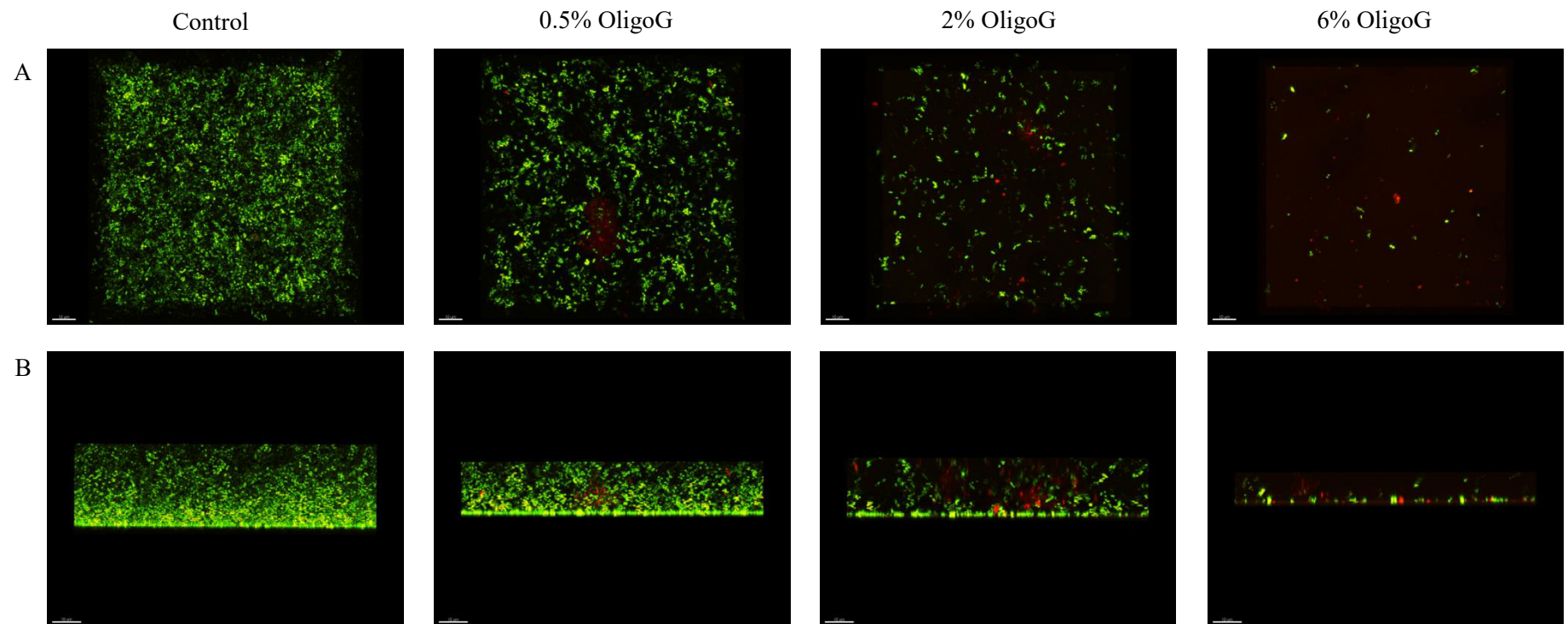


Fig 3.14: *P. aeruginosa* (NH 57388A) grown for 24 h in MH broth \pm TxRd-OligoG (0.5%, 2% and 6%). Imaged with SYTO[®] 9 stain using CLSM (x 60 magnification). A) Aerial view; B) side view (biofilm depth).

3.4.7 Effect of texas red-labelled OligoG as a treatment to disrupt an established biofilm

TxRd-OligoG treatment of an established *P. aeruginosa* (NH 57388A) grown for 24 h displayed comparable results to that of the un-labelled OligoG. As seen previously, 1 h of treatment with TxRd-OligoG showed no disruption of the biofilm, which was thin and compact in nature (**Fig 3.15**). Following 4 h of incubation with TxRd-OligoG there was no difference visible on the established biofilm (**Fig 3.16**), with both the treated and control biofilms appearing to have a more abundant growth after this treatment period. However, in accordance with the un-labelled OligoG, substantial disruption of the biofilm in a dose-dependent manner (0-6%) after 24 h of treatment with TxRd-OligoG was observed. In addition, TxRd (red colouration) was visible throughout the full depth of the disrupted biofilm, particularly at the highest concentration of (6%) OligoG (**Fig 3.17**).

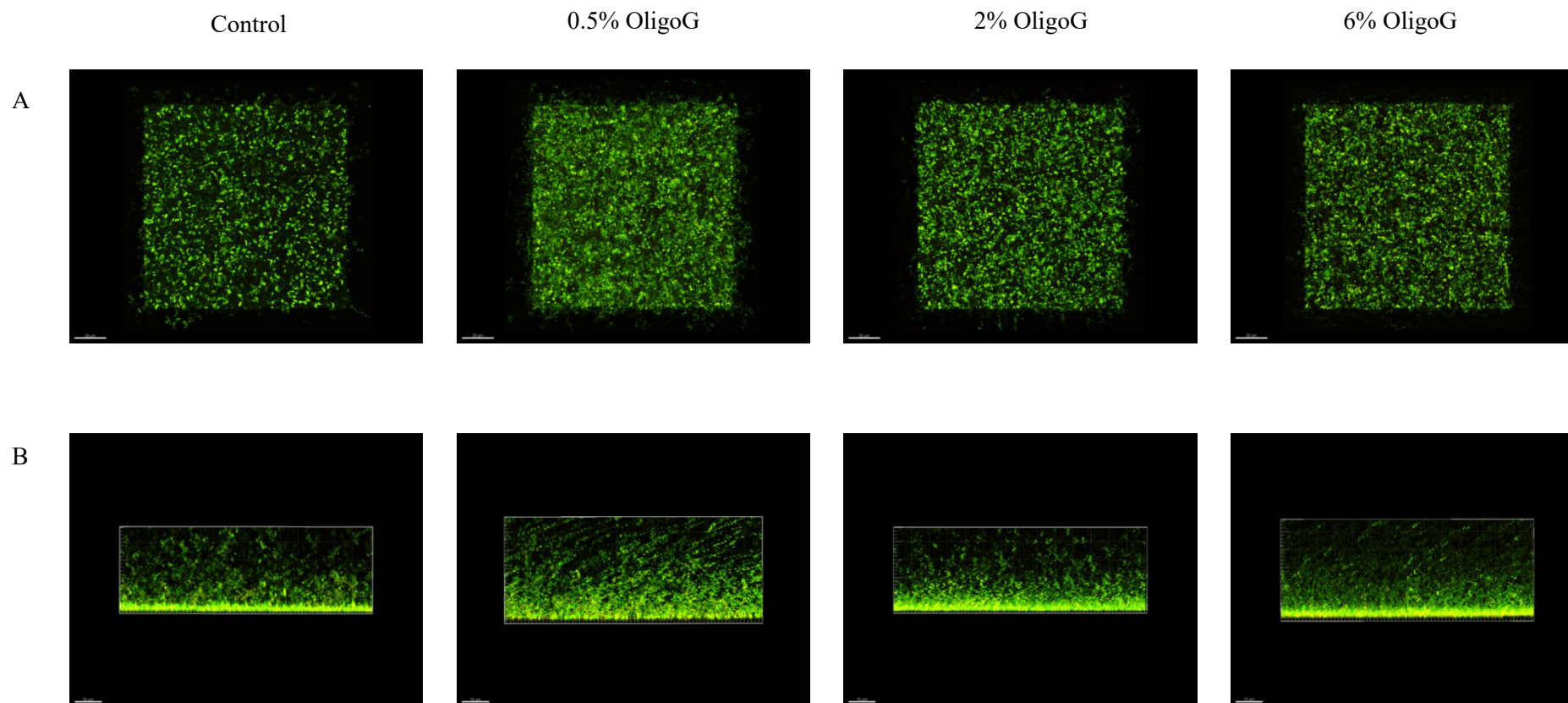


Fig 3.15: *P. aeruginosa* (NH 57388A) grown for 24 h in MH broth, followed by 1 h treatment of TxRd-OligoG (0.5%, 2% and 6%). Imaged with SYTO[®] 9 stain using CLSM (x600 magnification). A) Aerial view; B) side view (biofilm depth).

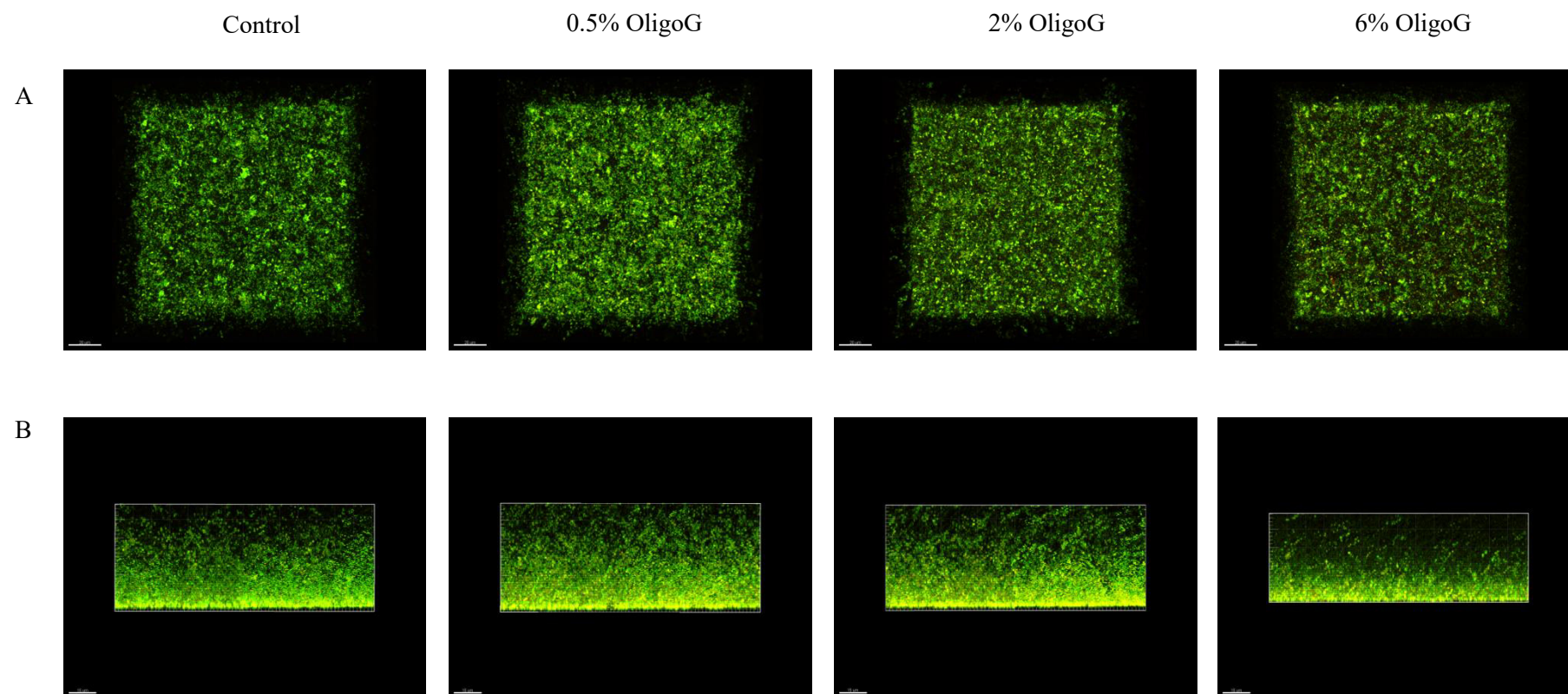


Fig 3.16: *P. aeruginosa* (NH 57388A) grown for 24 h in MH broth, followed by 4 h treatment of TxRd-OligoG (0.5%, 2% and 6%). Imaged with SYTO[®] 9 stain using CLSM (x600 magnification). A) Aerial view; B) side view (biofilm depth).

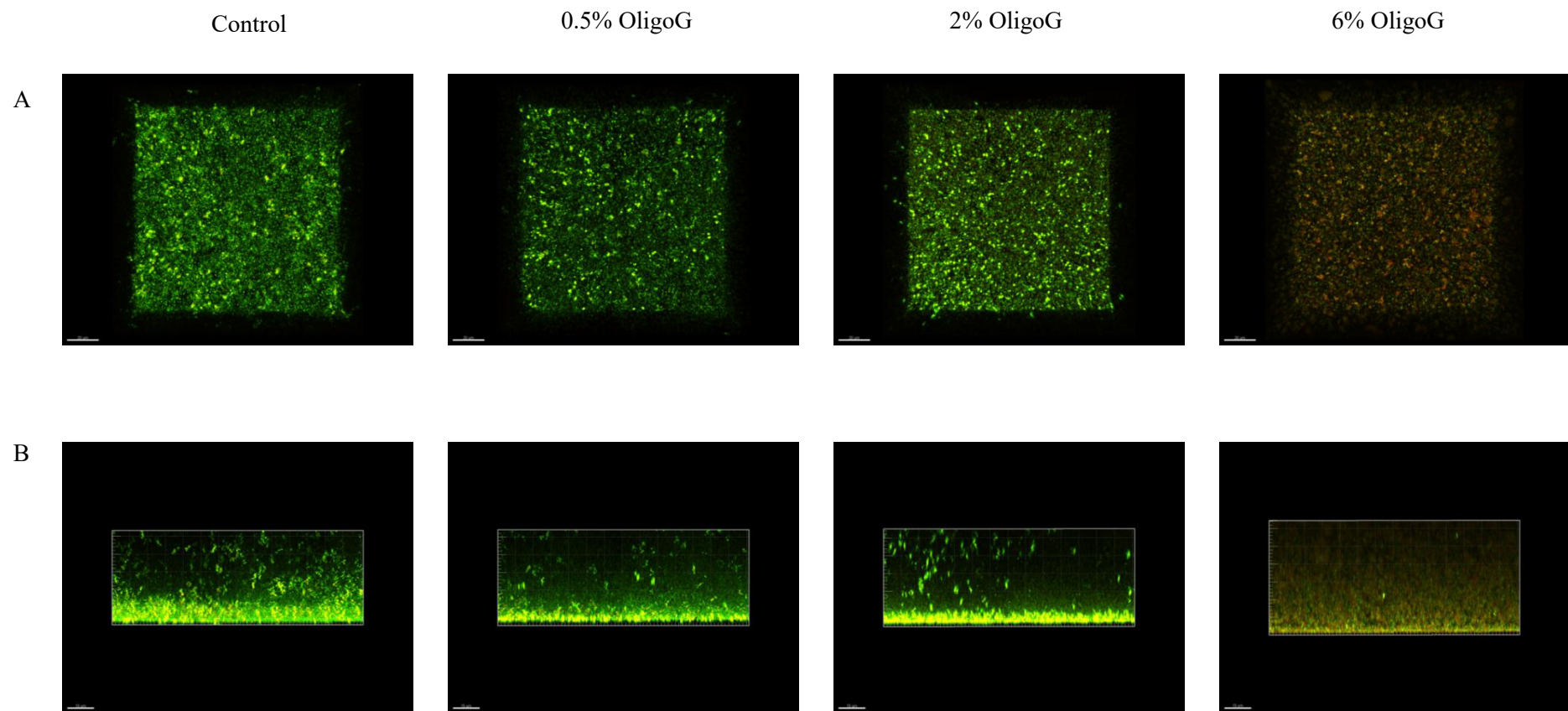


Fig 3.17: *P. aeruginosa* (NH 57388A) grown for 24 h in MH broth, followed by 24 h treatment of TxRd-OligoG (0.5%, 2% and 6%). Imaged with SYTO[®] 9 stain using CLSM (x600 magnification). A) Aerial view; B) side view (biofilm depth).

3.4.7.1 Effect of texas red-labelled OligoG as a treatment to disrupt an established biofilm: z-stack analysis

Analysis of the biofilm supernatant showed that no free TxRd was present (**Fig 3.18**), since TxRd only was found to increase in fluorescence at >5.5 ml elution in a PD-10 column (**Fig 3.10**), a trend not seen in these graphs. Interestingly, analysis of the supernatant from the 24 h treated biofilm with TxRd-OligoG showed a broader peak that eluted slightly later than the original TxRd-OligoG, suggesting that the OligoG chains had reduced in size during incubation with the biofilms. This was evident from the increase in surface area under each graph (expressed as percentage area >5.5 ml elution which was shown to increase as the incubation time of TxRd-OligoG increased; **Table 3.1**).

When investigating the biofilm structure of the different z-stacks, a halo of redness was clearly evident surrounding the bacterial cells at concentrations of TxRd-OligoG (6%) during both 4 h and 24 h treatment periods. This was evident throughout the biofilm depth (**Fig 3.19**). No statistical analysis was carried out on the biofilm surface area coverage values for TxRd-OligoG experiments since its anti-biofilm action may have been altered by conjugation.

3.4.7.2 Effect of a Texas red cadaverine only control as a treatment to disrupt an established biofilm

No biofilm disruption was observed following use of a “free” TxRd cadaverine control at 4 h or 24 h of treatment (**Fig 3.20**). However, when investigating the biofilm structure through the different z-stacks, it was evident that free TxRd cadaverine formed a halo effect around each bacterial cell, (**Fig 3.21**) as was seen with the TxRd-OligoG treatment, at both 4 h and 24 h (**Fig 3.19**).

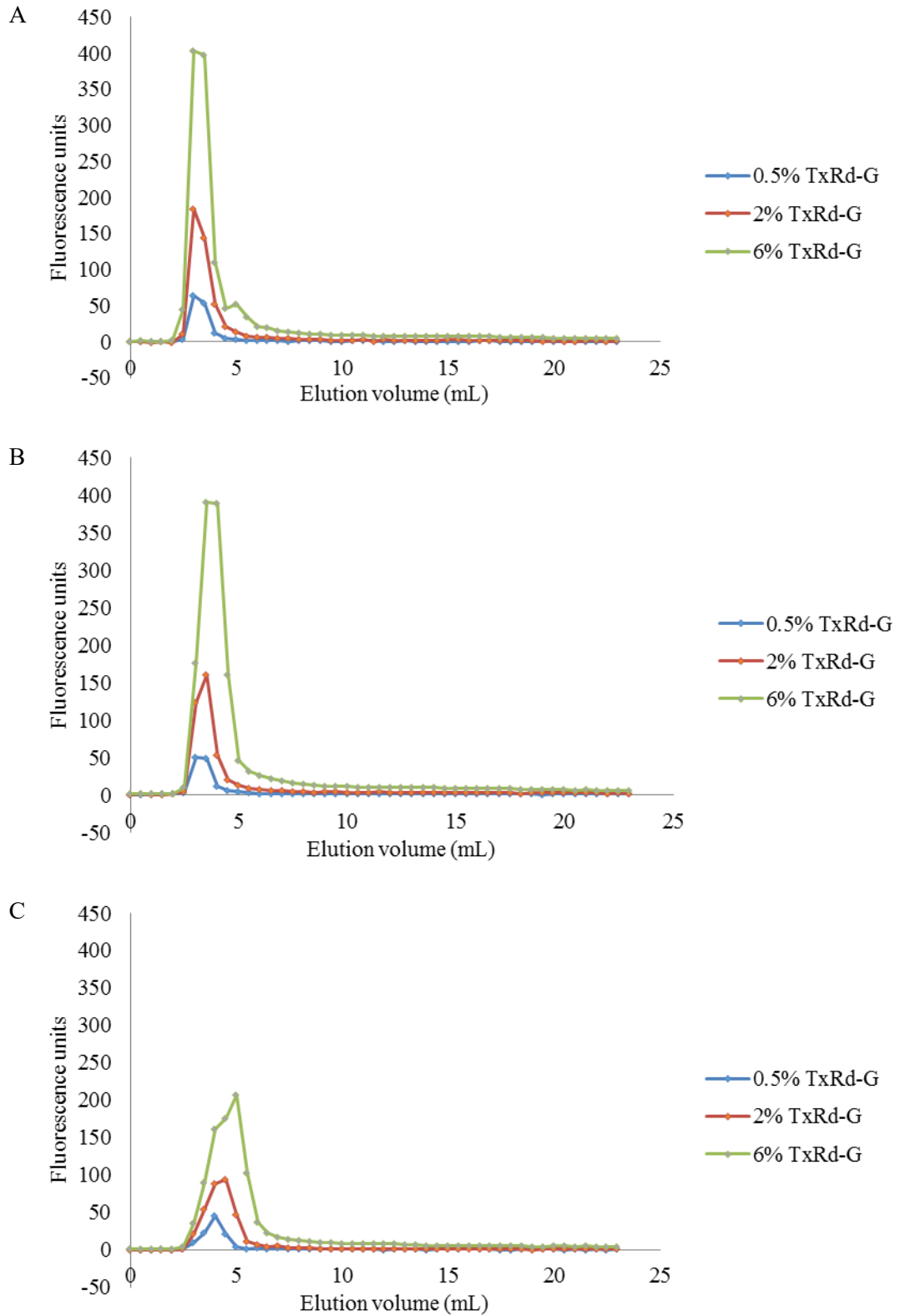


Fig 3.18: Quantification of TxRd-OligoG (TxRd-G) and unbound TxRd using PD-10 column analysis of supernatant from *P. aeruginosa* (NH 57388A) biofilms grown for 24 h in MH broth, followed by A) 1 h; B) 4 h and C) 24 h treatment with TxRd-OligoG (0.5%, 2% or 6%).

Table 3.1: Quantification of percentage surface area under graph at elution >5.5 ml under PD-10 analysis of supernatant (**Fig 3.18**).

TxRd-OligoG conc.	Percentage surface area under the graph at elution >5.5 ml following different incubation times (hours) with TxRd-OligoG		
	1 h	4 h	24 h
0.5%	13.5%	21.6%	22.1%
2%	14.5%	21.6%	14.7%
6%	22.0%	23.1%	31.7%

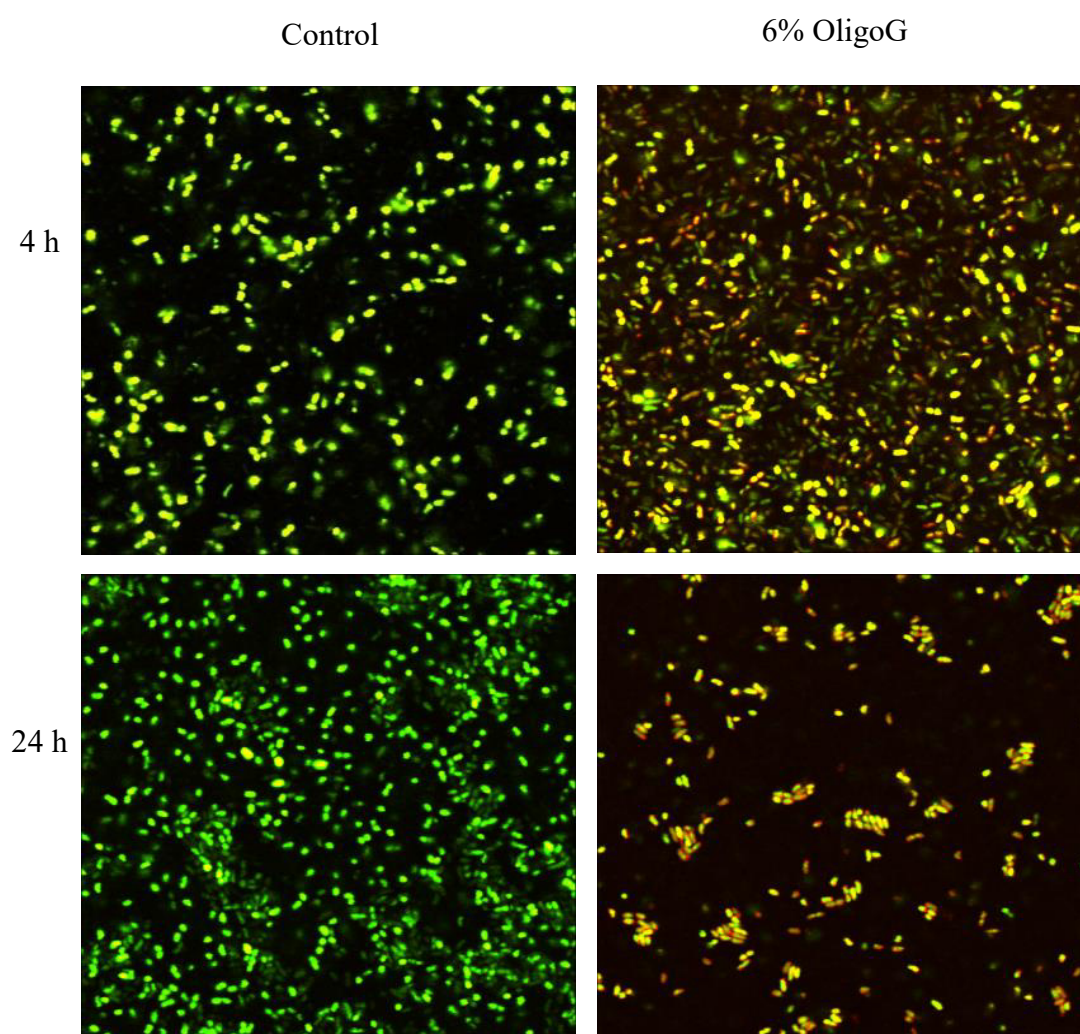


Fig 3.19: *P. aeruginosa* (NH 57388A) grown for 24 h in MH broth, followed by 4 h or 24 h treatment (MH broth control or 6% TxRd-OligoG). Imaged with SYTO[®] 9 stain using CLSM (x600 magnification, zoom x3.5).

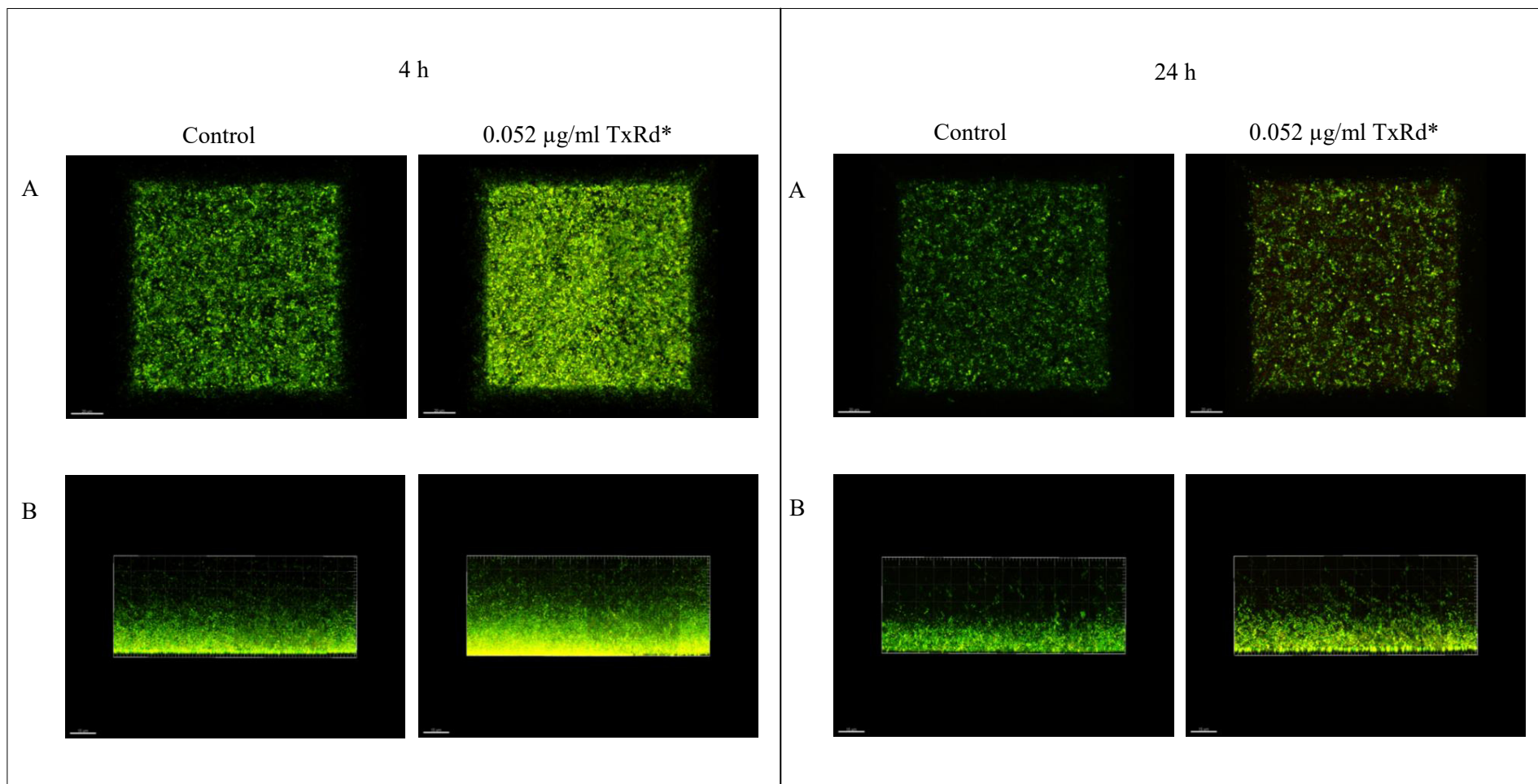


Fig 3.20: *P. aeruginosa* (NH 57388A) grown for 24 h in MH broth, followed by 4 h or 24 h treatment (MH broth control or TxRd control 0.052 µg/ml [*equivalent to 6% TxRd-OligoG conjugate]). Imaged with SYTO[®] 9 stain using CLSM (x600 magnifications). A) Aerial view; B) side view (biofilm depth).

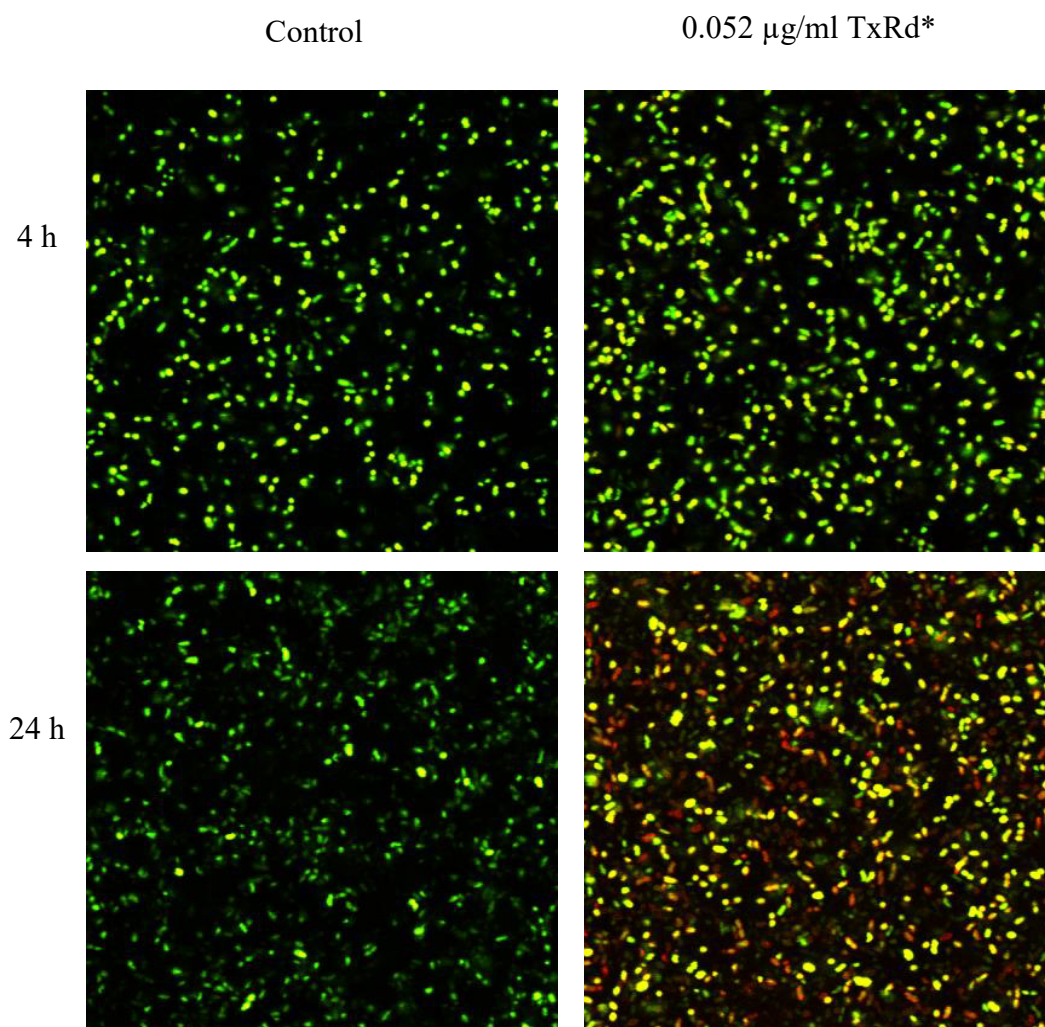


Fig 3.21: *P. aeruginosa* (NH 57388A) grown for 24 h in MH broth, followed by 4 h or 24 h treatment (MH broth control or TxRd control 0.052 $\mu\text{g/ml}$ [*equivalent to 6% TxRd-OligoG conjugate]). Imaged with SYTO[®] 9 stain using CLSM (x600 magnification, zoom x3.5).

3.5 Discussion

This chapter shows that OligoG possess important properties to both inhibit and disrupt *P. aeruginosa* biofilms. Its ability to provide inhibitory and disruptive functions was assessed against a mucoid *P. aeruginosa* strain isolated from the sputum of a chronically colonised CF patient. Several other synthetic compounds that both inhibit and disrupt biofilm formation have previously been investigated such as iron chelators used as adjunct therapy in the chronically infected lung (O'May et al., 2009), the surfactant polysorbate 80 (Toutain-Kidd et al., 2009) and a silver nano-coating for dental applications (Besinis et al., 2014).

Asymptomatic colonisation of CF lungs is often by non-mucoid strains of *P. aeruginosa*. Ultimately however, emergence of a mucoid form during chronic debilitating pulmonary infection typically occurs (Govan and Deretic, 1996). Conversion to the mucoid phenotype is often a response to the unique CF environment (Pritt et al., 2007). There is no defined interval between initial colonisation and the transition to the mucoid form, but emergence of a mucoid phenotype leads to its selection and dominance in the CF lung (Govan and Deretic, 1996). OligoG has previously been shown to disrupt the biofilm of the non-mucoid *P. aeruginosa* strain PAO1 (Khan et al., 2012). A similar dose-dependent effect of OligoG on mucoid strains in relation to biofilm assembly, biofilm inhibition and disruption, would be a distinct advantage for the CF patient.

Disruption of mucoid strains of *P. aeruginosa* is of particular importance in CF since, not only does the presence of mucoid colonies of *P. aeruginosa* indicate a poor prognosis for the patient (Sriramulu et al., 2005), but the mucoid phenotype confers greater resistance to antibiotic treatment (Waine et al., 2008). The mucoid matrix aids formation of protected biofilm microcolonies, thereby increasing resistance to opsonisation, phagocytosis, digestion and provides protection from dehydration for the bacterial cells (Pritt et al., 2007). Mucoid pseudomonal strains can be isolated in 90% of CF patients and are a typical feature of the disease, as other human infections, plants or animals are rarely colonised by it. Mucoid *P. aeruginosa* can, however, be found in non-CF patients such those with chronic bronchitis. *P. aeruginosa* colonises the CF lung following a history of general bacterial colonisation, antibiotic therapy and viral infections (Govan and Deretic, 1996). The

inhibition of biofilm growth in the presence of OligoG was evident in a dose-dependent manner, as well as producing a reduction in biofilm depth on the developing biofilms for up to 24 h. The potential ability of OligoG to disrupt mucoidal *P. aeruginosa* may be extremely useful in CF and other chronic lung diseases, as biofilm disruption may allow effective antibiotic doses to reach the diseased lung.

Mucoid pseudomonal strains synthesise large quantities of alginate exopolysaccharide due to genes such as *algD* (Pritt et al., 2007). Interestingly, the alginates derived from mucoid *P. aeruginosa* have already been a target for anti-biofilm therapies (Li et al., 2008). It is thought that OligoG may compete with these high MW alginates (Sletmoen et al., 2012) and prevent the cross-linking with mucin thereby reducing assembly and formation of a highly resistant EPS matrix. Other alginates have already been discovered from marine algae, e.g. A101, which not only inhibits the biofilm formation of many bacteria, but also disrupts the established biofilms of certain strains (Jiang et al., 2011). It has also previously been found that co-administration of rhDNase I and *algL* enhanced their activity, reducing both biofilm growth and sputum bacterial counts (Alipour et al., 2009) as well as increasing the efficacy of antibiotics (Alkawash et al., 2006). This work relates directly to the research with OligoG, suggesting that OligoG could also have enhanced (synergistic) efficacy if used in combination with rhDNase I as an *in vivo* CF therapy.

The AS medium utilised in this work was adapted from earlier studies (Sriramulu et al., 2005, Russo et al., 2013, Kirchner et al., 2012). The AS medium model has previously been used to aid understanding of how sub-inhibitory concentrations of specific antibiotics help to drive phenotypic diversity in *P. aeruginosa* populations (Wright et al., 2013). AS medium was used to study the potential biofilm inhibition of OligoG in a more clinically-relevant environment, although the model is limited by having only key components present. It is a given that the AS medium used here is not entirely representative of sputum in the CF lung particularly as other biologically active components present as nutrients were omitted, such as lactoferrin and oligopeptides. Therefore, AS medium does not resemble the acute phase of infection but rather, is more representative of the disease state with an established colonisation of *P. aeruginosa* (Sriramulu et al., 2005). SEM

imaging of AS medium alone showed a larger, more open porous structure, this may aid bacterial attachment and aid biofilm formation.

The microcolonies observed in this study have also been noted *in vivo*. Animal studies infecting healthy rats with a mucoid strain of *P. aeruginosa* to induce pulmonary infections via the “agar-bead” method, have shown intact Gram-negative bacteria enclosed with cell fragments within microcolonies which were morphologically similar to those found in the bronchial mucus of CF patients (Lam et al., 1980). Pseudomonal growth within the CF lung naturally selects for variants that produce large amounts of EPS. The bacteria in the CF lung are enclosed in this EPS which appears to drive microcolony formation.

In the early stages of *P. aeruginosa* lung infection, the bacteria readily form spherical micro- or macro-colonies, resembling biofilms, the only exception being that the bacteria are attached together and not to the surface (Haley et al., 2012, Fung et al., 2010). Previous pseudomonal growth in AS medium also demonstrated macroscopically visible “clumps” which could not be disrupted even by vigorous physical means (Sriramulu et al., 2005). In the AS medium, almost no planktonic cells were evident and cells were not attached to the polystyrene and glass surfaces. Similarly, structurally tight microcolony formation has been shown to form with a range of other *P. aeruginosa* isolates including CF epidemic and non-epidemic strains (Fung et al., 2010). The SEM study with AS medium confirmed the lack of attachment to the polystyrene surface, leading to the formation of distinct microcolonies. Unlike other studies, individual cells could be clearly seen, but this may have been associated with the ‘young’ age of the biofilms being studied. From previous studies, it has been shown that the total surface area exposed to nutrients and surface roughness coefficient values were significantly reduced when grown in AS medium (Haley et al., 2012). When the medium was replenished, new microcolonies appeared on the surface of the underlying growth, or formed detaching segments from the biofilm mass (Haley et al., 2012, Sriramulu et al., 2005). Similar observations could also be made in many of the OligoG samples, with an increasing quantity of detached segments produced as the concentration of OligoG increased. This may reflect the stressed environment created by OligoG with increased branching of biofilms from the spherical microcolonies.

At higher OligoG concentrations (>2%), the SEM images of *P. aeruginosa* (NH 57388A) grown in AS medium possessed microcolonies which produced “wiry spindles” protruding radially from the central core. It is unclear exactly what these were, but they may be mucin strands or potentially elongated bacterial cells which have arisen due to the reduced nutrient environment (Steinberger et al., 2002). Such cell elongation has also previously been linked to defective cell division (Yoon et al., 2011).

Image J analysis has been widely employed to compare digital images (Ghosh et al., 2004, Collins et al., 2002, Bruton et al., 2003) including those of biofilms (Hope and Wilson, 2004, Thomas et al., 2008, Villena et al., 2010). Automated image analysis reduces bias (to a marked extent) and facilitates analysis of images generated during high-throughput screening (Schindelin et al., 2012). Image J was utilised here to confirm the decrease in biofilm coverage that occurred in OligoG-treated samples was statistically significant.

Fluorescent-labelling is associated with technical problems, including dye-membrane interactions, a lack of specificity and dye-bleaching (Zanetti-Domingues et al., 2013). In the choice of a fluorescent dye, features such as photo-stability and brightness need to be measured against specificity of interaction (Zanetti-Domingues et al., 2013). No clear trend or factor can reliably predict the level of membrane-dye interaction for a given dye in a particular model (Hughes et al., 2014). These only become evident after laboratory experimentation. In these experiments, binding of TxRd-OligoG to the bacterial cell wall was apparent. Fluorescently-labelled molecules need to be characterised in terms of bound and free fluorescent marker. Potential release of free fluorophore from OligoG was eliminated as a problem, as analysis of the supernatant after incubation with the biofilm confirmed the TxRd-OligoG remained intact, potentially reflecting the TxRd itself binding non-specifically to the cell wall. The labelled OligoG retained its biofilm inhibition and disruption properties, as the TxRd only control confirmed that the biofilm disruption in the TxRd-OligoG samples was due to OligoG alone. However, localisation of OligoG within the biofilm could not be confirmed, since free TxRd also showed binding to the biofilm, albeit without conferring any anti-biofilm properties.

Fluorescent probes aid several optical techniques, but further challenges of conjugation arise as it cannot be assumed that the fluorophore itself does not alter the

properties of the sample in some way. Fluorescent imaging has been extensively employed in bacterial analysis (Moore et al., 1986). Organic fluorophores are ubiquitous tags for a range of biological targets, and many have been studied in systems that contain membrane lipids (Hughes et al., 2014). Previous studies have found that fluorescent probes significantly impacted the properties of a lipid bilayer, even at low concentrations (Skaug et al., 2011). Interaction between dyes and lipid bilayers can lead to several complications. For example, if the dye is conjugated to a biological target, it could potentially alter the target's interaction with lipid bilayers (Hughes et al., 2014). Dansyl-polymyxin is a fluorescent derivative of polymyxin B, which shows a 20-fold increase in fluorescence after binding to lipopolysaccharide (Moore et al., 1986). Due to the positively-charged amino group of TxRd cadaverine, it is likely that this molecule has a high affinity for the negatively-charged bacterial cell wall of the studied *P. aeruginosa*, and it is this that has likely caused it to form the homogenous 'red' halo observed around the cells.

Clear bottom black 96-well plates were used to grow the biofilms, allowing minimal preparation and disruption of the biofilms prior to live imaging (Richardson et al., 2008). Misinterpretation of images can also occur in probes that show pH- and concentration-dependence of the fluorescent output (Seib et al., 2007) which could induce pH- or concentration-dependent fluorescent quenching of the fluorophore (Seib et al., 2007). Previous studies have shown alteration in fluorescence with a change in pH when investigating OG conjugates (Seib et al., 2007). Treatment of the samples with OligoG did not alter the pH, therefore leaving the fluorescent output unaffected. Indeed, TxRd was shown to be unaltered at both pH 5 and 7. Concentration-dependent quenching has also been reported in previous studies using doxorubicin, which produced a bell-shaped curve of fluorescence (Seib et al., 2006), which remained independent of pH. The linear relationship seen with increasing concentration of TxRd cadaverine confirmed no concentration dependent quenching of the fluorophore had occurred.

3.6 Conclusion

OligoG was shown to have inhibitory and disruptive properties against biofilms of a mucoid *P. aeruginosa* strain isolated from CF sputum. This effect was maintained when also grown in the less nutritious AS medium, showing that OligoG could have utility and efficacy against the *in vivo* CF condition. TxRd-OligoG maintained the biofilm inhibition and disruption properties of the unlabelled OligoG, but failed to provide reliable data for the localisation of OligoG within the biofilm due to the affinity of TxRd for the bacterial cell wall.

Chapter 4:
Characterisation of mucin interactions
with OligoG

4.1 Introduction

Mucosal tissues account for the route or site of infection for most viruses, bacteria, yeast, protozoa and multicellular parasites (Linden et al., 2008). Mucosal epithelial tissues have adapted innate responses to these pathogens (Kagnoff and Eckmann, 1997). Important components of the innate immune system are mucins which form a physical barrier against chemical, enzymatic and mechanical insults and provide a “first line” defence against pathogens (Kagnoff and Eckmann, 1997).

Whilst important in defence, mucin barriers may impede drug delivery to the lung since inhaled agents bind to the mucins and are removed by mucociliary clearance (Widdicombe, 1997). Methods to disrupt these muco-adhesive interactions allowing crossing of the mucin-protective layer of the lung would greatly improve drug delivery to this site (Bansil and Turner, 2006). Although mucin-alginate interactions have been documented in the literature (Sletmoen et al., 2012, Nordgard and Draget, 2011, Nordgard et al., 2014), a greater understanding of the interplay of OligoG with mucin within sputum samples, needs to be investigated.

4.1.1 Mucin

Mucins are produced in the goblet cells and glycosylation occurs through the endoplasmic reticulum and golgi complex. Mucin oligomers are condensed in secretory granules prior to exocytosis and once released, rapidly assemble into a cross-linked network (King and Rubin, 2002). Rapid hydration of mucins occurs once they reach the epithelial surface, becoming 95% water by weight (Taylor et al., 2005a). Each mucin polymer is composed of a single subunit type, consisting of a protein backbone encoded by various genes. Mucins possess a large tandem repeat region which contains proline and is rich in serine and/or threonine residues known as apomucins (Lewis et al., 2013b). Apomucins are the site of *O*-glycosylation (Rose and Voynow, 2006) forming the typical bottle brush structure; **Fig 1.9** (Taylor et al., 2005a). The one structural element shared by all mucins is the attachment to the peptide by *O*-glycosidic linkages between *N*-acetylgalactosamine (GalNAc) and the apomucins (Lamblin et al., 2001). *O*-glycosylation requires an *N*-acetylgalactosaminyl peptidyltransferase and one or more glycosyltransferases depending on the final *O*- glycan structure (Rose and Voynow, 2006). The

glycosylation of proteins involves a stepwise progression of covalent attachments of oligosaccharide chains, which are then sequentially elongated and branched by a number of glycosyltransferases (Potapenko et al., 2010a, Groux-Degroote et al., 2008). The mucins found in humans frequently contain fucose (Fuc), galactose (Gal), *N*-acetylglucosamine (GlcNAc), sialic acid and mannose (Lamblin et al., 2001, Lewis et al., 2013a). Further to these sugar modifications, the carbohydrate chains may also be substituted by *N*-acetylneuraminic acid and/or sulfate (Davril et al., 1999). It is the glycan moiety that often defines the functional characteristics of the mucin (Potapenko et al., 2010a).

Further important changes in the core glycan chains, linked to respiratory disease, are Lewis antigens (Lewis et al., 2013a). These are tri- or tetra-saccharide terminal glycan epitopes and have 2 main sub-divisions of Lewis antigens, type 1 and type 2 (Degroote et al., 1999), depending upon the building site of the terminal galactose to the GlcNAc. Type 2 Lewis antigens are synthesised by transferring β -1,4-galactose to the GlcNAc saccharide, by β -1,4-galactosyltransferases, and they include Lewis x. Lewis x contains α -1,3-Fuc residues on the GlcNAc via fucosyltransferase. The galactose may or may not be modified with sialic acid to form sialyl Lewis x (Potapenko et al., 2010a)(Potapenko et al., 2010a). Further modifications of Lewis x may involve sulfation of GlcNAc (3-sulfo Lewis x); see **Fig 4.1** (Degroote et al., 1999)

4.1.2 Mucins associated with cystic fibrosis

Mucins are an important constituent in CF sputum (Lamblin et al., 2001) since they are gel-forming (King and Rubin, 2002, Jonckheere and Van Seuning, 2008), and represent <1% (w/v) of respiratory secretions (Henke et al., 2007, Phillips et al., 2006, King, 2005). In diseased sputum, altered terminal carbohydrate moieties affect differences in the viscoelastic properties of mucus, since the addition of a charged residue will influence mucin aggregation (Lewis et al., 2013a). In addition, the mucin-to-water ratio has been shown to be significantly increased to ~5-10 times greater than in healthy individuals (Lai et al., 2009b).

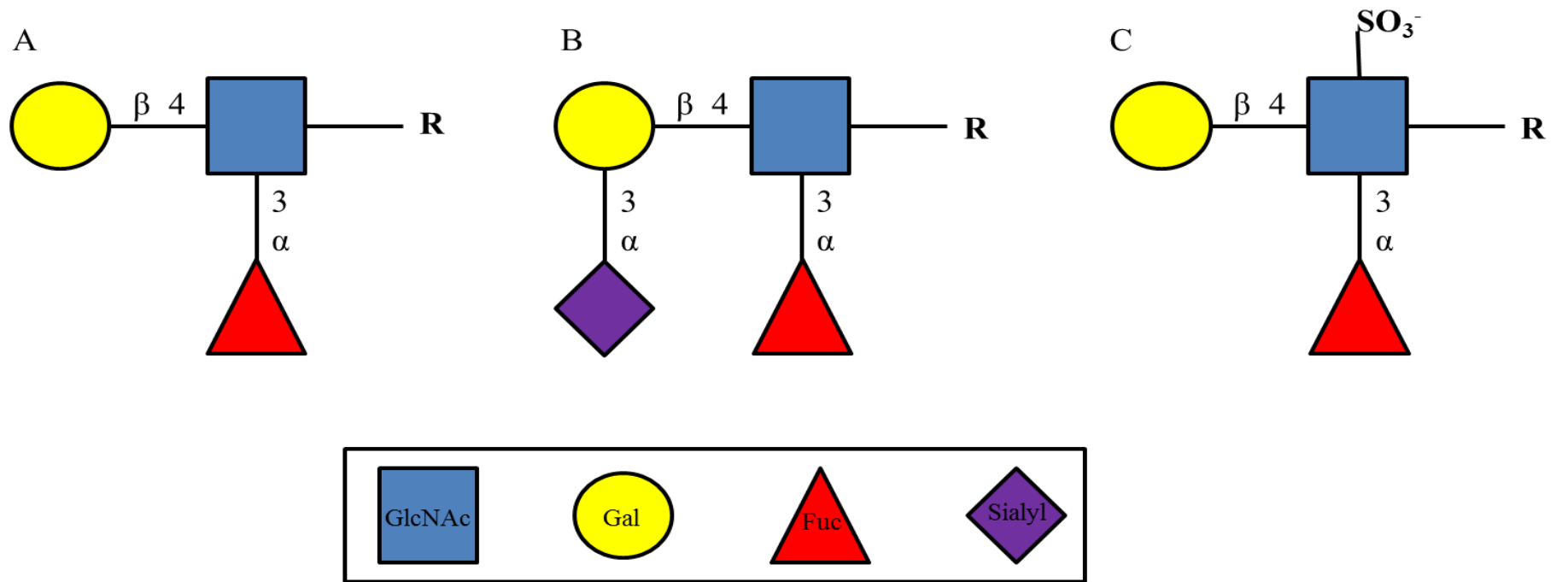


Fig 4.1: Schematic representation of glycan oligosaccharide A) Lewis x, B) Sialyl Lewis x and C) Sulfo Lewis x.

High mucin levels in the CF lung have been described (Thornton et al., 1991), although this has recently been questioned (King and Rubin, 2002) and mucin concentrations may even be decreased compared to healthy controls (Henke et al., 2004). CF mucins are however, more dense than seen in healthy patients, with highly glycosylated ends and increased levels of fucose, galactose, *N*-acetylglucosamine, (Bhat et al., 1996), sialic acid and sulfate (King and Rubin, 2002). Furthermore, increases in glycosylation and branching in CF mucins have been shown to lead to a higher tendency to “gel” and obstruct transport *in vivo* (Bhat et al., 1996). Mucin levels increase expression of sialylated and sulfated Lewis x determinants during inflammation and infection (Henke et al., 2007).

4.1.3 Pig gastric mucin

Due to the difficulties in obtaining mucin from human sources, pig gastric mucin (PGM) is often employed in studies, being a homologue of MUC5AC of the human lung (Felgentreff et al., 2006, Bhat et al., 1996, Crater and Carrier, 2010, Chen et al., 2012).

4.1.4 Interaction of alginate oligomers with components of sputum

Guluronate oligomers are polyelectrolytes and may inhibit interactions between matrix mucins and mobile components such as carboxylate-modified nanoparticles. Nordgard et al. (2014) hypothesised that guluronate oligomers could reduce the steric barrier of mucin networks by inhibition of mucin matrix crosslinks. “Force unbinding” events between non-commercial PGM and high molecular weight (MW) alginates have previously been quantified using atomic force microscopy (AFM; Sletmoen et al., 2012). In these experiments, on addition of guluronate oligomers to the buffer, a concentration-dependent suppression of PGM high MW alginate interaction was observed. The study concluded that the low MW guluronate oligomers-PGM interaction was the main mechanism underlying the suppression of mucin-high MW alginate interactions. Bacterial alginates are considerably larger than OligoG, with some reported to have a MW as high as 4000 kDa (Pena et al., 2002) as well as a low fraction of G residues; F_G 0.33 (Gimmestad et al., 2003). The interaction sites on the mucin molecule which are available for alginate binding may

be blocked by low MW alginate due to the difference in steric constraints of immobilised OligoG when compared to larger bacterial alginates (Sletmoen et al., 2012).

4.1.5 Fourier transform infrared spectroscopy

Monitoring and diagnosing lung disease is complex. For example, alterations in mucin expression, secretion and glycosylation, as well as in the Lewis antigen structures can all be used to characterise respiratory disease such as CF and chronic bronchitis (Davril et al., 1999, Degroote et al., 2003, Kirkham et al., 2008). There are still no sensitive tools to predict which chronic obstructive pulmonary disease (COPD) patients are at risk of exacerbation or rapid deterioration, or to monitor disease progression and outcome. Fourier transform infrared spectroscopy (FTIR) is a simple procedure which only requires a small quantity of test sample (Bosch et al., 2008, Lamblin et al., 2001). A study analysing COPD sputum using FTIR found statistically significant changes in the amide II regions and glycogen rich region of mucin between COPD patients and healthy controls (Whiteman et al., 2008) showing its utility for this application.

Early detection of lung cancer is poor, and since long term smokers share common symptoms such as coughing, dyspnoea and haemoptysis, with other respiratory diseases, symptoms are often dismissed by clinicians. By analysing the FTIR spectra, clear regions which differed in peaks between the healthy sputum and lung cancer patient were identified (Lewis et al., 2010). FTIR was able to detect cancer in 48% of cases where no tumour was visible during bronchoscopy. FTIR is also being developed to diagnose oropharyngeal tumours from healthy tissue (Menzies et al., 2014, Schultz et al., 1998, Pallua et al., 2012, Fukuyama et al., 1999), as well as diagnosing laryngeal tumours by detecting a single set of biomarkers (Menzies et al., 2014). As it is easy to use, FTIR could be developed as a simple tool for use by the non-specialist. It could also be used as a non-invasive way to monitor disease progression and bacterial identification (Bittar and Rolain, 2010).

4.1.6 DNA in cystic fibrosis sputum

The dominant polyanion found in CF sputum is extracellular DNA (eDNA). The concentration of eDNA in CF patients is 10 times higher compared to other chronic respiratory diseases such as chronic bronchitis (Kim et al., 2001, Kater et al., 2007). The majority of eDNA in the CF lung is believed to be from the host although bacterial eDNA may also be present (Lethem et al., 1990). The chronic inflammation seen in CF drives epithelial damage (Konstan and Ratjen, 2012), with increasing IL-8 production activating neutrophils which releases further eDNA into the already purulent sputum (Kim et al., 2001). Although obtaining an eDNA FTIR spectra from CF sputum represents a challenge, for accuracy however, it is vital to eliminate any “cross-over” between eDNA in the spectra analysed for mucin glycoprotein.

4.2 Aims

Mucin is an important secretion of the lung which contributes significantly to the viscoelasticity and biofilm formation in CF sputum. A greater understanding of the interactions between OligoG and mucin is required to elucidate possible interactions within the CF lung.

The hypothesis of the study was that the polyanionic nature of OligoG would alter the conformation of mucin, leading to structural changes of the glycans. The specific aims of the study were:

- To quantify changes in mucin surface charge induced by OligoG using zeta potential analysis through electrophoretic light scattering (ELS).
- To utilise different imaging techniques to visualise changes in mucin and sputum structure in the presence of OligoG.
- To characterise changes in hydrogen bonding and electrostatic interactions when treating sputum with OligoG using FTIR, and determine how it is related to the CF sputum DNA spectrum.

4.3 Materials and Methods

4.3.1 Extraction of pig gastric mucin

Mucin was collected from pigs immediately after slaughter (courtesy of Professor J. Pearson, Newcastle University). Briefly, the pig gut was surgically opened and the surface gently washed with water. The surface gel was then scraped off with a microscope slide, placed into a beaker and cooled on ice. The mucin was then transported to the laboratory at 4°C for processing. Purified mucin was then prepared as described in Pearson et al. (2000), and used in all the following studies.

4.3.2 Zeta potential analysis of pig gastric mucin-OligoG interactions (surface charge)

PGM (0.03% w/v) and OligoG (0.02% w/v) solutions were immersed in NaCl buffer (0.001 M) at pH 5 and pH 7, followed by filter sterilisation, 0.22 µm pore size (Klemetsrud et al., 2013). These were the control samples. OligoG treated samples of PGM were made up to a final concentration of 0.03% PGM and 0.02% OligoG (v/v). Control and treated samples were then incubated at room temperature (20 mins) prior to ELS using the Zetasizer Nano ZS (Malvern Instruments) and disposable capillary cells (Malvern instruments). Electrophoretic mobility of samples (25°C) was analysed using Smoluchowski's equation (Klemetsrud et al., 2013) as described in section 2.1.3.

4.3.3 Atomic force microscopy imaging of pig gastric mucin

In these studies, 0.004% (w/v) PGM in dH₂O alone and combined with 0.001% (w/v) of OligoG in dH₂O was stirred until fully dissolved (20 mins). A fresh mica plate (Agar Scientific) was cleaved and a 1 µl droplet of PGM ±OligoG was placed in the centre, and air-dried at room temperature for 20 mins. Imaging was performed using a Dimension 3100 AFM (6 samples per treatment group).

4.3.4 Scanning electron microscopy imaging of pig gastric mucin

PGM at 0.2% (w/v) was dissolved in dH₂O, and placed on a roller at 37°C for 2 h, prior to being filter sterilised (0.22 µm pore). Dissolved PGM (0.2%) was then

added to OligoG powder; producing a final OligoG concentration of 0.2%, 2%, 6% and 10% (w/v). These were then allowed to dissolve for 10 mins. Controls consisted of 0.2% PGM (w/v) only and 6% OligoG (w/v) alone. Samples (900 μ l) were placed on Thermanox glassTM slides (Agar Scientific) in 12-well plates (Grenier Bio-One, Stonehouse, UK), and incubated at 37°C (1 h). Samples were fixed by directly adding 100 μ l 25% glutaraldehyde (TAAB, UK, No. G004) to give a final concentration of 2.5% (v/v), and then left O/N. Samples were then washed with dH₂O (x4) before a final addition of 1 ml of dH₂O. Samples were then placed frozen at -20°C and freeze dried for 24 h. Imaging was performed using Hitachi S4800 scanning electron microscopy (SEM) without sputter coating.

4.3.5 Ultra-structural analysis of cystic fibrosis sputum

SEM of sputum samples were undertaken to determine whether treatment with OligoG led to structural changes in the CF sputum. Non-induced CF sputum samples (ethics number: 11/WA/0318) were collected and stored at -80°C until required. Samples were thawed O/N at 4°C. Samples (0.1 ml) were incubated \pm 0.2% or 2% (w/v) OligoG for 20 mins at 37°C. Non-homogenized CF sputum (0.1 ml) was placed on freshly-cleaved mica plates (Agar Scientific) as previously described and air-dried (5-10 mins). Non-adherent sputum was removed by washing gently with phosphate buffered saline (PBS; pH 7.4; x3). The slides were then fixed (1 ml of 2.5% [v/v] glutaraldehyde) in a 12-well plate, at 21°C (24 h). Complete dehydration of the samples was achieved using the ethanol dehydration method (Manzenreiter et al., 2012). Imaging was performed using Hitachi S4800 SEM, without sputter coating at high resolution and with chromium coating at low resolution.

4.3.6 ImageJ analysis and quantification

AFM images (20 μ m) were “smoothed”, prior to a standardised adjustment of the threshold in black and white. SEM of sputum samples were processed for “sharpening” to enhance the contrast at a set value. The images were then adjusted to highlight dark porous areas within the sputum samples. Both AFM and SEM images

were then converted into binary mode to allow measurement of surface area coverage and quantification.

4.3.7 Fourier transform infrared spectroscopy

4.3.7.1 Fourier transform infrared spectroscopy of cystic fibrosis sputum

Sputum samples were subjected to FTIR analysis to gain data on the possible interaction between mucin in sputum samples and OligoG, using a Bruker Alpha Fourier Transform IR instrument (equipped with a platinum attenuated total reflectance [ATR] single reflection diamond sampling module; Bruker Optics). Prior to each run, the ATR crystal was thoroughly cleaned using 70% (v/v) alcohol in dH₂O and air-dried. Infrared spectra were recorded as a mean of 24 scans per sample (each repeated on 3 separate occasions) between the wave number range of 4000-450 cm⁻¹, at a resolution of 4 cm⁻¹, controlled by Optics User Software (OPUS) version 6.5 (Bruker Optics). Although water was not expected to contribute to a spectrum after evaporation, each spectrum was assessed to ensure a smooth baseline existed between 1800 and 900 cm⁻¹ (Dong et al., 1992).

Initial test experiments were carried out on 10% (w/v) OligoG in dH₂O. A background spectrum was measured using 24 scans and subtracted from the sample spectrum acquired. Sputum samples from 9 patients (see **Table II.i**) were then collected and initially divided into Control, 0.2% OligoG and 2% OligoG (w/v) treatment categories. Approximately 3 µL of each sample was spotted directly onto the ATR sampling module, and allowed to slowly evaporated at room temperature. From preliminary results, it was apparent that the signal from the 2% OligoG test samples was dominated by OligoG, so subsequent studies employed a concentration of 0.2% (w/v) OligoG.

4.3.7.2 Fourier transform infrared spectroscopy data processing and analysis

Spectra were pre-processed using OPUS[®] software by subtracting a baseline between 4000-450 cm⁻¹. Baseline correction was performed followed by minimum/maximum normalisation and offset correction. A mean IR spectrum was generated across each group of replicates. The mean control sample was then subtracted from the mean OligoG treated sample for each patient.

Analysis focused on the 1240 cm⁻¹ peak, a region that does not include OligoG absorbance. This value was also selected as it is a measure of levels of sulfation (Lewis et al., 2013a), an important characteristic of the CF sputum and defining lung disease.

4.3.7.3 DNA extraction from cystic fibrosis sputum samples

DNA extraction was carried out on all CF sputum samples using a DNeasy Blood & Tissue Kit[®] (Qiagen). Sputum (1 ml) was processed as per the manufacturer's instructions. The DNA and protein content of the extracted samples was analysed using a Nanodrop spectrophotometer. For this, the Thermo Scientific[™] Nanodrop surface was thoroughly cleaned with isopropyl alcohol in dH₂O and a blank consisting of 1 µl of nuclease-free water used for calibration. A 1 µl sample of extracted DNA was measured and the DNA and protein contamination (absorbance_{260/280} nm) concentrations determined (n=3). The samples then underwent FTIR (as described in section 4.3.7.1 and 4.3.7.2), followed by secondary derivative analysis of the peaks.

4.3.8 Statistical analysis

Graph Pad Prism[®] statistical software was used to carry out statistical analysis. Zeta potential analysis of mucin-OligoG interactions and the surface area coverage of ImageJ binary images of the AFM mucin and SEM CF sputum samples was analysed using a paired t-test and the Tukey-Kramer multiple comparisons test based on a one-way ANOVA test, respectively. P<0.05 was considered significant.

4.4 Results

4.4.1 Zeta potential analysis of pig gastric mucin-OligoG interactions (surface charge)

The zeta potential for mucin in 0.001 M NaCl, pH 7 was stable at $-16.7 \text{ mV} \pm 0.85$. However, when OligoG (0.02%) was added, it became significantly more negative at $-23.1 \text{ mV} \pm 0.98$ ($P < 0.0001$). Due to the low concentration of the OligoG control in this buffer, only multiple weak unstable peaks were seen (**Fig 4.2A**). When the pH of the 0.001 M NaCl buffer was reduced to pH 5, the mucin produced a similar reading at $-16.0 \text{ mV} \pm 0.732$. Again, the addition of OligoG led to a significantly more negative result of $-24.2 \text{ mV} \pm 0.45$ ($P < 0.0001$), very similar to that in the pH 7 buffer. Similarly, the readings for the OligoG control were again unstable, producing multiple peaks (**Fig 4.2B**).

4.4.2 Atomic force microscopy imaging of pig gastric mucin

Treatment of mucin with OligoG was shown to disrupt the mucin network and change its morphology, forming a more disperse structure compared to the untreated control (**Fig 4.3**). The topography images were quantified using ImageJ analysis of binary images, clearly showing a significant 23% increase in the amount of area covered by the mucin when treated with OligoG compared to the untreated control; $52.06\% \pm 12.37$ Vs $28.81\% \pm 5.84$ respectively (**Fig 4.4**; $P < 0.005$). The samples remained reproducible throughout due to the low droplet size of $1 \mu\text{m}$.

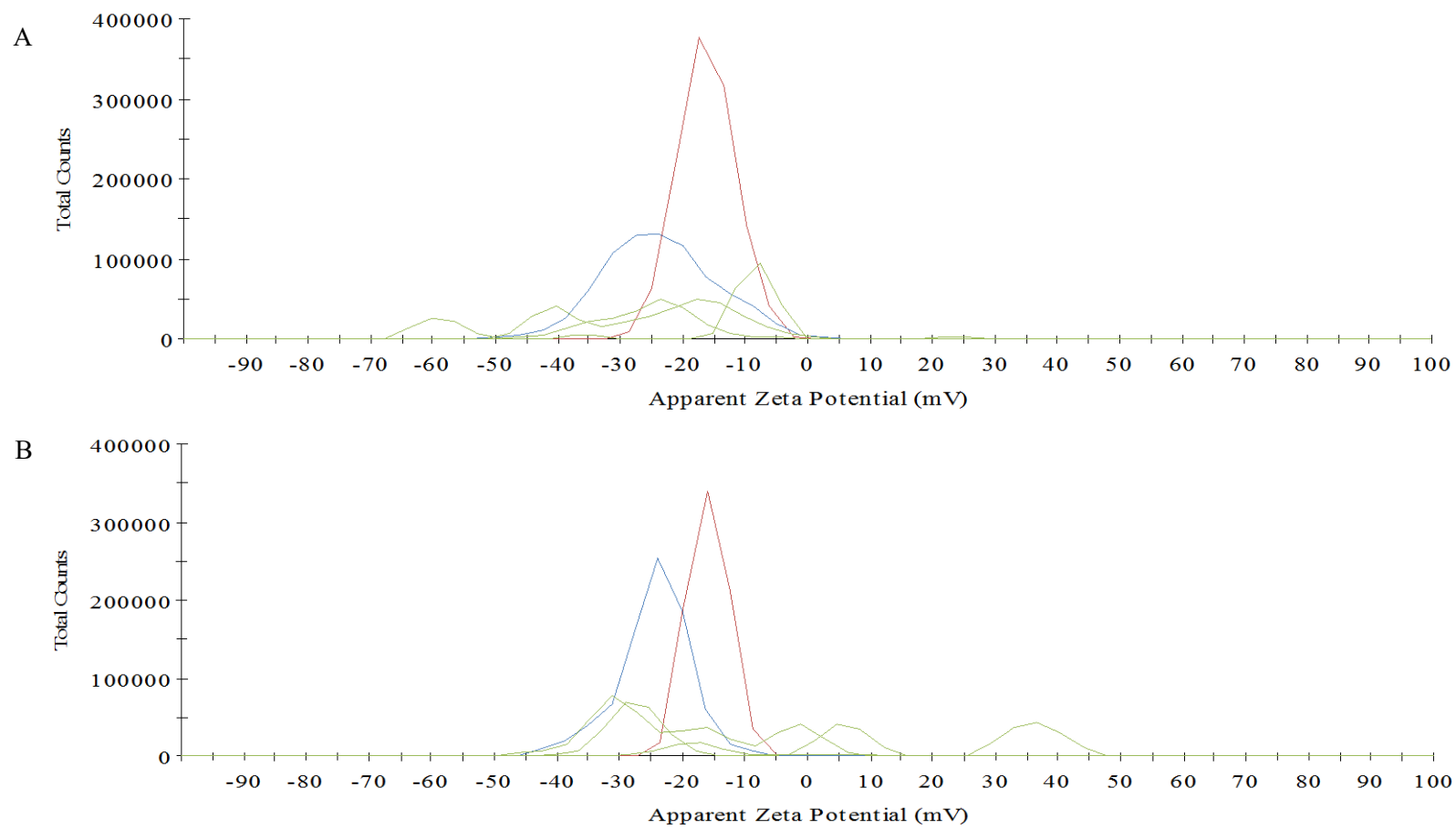


Fig 4.2: Zeta potential (surface charge) analysis (mV) of untreated PGM (red solid line), OligoG treated PGM (blue solid line) and OligoG only (green solid line). Buffer concentration 0.001 M NaCl A) pH 7, B) pH 5.

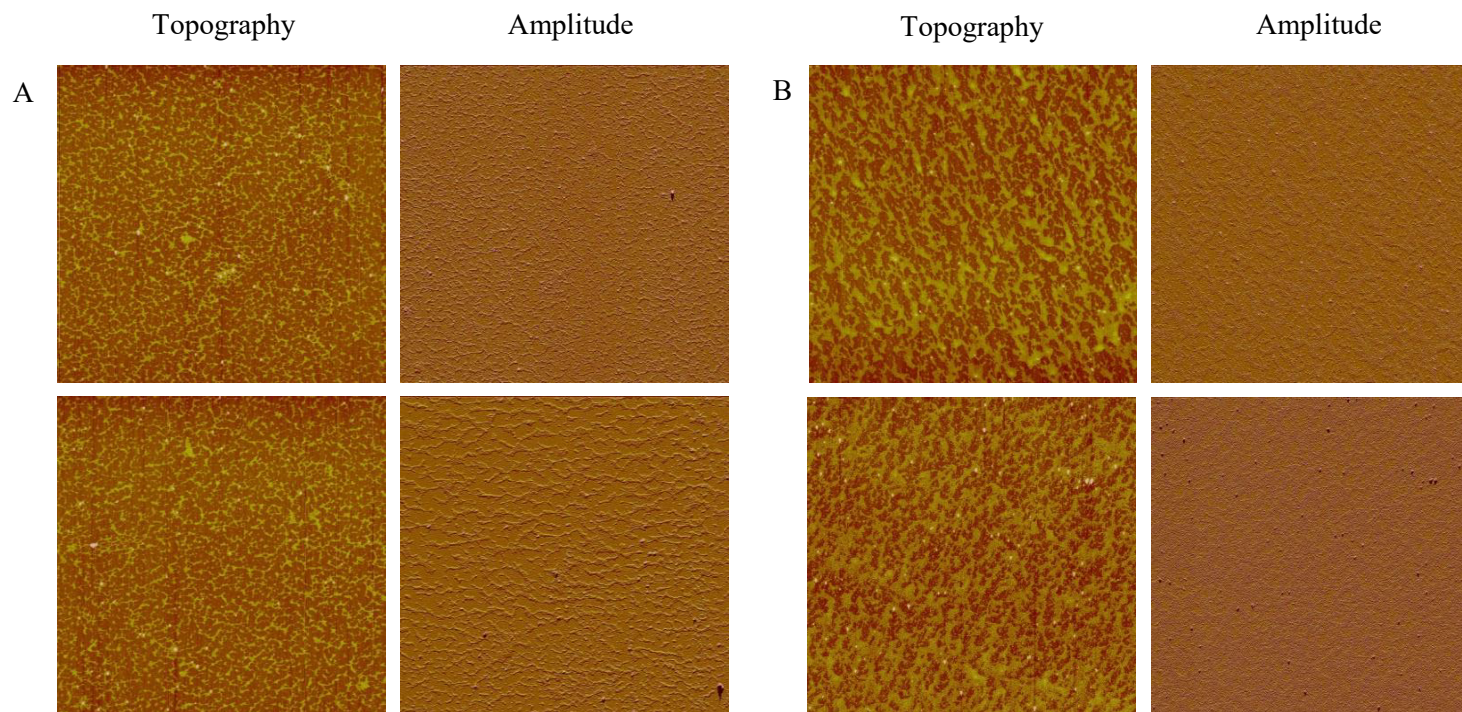


Fig. 4.3: AFM images (20 μm) of A) PGM only control (0.004%); B) PGM (0.004%) with OligoG (0.001%). Z scale of 9 nm.

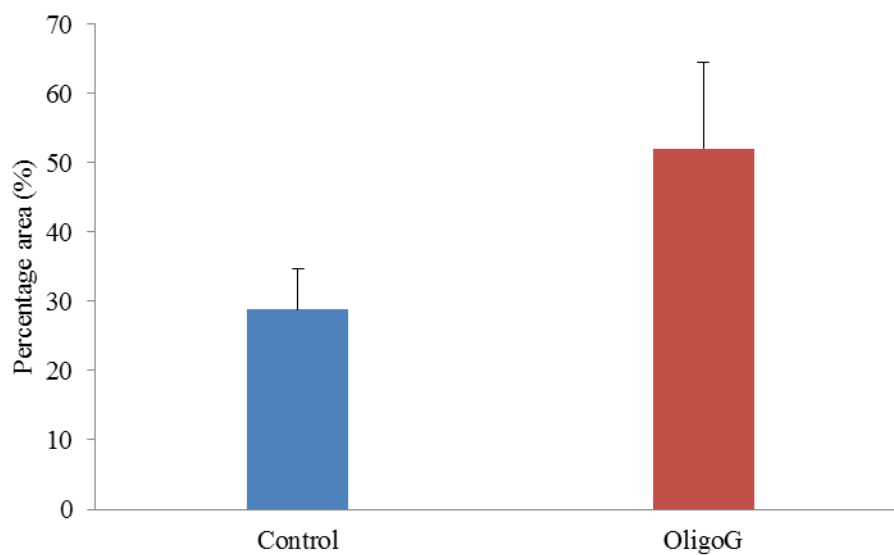


Fig 4.4: ImageJ analysis of the percentage surface area coverage of PGM AFM images (20 μm).

4.4.3 Scanning electron microscopy of pig gastric mucin

The PGM formed symmetrical smooth spherical shapes in the absence of OligoG similar to the microcolonies seen in **Chapter 2** in the AS medium (**Fig 3.7**). The OligoG only control (at 6%) formed a homogenous structured pattern. Treatment with 0.2% OligoG did not disrupt the formation of these spheres, although a number appeared to be less spherical and hence more bound to the Thermanox™ glass slide (**Fig 4.5**). As the concentration of OligoG increased (>0.2%), partial disruption of the spherical structures occurred (2% OligoG) with complete destruction observed at 6% OligoG (**Fig 4.5**).

4.4.4 Ultra-structural analysis of cystic fibrosis sputum

The control CF sputum samples produced a dense, tight woven network under SEM (18.75% ±4.17 porous). A more open porous sputum structure was seen when treated with 0.2% OligoG (25.78% ±5.46 porous). The 2% OligoG treated sputum structure was significantly more porous compared to the control; 32.17% ±3.90 (**Fig 4.6**; P<0.05). More detailed images at higher magnification of the sputum samples (**Fig 4.7**) demonstrated a smooth, non-porous structure in the control samples which became visibly more porous as the concentration of OligoG increased.

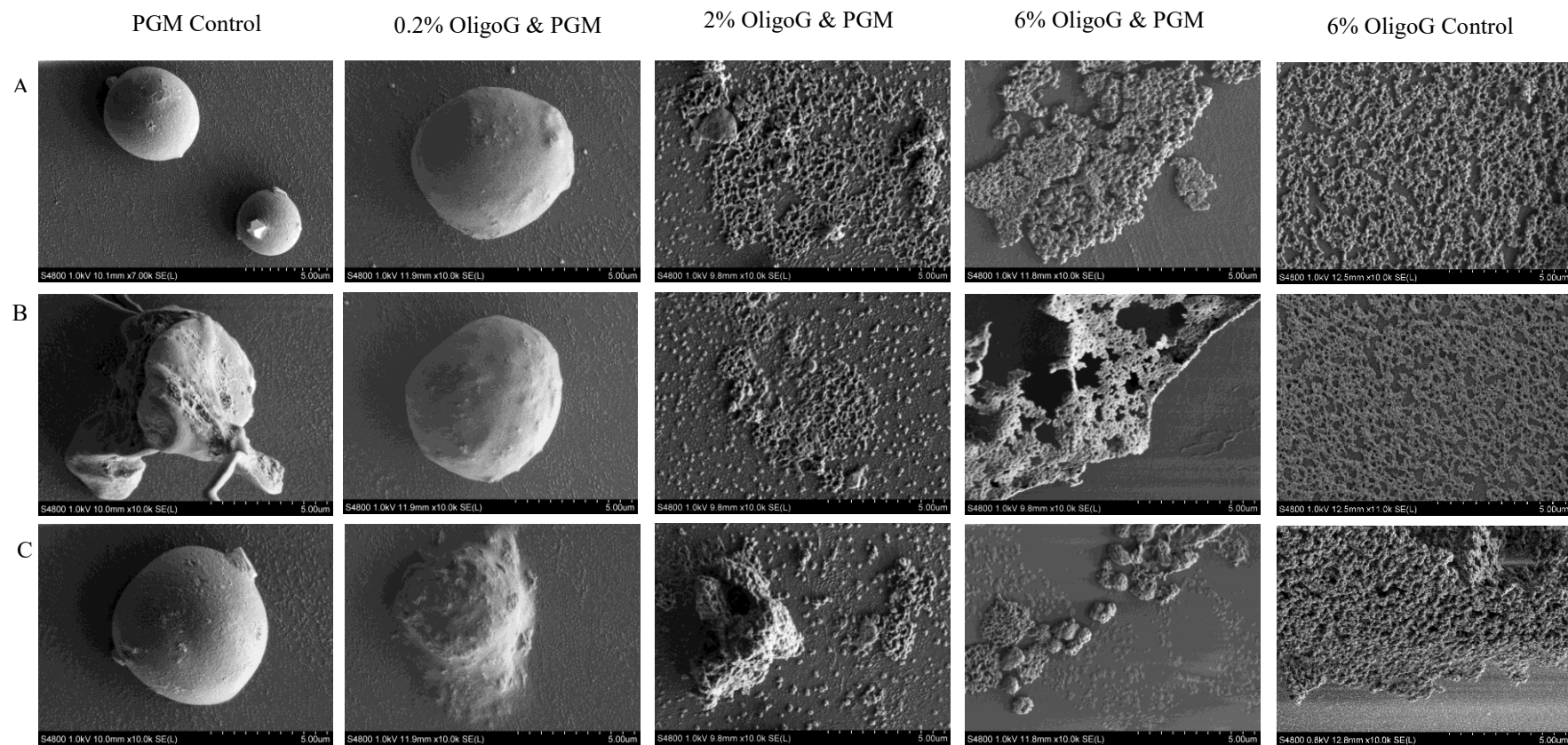


Fig 4.5: SEM of PGM \pm OligoG at 0.2%, 2% and 6% (repeats A-C). Scale bar 5 μ m.

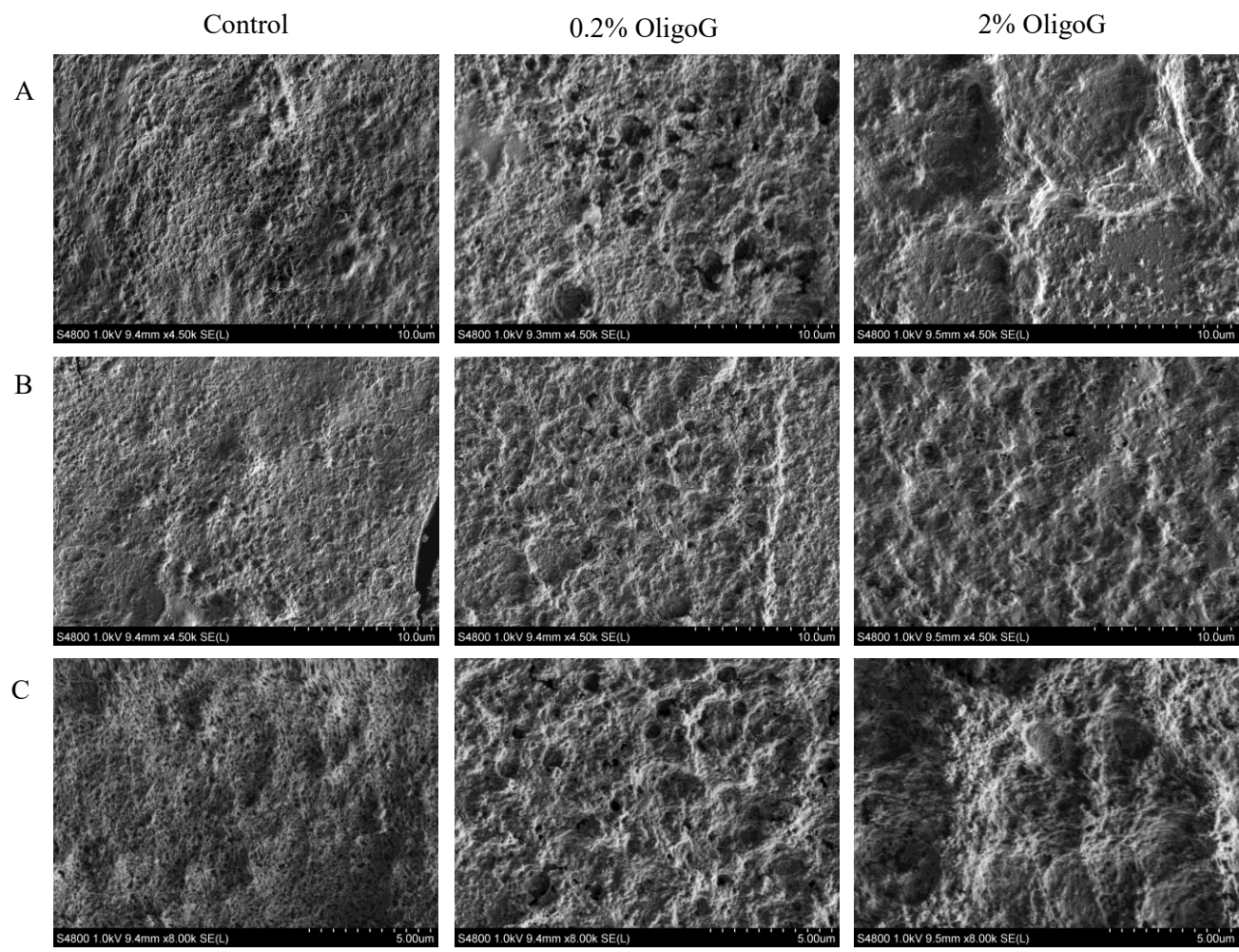


Fig 4.6: SEM imaging (without gold coating) of CF sputum \pm OligoG (0.2% and 2%). Scale bar A-B) 10 μ m; C) 5 μ m.

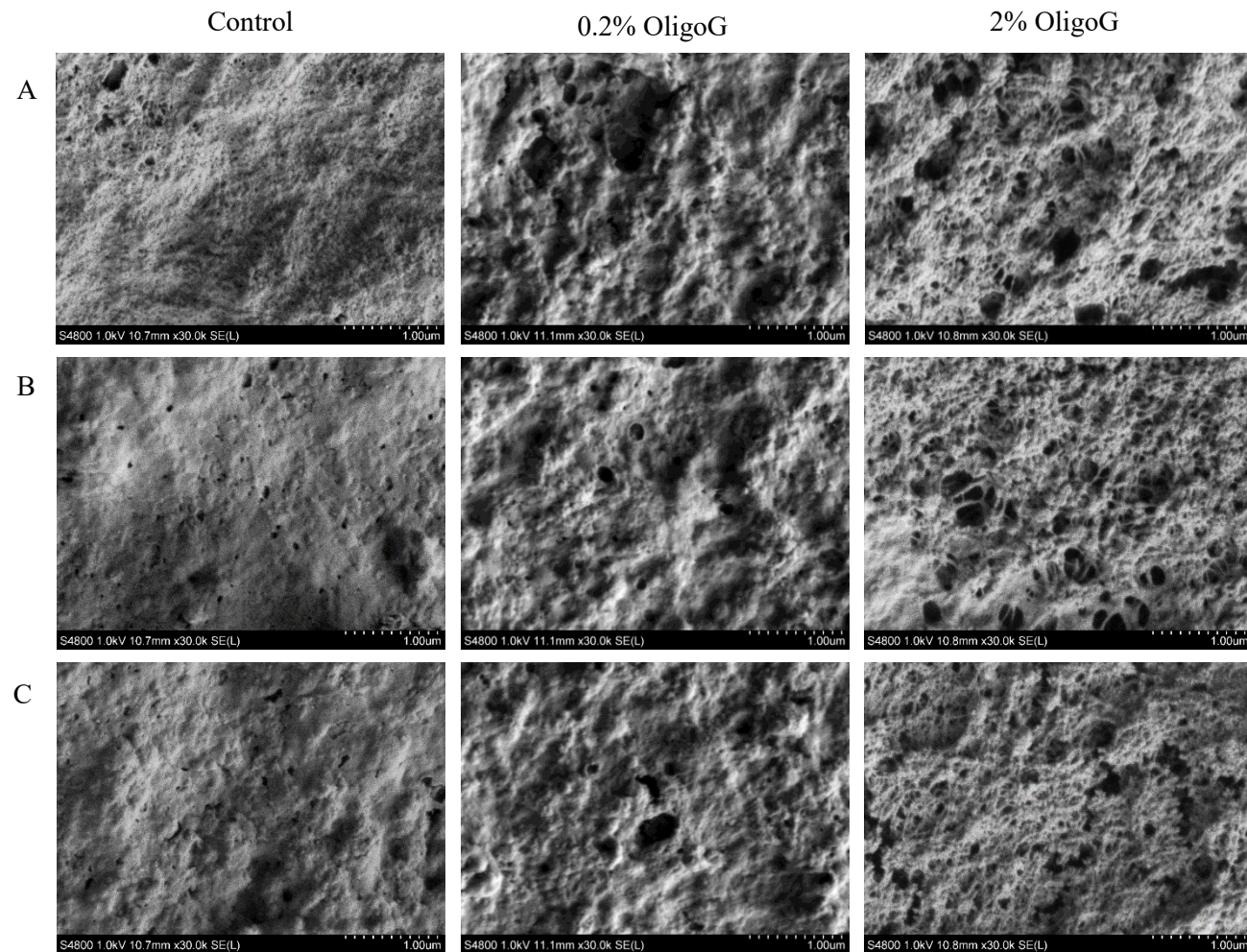


Fig 4.7: SEM imaging (with chromium coating) of CF sputum \pm OligoG (0.2% and 2%). Scale bar 1 μ m (A-C; triplicates).

4.4.5 Fourier transform infrared spectroscopy of cystic fibrosis sputum

FTIR analysis was performed out by subtractive analysis (the untreated sputum spectrum was subtracted from the OligoG treated sputum for each case). Therefore, the area of the spectrum chosen to be analysed was 1240 cm^{-1} which represents a sulfate peak (Lewis et al., 2013a). This area did not relate to OligoG and hence it allowed an unbiased analysis of any changes observed (**Fig 4.8A**). Focus was placed on negative peaks since these have the potential to demonstrate change by OligoG binding. Some sputum samples are likely to have higher levels of sulfation, and DNA phosphate may interact in this spectral region around 1230 cm^{-1} , **O–P–O** asymmetric stretching; DNA (Lipiec et al., 2012). Spectral reading from DNA from a CF patient confirmed the absence of a phosphate DNA peak at 1240 cm^{-1} , therefore strengthening the validity of the sulfate interaction (**Fig 4.8B**).

A change in absorbance was observed due to the interaction of OligoG with mucin. A decrease in absorbance of OligoG treated samples (**Fig 4.9A**) led to an overall negative peak following subtraction of the control sample from the OligoG treated sample (**Fig 4.9B**). This was seen in five of the OligoG treated samples at 1240 cm^{-1} , indicating hydrogen bonding and electrostatic interactions between the sulfate moiety (at this position) and OligoG. It is therefore likely that the energy between the **S⁺ – O⁻** bonds was shifted to an **S⁺ – O⁻ – H⁺** bond following treatment with OligoG (**Fig 4.10**), although this did not reach statistical significance.

Although the changes in wavenumber absorbance noted were minimal, again, five samples produced a negative peak after spectral subtraction. This again showed energy loss of a bond, resulting in a lowering of the frequency (i.e. having a higher wavelength, leading to a reduction in wavenumber; **Fig 4.10**).

All patients tested provided non-induced sputum and were taking antibiotics. However, due to the small sample size no correlation was found between sex, age, use of rhDNase I and forced expiratory volume in 1 second (FEV₁). Full details of the patient samples can be found in **Appendix II, Table II.i**.

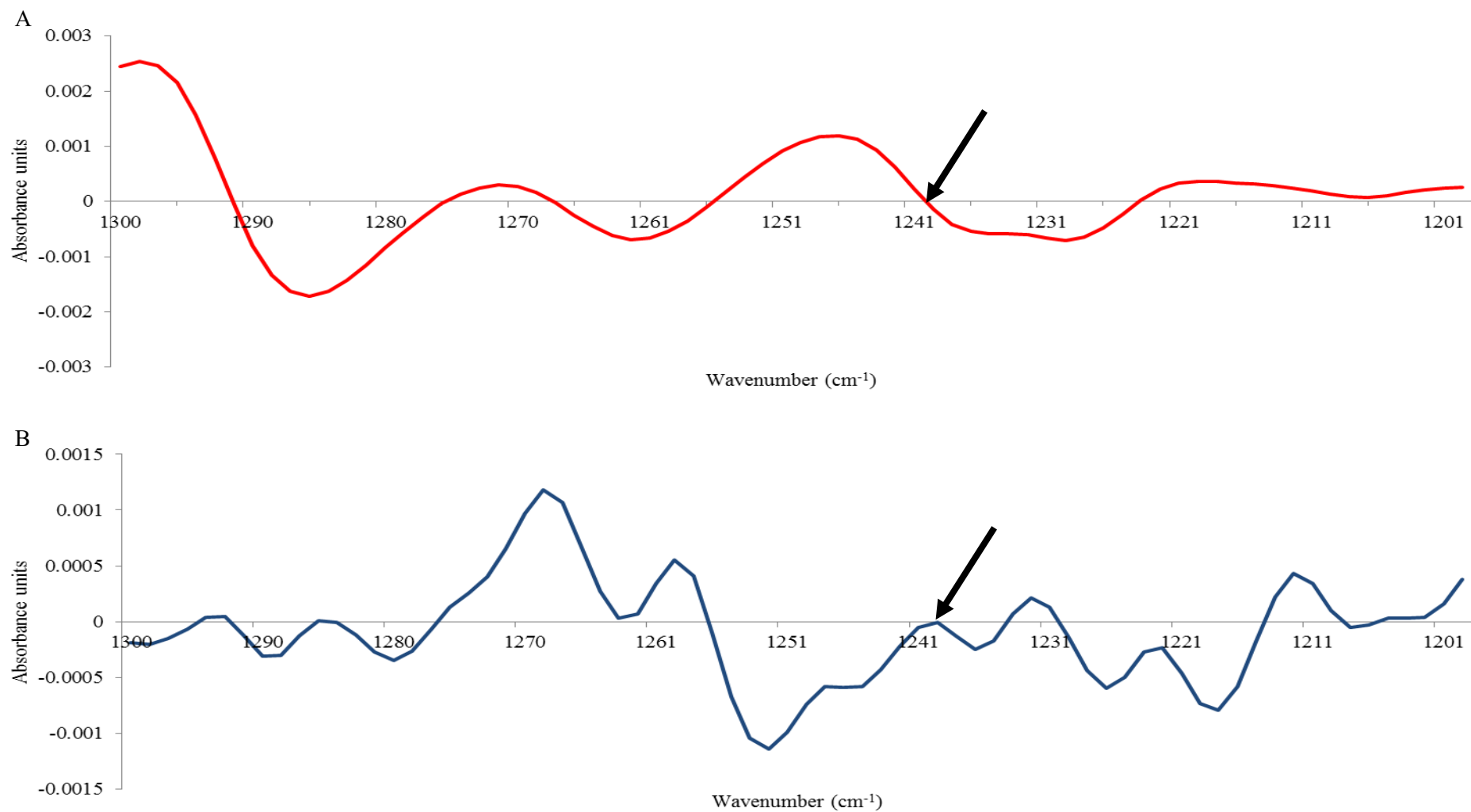


Fig 4.8: Second derivative of A) OligoG and B) CF DNA FTIR; confirming no interaction at sulfation peak 1240 cm⁻¹ (see black arrow).

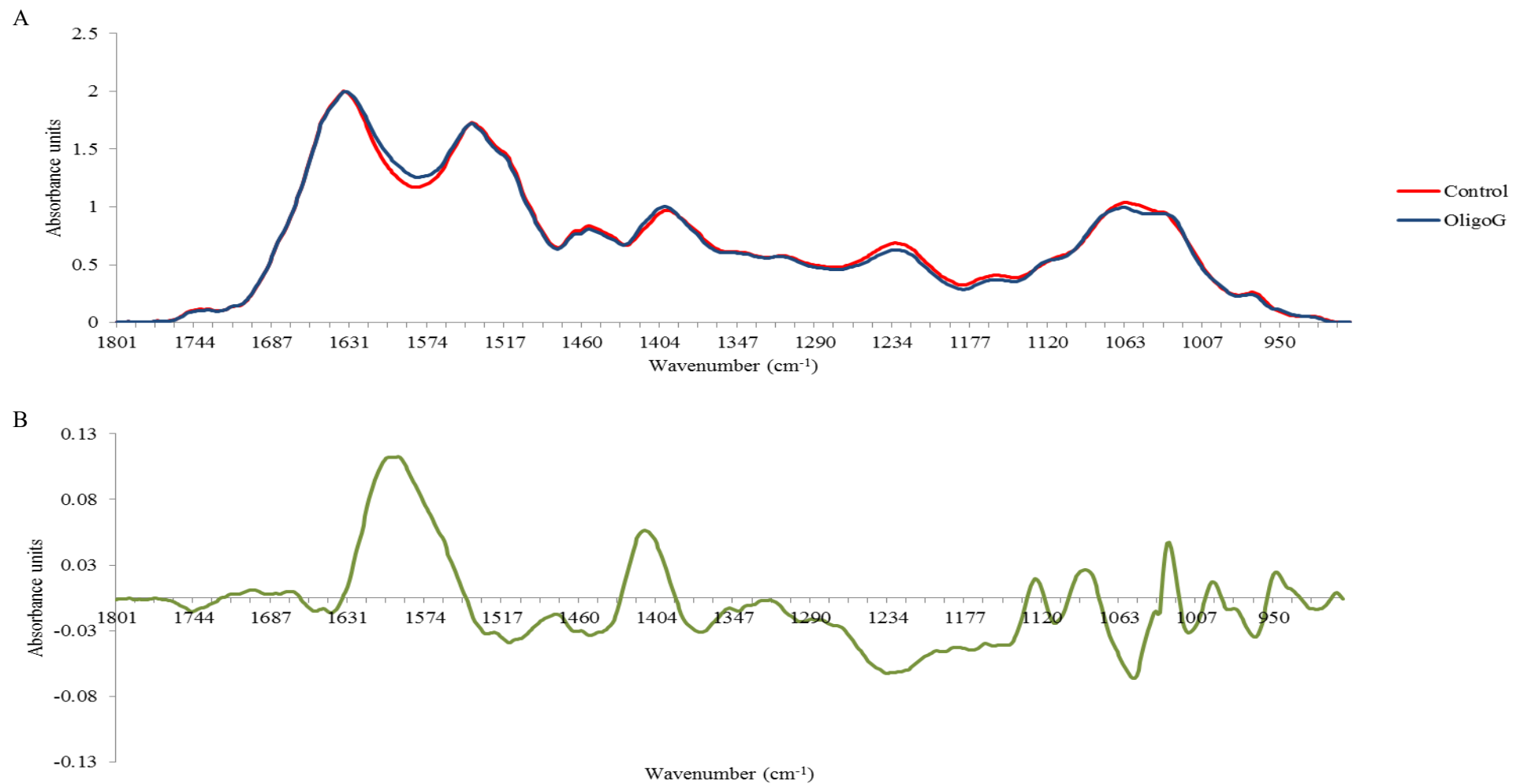


Fig 4.9: FTIR spectral peaks of sputum from patient 6 (**Table II.i**). A) Mean spectra for control and OligoG treated sputum. B) Subtraction of control sputum sample spectra from OligoG treated sample spectra.

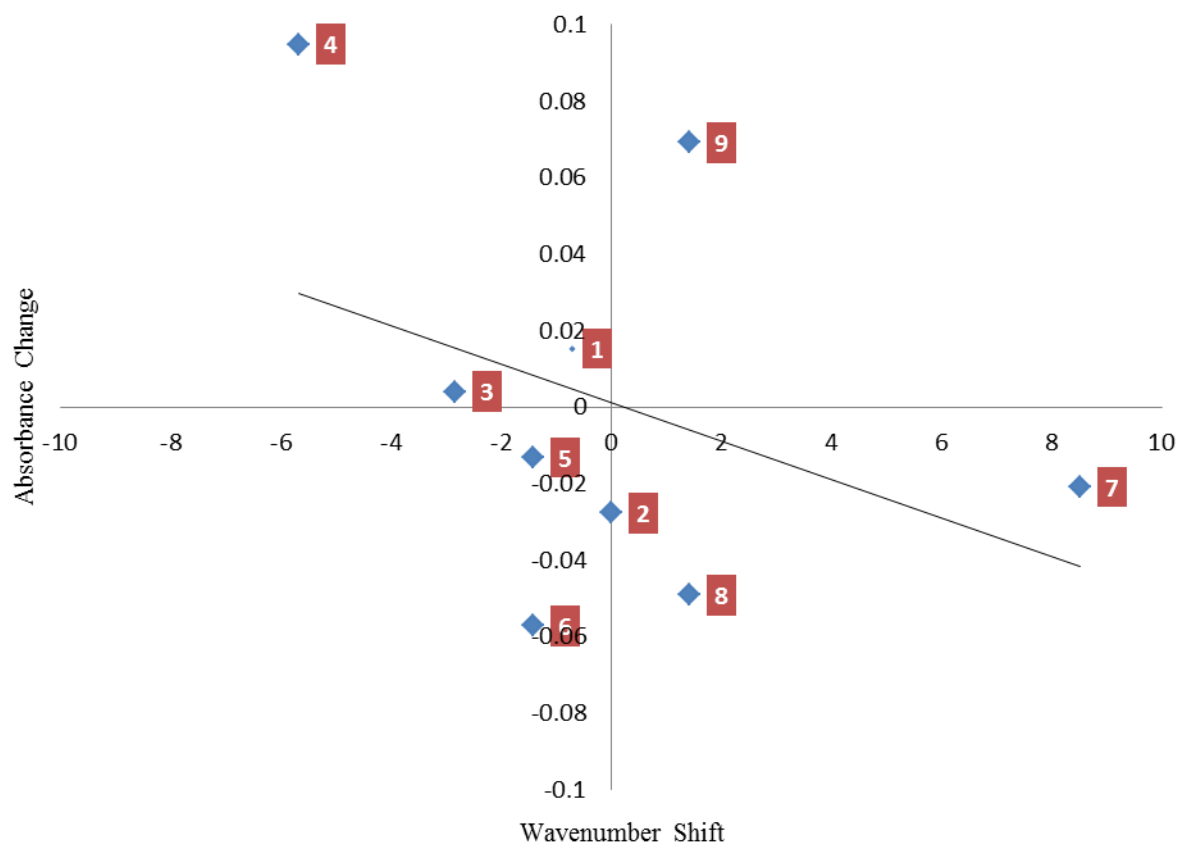


Fig 4.10: Scatter graph of FTIR readings at 1240 cm^{-1} representing patients 1-9 (see **Table II.i**). Change in absorbance and wavenumber shift of OligoG treated sample subtracted from the control.

4.5 Discussion

Modifying the properties of mucus may be beneficial in a range of conditions such as CF (Nordgard et al., 2014), reproductive medicine (Willits and Saltzman, 2001) and reducing the barriers to drug and gene delivery (Cone, 2009, Lai et al., 2009a). Negatively-charged biopolymers such as mucin, DNA and alginates, connect via physical entanglement of non-covalent bonds. As glycoproteins exhibit electrostatic, hydrophobic and hydrogen bonding interactions, mucin is therefore able to adhere to other substances. Although mucin serves as a barrier to bacteria, several pathogens such as *P. aeruginosa* reside within mucus and possess specific adhesins to bind to it (Bansil and Turner, 2006).

PGM does not provide a completely accurate model system of native human CF mucus. The decision to use commercial purified type II gastric mucin from porcine stomach as a reproducible model (Sigma Aldrich PGM) is common in many studies (Crater and Carrier, 2010, Felgentreff et al., 2006, Lee et al., 2005, Ritzoulis et al., 2012) but it is important to be aware that there is a risk that non-commercial PGM may have been denatured due to the solvents (CsCl/guanidium chloride) used in its purification. However, commercial PGM also has problems such as potential impurities like salts, immunoglobulins and secreted proteins which may still be present. Purification of mucin may lead to degraded viscoelastic behaviour of the commercial PGM in comparison to PGM which has not undergone any chemical treatment (Lee et al., 2005). In addition, freshly purified PGM gives greater inter-batch variability compared to commercial PGM, but is more comparable to the native secretion (Maleki et al., 2008). Commercial PGM however, is unable to produce rheological properties comparable to native mucus (KocevarNared et al., 1997). In contrast, the use of non-commercial PGM allows good comparison to the *in vivo* situation, particularly in relation to nanoparticle delivery (Nordgard et al., 2014). Therefore, non-commercial PGM was used for these studies as a standardised model system.

The zeta potential values obtained did not vary greatly between pH 5 and pH 7, typically being the pH range seen within the CF lung (Newport et al., 2009). The observed zeta potential values become more negative following OligoG treatment and this was highly suggestive of mucin-OligoG interaction. This could increase the

transport rate of therapeutics through PGM. Changes in surface charge may also affect the ability of bacteria to form biofilms since mucins have been shown to increase the attachment of *P. aeruginosa* in CF airways (Landry et al., 2006). It may also impede bacterial growth since mucins have also been shown to prolong bacterial survival (Mothey et al., 2014). A low concentration of OligoG (0.2%; w/v) was used in this study, with the OligoG control failing to provide an accurate zeta potential reading. As a result, the mucin-OligoG combined test was not “masked” by OligoG and reliable results were obtained.

Mucin interaction with *P. aeruginosa* has been shown to increase bacterial motility, which in part is directed by quorum sensing and the lubricating properties of mucin (Yeung et al., 2012). In contrast, OligoG has already been shown to reduce the motility of *P. aeruginosa* (Powell et al., 2014, Khan et al., 2012) and therefore may further explain its anti-biofilm properties in a more clinical setting. In addition to this, high MW alginates such as those produced by *P. aeruginosa*, have a lower interaction with PGM when treated with OligoG (Sletmoen et al., 2012).

Mobility of particles in PGM has been shown to be inversely correlated to the surface potential (or charge). Sulfate modified polystyrene nano-particles had the lowest surface potential and the highest transport rate, compared to amine modified particles which had the highest zeta potential and lowest transport rate (Crater and Carrier, 2010). Previous studies have also shown how similar results were obtained for the polysaccharide pectin when combined with commercial PGM, with the overall zeta potential becoming more negative following treatment (Klemetsrud et al., 2013). This may be a highly advantageous property since anionic particles diffuse 20-30x faster through gastrointestinal mucus, compared to cationic particles (Crater and Carrier, 2010). The anionic properties of the ‘mucin-OligoG’ molecule may therefore also allow easier access of therapeutics through the mucus network.

An understanding of the effect of pH on mucin-mucin interactions is important since the electrostatic charges are governed by the polypeptide backbone and the oligosaccharide side chains (Maleki et al., 2008). The pH of the stomach is 1-2 and the gastric epithelium remains unharmed under such acidic conditions primarily due to gelation of the gastric mucin (Cao et al., 1999). Due to the gastric environment being acidic, the conformation of PGM is expected to change at higher pH values. Non-commercial PGM was found to form a strong heterogeneous network of

intertwined chains at pH 2, which became more evenly dispersed and form a more homogenous network at pH >2 (Maleki et al., 2008). This clearly explains why no difference was found between pH 5 and pH 7 in the zeta potential studies. Extracting MUC5AC from CF sputum may allow for a more accurate comparison of mucin-OligoG changes when tested at pH 5 and pH 7.

AFM employs a non-invasive and non-destructive sample preparation (Deacon et al., 2000) and has been used extensively to visualise structures at the nanoscale level (Round et al., 2002, Round et al., 2004). Diluted solutions of mucins have been imaged to show its extended conformation when placed on untreated freshly cleaved mica plates (McMaster et al., 1999, Deacon et al., 2000, Hong et al., 2005, Klemetsrud et al., 2013). The methodology of imaging on mica plates was found to be reliable and reproducible (Round et al., 2002, Manzenreiter et al., 2012).

AFM mucin images have previously demonstrated a regular network structure (Klemetsrud et al., 2013) and have been a useful tool to show glycoprotein structure and aggregation (Hong et al., 2005). The AFM images in this study were as anticipated, with the zeta potential becoming more negative when mucin and OligoG were combined. These results were indicative of increased repulsion between the molecules and less inter-linking networks, potentially reducing its ability to interact with bacterial biofilms or increase the viscosity of sputum. The increase in molecules within the solution on addition of OligoG may partially account for the changes seen in surface area. However, even when treated with OligoG, the structural similarity of the mucin pattern was maintained with what appeared to be binding with OligoG.

Previous studies have reported mucin AFM imaging to show consistency with SEM studies (Deacon et al., 2000). Studies have also shown how SEM of commercial PGM (Sigma Aldrich) provides a visual representation, to establish the relationship between nanoparticle concentrations and mucin aggregation (Chen et al., 2010). Hence a similar approach was used for this study. The effect of OligoG on PGM was particularly dramatic, with the spherical mucin structures seemingly completely disrupted in the treated samples, with the mucin network instead appearing to have opened up and having fewer mucin network strands. The addition of low MW guluronate oligomers to mucin matrices has previously been shown to form less dense cross-linking network and an increased matrix pore size (Nordgard et

al., 2014). OligoG therefore has a potential application for improved delivery of nanomedicines.

Spherical mucin structures have previously been imaged by SEM, and are a recognised complication for contact lens wearers (Millar et al., 2003). Interestingly in this chapter, the spheres were formed under static conditions, and hence must have formed due to the charge on the mucin within the test solution. The lack of these spherical structures in the treated samples shows how significant the alteration in charge was following the addition of OligoG.

Difficulties arise during sample preparation for SEM imaging as the sputum microstructures are likely to contract (Schuster et al., 2013), and fixation and dehydration may therefore directly affect the resulting pore size obtained (Schuster et al., 2013). These specific hurdles are difficult to overcome, but the contrast between the identically-treated test and control samples validated the approach taken. Previous studies using SEM imaging of sputum samples, (Manzenreiter et al., 2012, Schuster et al., 2013, Sanders et al., 2000) showed that (similar to this study), healthy mucus samples produced a meshwork architecture. This mucus mesh ranged from tens to hundreds of nanometres in diameter, with many fibres smaller than 100 nm. The fibres were organised randomly suggesting that the mucus was isotropic (Schuster et al., 2013). The surface area coverage of pores increased with increasing concentration of OligoG, which may improve access for other therapeutics.

The comparison of PGM SEM and sputum SEM is vital since previous studies have shown that purified PGM showed increased nanosphere entrapment compared to native pig gastric mucus, possibly due to removal of non-mucin products leading to exposed interaction sites on mucins which were previously inaccessible (Nordgard et al., 2014). OligoG was shown to disrupt both PGM and sputum structure, but PGM to a greater extent. This may be due to an increase in exposed “mucin sites of interaction”. Further to this, non-commercial polymeric PGM samples were found to contain disulfide bridges/mucin polymers (Fogg et al., 1996) making it more comparable to the interactions seen in sputum samples.

Recent developments in pharmaceutical nanotechnology have attempted to use nanoparticles to aid transport of drugs or genes to target areas by inhalation as treatments for respiratory diseases such as CF (Chen et al., 2010). An understanding of nanoparticles as an inhaled therapeutic to treat respiratory diseases may improve

pharmacokinetic drug profiling and provide effective therapeutic outcomes (Schuster et al., 2013). These must penetrate the mucosal barrier to avoid rapid clearance and provide the pharmacokinetic effect required (Schuster et al., 2013, Sanders et al., 2000). Schuster et al. (2013) showed that both particle size and charge were key to facilitating transport through respiratory mucus, with the former being the greatest predictor of particle diffusion. Furthermore, perhaps unsurprisingly, rhDNase I had a significant effect on particle diffusion, confirming that eDNA is a large component of sputum (Sanders et al., 2000). Cationic complexes are less transport-efficient than anionic ones (Chen et al., 2010, Sanders et al., 2000, Ferrari, 1997) thereby giving the low MW anionic properties of OligoG a distinct advantage in terms of increased sputum penetration (Sanders et al., 2000).

Various mineral salts account for up to 1% of mucus mass, with the elasticity increasing with greater ion valency. Higher concentrations of multivalent cations (e.g. Ca^{2+} and Mg^{2+}) can facilitate reversible crosslinks between mucin monomers (Lai et al., 2009b). Cationic Ca^{2+} acts as a “cross-linker” which condenses the mucin matrices inside mucin granules before exocytosis. In this way, Ca^{2+} can interact with mucin and create complex insoluble mucus plugs (Bhat et al., 1996). Ca^{2+} concentration within the CF lung increases to 4 mM compared to 1 mM in normal individuals (Chen et al., 2010). Guluronic acid (G) subunits have previously shown preferential binding to cations such as Ca^{2+} (Lattner et al., 2003), and may therefore further reduce mucin cross-links.

Recent novel clinical approaches involve the use of portable FTIR for use on patient samples in a clinical setting to predict acute episodes of COPD (Lewis et al., 2013a) or to aid detection of lung cancer (Lewis et al., 2010, Yano et al., 2000, Yano et al., 1996, Wang et al., 1997). This tool could be further developed as an aid in the treatment of CF patients since it is known that sialylation and sulfation of the Lewis x antigen is associated with respiratory disease, and could be a useful biomarker for analysing disease progression and severity (Lewis et al., 2013a). SEM and FTIR have previously been used in combination to assess the chemical and morphological composition of animal mucins (Teubl et al., 2013b). Extending this analysis to sputum samples is complex, as the evaluation involves multiple chemical bond interactions due to the vast heterogeneity of the samples. Over sulfation in CF mucins has long been reported in the literature (Degroote et al., 1999, Xia et al.,

2005, Davril et al., 1999, Delmotte et al., 2002) and may be two fold greater than that derived from healthy individuals (Mendicino and Sangadala, 1999). It has also been shown that the sulfated Lewis x antigen is the main sulfated sugar in mucin in CF (Lewis et al., 2013a). Within a subtractive spectrum, positive peaks for OligoG were expected to increase overall absorbance in the treated samples, therefore making these areas of the spectrum uninformative.

The spectral analysis for this study was taken between 900-1280 cm^{-1} . This is the region of the IR spectrum where absorbance at **C-O** bonds in sugars occur (Khajehpour et al., 2006), as well as **C-C** stretching or **C-O-H** bending (Hounsell, 1994). Specific sugar peaks in this area also come from **C-H** “wagging” and **O-H** “flexing” vibrations (Kacurakova and Mathlouthi, 1996). IR spectra for sugar derivatives have previously been determined; the peak position and associated absorbance of the carbohydrate associated region being extremely similar to that found for Lewis x antigen, due to the monosaccharide composition. Lewis et al (2013) showed that the IR spectra for raw sputum from a COPD patient had a similar general pattern to the Lewis x antigen derivatives, with a 1240 cm^{-1} peak, which corresponded to the sulfation peak (Powell et al., 1994). In this way, the characteristic sulfate absorption allowed the sulfated Lewis x derivative to be distinguished from the non-sulfated antigen (Lewis et al., 2013a).

Glycan sulfation is thought to increase when bacterial infection is present, possibly to protect the underlying glycoproteins from enzymatic degradation by bacteria (Mendicino and Sangadala, 1999). Inflammatory leukocytes and *P. aeruginosa* are thought to recognise sulfated ligands and lead to an inflammatory response and increased pathogenesis of *P. aeruginosa* respectively (Xia et al., 2005, Ramphal and Arora, 2001). However, a xenograft CF model demonstrated an increase in sulfation in the absence of bacterial infection, which implies it may be a primary defect of the disease (Zhang et al., 1995). Other studies have postulated that increased sulfation may be inherent in CF patients and only partly dependent on chronic bacterial infection (Robinson et al., 2012). Equally though, some studies have also reported a reduction in sulfation in CF patients compared to healthy control, and therefore may not be an accurate model for all CF patients (Schulz et al., 2007). Changes in this peak in sputum suggest that OligoG was able to bind to the sulfate moieties on the glycans and in this way, may counteract the effects of

pathogen recognition and binding (Robinson et al., 2012). Hence, OligoG's ability to interact with the sulfate moiety could potentially reduce the severity of bacteria-induced exacerbations. Importantly, this study was limited due to lack of healthy control sputum and the small sample size and further work is needed to confirm these results.

The viscosity of mucin was previously found to be pH dependent in artificial gastric juices with a gradual rise <pH 5 of approximately 100-fold compared to pH 7. It was found that when the PGM was treated with neuraminidase it removed over 90% of the sialic acid, yet had no effect on the viscosity (Bhaskar et al., 1991). In contrast, proteolytic digestion of the mucin with trypsin, or reduction of disulfide bonds with dithiothreitol, completely prevented changes in viscosity at low pH. This study shows the importance of targeting mucin in the study of sputum viscoelasticity, as well as highlighting the need to also focus on other sputum components.

Sputum samples have an inherent heterogeneity and represented a risk of bias, therefore, replication was key to the detection of outliers (Bhat et al., 1996). However, the results proved to be very reproducible from the same sample. It was expected that there could be large outliers within the samples due to this inherent heterogeneity, but again this was not the case. The results presented here may be used to create a hypothesis regarding the interaction of OligoG with the sulfate moiety of mucin, and to drive further research in patients and possible use of FTIR as a tool for clinical analysis of patient samples.

FTIR does have its limitations. It cannot determine the exact molecular structure of compounds, only which chemical groups are present in a sample. Also, some vibrations detected by FTIR are attributable to multiple chemical groups. Such problems may be overcome, for example, by the development of an FTIR reference library for monosaccharides (Lewis et al., 2013a). FTIR can also lead to extremely complex readings when multiple components are present within a sample. In this study, choosing an area of the spectrum which did not include an OligoG tracing was vital to obtaining usable data. Also the exact composition of sputum and clearance rate will differ depending on the microbiota, anatomical site and disease state (Schuster et al., 2013). Hence, had time and resources allowed, use of a much larger sample size would have been more informative.

4.6 Conclusion

Interaction of OligoG with mucin produced a more negative surface charge leading to a more disperse structure, as seen in the AFM images. The tight untreated mucin spheres (SEM) were disrupted by OligoG in a dose dependent manner. This was further reflected in the complex polyanionic CF sputum, as the pore size increased and the tangled meshwork opened, when treated with OligoG. A hypothesis was drawn from the FTIR analysis suggesting that OligoG interacts with the sulfate moiety of mucin. Since an increase in sulfation within the CF lung is associated with reduced pulmonary function, this finding may lead to elucidation of another mechanistic effect of OligoG within the CF lung.

Chapter 5:
Studies on the rheological changes
induced in cystic fibrosis sputum by
OligoG

5.1 Introduction

Rheology has been extensively used to analyse the properties of sputum (Nordgard and Draget, 2011) since its viscoelasticity is directly altered in many pathological conditions of the lungs (Nielsen et al., 2004). In cystic fibrosis (CF) patients, the sputum has an increased elasticity and viscosity which impairs clearance from the lungs. As such a major goal of therapy is effective removal of this thick tenacious sputum (Robinson et al., 1997). The physico-chemical structure of mucus is therefore an important therapeutic target in diseases such as CF and chronic obstructive pulmonary disease (COPD; Nordgard and Draget 2011). In this study, a direct comparison of the effects of the alginate oligomer OligoG with another therapy currently employed to alter the viscoelastic properties of sputum in CF patients, rhDNase I, was performed *ex vivo*.

5.1.1 Sputum

In chronic respiratory disease, production of sputum with abnormal viscoelastic properties (i.e. increased viscosity and elasticity) impedes effective mucus clearance, which prolongs infection and triggers airway inflammation (Nielsen et al., 2004, Livraghi-Butrico et al., 2012). A significant correlation has been found between polyanions, mucin and DNA, and rheological changes in CF sputum (Sanders et al., 2000). Impaired clearance ultimately results in a reservoir of pathogens as well as both host and bacterial derived inflammatory mediators (e.g. interleukins and lipopolysaccharide; LPS), which perpetuate damage of the respiratory epithelium and drive chronic inflammation via direct (e.g. protease) and indirect (e.g. cytokine and Toll-like receptor) mechanisms (Livraghi-Butrico et al., 2012). The altered viscoelasticity of mucus also effectively reduces the ability to deliver specific therapies to the diseased lung.

5.1.2 Mucolytics

Mucolytics aim to free adherent secretions from the epithelium and decrease their elasticity and viscosity. Mucolytics are used as a therapy for mucus clearance

in CF patients and work in conjunction with bronchodilators, chest physical therapy and good nutrition (King and Rubin, 2002) to improve lung function in the patients.

In a previous study, treatment with a prototype, low molecular weight (MW) alginate oligomer (DP_n10) was shown to alter the rheology of mucin/alginate gels, mucin/DNA gels and sputum from a CF patient (Nordgard and Draget, 2011).

5.1.2.1 rhDNase I

CF patients undergo a continuous cycle of obstruction, infection and inflammation which releases large amounts of extracellular (e)DNA (Konstan and Ratjen, 2012). eDNA is a viscous polyanion and is primarily released by neutrophil-induced cell death in the lung mucus. eDNA has been shown (via rheological investigations) to cause changes in viscoelasticity, leading to an increased complex modulus, a decrease phase angle and increased complex viscosity (Nordgard and Draget, 2011). The eDNA content of the sputum has also been shown to be directly proportional to the viscous and elastic response of the mucus (Zahm et al., 1995). This led to the development of a highly purified recombinant human DNase I; (rhDNase I; Shah et al., 1995), which enzymatically digests the eDNA fragments in sputum. rhDNase I treatment has been shown to decrease the viscosity and elasticity of infected mucus by hydrolysing the phosphodiester bonds of the DNA chains to form shorter oligonucleotides (Henke and Ratjen, 2007, Sanders et al., 2006, Visick and Fuqua, 2005), promoting improved airway clearance of secretions, resulting in increased pulmonary function, reduced pulmonary exacerbations (Fuchs et al., 1994, Jones and Wallis, 2010, Shah et al., 1995) and may prolong survival. Approximately 42.7% of CF patients regularly use a nebulised rhDNase I treatment (Bilton and Osmond, 2010). Interestingly, the greatest improvement in CF patient survival occurred between 1994 and 1997 and coincided with a “step” increase in the use of nebulised rhDNase I (George et al., 2011). The higher the initial eDNA content of treated sputum, the greater the effect of rhDNase I (Zahm et al., 1995). It should be noted that other authors have suggested that there is no direct relationship between the concentration of eDNA found within sputum and its viscosity. In contrast, COPD sputum samples have been shown to possess a decreased eDNA concentration

and viscoelasticity compared to CF sputa, suggesting that the higher elasticity and viscosity found in CF may be due to the presence of eDNA (Sanders et al., 2000).

5.1.2.2 Mannitol

Mannitol is a recently licensed (2012) sugar alcohol developed to improve surface hydration of the lung epithelium in CF patients and is inhaled as a dry powder (Bronchitol[®]). It is believed that mannitol induces a sustained osmotic gradient to increase the amount of water in the airway lumen, thereby increasing hydration of the periciliary fluid and improving mucus clearance. A phase II, randomised, open-label, dose response crossover study was carried out using mannitol showing a statistically significant increase in forced expiratory volume in 1 second (FEV₁) at 400 mg compared to 40 mg (Teper et al., 2011) which was maintained for the whole of the 26 week study (Bilton et al., 2011). However, overall perseverance with mannitol therapy has been poor. A study revealed that 27 out of 85 (32%) patients were excluded from even commencing the trial due to failed mannitol tolerance tests, MTT (Teper et al., 2011), with a larger study finding 27 (7.1%) failed the MTT out of 378 patients (Bilton et al., 2011). Up to 22.4% of patients were thought to have an adverse event during the life time of this study due to the test medication mannitol. The most common adverse events are bronchospasm, headache, cough and pharyngeal pain (Teper et al., 2011, Minasian et al., 2010) as well as lack of time in taking the medication (Aitken et al., 2012, Bilton et al., 2011). Studies have shown no change in microbiology results during treatment. This is a particularly important finding, since many organisms are able to use mannitol as a carbon source (Aitken et al., 2012).

5.1.3 Rheology

Rheology is used to assess the effect of mucolytics on sputum properties (Hoffer-Schaefer et al., 2014). Modulating the rheological properties of mucus is often a desirable therapeutic measure aimed at changing these parameters to those levels found in health (Nielsen et al., 2004) and can be achieved by targeting exogenous polymers (Nordgard and Draget, 2011). However, before the use of

therapeutic products to alter the rheological properties of mucus or sputum, the initial state of the mucus needs to be assessed (King, 1998).

Liquid elements undergo shear flow over or past each other, whilst adjacent elements undergo extensional flow towards or away from each other (Barnes, 2000). It has been shown that the most reliable information regarding the properties of sputum can be gained via shear rheology oscillatory techniques (Nielsen et al., 2004), and the cough clearance index (CCI; King, 1987) can be calculated from these tests;

$$\text{CCI} = 3.44 - (1.07 \times \log G^*100) + (0.89 \times \tan\delta 100)$$

However, a direct comparison of sputum samples can be difficult as observed viscoelasticity may vary with the physiology/pathology of the specimen provider (Nordgard and Draget, 2011). Moreover, large inter- and intra-patient variation may occur due to variations in water content, actin, DNA and glycoprotein content.

5.2 Aims

As OligoG has previously been shown to cause disruption of mucin and alginate interactions (Sletmoen et al., 2012), we hypothesised that the alginate oligomer could potentially be chronically delivered, via an inhaled route to alter the viscoelastic properties of sputum in patients with chronic respiratory disease. The specific aim of this chapter was to test the use of OligoG in the management of chronic lung disease by studying its ability to modify the rheological properties of CF sputum.

The specific aims of this study were:

- To investigate the ability of OligoG to modulate the viscoelastic properties of CF sputum *ex vivo*.
- To assess changes in sputum rheology longitudinally *ex vivo*.
- To compare OligoG treatment to currently available mucolytics *ex vivo*.

5.3 Materials and Methods

5.3.1 Patients and samples

Non-induced sputum samples (n=23) were collected by expectoration from 7 patients with CF (mean age 26 years; range 17-39) with mean FEV₁ 0.80-1.93 L (mean percent predicted FEV₁ was 46%; range 20-65%). All subjects were under the care of the Cystic Fibrosis Service, Cardiff and Vale University Health Board and gave written informed consent. The study was approved by the Local Research Ethics Committee (ethics number: 11/WA/0318). Sputum samples with visible quantities of saliva were not used. The patients were hospitalised due to pulmonary exacerbation at the time of sampling. *P. aeruginosa* was isolated from all patients on airway culture and all were receiving oral, inhaled and/or intravenous antibiotics. Serial analysis of sputum collected from Patient 1 was employed in the longitudinal study (*vide infra*). Patient data is shown in **Table 5.1**.

Sputum samples were stored at -80°C prior to use as in previous studies (Dasgupta et al., 1998, Stressmann et al., 2011, Wills et al., 1997, Serisier et al., 2009, Horsley et al., 2013, Hoffer-Schaefer et al., 2014). Initial experiments (data not shown) confirmed that freezing samples did not affect sputum rheology. Previous literature has also shown that freezing the samples does not significantly change viscous or elastic response (G' or G'' ; Sanders et al., 2000).

Table 5.1: Patient data, including antibiotic and rhDNase I (if applicable) regimen at time of sampling.

Patient No.	Age (Yrs)	Sex	rhDNase I	Antibiotic regimen at time of sampling			Recent sputum microbiology	FEV ₁ (%)
				IV	Oral	Inhaled		
1 [#]	17	F	Y	Tobramycin Meropenem	Flucloxacillin Azithromycin	Colistin (alternate month with) Tobramycin	<i>P. aeruginosa</i>	1.10 L (37%)
2	31	M	N	Colistin Meropenem Chloramphenicol		Colistin (alternate month with) Tobramycin	<i>P. aeruginosa</i>	1.85 L (51%)
3	28	M	Y	Tobramycin Ceftazidime			<i>P. aeruginosa</i>	1.93 L (54%)
4	39	M	Y		Azithromycin Flucloxacillin	Colistin (alternate month with) Tobramycin	<i>P. aeruginosa</i> <i>S. aureus</i>	1.85 L (50%)
5	30	F	N	Tobramycin Aztreonam	Azithromycin	Colistin (alternate month with) Tobramycin	<i>Pseudomonas</i> sp. <i>P. aeruginosa</i>	1.93 L (65%)
6	20	M	Y	Tobramycin Meropenem	Azithromycin	Colistin	<i>Pseudomonas</i> sp.	0.80 L (20%)
7	18	M	Y	Tobramycin Ceftazidime	Flucloxacillin Azithromycin	Colistin (alternate month with) Tobramycin	<i>P. aeruginosa</i>	1.30 L (43%)

[#]Sputum from Patient 1 was used for the longitudinal study. FEV₁; forced expiratory volume in 1 second.

P. aeruginosa, *Pseudomonas aeruginosa*; *S. aureus*, *Staphylococcus aureus*.

5.3.2 Extensional rheology

A total of 4 repeat experiments were performed on samples collected from 3 patients (patient 1, 2 and 7 in **Table II.i**). The sputum samples were treated with 2% OligoG and a dH₂O control. The minimum volume of sputum used for the extensional rheology was 0.2 ml. The treated samples were rocked gently side to side 4 times to mix them whilst preventing any change in rheological properties. Vigorous agitation was avoided to prevent spontaneous gelling or introduction of air into the gel. The samples were then incubated at 37°C for 4 h before rheological measuring.

Capillary Break-Up Extensional Rheometry (CaBER) was employed to measure the extensional properties of sputum samples. Briefly, two 7 mm plates were placed on the rheometer and the upper plate (no. 2) was aligned manually to the lower one (no. 1; **Fig 5.1**). For live recording of the experiment, the sputum samples were placed between the two plates and plate 2 was slowly moved upwards, subjecting the sample to a known “step-strain”.

There was a delay between loading and testing relaxation time. This was altered until the specimen fell at a time lag. The surface tension and density was measured for each sample.

An imposed step strain ϵ resulted in the formation of an unstable filament with a diameter (D) that decayed as a function of time due to surface tension σ .

In the final stages of filament break-up, the thinning phenomena was dominated by surface tension effects which allowed analysis of the rate-change of the mid-filament diameter to determine the extensional viscosity of the sample.

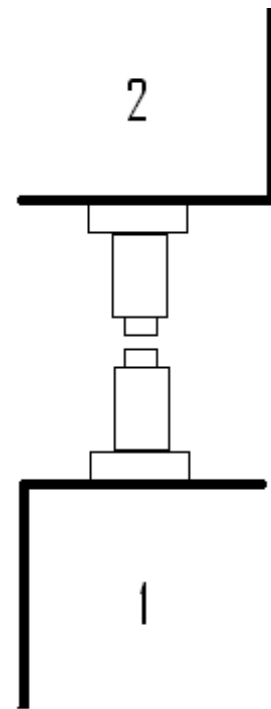


Fig 5.1: Set up of two (1 and 2) plates (7 mm) for extensional rheology.

5.3.3 Shear rheology

The rheological properties of sputum samples were measured using a parallel 60 mm aluminium plate on an AR-G2 (TA instruments, UK) Controlled Stress Rheometer. Prior to starting the experiments, the instrument's geometry inertia and rotational mapping were calibrated, followed by measurement of the rheometer's zero gap. Samples were placed on the lower plate with the upper plate being lowered onto the sample until the gap reached a pre-defined value (set after the initial wall slip test) between 400-1000 μm . This gap was then adjusted so that the sample adequately filled the gap between the rheometer plates.

All rheological experiments were conducted at a fixed temperature of 37°C using Peltier control, to replicate the mean body temperature for clinical comparison (Sanders et al., 2000). Torque sweeps were initially performed (0.1-10 Pa) to determine a stress at which the response of G' and G'' were within the linear viscoelastic region of the sample (Serisier et al., 2009). The strain was therefore set at 2%, a level deemed to be within the linear viscoelastic range.

An oscillation procedure was set up to carry out a frequency sweep, between 0.1-10 Hz (Serisier et al., 2009). The upper frequency was chosen since the ciliary beat frequency is estimated to be 10 Hz. Studies investigating the effect of normobaric oxygen on cilia beat frequency have reported frequencies of 10.2 Hz (\pm 0.9) and 9.5 Hz (Stanek et al., 1998, Shah et al., 1996). This biologically relevant frequency has been used for similar studies (Nielsen et al., 2004). The lower frequency of 0.1 Hz was chosen since the mucociliary clearance index has been estimated at 0.16 Hz (King, 1980), and a plateau was reached at frequencies lower than 0.1 Hz, possibly due to sputum reaching a permanent network structure (Nielsen et al., 2004). Other rheological studies have focused on and used 0.16 Hz or 1 Hz as their test frequency due to its low inertia, leading to highly reproducible results (Sanders et al., 2000, Sanders et al., 2006, Wills et al., 1997).

5.3.3.1 Sample heterogeneity

Visual inspection of patient sputum samples highlighted the heterogeneous nature of the sputum, varying from near liquid to relatively solid. Small CF volume samples have been shown to produce large variations in viscoelasticity when

analysing separate aliquots from the same sputum sample (Serisier et al., 2009). Hence a control was included within each treated sample. However, previous experiments of sputum heterogeneity have also shown that a sample could be divided into different treatment modalities and still remain comparable for analysis (Sanders et al., 2000). For example, using a minimum sample size of 0.9 ml good reproducibility of both G' and G'' was evident, with larger volume fractions shown to reduce the inherent variability between samples (Sanders et al., 2000). In the majority of cases, it was not possible to include control sputum samples from healthy individuals, as they are induced using 4.5% hypertonic saline (Serisier et al., 2009). This process not only has an effect on sample rheology, but also does not produce an adequate sample size. The 'gold standard' for obtaining normal respiratory secretions is an invasive procedure, where sputum is collected directly from endotracheal tubes at surgery. Again, this route does not provide adequate sputum sample sizes for rheological research (Serisier et al., 2009). To test sample variability in the samples used in this study, a single patient's samples were divided ($n=8$) for rheological testing and it acted as its own control.

5.3.3.2 Wall-slip testing

Dynamic effects within test samples may be present, which enhance the wall-slip effect (section 1.7.4). Shear rate and/or shear rate gradient will be present next to the smooth wall within the fluid. This leads to the movement of particles further from the wall. The resulting effect of these dynamic and static elements of lubrication is greater for larger particles since the particle-free layer will be bigger. Slip becomes more important at higher concentrations, greater particle size, reduced viscometer gap-size and when shear rates are decreased (Barnes, 2000). Hence, wall slip tests were completed to optimize the experimental set-up. To detect any presence of wall slip in sputum, 3 samples were tested from patient 1. The set-up was as initially described, and a frequency sweep (0.1-10 Hz) was carried out at a set gap of 1000, 800, 600, 400 and 200 μm .

5.3.3.3 Sample incubation times

Samples were incubated at different time points to assess the optimal incubation period for experiments with OligoG, and hence gain the maximum therapeutic benefit. Samples were treated with 2% OligoG and incubated for 5, 30, 60 and 240 mins (4 h). These samples then underwent a frequency sweep (0.1-10 Hz) to analyse changes in the viscoelastic properties of each test sample.

5.3.3.4 Longitudinal study

To monitor potential changes in the efficacy of OligoG with disease state, a longitudinal study of sputum rheology was conducted over 9 days on samples from patient 1, who was chronically infected with *P. aeruginosa* (**Table 5.1**). Aliquots of each sputum sample were divided into six different treatment protocols. Each sample was treated with 10% of total volume using the following treatment modalities: (1) dH₂O (v/v); (2) 100 nM rhDNase I v/v (Pulmozyme[®], Pz; Genentech Inc. San Francisco, CA); (3) 0.2% OligoG (w/v); (4) 2% OligoG (w/v); (5) rhDNase I and 0.2% OligoG; (6) rhDNase I and 2% OligoG. A final rhDNase I concentration of 2.5 µg/ml (approximately 100 nM) was chosen in line with previous studies (King et al., 1997). After addition of each treatment regime to the sputum, the samples were inverted gently (x4) prior to incubating for 4 h statically at 37°C.

5.3.3.5 Comparative study

To further observe the effectiveness of 2% OligoG (w/v), an additional 23 patient sputum samples were collected, treated and analysed as described above. All samples underwent a frequency sweep using the same parameters as before. Non-induced sputum samples (n=23) were collected by expectoration from 7 patients with CF (patients 1-7 in **Table 5.1**) attending the Cystic Fibrosis Unit, Cardiff.

In a separate experiment, a series of three samples were also used to compare treatment with OligoG and ability to modulate sputum rheology with mannitol. At the time of testing, mannitol was not licensed in the UK as an inhalation therapy for CF. These studies consequently employed Aridol[®], which is essentially the same drug, but currently used for the treatment of asthma. In these studies, and based on product information, we compared 2% mannitol with 2% OligoG.

5.3.4 Statistical analyses

Statistical analysis was performed using Graph Pad Prism[®] statistical software. The longitudinal study was analysed using Dunnett Multiple Comparisons test in conjunction with analysis of variance (ANOVA) to compare the means. The characteristics of the samples in the comparative study between the control group and 2% OligoG treated samples were tested using Wilcoxon matched-pairs signed-ranks test. Confidence intervals were set at 95% and $P < 0.05$ was considered significant.

5.4 Results

5.4.1 Extensional rheology

The extensional rheology showed a large degree of variation within the extensional viscosity of the control samples when repeated. The value for extensional strain rates also varied hugely between samples, as to be expected.

Graphs were plotted using a curve fitting step. Interestingly the degree of variation seemed to decrease when the sample was treated with 2% OligoG (**Fig 5.2**). Also, whilst patients 1 and 2 appeared to show similar curves for test and controls (i.e. untreated sample curves below those of the treated sample curves), those for patient 7 were distinctly different, with the test curves sitting between those of the various controls.

5.4.2 Shear rheology

5.4.2.1 Sample heterogeneity

A test for heterogeneity was carried out to ascertain if a single patient sample could provide reproducible results when divided into 8 individual samples for testing. The phase angle was found to have a mean of 17.95 ± 1.41 (**Fig 5.3A**) with the ratio of G'' to G' ($\tan \delta$) remaining stable throughout the test for variability. The mean $\tan \delta$ was 0.32 ± 0.03 (**Fig 5.3B**).

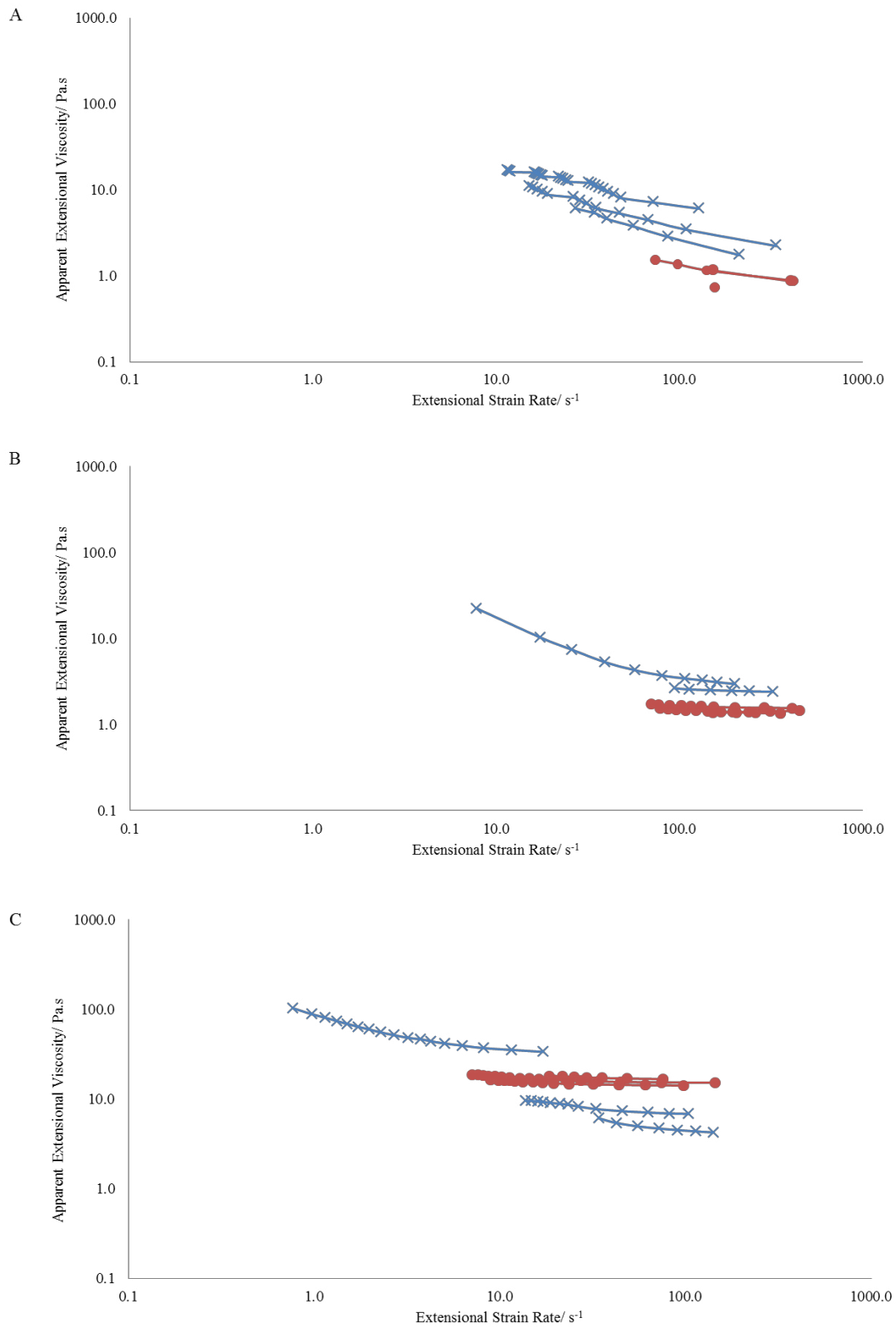


Fig 5.2: Extensional viscosity of CF sputum showing untreated (blue cross) Vs 2% OligoG treated (red circles) on patient 1, patient 2 and patient 7 respectively (A-C).

These tests revealed that a sample from a single patient can deliver reproducible results on being divided into different aliquots of 0.9 ml for testing. Furthermore, these results suggested that a single sample could be divided to compare different treatment regimens. Further control studies were then required to discover which plate gaps were the most reliable and reproducible for such comparisons.

5.4.2.2 Wall slip testing

Wall slip tests were performed on CF sputum samples (n=3) across a wide frequency range of 0.1-10 Hz. The results were plotted as complex modulus values to analyse the rigidity of the samples across the range of frequencies tested. The values across the frequencies of 0.1-10 Hz are shown in **Figs 5.4A-C**.

The values for all set gaps varied more at >1 Hz, with the greatest variation seen at >4 Hz. **Fig 5.4A** and **Fig 5.4C** revealed a high level of inertia when the gap between the sample and the upper plate was 200 μm at frequencies >1 Hz. The second run (**Fig 5.4B**) revealed an even higher effect of inertia at a set gap of 200 μm , giving erroneous results. The findings confirmed previous studies (King 1980) where the mucociliary clearance value of 0.16 Hz was used as it produced the most reliable results.

The wall slip results (n=3) were analysed further and the results were focused on 0.16 Hz. The values found at this frequency for the elastic response (**Fig 5.5A**) indicates that when the plate is lowered to 200 μm (seen for sample 2 only), the possibility of probing large clumps of sputum instead of bulk properties may occur, decreasing the homogeneity of the analysis. Similar results were seen for the viscous response with sample B again showing erroneous results when compared to the other two samples (**Fig 5.5B**). These results suggested that all subsequent testing should be carried out at a set gap of $\geq 400 \mu\text{m}$.

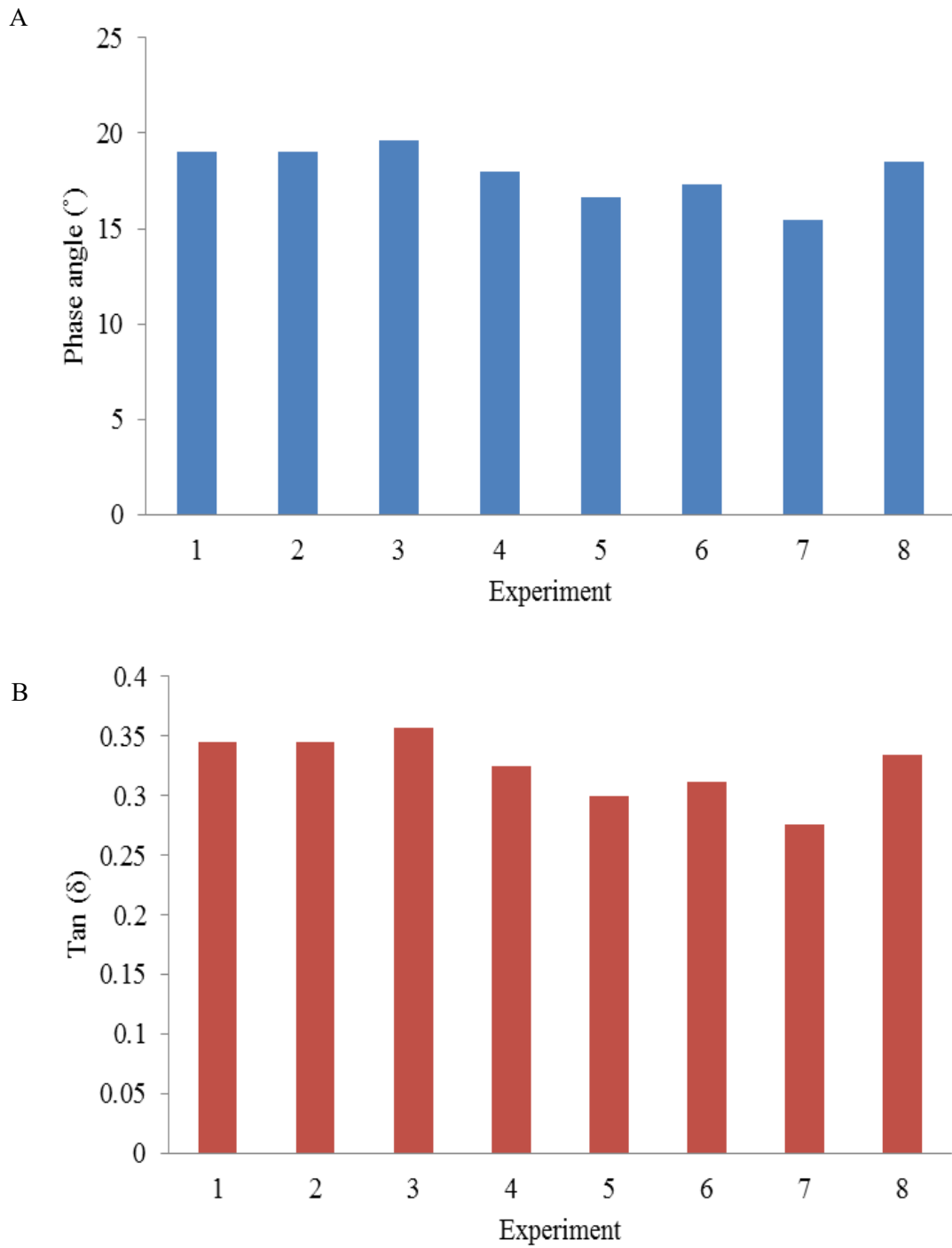


Fig 5.3: Rheological testing of a single patient sample divided into 8 aliquots to demonstrate experimental reproducibility showing; A) Phase angle (°) and B) Tan (δ) at 0.16 Hz.

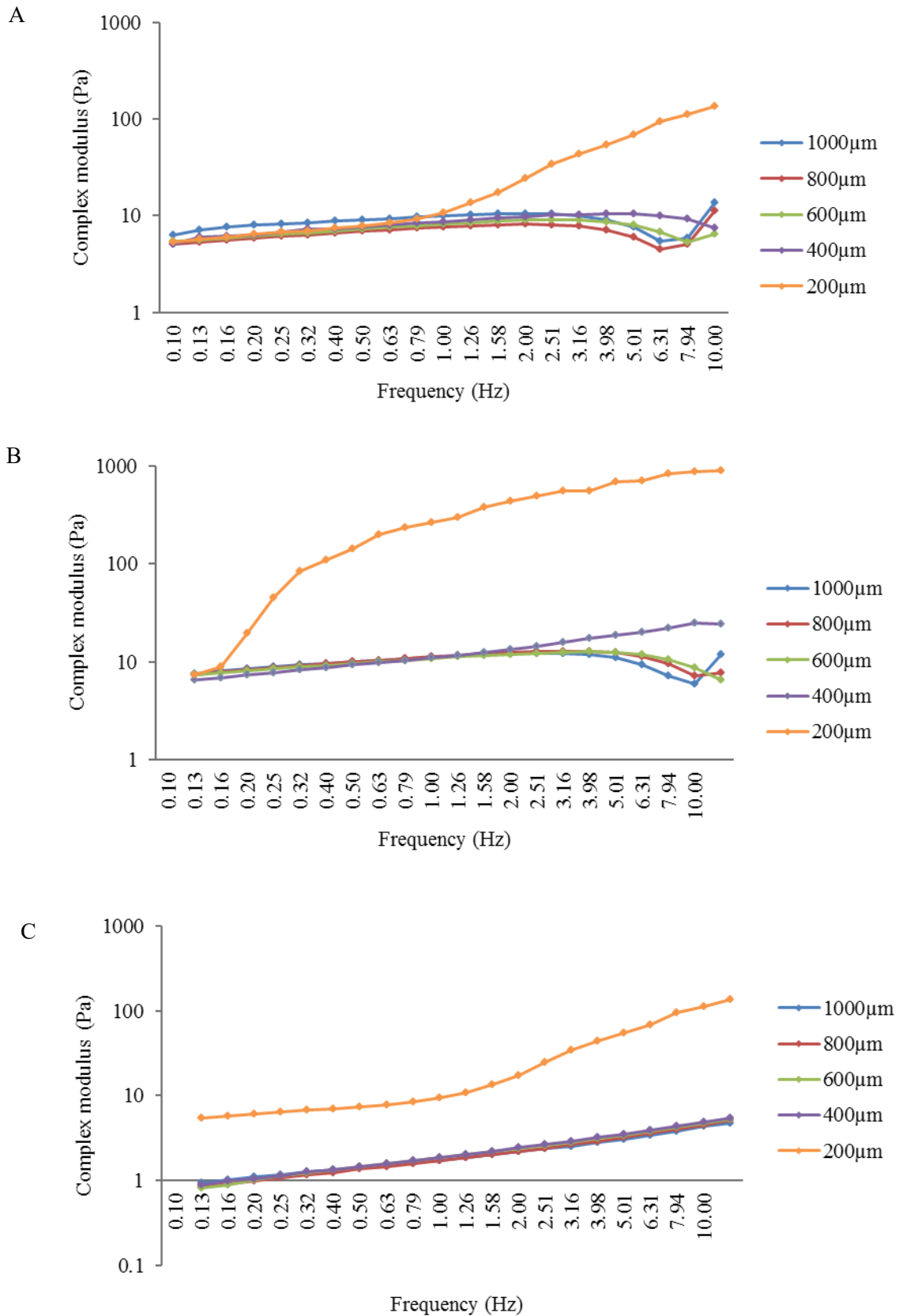


Fig 5.4: Wall slip tests showing complex modulus (G^*) values in triplicate A), B) and C) over the frequency range 0.1- 10 Hz at set gaps 200, 400, 600 and 1000 μm ($n=3$).

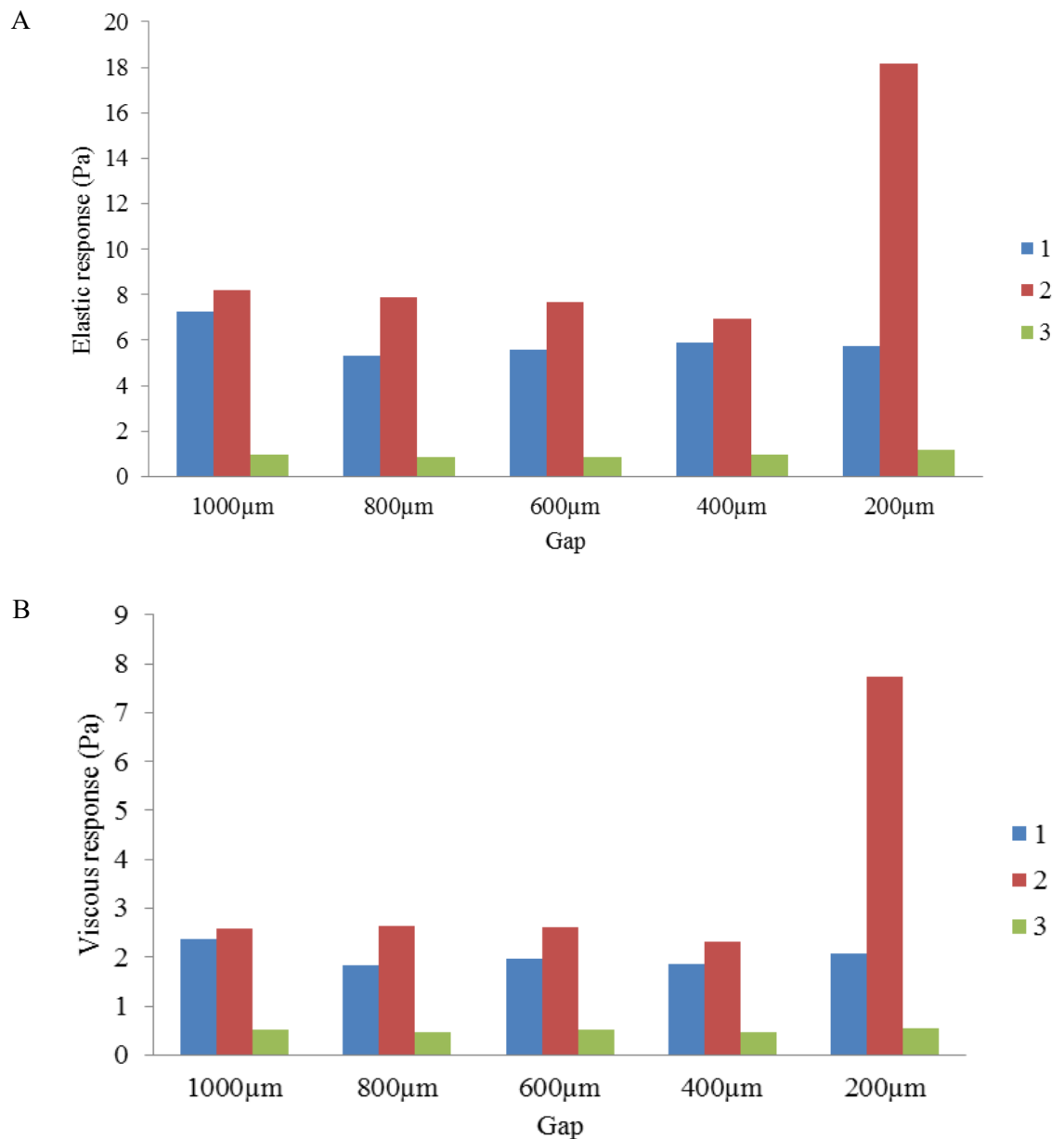


Fig 5.5: Wall slip testing at 0.16 Hz at set gaps 200, 400, 600 and 1000 μm showing A) Elastic response (G'). Mean response for pre-set gaps \pm standard deviation: 1=6.01 \pm 0.86, 2= 7.68 \pm 0.54 and 3 = 0.91 \pm 0.048. B) Viscous response (G''). Mean response for the pre-set gaps \pm standard deviation: 1= 2.01 \pm 0.25, 2= 2.54 \pm 0.14 and 3= 0.91 \pm 0.05.

5.4.2.3 Incubation time

The optimal incubation time with OligoG was determined by analysing the effect of time on both elastic and viscous response ($n=3$). The optimum incubation time could be used as an aid to determine when physiotherapy (in an *in vivo* setting) would be most beneficial after inhalation treatment with OligoG. The elastic response (G') was found to decrease after 1 h, with an even greater effect seen after 4 h (**Fig 5.6A**). Comparable results were seen with the viscous response for these incubation times (**Fig 5.6B**). Conversely, the phase angle increased considerably at 4 h incubation time (**Fig 5.6C**) suggesting that 4 h should act as the incubation period for all subsequent tests.

5.4.2.4 Longitudinal study

The longitudinal study on sputum samples collected from the same patient over 9 days demonstrated marked intra-individual variation (at 0.16 Hz) in control values of elastic response (G' ; 0.16-0.79 Pa; **Fig 5.7**) and viscous response (G'' ; 0.13-0.32 Pa; data not shown), showing considerable heterogeneity in the observed viscoelastic properties of the sputum during periods of exacerbation and hospital admission, even for samples obtained on the same day.

This study confirmed the effectiveness of the 2% OligoG treatment at reducing both the elastic response (G') and viscous response (G'') of CF sputum samples (**Figs 5.8A-B**) to approximately half those of the control ($P<0.01$). However, the data revealed an inconsistent response to rhDNase I alone, failing to demonstrate statistically significant reductions in either G' or G'' ($P>0.05$) for 6/9 test sputum samples. In contrast, rhDNase I used in conjunction with 2% OligoG showed statistically significant differences in both G' and G'' ($P<0.01$). This result suggests a potentiating effect of the combined treatment, with the observed values of both G' and G'' , being less than those for 2% OligoG or rhDNase I alone (**Fig 5.8**). A potentiating effect was also seen using 0.2% OligoG, although significant effects were observed only for G'' ($P<0.01$) and not G' ($P>0.05$).

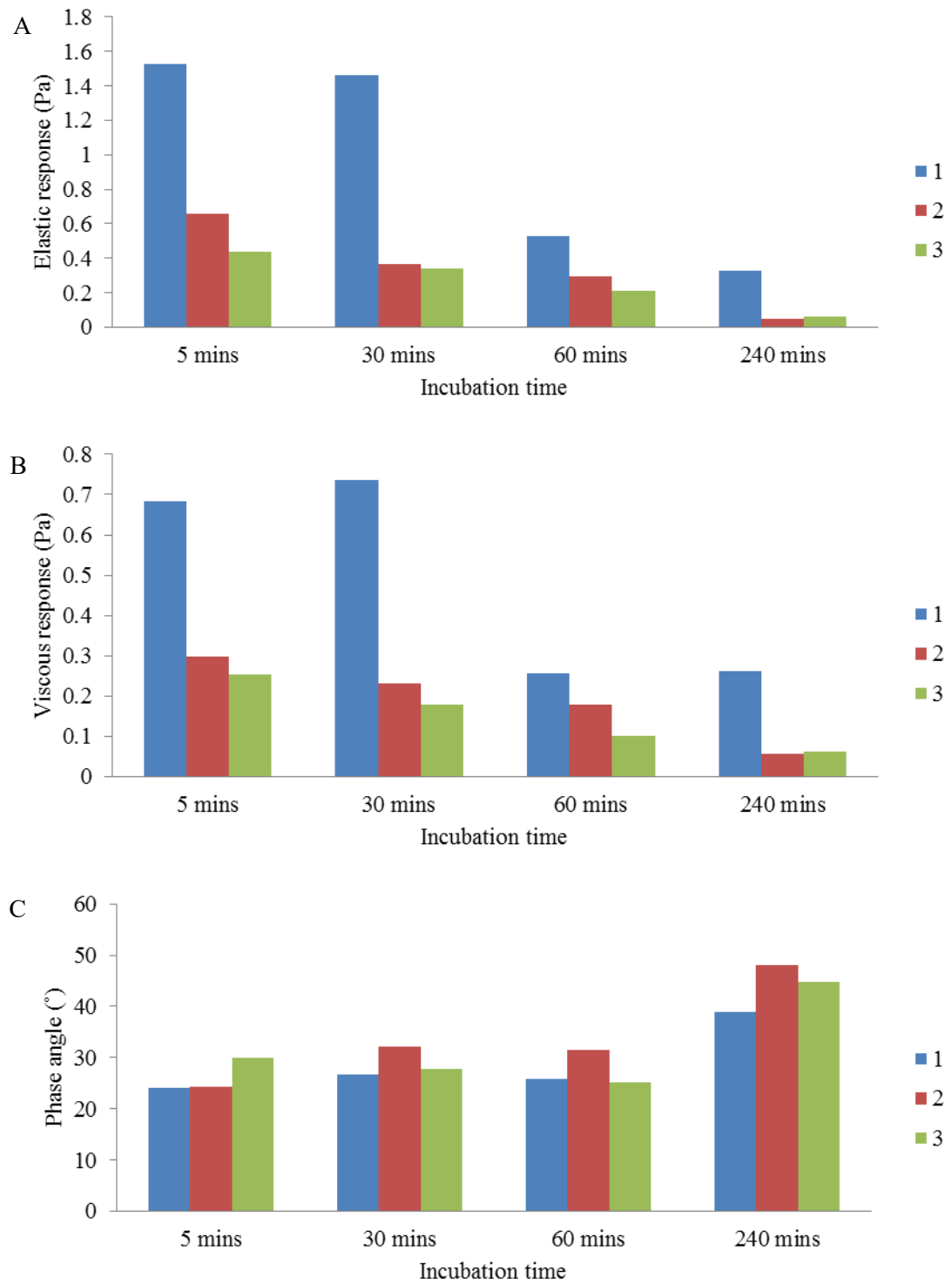


Fig 5.6: Effect of incubation time on rheological testing of OligoG treated sputum (2%) at 0.16 Hz. A) Elastic response (G'); B) Viscous response (G'') and C) Phase angle ($^{\circ}$). Set-gap $\geq 400 \mu\text{m}$ (1-3, replicates).

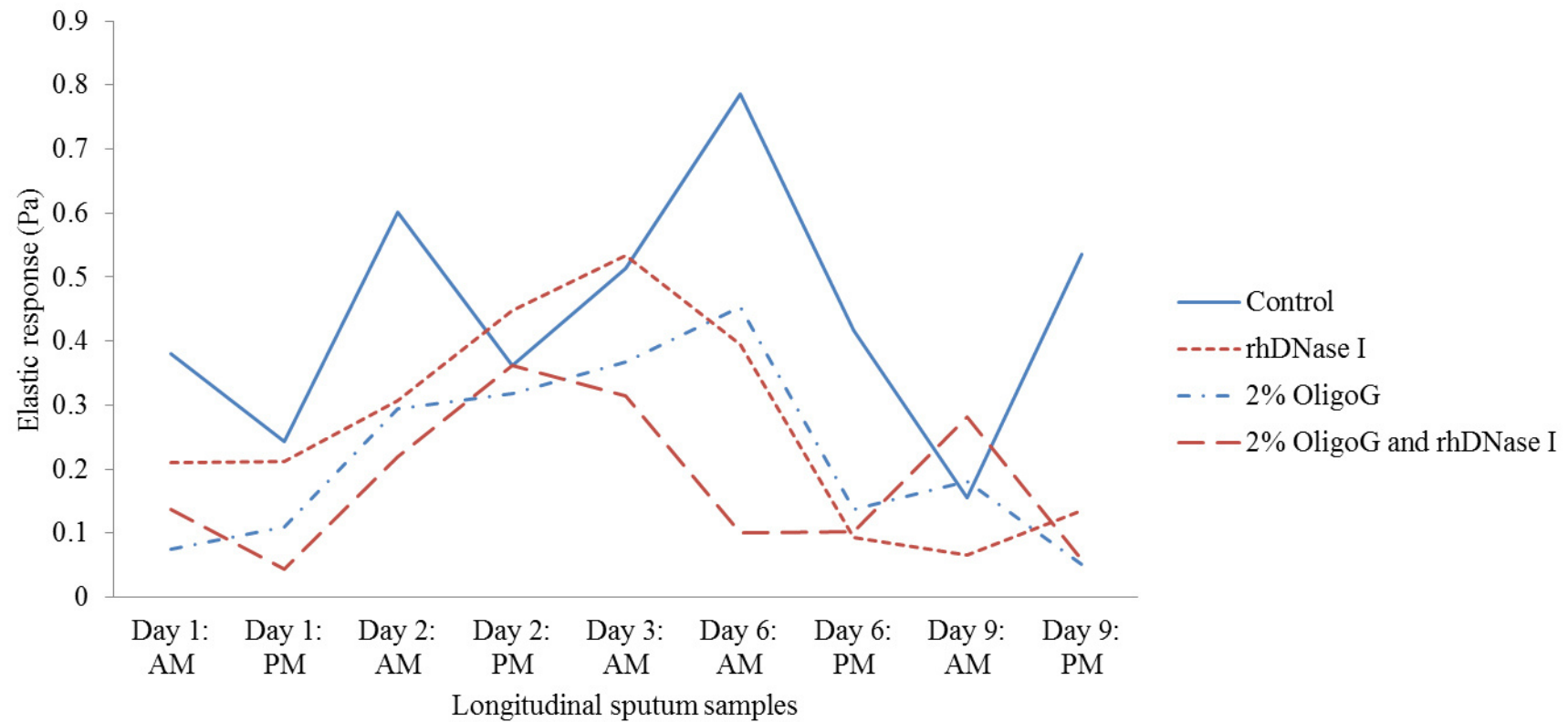


Fig 5.7: Longitudinal study of sputum samples (n=9) from a single CF patient collected over a period of 9 days, showing change in elastic response (Pa), compared to controls, when treated with 100 nM rhDNase I and/or 2% OligoG (at 0.16 Hz).

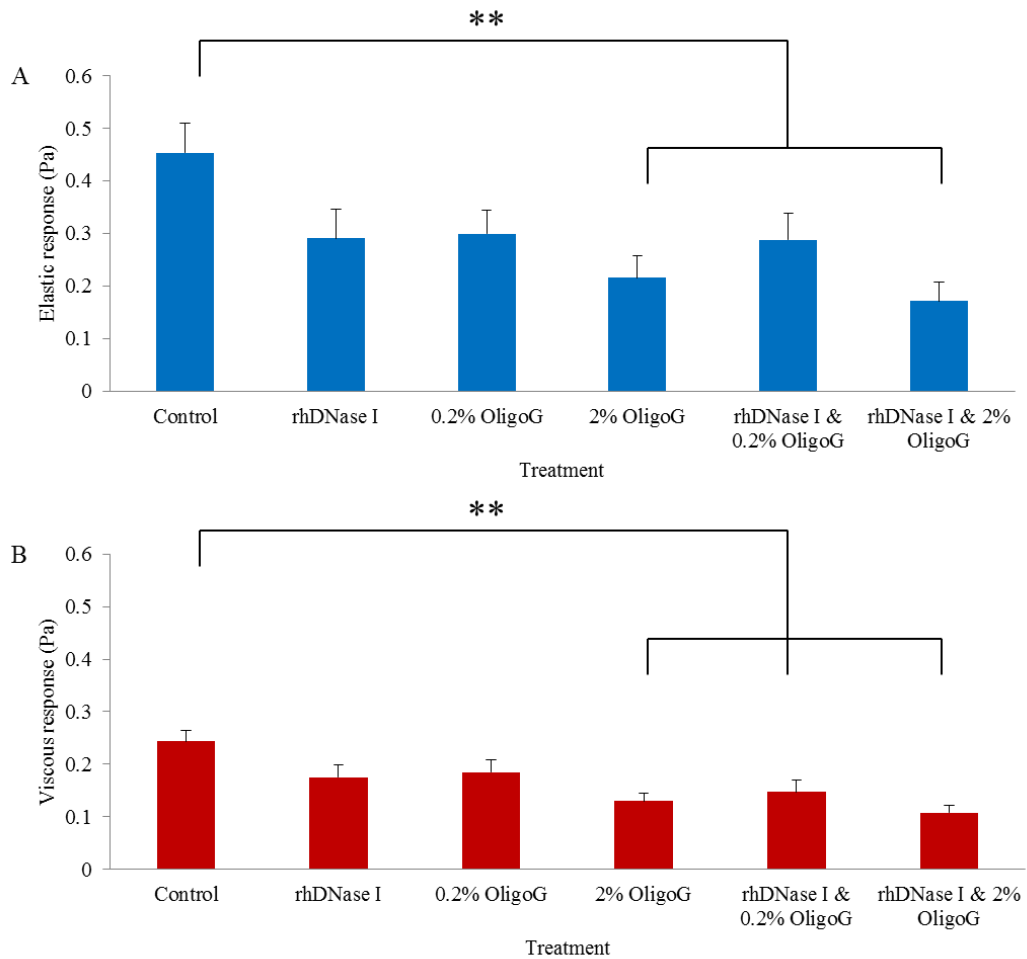


Fig 5.8: Longitudinal study for samples from a single patient collected over 9 days showing values for: A) elastic response (G'), B) viscous response (G'') at 0.16 Hz for various sputum treatments with/without 0.2% or 2% OligoG and/or rhDNase I (100 nM; n=9), ** $P < 0.01$. The error bars represent the standard error of the mean.

5.4.2.5 Comparative study

Shear rheology studies with 2% OligoG treatment showed a dramatic and significant reduction in both elastic (G') and viscous response (G'') of CF sputum compared to the dH₂O-treated control. A model has been previously developed to predict mucociliary clearance *in vivo* (King, 1980) and focused on the low frequency of 0.16 Hz, chosen to analyse mucus clearance, $P < 0.0001$; **Fig 5.9A** (Nordgard and Draget, 2011) and cilia beat frequencies 10 Hz, $P < 0.02$; **Fig 5.9B** (Nielsen et al., 2004, Stanek et al., 1998, King, 1987). There was no statistically significant change in the $\tan \delta$ value at between 0.16 Hz and 10 Hz (i.e. the ratio of G'' to G' remained comparable). The CCI modelled from the 10 Hz rheological data, showed that treatment with 2% OligoG significantly increased the predicted CCI (3.92 Vs 3.61 for the dH₂O control; $P = 0.02$).

5.4.2.6 Mannitol study

The elastic and viscous response of sputum after treatment with mannitol or OligoG was found to decrease (**Fig. 5.10**). The graphs highlight the greater effect of 2% OligoG on both elastic response (G') and viscous response (G'') in comparison to 2% mannitol treatment.

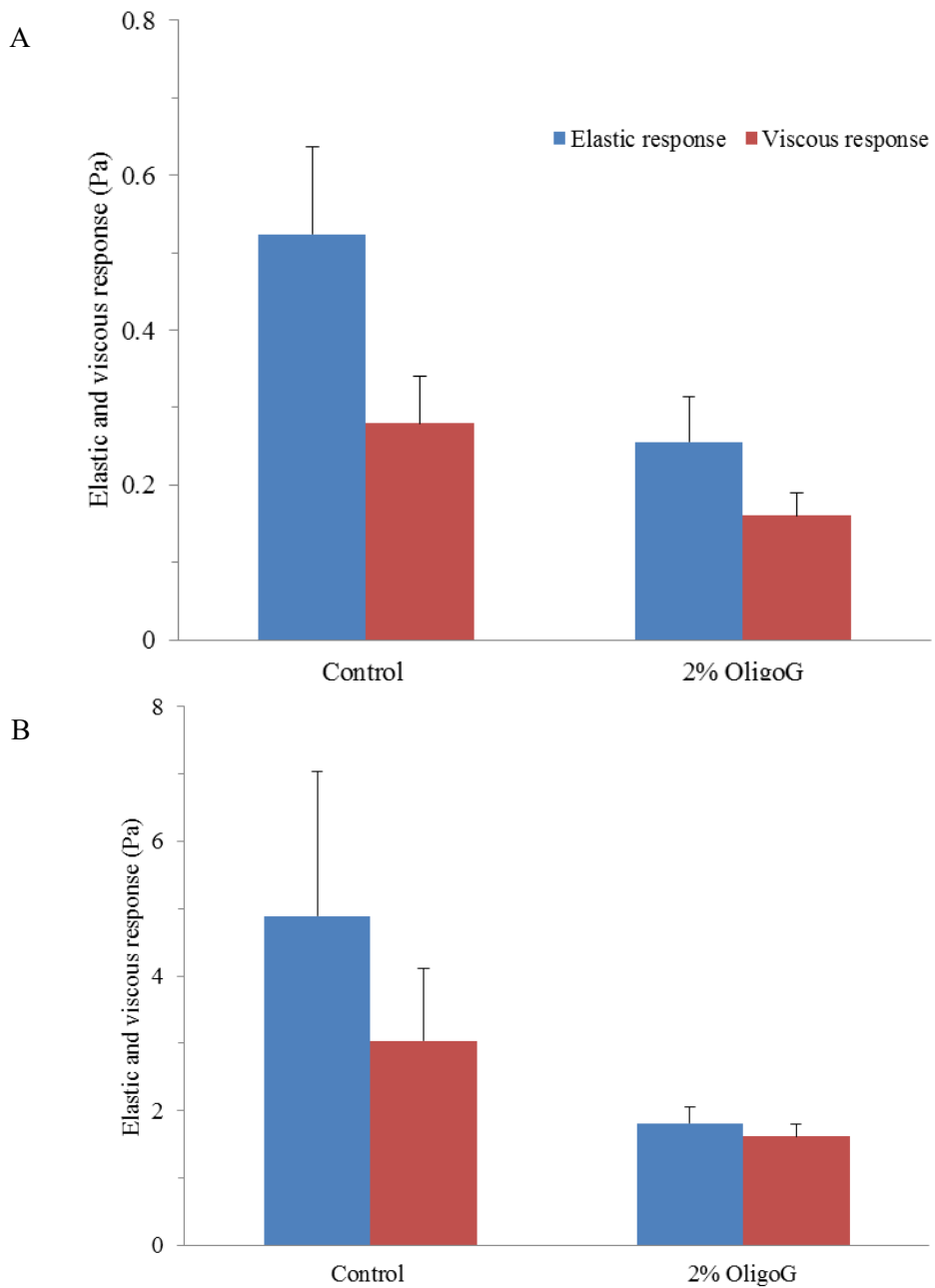


Fig 5.9: Changes in elastic response (G') and viscous response (G'') for 2% OligoG treatment of sputum samples compared to dH₂O treated controls measured at A) 0.16 Hz (n=23) and B) 10 Hz (n=21).

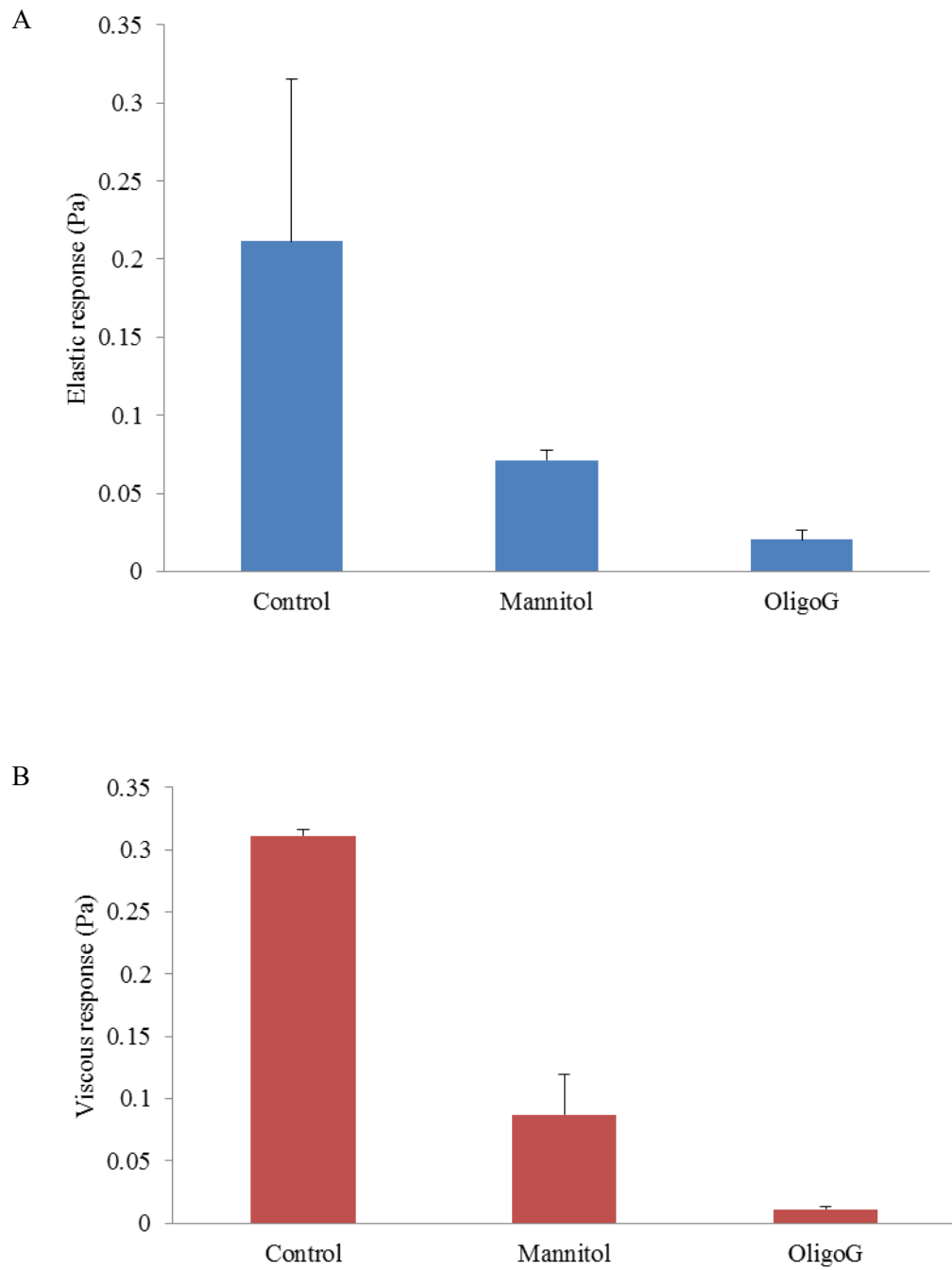


Fig 5.10: Changes in sputum rheology at 0.16 Hz showing A) elastic response (G') and B) viscous response (G'') for dH_2O treated control compared to 2% mannitol and 2% OligoG treatment.

5.5 Discussion

Potential new therapies to decrease exacerbations and aid reduction of antibiotic resistance by the breakdown of the sputum biofilms are highly desirable to decrease both morbidity and mortality in CF.

Extensional rheology experiments highlighted the heterogeneous nature of CF sputum in analysis when low sample volumes were used. The findings showed OligoG treated samples to be more homogenous, but interpretation of findings should be made with caution since the sample number was low ($n=3$). Oscillatory techniques, used to measure viscoelastic properties (i.e. G' , G'') represents a potentially useful method for testing the efficacy of mucolytic agents *in vitro* (Nielsen et al., 2004). This study employed a frequency range of 0.1-10 Hz, which was relevant to biological processes in the airway; the mucociliary clearance index having been studied at 0.16 Hz (King, 1980, Sanders et al., 2000, Sanders et al., 2006, Wills et al., 1997, Nielsen et al., 2004) and cilia beat frequency at approximately 10 Hz (Nielsen et al., 2004, Stanek et al., 1998, King, 1987).

To analyse shear rheology as accurately as possible, several control experiments were carried out. These demonstrated that dividing a single sputum sample into different treatment groups was valid and relevant for comparative analysis as long as the samples were not too small (≥ 0.9 mL) and showed that up to 4 h incubation time was optimal for 2% OligoG treatment. Time-dependent analysis of CF sputum has previously been carried out using other mucolytic targets (Kater et al., 2007). These previous studies demonstrated a time-dependent decrease in sputum cohesivity with gelsolin (Kater et al., 2007), highlighting the importance of selecting an optimum time of incubation for rheological testing, as observed here for OligoG. Although incubation may alter the properties of the mucins in the sputum sample by lowering the elastic response (Horsley et al., 2014), the results of this study remained comparable, as both treated and untreated were incubated for the same length of time.

Altered sputum rheology can impair mucociliary and cough clearance, so assessing the rheological properties of sputum is vital for determining disease progression. Various types of rheological analysis have shown the importance of measuring both elastic and viscous parameters. Sputum is a true viscoelastic material, with the elastic response (G') remaining greater than the viscous response

throughout the frequency sweep. Early rheological measurements on sputum were carried out over large deformation and forces, which led to disruption of the elastic component. However, it is important that the biopolymer structures within CF sputum are not damaged when measuring elastic and viscous responses (Nielsen et al., 2004). The untreated samples in this study showed this response across all frequency ranges were within the linear viscoelastic range.

Elastic forces have been found to impede clearance by coughing more than viscous forces. These findings may relate to a balance which exists between elasticity and viscosity of mucus in healthy individuals to optimise both forms of airway clearance (cough and mucociliary action). It has been postulated that a rheological shift may occur during airway injury (King et al., 1985). Monitoring of the viscoelastic properties of mucus is therefore important, particularly in compromised patients, since the optimal range needs to be a balance between mucociliary and cough clearance (King, 1998). The elastic properties need to be high enough to ensure that mucus is propelled by the cilia and to prevent movement down the lung, but not to the point where it resists propulsion by the cilia (Nordgard and Draget, 2011, Shah et al., 1996) since causing the mucus to become too liquid may lead to another potential hazard (King, 1998).

Another major independent variable linked to mucus clearance in a simulated cough is viscosity (King et al., 1989). When looking at the viscoelastic properties of mucus gel stimulants across a range of bronchial values found in COPD patients, a negative correlation was found between cough clearance and increased viscosity, spinnability and adhesivity, but not with elastic response (King et al., 1989). It was found that viscosity was the dominant variable. Based on the Newtonian relationship, we can see that a sample of low viscosity (η) will displace one with a higher value since:

$$F=k\eta X$$

For a given force (F), the displacement (X) is proportional to $1/\eta$. η is an important factor in governing the displacement of a given force. The wave formation created during cough clearance is influenced by the surface tension, which in turn can inhibit changes in surface architecture and hence reduce clearing. Lowering the mucus surface tension is beneficial for both forms of clearance (King et al., 1989).

As a result, the effects of OligoG (2%) in lowering the viscous response of sputum, could potentially aid clearance of sputum from the lungs *in vivo*.

The ratio of viscous response to elastic response ($\tan \delta$) is also important in mucociliary clearance. An increase $\tan \delta$ results in sputum having greater clearance potential by coughing, but less easily cleared by ciliary action (King, 1987). When viscosity is increased at constant elasticity, there is a pronounced reduction in the mucociliary transport rate (King, 1980). As CF sputum becomes too difficult to clear by the cilia, clearance by coughing becomes increasingly important (Kater et al., 2007). The ratio between viscous response and elastic response within coughing is opposite to that found for ciliary clearance. The natural balance between viscous and elastic response allows mucus to be cleared by both mechanisms (King, 1987). The ratio of viscous to elastic response was maintained by OligoG; a feature which is important clinically for the optimum clearance of mucus by both cough and mucociliary actions (King et al., 1997, Henke and Ratjen, 2007). Rheological testing could be used on samples obtained from an *in vivo* clinical trial using OligoG to confirm the findings, and detect any clinical changes found.

The results of this study (at 2% OligoG) were consistent with those previously demonstrated for another prototypical alginate oligomer, DP_n10, FG 0.89, which showed an ability to decrease the elasticity of sputum (Nordgard and Draget, 2011). DP_n10 (at a concentration equivalent to 0.06%) led to a decrease in complex modulus (G^*) and an increase in phase angle δ of treated sputum samples (in the frequency range of 0.01 to 3 Hz) indicative of electrostatic competitive inhibition, reduced cross-linking networks and weakened gel matrix. It is likely that OligoG utilises these mechanisms to target the mucin (and non-mucin) components of the CF sputum and induce the observed changes in viscoelasticity. The finding that OligoG was not immediately effective, (requiring a 60-minute incubation period to induce any effect), supported this theoretical mode of action, i.e. the “smaller” low MW alginate oligomers require time to disrupt/compete for the high MW binding sites on the mucin in the sputum (Nordgard and Draget, 2011).

Treatment with OligoG was shown to induce highly significant and reproducible changes in elastic and viscous responses (G' and G'') of sputum from CF patients over the entire frequency range studied. This study has shown that OligoG modulates the elasticity of mucus leading to a decrease in stiffness. A mixed

mucin-alginate gel will contain a combination of mucin-mucin and mucin-alginate interactions. The mucin-alginate interaction is thought to be electrostatic in nature (Taylor et al., 2005b). Low MW alginate oligomers (such as found in OligoG) have a small radius of gyration surrounding them due to their low MW, making the mucins unable to form cross-links (Nordgard and Draget, 2011). These findings (at the macroscale) accord with recent nanoscale studies, which demonstrated the ability of alginate oligosaccharides to disrupt mucin/alginate interactions (Sletmoen et al., 2012) and again reflect lower resultant cross-linking densities in the sputum (Nordgard and Draget, 2011). They also concur with the ability of OligoG to modify the extracellular polymeric substance (EPS) matrix (and structure) of bacterial biofilms *in vitro* (Powell et al., 2013). Within the mucus of CF patients, these mucin/alginate interactions appear to be enhanced (and viscosity and elasticity increased) by the excessive production of bacterial alginates by for example, *P. aeruginosa* (Fuongfuchat et al., 1996) thereby inhibiting mucociliary transport.

Contrary to previous studies, statistically significant results were not obtained in this study when treating sputum with rhDNase I. Previous studies investigating the *in vivo* treatment of CF patients with rhDNase I for ten days (Shah et al., 1996) found an immediate drop in G' , G'' and G^* values (i.e. decreased viscoelasticity) compared to the placebo ($P < 0.001$). In addition, clinical improvement in FEV₁ immediately after termination of treatment was found, but the effect did not persist. There was also no change in sputum DNA concentration after the ten days of treatment, in comparison to the placebo control group. In addition, the rheological properties of sputum were not influenced by colonisation of the lung with mucoid *P. aeruginosa* (Shah et al., 1996). These original landmark rheological studies of rhDNase I pre-date its widespread use. In our hospitalised patients receiving intensive therapy, it was ethically unacceptable to withdraw treatment with regular nebulised rhDNase I prior to sample collection. Previous studies have also found it was ethically difficult to stop patients receiving rhDNase I, so to mitigate this, sputum was collected in the morning before treatment with mucolytic agents (Sanders et al., 2006).

The variation in rhDNase I efficacy noted in the longitudinal study may reflect variations in the eDNA component of the sputum in association with inflammatory cell content and disease exacerbation (Jiang et al., 2011, Kim et al., 2006). Since

Patient 1 in this longitudinal study was already on a twice daily rhDNase I regime, its maximum effect in the samples used for the *in vitro* testing may also have been reached. However, other studies investigating the relationship between DNA content in sputum and viscosity have found no significant correlation between any classification of sputum whether mucoid, purulent or mucopurulent (Picot et al., 1978). This was hypothesised to be due to an increase in exudates, resulting from inflammatory reactions possibly diluting the DNA/glycoprotein content of the sputum (Picot et al., 1978). It may also explain why rhDNase I does not always have an optimal effect on decreasing the viscous and elastic responses (G' and G''), and why it was found only to work on 6/9 of the samples tested in this longitudinal study. Consequently, the effect of OligoG treatment at 2% dominated the changes in viscoelastic properties observed. The combined effect of rhDNase I with 0.2% OligoG revealed a synergistic effect and may in fact be a novel way to enhance the effect of rhDNase I.

rhDNase I has previously been shown to be ineffective in specific CF patients. They are known as the non-responders. Testing of responders against non-responders found a statistically significant difference between both groups, with sputum found to be extensively degraded in the former compared to the latter, where it was not degraded at all. The median decrease in sputum elastic response (G') in both groups was 32% and 5% respectively (Sanders et al., 2006). There are several hypotheses why this group of patients do not respond to treatment, including difficulty of penetration of the therapeutic through sputum.

The ability of new therapies to gain access through the complex sputum matrix is a challenge. It has been shown that fluorescently-labelled negatively-charged polystyrene nanospheres, in a range of sizes, varied in their penetration through sputum samples (Sanders et al., 2000). Larger nanospheres 270 nm and 560 nm seemed to have poor penetration due to steric obstruction. However, the water channels in CF sputum seemed to allow passage of the smallest nanospheres (124 nm). Furthermore, electron microscopy revealed pores in the sputum, ranging in diameter between 100-400 nm (Sanders et al., 2000). Interestingly, treatment with rhDNase I only, led to a minor increase in nanosphere transport. DNA fragments from degradation by rhDNase I may hinder the transport of these nanospheres through viscous effects. Another possibility is low Mg^{2+} levels which are necessary

for optimal rhDNase I activity (Sanders et al., 2000). Mg^{2+} levels in responders to rhDNase I were found to be significantly higher than those in the non-responder group. Moreover, there was a significant positive correlation between Mg^{2+} concentration and decrease in sputum elastic and viscous responses upon treatment with both rhDNase I and Mg^{2+} in the non-responder cohort (Sanders et al., 2006). Mg^{2+} is thought to be a co-factor in the enzymatic degradation of DNA by rhDNase I with a minimum concentration of Mg^{2+} required for its activity.

Actin plays a key role in rhDNase I activity. It has been shown that in a DNA concentration typically found in CF sputum (2.6 mg/ml), without actin, the activity of rhDNase I is independent of Mg^{2+} concentration (Sanders et al., 2006). It has been hypothesised that G-actin inhibits rhDNase I, and that Mg^{2+} promotes its polymerisation into F-actin, which does not interact with rhDNase I.

rhDNase I has previously been investigated for possible synergistic effects with saline, where viscoelasticity was analysed using a magnetic microrheometer technique. A significant difference was seen between 3% saline and rhDNase I compared to 0.9% saline and rhDNase I, with a decrease in the sputum rigidity index ($\log G^*$ at 1 rad/s) with the latter. Saline at 0.9% did not show a statistically significant improvement compared to the untreated control or when combined with rhDNase I. These figures also showed a reduction in spinnability when this combined treatment was used, but the reduction was less than additive, suggesting that combination treatment between saline and rhDNase I may not lead to synergy. It was postulated that the high salt concentration may have hindered the activity of rhDNase I since they were combined prior to the sputum treatment (King, 1998). OligoG on the other hand, seemed to target different areas of sputum, without hindering the efficacy of rhDNase I.

Possible synergy between physical disruption of sputum using positive expiratory pressure (PEP) and rhDNase I treatment has also previously been tested (Dasgupta et al., 1998). Flutter[®] valve (producing PEP) therapy and/or rhDNase I was carried out on sputum samples. Flutter[®] and rhDNase I treatment alone did not significantly change sputum rigidity, but when used in combination, a substantial decrease in rigidity was found ($P < 0.001$). The same trends were found when calculating CCI, as rhDNase I failed to reach significance unless combined with Flutter[®]. The authors hypothesised that the dose of rhDNase I was sub-threshold, but

potentially acted to prime the gel network, which was then degraded by the applied PEP oscillations (Dasgupta et al., 1998). Other studies have shown that combined mucolytic treatments have a greater potential patient benefit than single treatments alone (King et al., 1997, Dasgupta et al., 1998).

CF patient exacerbations are related to cough, sputum production, dyspnoea, and lowering of energy levels and appetite, which can lead to weight loss. Lowering the incidence of exacerbation is vital, since it is related to morbidity, and is consequently a strong predictor of survival (Stressmann et al., 2011). There was no significant difference found in sputum bacteriology before and after treatment with rhDNase I (Shah et al., 1996). The additive effect of OligoG may therefore be of additional benefit.

This present study showed that mannitol lowered both the elastic and viscous response, but that the effect was not as great as that observed with OligoG. Minasian et al. (2010) found that treatment with mannitol was comparable to that of rhDNase I, with a 7% increase in FEV₁ from baseline. Other studies have also found improvement in the treatment groups, irrespective of the use of rhDNase I (Bilton et al., 2011). However, mannitol did not enhance the effect of rhDNase I when used in combination. A similar reduction in exacerbation has been reported for mannitol and 7% hypertonic saline (HS); 35% and 37% respectively (Bilton et al., 2011). Mannitol and HS are not true mucolytics as they target osmolarity rather than distinct network junctions. Since the increase in G' and G'' of sputum originates from the high number of junctions between biopolymer chains per volume unit of sputum (Sanders et al., 2000), combination effects with rhDNase I was probably not to be expected.

During CF exacerbation, as well as the increase in polymeric eDNA levels, F-actin also increases significantly, contributing to the 'stickiness' of purulent CF sputum (Henke and Ratjen, 2007). The change in viscoelasticity due to the actin component of sputum has also been studied. Gelsolin is an actin-severing peptide which cleaves non-covalent bonds between actin monomers within actin filaments, whilst thymosin β 4 (T β 4) is the major actin-sequestering peptide. The viscosity of CF sputum treated with gelsolin *in vitro* has been shown to be significantly lowered at low shear (Vasconcellos et al., 1994). In contrast, no dose response change in elasticity was found when sputum was treated with thymosin β 4 (T β 4), unless it was

combined with rhDNase I (Kater et al., 2007). This synergistic response with gelsolin and rhDNase I produced a larger reduction in G' and G'' than seen with either reagent alone. This highlights distinctive targets within sputum samples and the possibility that synergistic effects can cause an amplified therapeutic treatment.

In the CF airway surface liquid (ASL), polycationic elements become entangled within the network and lower the effect of secreted antibacterial factors. Cationic antibacterial peptides such as cathelicidin LL-37 have reduced activity due to their interaction with the polyanionic nature of DNA and F-actin. This results in aggregation leading to reduced effectiveness, which is enhanced also by bacterial LPS. Breaking up the filaments of F-actin has been shown to increase effectiveness of endogenous antibacterial factors (Bucki et al., 2007). An increase in the proportion of free IL-8 and IL-8 dependent neutrophil chemotactic activity of sputum supernatants was found following *in vitro* addition of rhDNase I and gelsolin (Perks and Shute, 2000). The polyanionic nature of eDNA and actin may be repelled by OligoG to open the structure.

Respiratory failure due to chronic suppurative lung disease is the major cause of death in CF patients (Cohen-Cymbarknoh et al., 2011), with pulmonary function and chronic *P. aeruginosa* infection being the major prognostic indicators (Emerson et al., 2002). OligoG can modify the EPS of pseudomonal biofilms and increase bacterial susceptibility to antibiotic treatment *in vitro* (Khan et al., 2012). The ability of OligoG to significantly modify the viscoelastic properties of CF sputum was also evident, the characteristics of which are known to vary in the lung in association with both inflammation and infection, representing an important therapeutic target (King, 1998, Shah et al., 1996) although the exact rheological determinants of optimum ciliary transportability however, remain to be defined (Wills et al., 1997).

The ability of OligoG at lower concentrations (0.2%) to potentiate the viscoelastic changes induced by rhDNase I may reflect the distinct “targets” of the agents. rhDNase I modifies the extracellular high MW macromolecular structure of the sputum (i.e. DNA). OligoG disrupts both mucin and macromolecular mucin/alginate interactions; probably disrupting the hydrogen bonds between mucin molecules (Fuongfuchat et al., 1996). In this study, treatment with 2% OligoG more reliably decreased the elastic and viscous response compared to controls; reflecting

the universal alteration in the structural assembly of mucin in CF sputum and its value as a therapeutic target in the mucolytic treatment of CF (Davril et al., 1999).

5.6 Conclusion

There remains a need for new and improved therapies in CF, as the treatments are not universally effective and may be problematic. These studies highlight the potential usefulness of therapies to alter the macromolecular structure of mucus and affect changes in its rheology in chronic respiratory disease. The previously-described ability of OligoG to potentiate antimicrobial activity against Gram-negative bacteria (Khan et al., 2012) and modulate biofilm EPS alongside its ability, as demonstrated here, to reduce the elastic and viscous response of mucus, may be of particular use in the treatment of chronic respiratory disease (Henke and Ratjen, 2007, Elkins and Bye, 2006).

Chapter 6:
**Characterisation of the antifungal
properties of OligoG**

6.1 Introduction

The increase in adverse health effects in patients due to *Candida* species is rising at an alarming rate with soaring economic consequences (Ramage et al., 2005, Lin et al., 2005). *C. albicans* represents the most prevalent candidal species in humans but the incidence of other non-albicans *Candida* species infections is also increasing (Silva et al., 2011b, Fidel et al., 1999), many of which have high levels of resistance to conventional antifungal treatment (da Silva et al., 2013). The most frequent causes of candidiasis are *C. albicans*, *Candida glabrata*, *Candida parapsilosis*, *Candida tropicalis* (Silva et al., 2012) and *Candida krusei* (Lass-Floerl, 2009). Virulence in *Candida* species is attributed to an ability to adhere readily to host tissue, to undergo morphological alteration and to secrete hydrolytic enzymes which facilitate invasion (Silva et al., 2011b). In addition to candidal infections, fungal infections other than *Candida* species are also on the rise such as aspergillosis, zygomycosis and fusariosis (Lass-Floerl, 2009).

The prevalence of *C. albicans* in CF patients has for many years been overlooked. A prospective observational study found that 60.7% of CF patients grew *C. albicans* (Chotirmall et al., 2010). Those with the lower BMI were found to be chronically colonised. It was also found that *C. albicans* was generally isolated from those with a more advanced disease and with those colonised having more hospital treated exacerbations. Although the colonisation of *C. albicans* was not the strongest predictor of BMI or FEV₁, both parameters significantly decreased following the first acquisition found in sputum culture. It is still debated if the fungal colonisation growth represents harmless sputum positivity or a potential pathogen (Chotirmall et al., 2010).

6.1.1 Non-albicans *Candida* species

Non-albicans *Candida* species have been estimated to account for 43.5-56.5% of all reported candidemia; *C. tropicalis* being the most frequent non-albicans *Candida* species in invasive candidiasis, especially in cancer patients (da Silva et al., 2013). *C. tropicalis* is now widely recognised as an important pathogen and a greater understanding of its virulence is required.

In vitro studies employing *C. tropicalis* 519468 showed it was found to form predominantly filamentous growth on reconstituted human oral epithelium (RHE), with clear disruption of epithelial tissue being evident at 24 h, leading to tissue alteration and detachment of the superficial keratinocyte layer (Silva et al., 2011b). An increase in the level of lactate dehydrogenase activity (LHD) was also found, which correlated with the observed tissue damage. This study supported the view that the pseudohyphal form facilitated tissue invasion.

6.1.2 Morphology

Yeast-like fungi are the most common cause of fungal infections in humans (Kamysz et al., 2006). *Candida* species are polymorphic having several growth forms and can grow as both yeast and filamentous form. Pseudohyphae are formed by budding from yeast cells or hyphae, with the new growth remaining attached to the parent cells as it elongates. Pseudohyphae lack internal cross walls and have filaments with constrictions at cell-cell junctions. In contrast, true hyphae form either from an existing hyphae or a yeast cell, and are initiated by germ tube projection. This elongates and branches which divides the hyphae into a separate fungal unit (Silva et al., 2012). Certain *Candida* species may exhibit reversible transition from each growth form, conferring the advantage of rapid and efficient environmental adaptation. Different environmental signals which induce these changes in morphology include: serum, *N*-acetylglucosamine, pH changes, hypoxia, hypercapnia, temperature, starvation and adherence (De Sordi and Muhlschlegel, 2009). Not all *Candida* species form hyphae and/or pseudohyphae. *C. glabrata* is not polymorphic and can only grow as a blastoconidia (Silva et al., 2012).

6.1.3 Virulence and adherence

The invasion of host tissue by *Candida* is a complex combination of physical, mechanical and enzymatic processes. Adhesion to host tissues and morphogenesis both contribute to candidal virulence (Jayatilake et al., 2005). In addition, there are multiple virulence factors associated with *Candida* species (Shimizu et al., 1996) and four main enzymes have been associated with virulence produced by *C. albicans* strains including hyaluronidase, chondroitin sulphatase, secreted aspartyl proteinases

(SAPs) and phospholipases (PLs), which help *Candida* species to invade tissues. Interestingly, these factors have been shown to be increased in antifungal resistant strains (Ying and Chunyang, 2012).

Secretions of hydrolytic enzymes, e.g. SAPs, are key virulence factors during *C. albicans* mucosal and disseminated infections, which are important in determining pathogenicity (Schaller et al., 1999). The proteinases of *C. albicans* are made up of isoenzymes encoded by at least 10 SAPs genes that are implicated in both local and systemic infections (Schaller et al., 1999). It has been found that *SAP1-3* have a direct role in tissue damage during superficial infections, whilst *SAP4-6* are important for invasion and interaction with components of cellular defence (Schaller et al., 2001). *SAP6* expression occurs during yeast to hyphae transition (Schaller et al., 1998). Interestingly, PL was found to be particularly concentrated at the peripheries of the hyphal tips and at the initial sites of bud formation (Jayatilake et al., 2005) acting as a mechanical “anchor” for yeast survival on oral epithelium, preventing displacement by hydrodynamic shear due to morphological alteration to facilitate adhesion. Fungi are known to produce cell surface proteins such as the adhesins *HWPI* (Nobile et al., 2006). Target genes such as *ALS3* (Nobile et al., 2008) and the cell wall related protein *SUN41* (Norice et al., 2007) have been identified as important factors in biofilm adhesion and virulence in *C. albicans*.

To establish an infection, *Candida* species must mount effective stress responses to counter host defences, and adapt to dynamic changes in nutrient status within different environments (Ene et al., 2012). Changes in carbon source have been shown to dramatically affect their cell wall architecture (Lowman et al., 2011). For example, a carbon source such as lactate can strongly influence the resistance of *C. albicans* to antifungal drugs, osmotic and cell wall stresses. Furthermore, an increase in stress resistance was associated with major changes in architecture and biophysical changes independent of key stress (Hog1) and cell integrity (Mkc1) signalling pathways (Ene et al., 2012). In this respect, it is well known that *Candida* species are able to respond to changes in their immediate environment, being able to undergo reversible morphological changes between yeast (spherical cells) and hyphal (filamentous) forms of growth (Ene et al., 2012). *C. dubliniensis* and *C. albicans* have been shown to react to changes in environmental pH by changing cell shape via differential gene expression, which they use as a means of adaptation to different

ecological niches (Sosinska et al., 2011). OligoG may exert its effect on the cell wall through its use as an alternative carbon source. OligoG does not, however, significantly alter the pH of the media (Khan et al., 2012).

6.1.4 Models to assess candidal biofilm formation

In health, the intact human epithelium acts as a discrete physical and chemical barrier against *Candida* species infection. The ability to study these interactions experimentally has presented a number of problems. Animal models fail to completely mimic the human *in vivo* condition and their use poses ethical issues (Schaller et al., 1998) so more suitable *in vitro* experimental models are required. Primary oral keratinocyte mono- and multi-layered and organotypic cultures of human origin have all been previously explored as model systems to study these interactions (Oda et al., 1998, Sundqvist et al., 1991, Easty et al., 1982). The use of such human primary cell culture models is however limited due to a lack of available tissue, inter-donor variation (and hence insufficient reproducibility), as well as fibroblast contamination and limited duration of exposure. Novel alternatives to overcome these problems have used primary cell culture models with specific cell lines (Jacobsen et al., 1999) and *ex vivo* models employing biopsy tissue and the chick chorioallantoic membrane (Pugh and Cawson, 1975, Reichart et al., 1995). The reconstituted human oral epithelium (RHE; SkinEthic Laboratories, Lyon, France) provides a reproducible multi-layer keratinocyte model structure where it is possible to reproduce the internal milieu of the oral cavity within the appropriate pH range, although it has a time limit due to the multi-layer nature of the model.

6.1.5 Reconstituted human oral epithelium

The RHE model consists of well-stratified keratinocytes which are devoid of stratum corneum (**Fig 6.1**), being structurally comparable due to routine culture conditions (Schaller et al., 1998). It is essentially an ‘off the shelf’ use model for time-limited experiments (Jayatilake et al., 2005). RHE are organotypic cultures of spontaneously immortal TR146 cells originally obtained from a squamous cell carcinoma of the buccal mucosa. The tissues exhibit stratification, epithelial

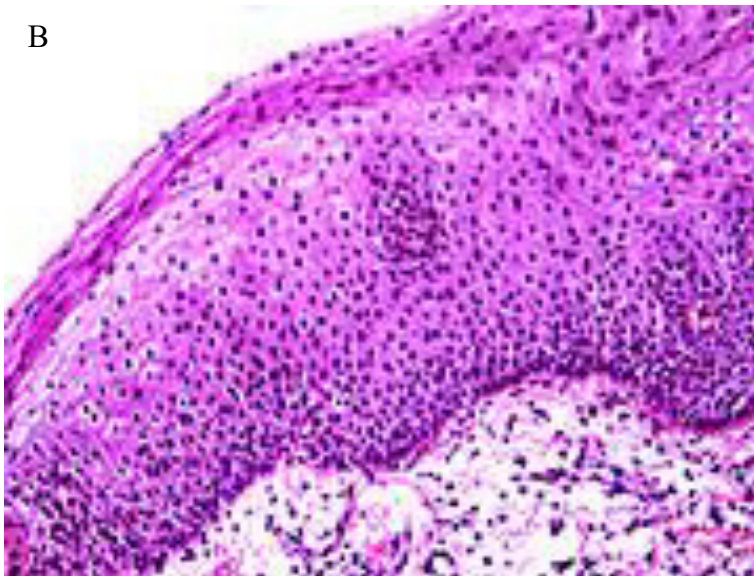
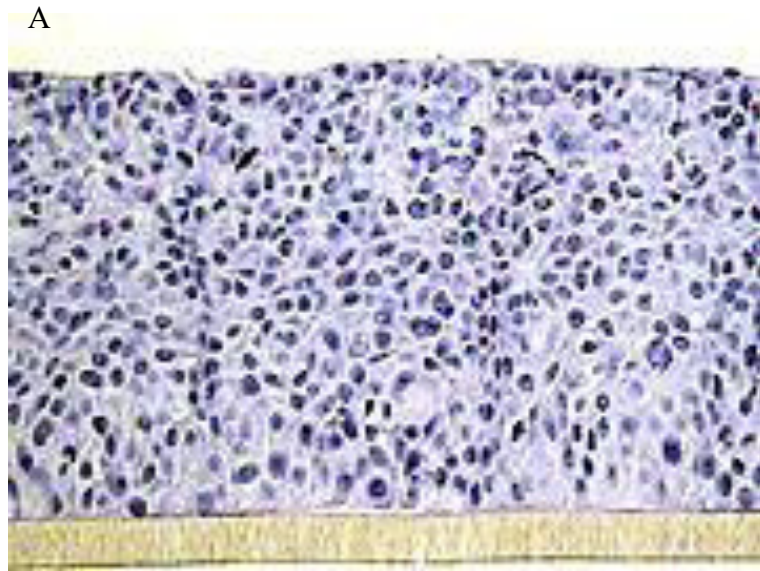


Fig 6.1: A) Reconstituted human oral epithelium (SkinEthic Laboratories, Nice, France); B) Oral epithelium *ex vivo* (SkinEthic Laboratories, Nice, France).

morphology and permeability, and express keratins in a pattern which mimics intact human epithelia (Jacobsen et al., 1999).

The suitability of the RHE model as an *in vitro* model to study chronic candidal epithelial interaction and invasion in chronic hyperplastic candidosis has been confirmed in a number of studies (Bartie et al., 2004, Jayatilake et al., 2005, Schaller et al., 2001, Malic et al., 2007). In the RHE model, differing patterns of *Candida* species tissue invasion highlight its ability to demonstrate strain-specific differences in the ability of similar strains to invade the tissue. In the model, invasion correlated with the expression of SAP and morphological changes (Bartie et al., 2004, Schaller et al., 1999). RHE has therefore been shown to be a useful test for oral pharmacology experiments (Schaller et al., 1998). RHE has also been used in permeability studies for therapeutic applications, for example, to detect diffusion of naltrexone across the oral mucosa (Giannola et al., 2007).

More recently, site specific keratinocyte (including reconstituted human vaginal epithelium) models have been employed to analyse cytokine responses using quantitative PCR and fluorescence-activated cell sorting (Schaller et al., 2005). This study showed that specific *SAPs* causing tissue damage correlated with an epithelial induced pro-inflammatory cytokine response.

Whilst the RHE model lacks humoral or cell-mediated immune responses (Bartie et al., 2004), which are pivotal in regulating candidal epithelial interaction in humans, the model system is pliable, reproducible and of value in studying the interaction of potential antifungal agents with fungal adhesion and invasion of epithelia. Often patients predisposed to candidal infection will have an altered or depressed immunity (Schaller et al., 1998) which therefore cannot be completely replicated using this model.

6.1.6 Antifungal agents

Fungi are eukaryotic cells which means their mechanism of gene expression, replication and some structural features are similar to those found in human cells, which makes development of highly specific antifungals difficult (Kamysz et al., 2006). An antifungal agent is a substance of biological, semi-synthetic or synthetic origin which inhibits the growth of, or kills fungi (Rodriguez-Tudela et al., 2008).

Various chemical classes of antifungal agents are in widespread clinical use to treat *Candida* species infections and include polyenes, azoles, echinocandins, pyrimidine analogue and flucytosine. Fluconazole is the most commonly prescribed antifungal agent (des Champs-Bro et al., 2011, Prasad et al., 2008) and is used prophylactically as well as for treatment (da Silva et al., 2013). Fluconazole activity is mediated by inhibition of the enzyme responsible for converting lansterol to ergosterol, which is a key component in fungal cell membranes. Exposure to fluconazole results in cell lysis and death. It is available in either intra-venous or oral formulations and is rapidly absorbed from the gastrointestinal tract (Watt et al., 2011, Morschhauser, 2010).

In contrast to the studies of bacterial biofilm resistance to antibiotics, the mechanisms by which biofilms resist the action of antifungal agents is not well characterised. It has been postulated that the mechanism may include drug exclusion by the biofilm matrix and phenotypic changes due to nutrient limitation or a switch to a low growth rate (Baillie and Douglas, 2000). Mutations in *ERG11* which encodes sterol 14 α -demethylase can affect binding of azoles to the enzyme, which results in drug resistance. An increase in expression of *ERG11* can also lead to azole resistance and alterations in the sterol biosynthesis pathway that bypass the accumulation of toxic sterol (Morschhauser, 2010). It has also been found that diffusion through a mixed-species biofilm comprising of *C. albicans* and *Staphylococcus epidermis* is very slow (Al-Fattani and Douglas, 2006). Resistance is the main disadvantage for the clinical use of azole antifungals like fluconazole, itraconazole and voriconazole (Aperis et al., 2006). The efficacy/toxicity ratio of some antifungal agents such as amphotericin B is unfavourable and can lead to hepatic and kidney damage at high concentrations (Giordani et al., 2004). Another factor limiting amphotericin use is neutropenia (Kamysz et al., 2006).

New targets for antifungal activity have been developed with echinocandins being the newest addition, approved by the FDA (Cappelletty and Eiselstein-McKitrick, 2007). Echinocandins are the first new antifungal drug classes introduced in more than 20 years (Denning 2002). Echinocandins inhibit 1,3- β -D-glucan synthetase and have a broad spectrum fungicidal activity against *Candida* species (Chamilos et al., 2007). Echinocandins have low host cell toxicity and have a rapid fungicidal activity against most *Candida* species with predictable kinetics

allowing once-a-day dosing (Denning, 2002). Voriconazole and amphotericin B have shown synergy with echinocandins, but unfortunately the clinical response has been variable (Cappelletty and Eiselstein-McKittrick, 2007).

6.1.7 Combination therapy

The number of antifungal drugs available for clinical use is limited in comparison to antibacterial drugs, and there has also been an increase in cross-resistance thereby driving the need for new therapeutic strategies in this area (da Silva et al., 2013). Antifungal treatments are also often limited due to their toxicity and adverse side effects leading to chills, fever, headache, nausea and vomiting, and dose-limiting nephrotoxicity (Dismukes, 2000, Lewis, 2011). The use of combined antifungal therapy has been postulated as a means to promote efficacy and lower the observed systemic toxicity of antifungal agents (Harris and Coote, 2010, da Silva et al., 2013). Examples of this include the combined use of amphotericin B with an azole to target ergosterol and its synthesis, respectively (Kalkanci et al., 2010), administration of the fungicide amiodarone with fluconazole to broaden its antifungal activity (da Silva et al., 2013) and effective treatment against the protozoan *Trypanosoma cruzi* using the antifungal posaconazole in combination therapy with amiodarone (Veiga-Santos et al., 2012). Naturally occurring peptide antibiotics have considerable potential as novel antifungal compounds (Kamysz et al., 2006) and show synergy with of a range of antifungal agents (Harris and Coote, 2010). Iron chelation alone or in combination with antifungal drugs may be another useful means for the prevention and treatment of mycoses (Zarembek et al., 2009). Essential oil from *Cinnamomum cassia* (Giordani et al., 2006), *Thymus vulgaris* thymol chemotype (Giordani et al., 2004) and acteoside isolated from the aerial parts of the shrub *Colebrookea oppositifolia* (Ali et al., 2011) have been shown to potentiate amphotericin B, with the latter having fungitoxic properties against various *Aspergillus* species. Citrinamides A and B are aromatic alkaloids isolated from *Penicillium* species FKI-1938. Such alkaloids have shown moderate potentiation of miconazole activity against *C. albicans* (Fukuda et al., 2008). However, limiting factors such as the allergenic potential of natural oil needs to be taken into account for *in vivo* application (Giordani et al., 2006).

A newer approach is to incorporate substances not classified as antimicrobials, for example, enzymes such as alginate lyase (AlgL; Bugli et al., 2013) and in this regard, therapeutic dose of polyene antifungals on *Aspergillus fumigatus* infections was shown to reduce in the presence of AlgL. Although alginate is not found in *A. fumigatus* extracellular matrix, other polyuronates are found, which can be degraded by AlgL. The hyphae are cohesively bonded together by a hydrophobic EPS and nonspecific degradation by the enzyme, enables polyenes to exert their antifungal action (Bugli et al., 2013).

6.2 Aims

Whilst the mechanism by which OligoG affects the growth of *Pseudomonas* species remains largely unknown, this effect is however, striking. Conceivably, OligoG therefore could also affect the formation and assembly of candidal biofilms and subsequent interaction with epithelial surfaces.

The hypothesis of this study was that exposure of *Candida* species to OligoG might induce a disrupted morphology and a decreased biofilm mass, and this could be studied in an established biofilm model. The specific aims of the study were:

- To utilise scanning electron microscopy (SEM) and atomic force microscopy (AFM) to characterise changes in biofilm assembly in the presence of OligoG.
- To utilise electrophoretic light scattering (ELS) to analyse changes in surface charge by OligoG treatment.
- To utilise the RHE model to study the changes in fungal adherence and invasion induced by OligoG treatment.

6.3 Materials and Methods

6.3.1 Culture media and fungal strains

Sabouraud Liquid Broth (SAB; LabM, Heywood, Lancashire) and Sabouraud Dextrose Agar (SDA; Lab M) were used for routine maintenance and growth of *Candida* species. A completely synthetic medium, RPMI-1640 (Sigma-Aldrich) traditionally used for susceptibility testing of fungi was also employed for additional

experiments where limited fungal growth was required e.g. testing of antifungal therapeutics (Rodriguez-Tudela et al., 2008). Media was filter-sterilised and stored at 4°C until use. Prior to each experiment *Candida* species were grown aerobically on SDA at 37°C for 18 h. Yeast Nitrogen Base (YNB; BD Diagnostics, Cowley, UK) medium supplemented with 0.5% glucose (w/v) was used for the RHE studies.

The strains chosen for these studies (**Table 6.1**) were those previously used for susceptibility testing with OligoG, MIC elucidation with various antifungals and germ tube formation tests. These strains were previously characterised in a preliminary study of co-culture with OligoG, undertaken by collaborators in Norway (see **Appendix III**).

Table 6.1: *Candida* strains and sources.

<i>Candida</i> strain	Strain source
<i>Candida albicans</i> CCUG 39343	Faeces
<i>Candida tropicalis</i> 519468	Urinary
<i>Candida glabrata</i> ATCC 2001	Faeces
<i>Candida albicans</i> ATCC 90028	Blood

6.3.2 LIVE/DEAD[®] staining of *Candida tropicalis* 519468 biofilms grown in OligoG

An overnight (O/N) culture of the fluconazole resistant, *C. tropicalis* 519468 was grown in RPMI-1640 broth. Biofilms were grown in 8-well chamber slides (BD Falcon), using an inoculum of 35 µl of O/N culture per well (10^7 cells; OD₆₀₀), followed by addition of either 350 µl of RPMI-1640 or 350 µl of 2% OligoG (w/v solubilised in RPMI-1640). The chamber slides were then incubated for 24 h at 37°C, with gentle rocking. The supernatant was removed and the biofilm stained with LIVE/DEAD[®] BacLight[™] Bacterial Viability Kit (Invitrogen, Paisley, UK) containing SYTO[®] 9 dye and propidium iodide, prior to imaging under a fluorescent microscope (Olympus Provis AX70). The Bacterial Viability Kit was used preferentially to Yeast viability kits (personal communication: Dr S. Malic) in this study.

6.3.3 Effect of growth in OligoG on *Candida* species biofilm formation

6.3.3.1 Scanning electron microscopy imaging

Three *Candida* species from a variety of clinical sources were chosen to detect changes in biofilm formation in the presence of OligoG. These isolates were *C. tropicalis* 519468, *C. glabrata* ATCC 2001 and *C. albicans* 39343. Thermanox™ glass slides (15 mm diameter; Agar Scientific) were inserted into each well of a 12-well Cellstar® plate (Grenier Bio-One, Stonehouse, UK) and 1 ml SAB ±2%, 6% and 10% OligoG (w/v) was added. The O/N *Candida* cultures were diluted 1 in 10, and 20 µl added to each test well which were then mixed well prior to being incubated for 24 h (with gentle rocking) at 37°C. The supernatant was removed and each well immersed in 2.5% (v/v) glutaraldehyde for 1.5 h prior to being washed (x 4) with dH₂O. After addition of 1 ml dH₂O to each well, the biofilms were frozen (-20°C) before being placed in a freeze-dryer for 24 h. Imaging was performed using a Hitachi S4800 SEM, without sputter coating.

6.3.4 Effect of OligoG and fluconazole combination therapy on growth of *Candida tropicalis* 519468 biofilms

6.3.4.1 Scanning electron microscopy imaging

C. tropicalis was inoculated in RPMI-1640 medium and incubated aerobically at 37°C O/N for 24 h, at 160 rpm. The O/N culture was diluted to 4×10^6 cfu/ml as determined by an OD₆₀₀ reading of 0.3 (Muter et al., 2001). One ml of the diluted culture was incubated with gentle rocking (4 h, 37°C) on Thermanox™ slides in the bottom of 12-well Cellstar® plates. Each well was washed (x 3) with pre-warmed RPMI-1640 medium. To each well, 1 ml of either 0.5, 1 or 2 mg/l fluconazole and/or 2% OligoG (w/v) in RPMI-1640 was added and further incubated with gentle rocking (24 h, 37°C). The cell preparations were fixed and freeze dried as described in 6.3.3.1 above. Imaging was performed using a Hitachi S4800 SEM, without sputter coating.

6.3.4.2 Atomic force microscopy imaging

Sample preparation for AFM was as previously described (Murillo et al., 2005). Briefly, *C. tropicalis* 519468 was grown O/N in SAB by gently rocking. Then, 10 ml of this O/N culture was centrifuged (2,100 x g, 10 mins) and the pellet re-suspended in pre-warmed SAB to attain an inoculum of 4×10^6 cfu/ml (OD₆₀₀). Biofilms were formed in polystyrene petri dishes (90 mm x 16.2 mm; Fisher Scientific) using 6 ml of inoculum, by shaking incubation at 37°C for 5, 30, 90 or 240 mins. Initial studies (data not shown) determined that the depth of biofilm formed after 240 mins was too dense for AFM analysis and a maximum growth time of 90 mins was chosen for subsequent experiments. The concentration of fluconazole used was set at the conventional MIC value i.e. 1 mg/l (see **Appendix III, Table III.i**, undertaken by collaborators in Norway).

Separate experiments investigating biofilm inhibition and disruption employed 6 ml of inoculum (prepared as above) \pm 2% OligoG (w/v) and/or fluconazole (1 mg/l). Biofilms were incubated at 37 °C for 90 mins. Biofilm disruption studies grew the initial inoculum (6 ml) for 30 mins and then replaced the medium with fresh SAB for a further 90 mins in the absence or presence of \pm 2% OligoG (w/v) and/or fluconazole (1 mg/l).

Prior to AFM imaging, biofilms were rinsed with dH₂O (x 2) and air dried at room temperature for 1 h. Imaging was performed using a Dimension 3100 AFM (Bruker), scan speed of 0.7 Hz.

6.3.5 Effect of OligoG on zeta potential (surface charge) of *Candida* species

O/N cultures of *C. tropicalis* 519468 and *C. albicans* 39343 were grown statically in SAB at 37°C; 100 μ l of each culture was used to inoculate fresh SAB, before culture at 37°C for 19 h at 80 rpm. One ml of this culture was removed and washed at 5,500 g (3 mins) in dH₂O (x2) to remove growth medium. The pellet was re-suspended in 100 μ l of appropriate buffer and 20 μ l of this suspension added to 1 ml of the relevant electrolytic solution at a salt concentration of 0.01 M NaCl, pH 5, 7, and 9, with or without OligoG (10%; w/v). *Candida tropicalis* 519468 and *C. albicans* 39343 were incubated in the relevant solution for 20 mins, before the sample was subjected to further washing and centrifugation at 2,500 g (6 min) to

remove excess OligoG. ELS analysis of zeta potential was performed before and after the last centrifugation step. *Candida* species cells exposed to lower concentrations of OligoG (0.2-1%) were not subject to further washing and centrifugation since at lower concentrations excess OligoG was unlikely to mask the results. ELS was therefore tested immediately after the 20 mins incubation step. A Zetasizer Nano ZS (Malvern Instruments) and disposable capillary cells (DTS1061 Malvern instruments) were used. The zeta potential of *C. tropicalis* 519468 and *C. albicans* 39343 was calculated by applying Smoluchowski's model, as described in section 2.1.3.

6.3.6 *In vitro* reconstituted human oral epithelium infection model

6.3.6.1 Growth curves and effect of OligoG

C. albicans ATCC 90028 was grown O/N in Yeast Nitrogen Base (YNB; BD Diagnostics, Cowley, UK) medium supplemented with 0.5% glucose (w/v) at 37°C without agitation. This culture was diluted to 5×10^7 cfu/ml in 0, 0.2, 2, 6 or 10% OligoG (w/v) for use as the inoculum for growth curve experiments. Each growth curve was conducted in triplicate using 200 µl of inoculum in a 96-well plate, with a YNB ±OligoG blank. Growth curves were conducted over a 24 h period at 37°C and results recorded on a Fluostar Omega plate reader (BMG LABTECH). Readings measuring change in cell density were recorded every hour.

6.3.6.2 Preparation of *Candida albicans*

C. albicans ATCC 90028 was cultured on SDA at 37°C for 24 h. A single colony from the resulting growth was sub-cultured into YNB and incubated for 12 h at 37°C under gentle agitation. This suspension was centrifuged and washed (x3) with phosphate buffered saline (PBS). The resulting yeast cells were enumerated using a haemocytometer and 50 µl of 2×10^6 cfu/ml was added to the RHE (SkinEthic Laboratories, Nice, France).

6.3.6.3 Preparation of RHE

RHE models were generated by SkinEthic Laboratories, Nice, France by culturing transformed human keratinocytes derived from the cell line TR146.

Cultures had been incubated in serum-free conditions (in line with the manufacturer's protocol, see **Appendix III, Fig III.i**). A chemically defined MCDB-153 medium containing 5 µg/ml insulin and 1.5 mM calcium chloride was used to grow the cells on a 0.5 cm² microporous polycarbonate filter for 5 days. The MCDB-153 medium contained essential amino acids, vitamins, inorganic salts, organic compounds and trace elements. The RHE *in vitro* model and all culture media were devoid of any antibiotics and antimycotics.

6.3.6.4 Culture and imaging of infected RHE

Immediately following delivery of the RHE, the tissue was removed from the agarose-nutrient solution and placed in a fresh 6-well tissue culture plate with 1 ml of SkinEthic maintenance medium (see **Appendix III, Fig III.i**) ± 0.2, 2 and 6% OligoG (w/v), prior to the addition of the candidal inoculum. RHE infected with 2 x 10⁶ cfu/ml *Candida* were incubated for 12 h at 37°C in a humidified atmosphere enriched with 5% CO₂. A non-infected control ± 6% OligoG (w/v) was included and all experiments were repeated in triplicate.

Cell viability was studied employing CLSM with LIVE/DEAD[®] staining. Following co-culture with *C. albicans*, RHE were placed on microscope slides and 100 µl of LIVE/DEAD[®] was placed directly on the tissue (containing 25 µM SYTO[®] 9 and 15 µM propidium iodide). The samples were incubated for 30 mins at 37°C in the dark prior to being transferred onto a clean glass slide. The tissue was covered with Vectashield[®] mounting medium to prevent “photo bleaching”. CLSM was performed using a Leica TCS SP2 AOBS spectral confocal microscope (Leica Microsystems GmbH, Wetzlar, Germany). All experiments were repeated in triplicate.

6.4 Results

6.4.1 LIVE/DEAD[®] Staining of *Candida* species biofilms grown in OligoG

LIVE/DEAD[®] staining (**Fig 6.2**) revealed that *C. tropicalis* 519468 biofilms grown in the presence of 2% OligoG possessed distinct differences in biofilm structure compared to the untreated control. OligoG treatment resulted in biofilm

disruption, as demonstrated by increased cell and hyphal death (red) in comparison to live cells (green) and a more 'open' and less densely-formed biofilm.

6.4.2 Effect of growth in OligoG on *Candida* species biofilm formation

The structural changes of candidal biofilms induced by OligoG were species-specific. SEM imaging of a range of OligoG concentration revealed the dose dependent effect of *C. tropicalis* grown in OligoG. Treatment with 2-10% OligoG induced potential elongation (length) and "flattening" of candidal cells (**Fig 6.3**). The biofilms exhibited less cell biomass, with a "looser" cellular structure as the OligoG concentration increased (**Fig 6.3**). In contrast, the same pattern was not seen with *C. albicans*, where cell size and shape appeared unaffected. Instead "cell flattening" was only apparent at the highest OligoG concentrations (10%), which corresponded to a "looser" biofilm structure, decrease in cellular biomass and an increase in water channels (**Fig 6.4**). The overall effect of OligoG on *C. glabrata* appeared negligible (**Fig 6.5**).

Control

2% OligoG

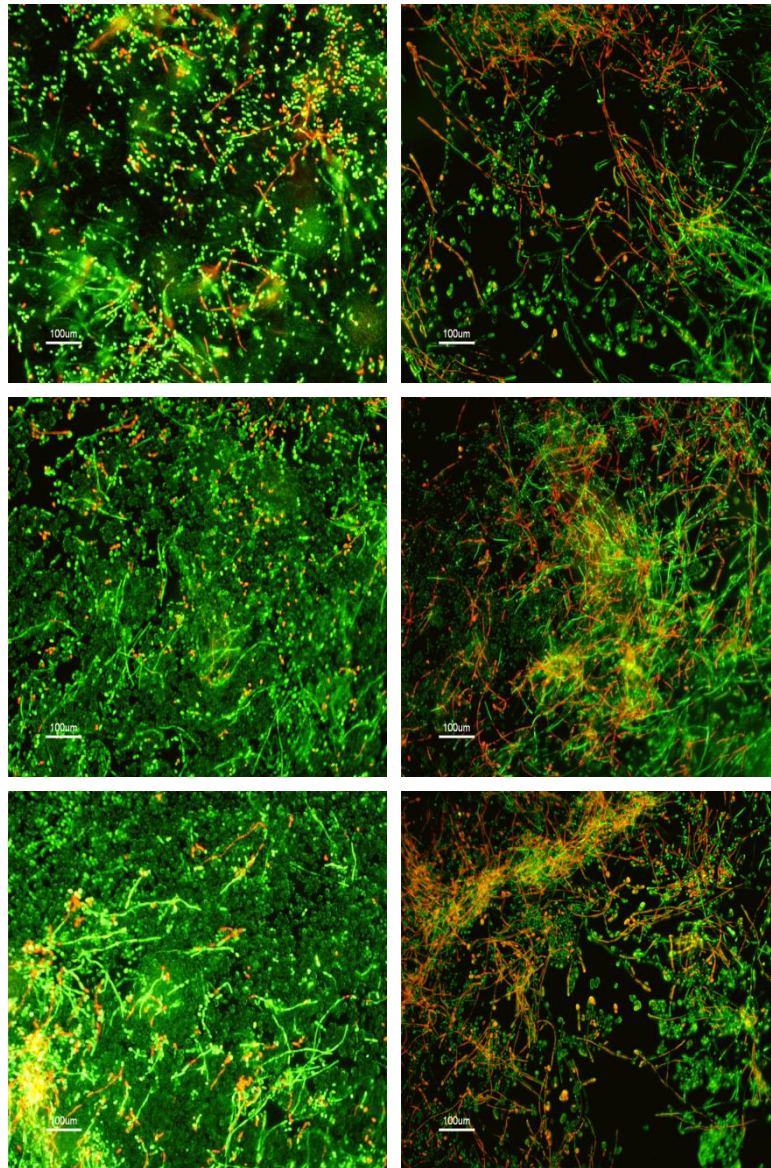


Fig 6.2: LIVE/DEAD[®] fluorescence imaging of *C. tropicalis* 519468 grown for 24 h at 37°C. Untreated control Vs 2% OligoG. Green and red represent live and dead cells respectively.

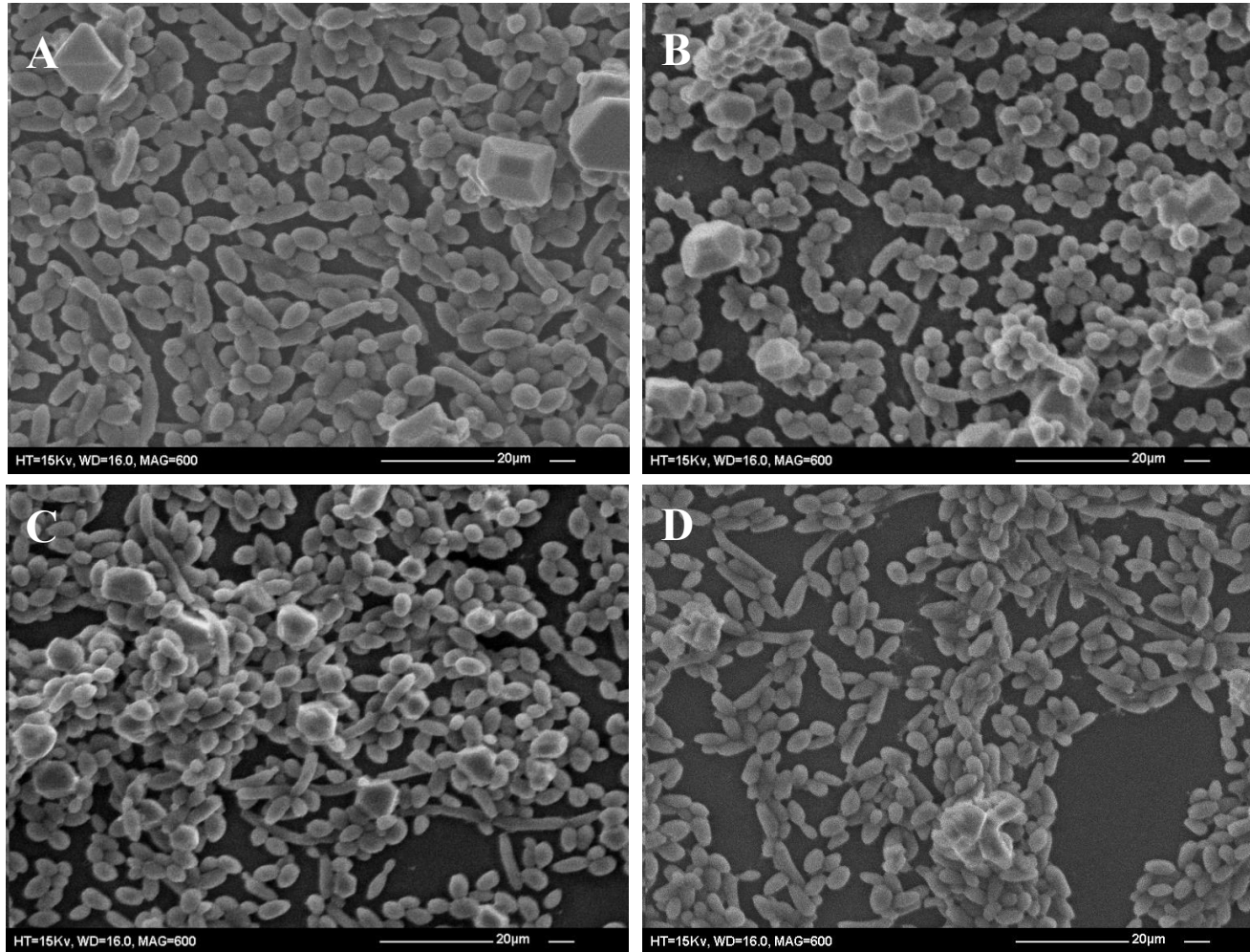


Fig 6.3: SEM of *C. tropicalis* 519468 (x1200) treated with OligoG at concentrations of A) 0% B) 2% C) 6% D) 10%. Scale bar is 20 µm.

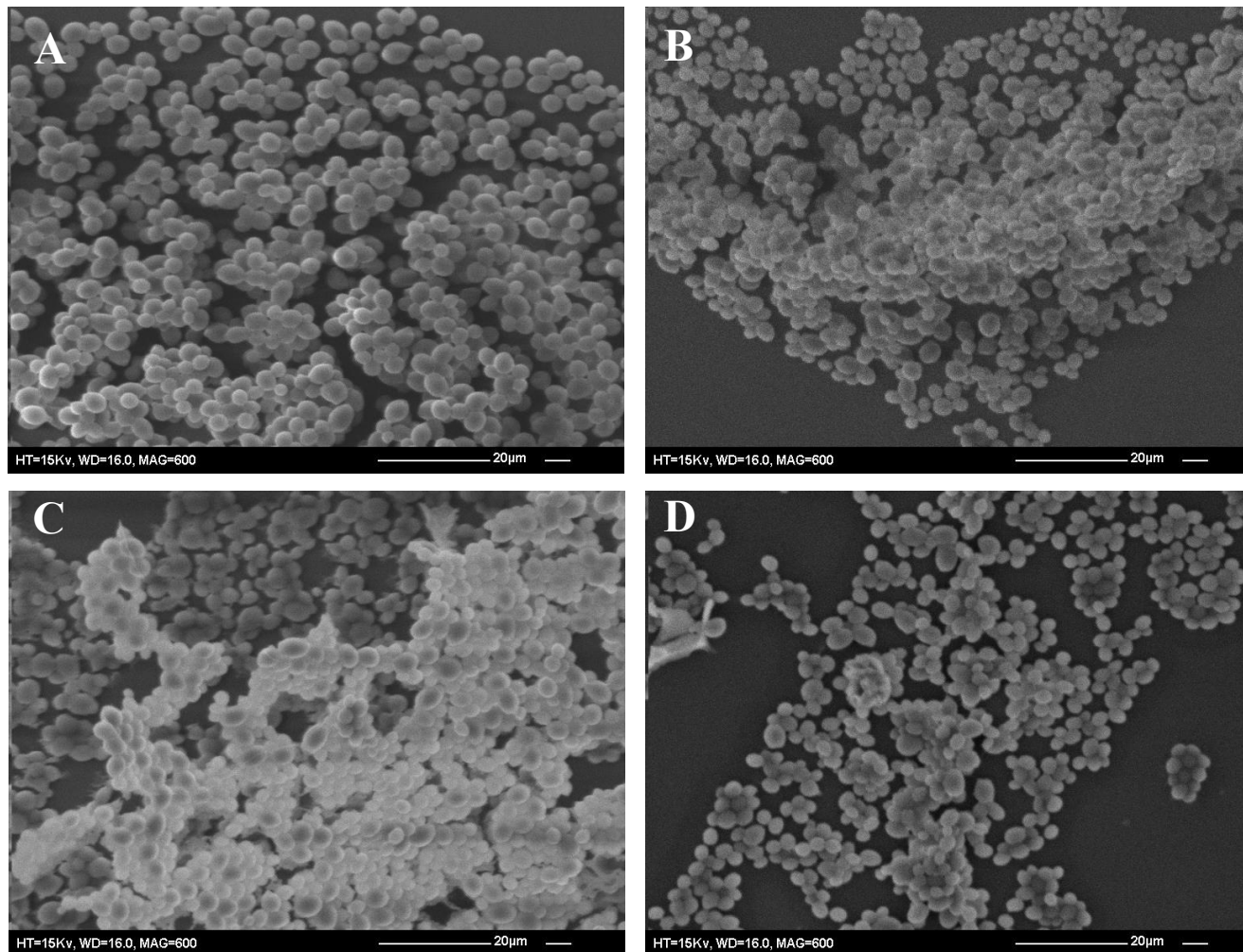


Fig 6.4: SEM of *C. albicans* 39343 (x1200) treated with OligoG at concentrations of A) 0% B) 2% C) 6% D) 10%. Scale bar is 20 μm .

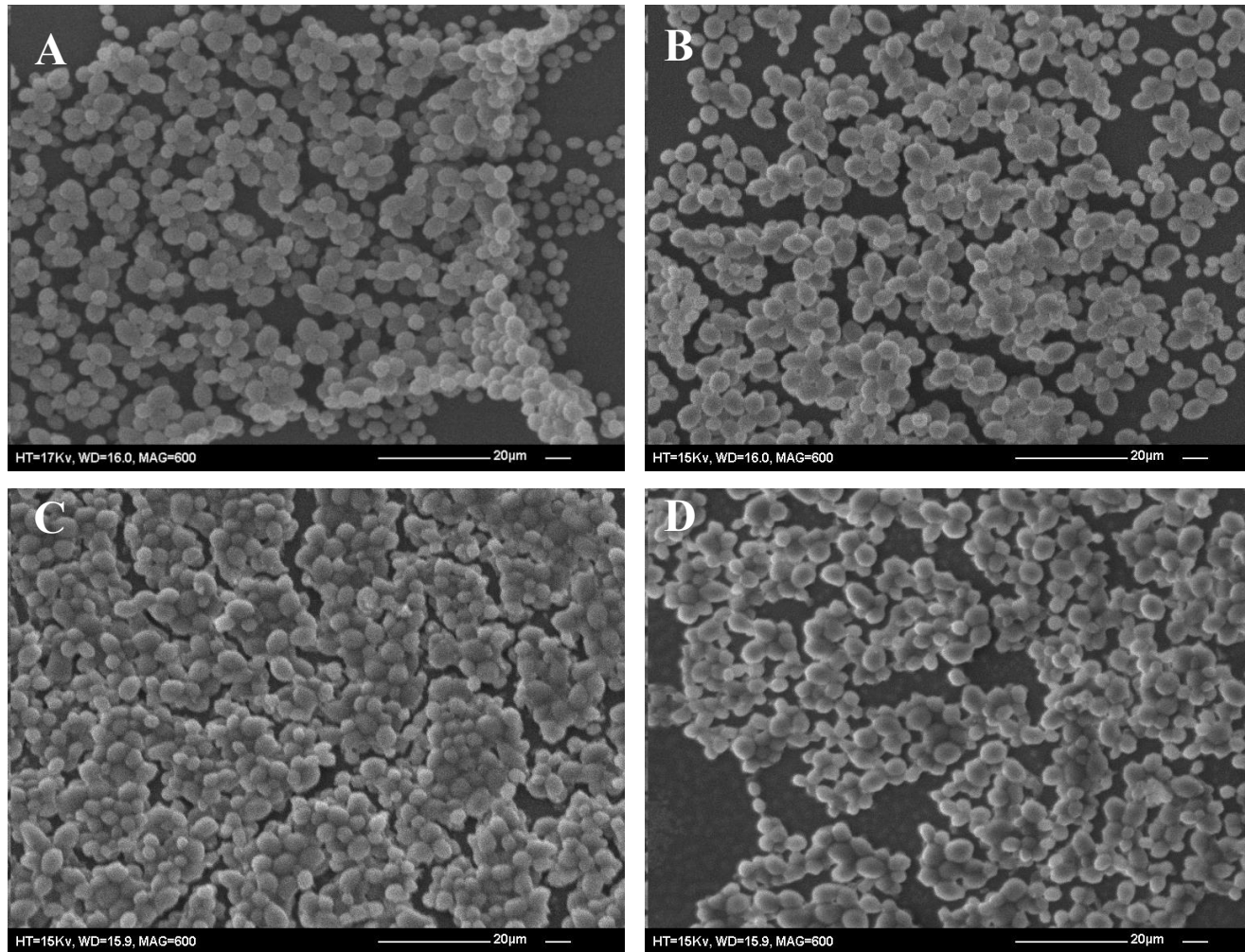


Fig 6.5: SEM of *C. glabrata* ATCC 2001 (x1200) treated with OligoG at concentrations of A) 0% B) 2% C) 6% D) 10%. Scale bar is 20 μm.

6.4.3 Effect of OligoG and fluconazole antifungal therapy on growth of *Candida tropicalis* biofilms

SEM revealed that when fluconazole was used at concentrations equivalent to ‘at’ and ‘above’ the MIC value (1 mg/l), a less dense biofilm with a decrease in hyphal growth was formed. However fluconazole treatment “below” the MIC value appeared to have no effect. Fluconazole used in conjunction with 2% OligoG however showed a potentiation effect on the establishment of *C. tropicalis* biofilms (**Fig 6.6**). The combined treatment, at every fluconazole dose studied, induced a less well-formed biofilm (i.e. decreased biomass and increased water channels) when compared to fluconazole treatment alone.

The differences observed in altered biofilm structure with 2% OligoG treatment were less marked when using AFM imaging (**Fig 6.7**), than with LIVE/DEAD[®] staining and SEM imaging. Interestingly, whilst the differences in gross biofilm structure were slight, the *Candida* species cells themselves exhibited marked changes in morphology following OligoG treatment. Treatment with OligoG and fluconazole resulted in less filamentous growth, OligoG treatment alone resulted in rounded cells, whilst fluconazole treatment produced cells that were decidedly more “flattened” in shape. The combination treatment however, produced the most distinctive morphological changes, with the cells having a roughened surface in comparison to cells treated with fluconazole or OligoG alone.

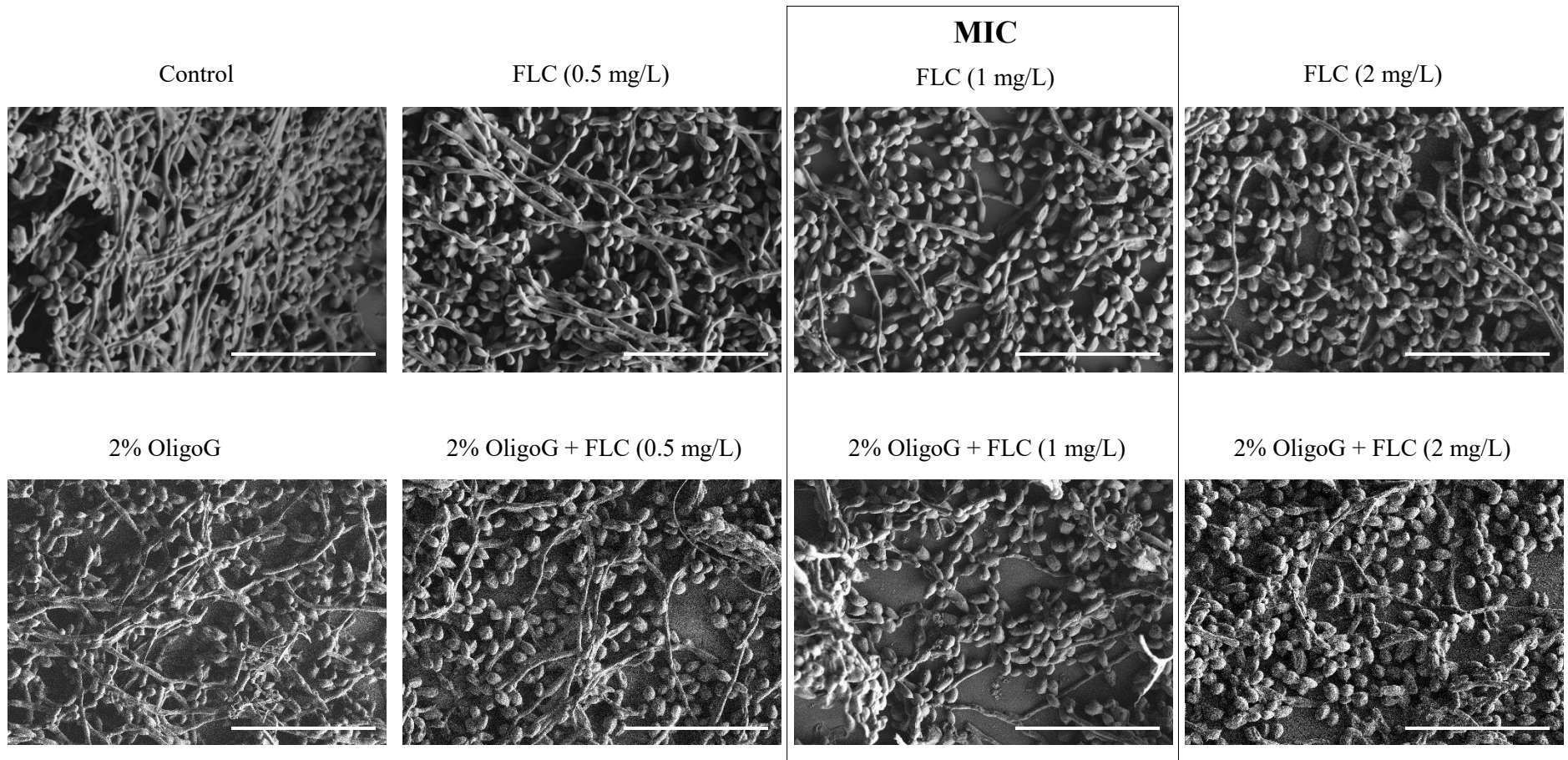


Fig 6.6: SEM of *C. tropicalis* 519468 (x1200) treated with 2% OligoG with/without fluconazole (FLC) at concentrations of 0.5, 1 and 2 mg/l (equivalent to 'below', 'at' and 'above' the MIC value respectively). Scale bar is 40 μ m.

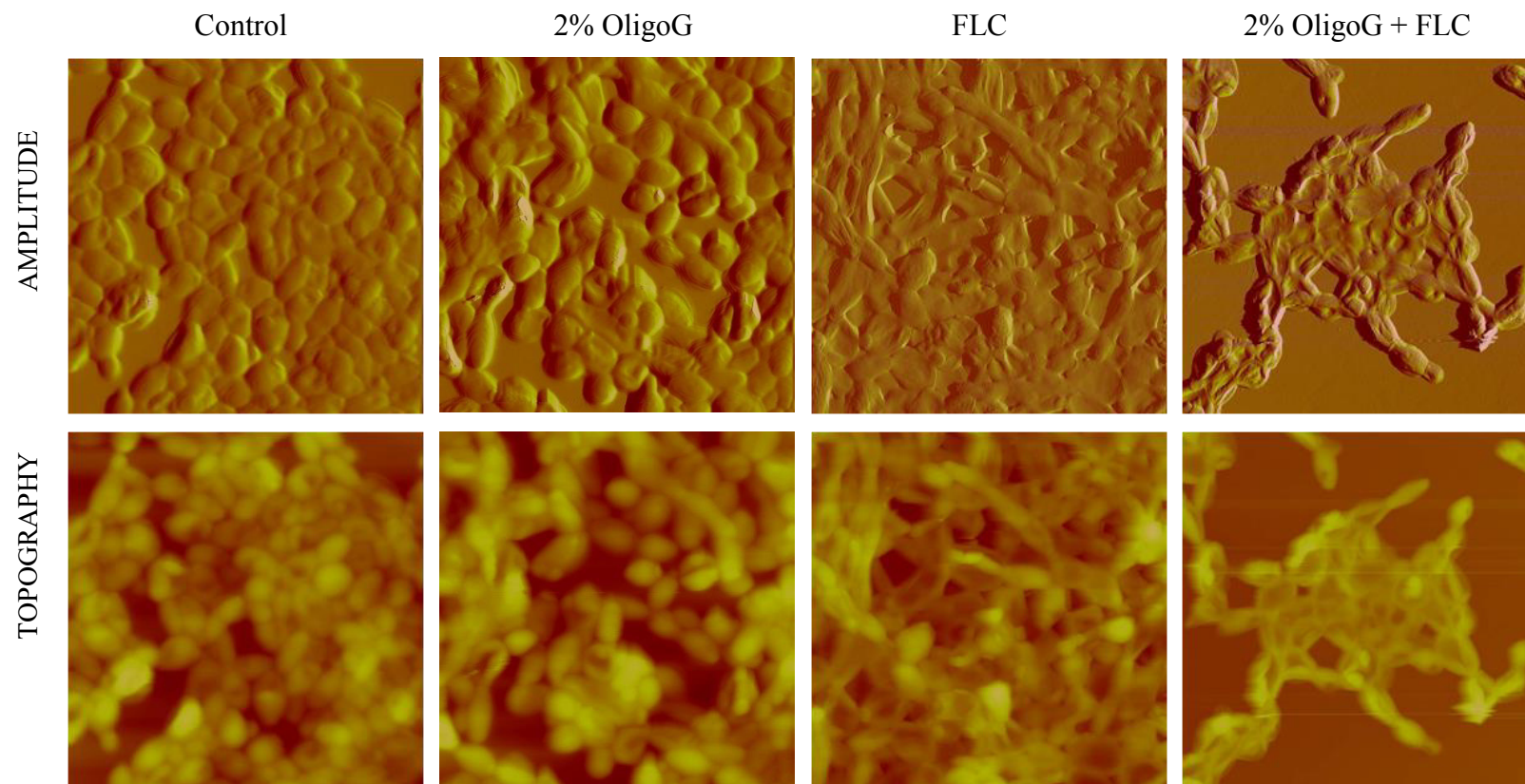


Fig 6.7: AFM imaging of *C. tropicalis* 519468 grown on polystyrene with and without 2% OligoG and/or fluconazole (FLC, 1 mg/l, equivalent to the MIC). Image area $50 \mu\text{m}^2$; Z-scale of $7.5 \mu\text{m}$.

6.4.4 Effect of OligoG and fluconazole combination therapy on disruption of immature *Candida tropicalis* 519468 biofilms

The effect of OligoG and fluconazole combination therapy on cellular structure was less evident on pre-formed biofilms (**Fig 6.8**). However, a decrease in cell biomass was seen, with an additive, and more marked effect when OligoG and fluconazole were used as a combined treatment. Interestingly, although the samples underwent vigorous washing, some areas were clearly seen to retain OligoG around the cells (**Fig 6.9**).

6.4.5 Zeta potential analysis of *Candida* species

Zeta potential values for both *C. albicans* 39343 and *C. tropicalis* 519468 were negative and there was no significant difference between values obtained at any pH tested. However, the mean value for *C. albicans* 39343 ($-22.3 \text{ mV} \pm 1.15$) was considerably more negative than for *C. tropicalis* 519468 ($-5.24 \text{ mV} \pm 0.43$) at 0.01 M, pH5 (**Fig 6.10**).

The zeta potential of treated *Candida* species was masked by OligoG prior to washing, and this masking was highlighted by the fact that *C. albicans* 39343 and *C. tropicalis* 519468 produced similar peaks ($-10.2 \text{ mV} \pm 0.65$ and $-10.9 \text{ mV} \pm 1.07$ respectively). Post-washing, no significant differences in the zeta potential value for the treated and untreated samples were observed (**Fig 6.11**). Lowering the OligoG concentration to 0.2%, 0.5% and 1% OligoG to analyse the surface charge without washing confirmed that there were no significant changes in zeta potential (**Table 6.2**). A less negative zeta potential was found at 1% OligoG with *C. albicans* 39343, which was not seen with *C. tropicalis* 519468, probably due to the masking effect of OligoG at this concentration.

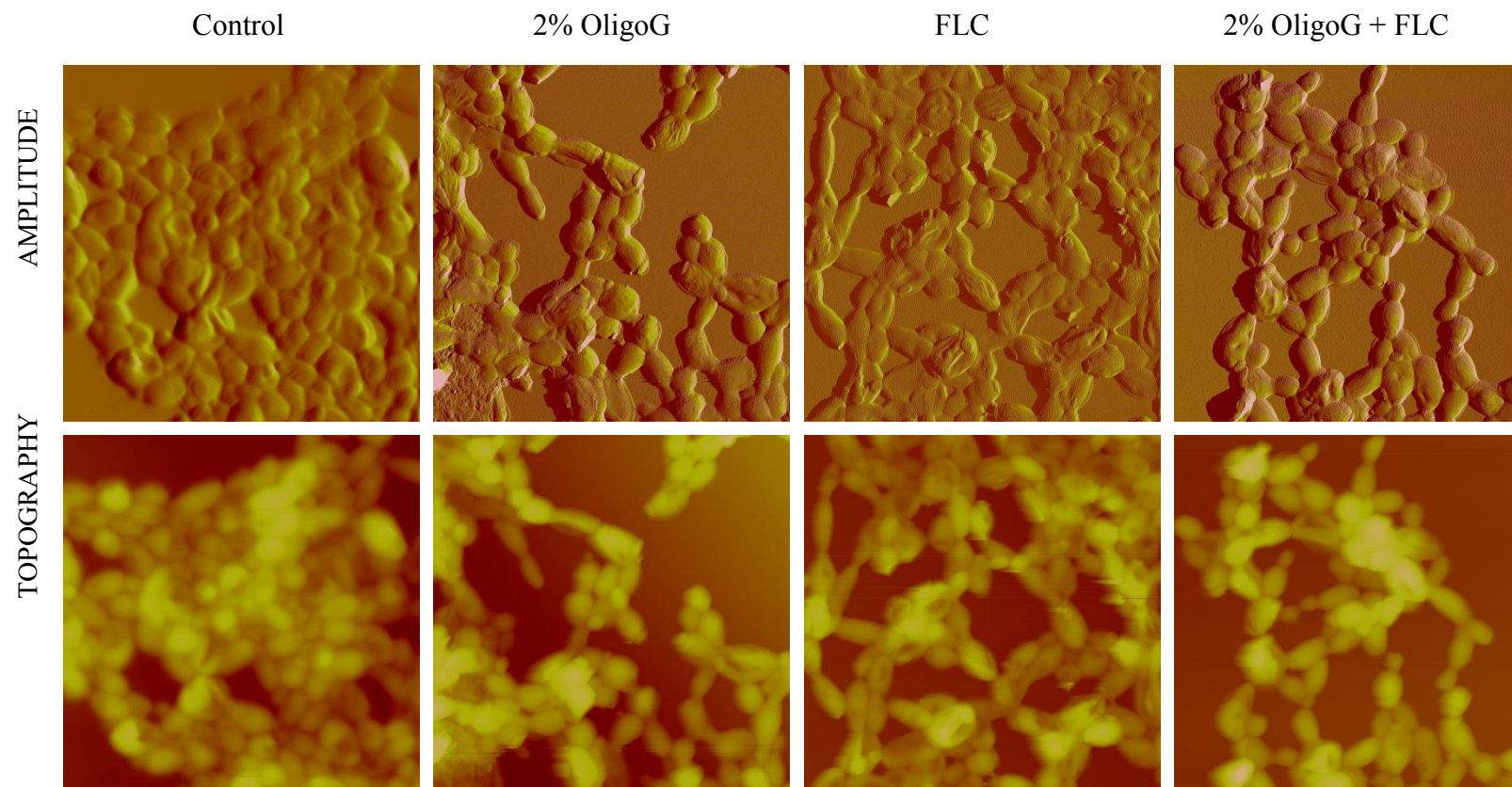


Fig 6.8: AFM imaging of *C. tropicalis* 519468 grown on polystyrene with and without 2% OligoG and/or fluconazole (FLC, 1 mg/l, equivalent to the MIC) on a 30 min established biofilm. Image area $50 \mu\text{m}^2$; Z-scale of $7.5 \mu\text{m}$.

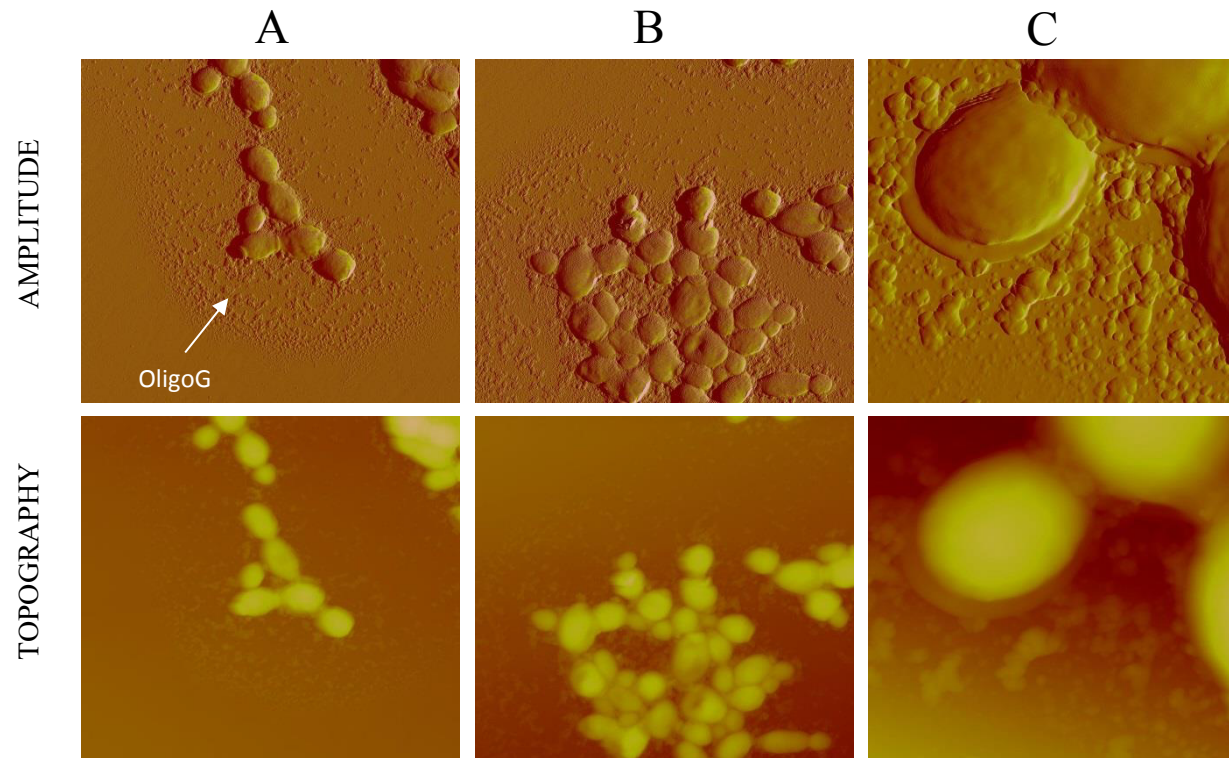


Fig 6.9: AFM imaging of *C. tropicalis* 519468 grown on polystyrene with and without 2% OligoG and/or fluconazole (FLC, 1 mg/l, equivalent to the MIC). A) Image area $50 \mu\text{m}^2$; Z-scale of $8 \mu\text{m}$. B) Image area $50 \mu\text{m}^2$; Z-scale of $9 \mu\text{m}$. C) Image area $8 \mu\text{m}^2$; Z-scale of $4 \mu\text{m}$.

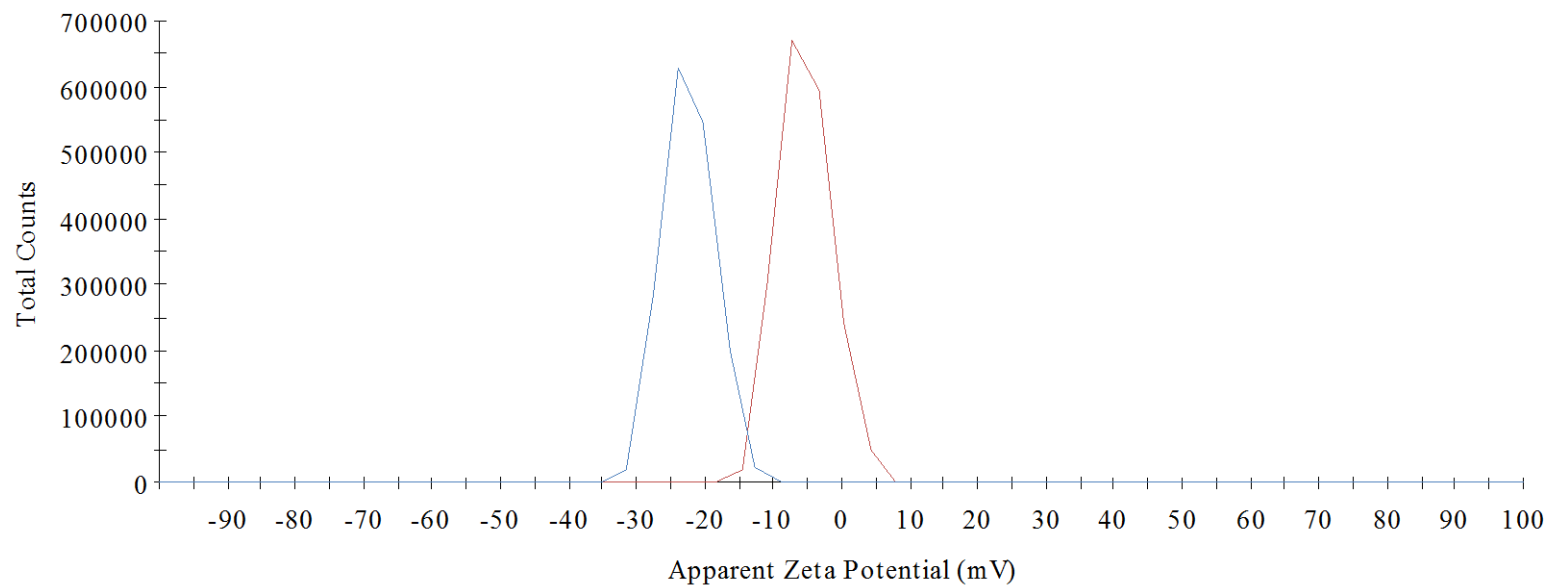


Fig 6.10: Typical zeta potential distribution for *C. albicans* 39343 (blue solid line) and *C. tropicalis* 519468 (red solid line) at 0.01 M NaCl, pH 5.

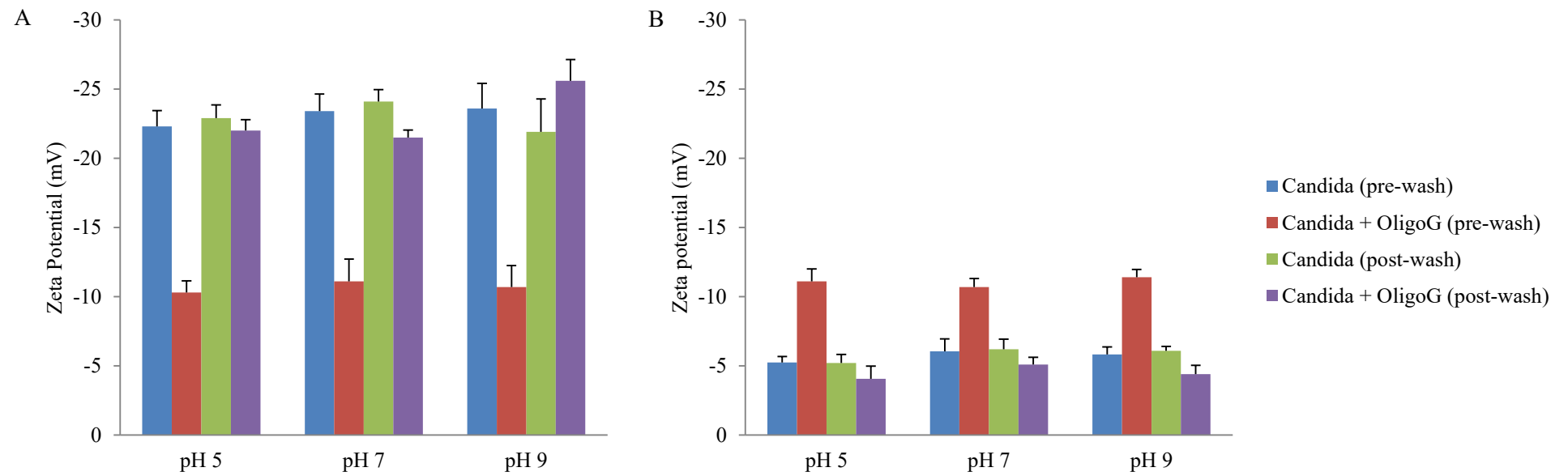


Fig 6.11: Mean Zeta Potential (mV) values for A) *C. albicans* 39343 and B) *C. tropicalis* 519468; untreated *Candida* (pre-wash), treated *Candida* with 10% OligoG (pre-wash), untreated *Candida* (post-wash) and treated *Candida* with 10% OligoG (post-wash) at 0.01 M NaCl, pH 5, 7 and 9.

Table 6.2: Pre-wash mean zeta potential values (\pm standard deviation) at 0.01 M NaCl, pH 5, of untreated *C. tropicalis* 519468 and *C. albicans* 39343 cells: control, 0.2% OligoG, 0.5% OligoG and 1% OligoG.

Mean Zeta Potential (mV)		
+% OligoG	<i>C. tropicalis</i> 519468	<i>C. albicans</i> 39343
<i>Candida</i> Only	-5.24 \pm 0.43	-22.3 \pm 1.15
<i>Candida</i> + 0.2% OligoG	-4.69 \pm 0.84	-21.8 \pm 2.25
<i>Candida</i> + 0.5% OligoG	-3.56 \pm 0.98	-24.0 \pm 1.23
<i>Candida</i> + 1% OligoG	-6.04 \pm 2.27	-12.7 \pm 2.36*

*possible masking effect of OligoG

6.4.6 Reconstituted human oral epithelium

6.4.6.1 Growth curves

The growth curves over 24 h of *Candida* species showed that there was a dose-dependent response when grown in the presence of OligoG. After 4 h, a clear reduction in cell growth with increasing concentration of OligoG could be seen. However, there appeared to be no difference between growth curves obtained for 0.2% and 2% OligoG. Interestingly, the presence of OligoG did not alter the time point (around 7 h) at which the cells went from exponential phase to stationary phase growth (**Fig 6.12**).

6.4.6.2 Confocal laser scanning microscopy of LIVE/DEAD[®] staining of RHE model infected with *Candida albicans* (\pm OligoG)

Healthy un-infected RHE samples exhibited few non-vital cells (**Fig 6.13**). Infected control RHE demonstrated abundant *Candida* species with vital filaments being evident throughout the samples. Interestingly as the concentration of OligoG increased there was a decrease in the amount of hyphal formation, with obvious increases in non-vital (red stained) hyphae at 2% OligoG. At 6% OligoG, an increase in live yeast at the surface of the epithelial cells was also observed (**Fig 6.13**).

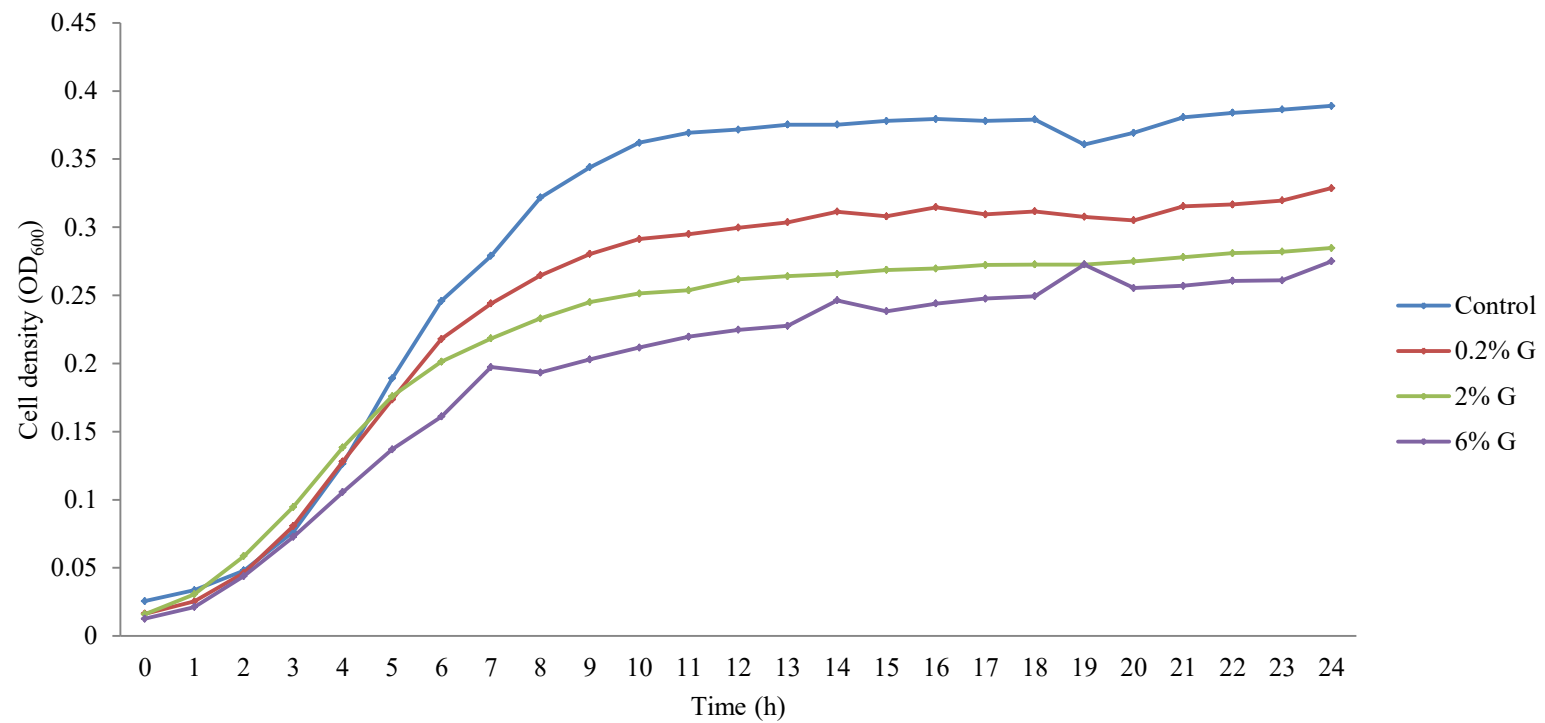


Fig 6.12: Growth curve over 24 h for *C. albicans* ATCC 90028 comparing growth in 0.2%, 2%, 6% and 10% OligoG with an untreated control.

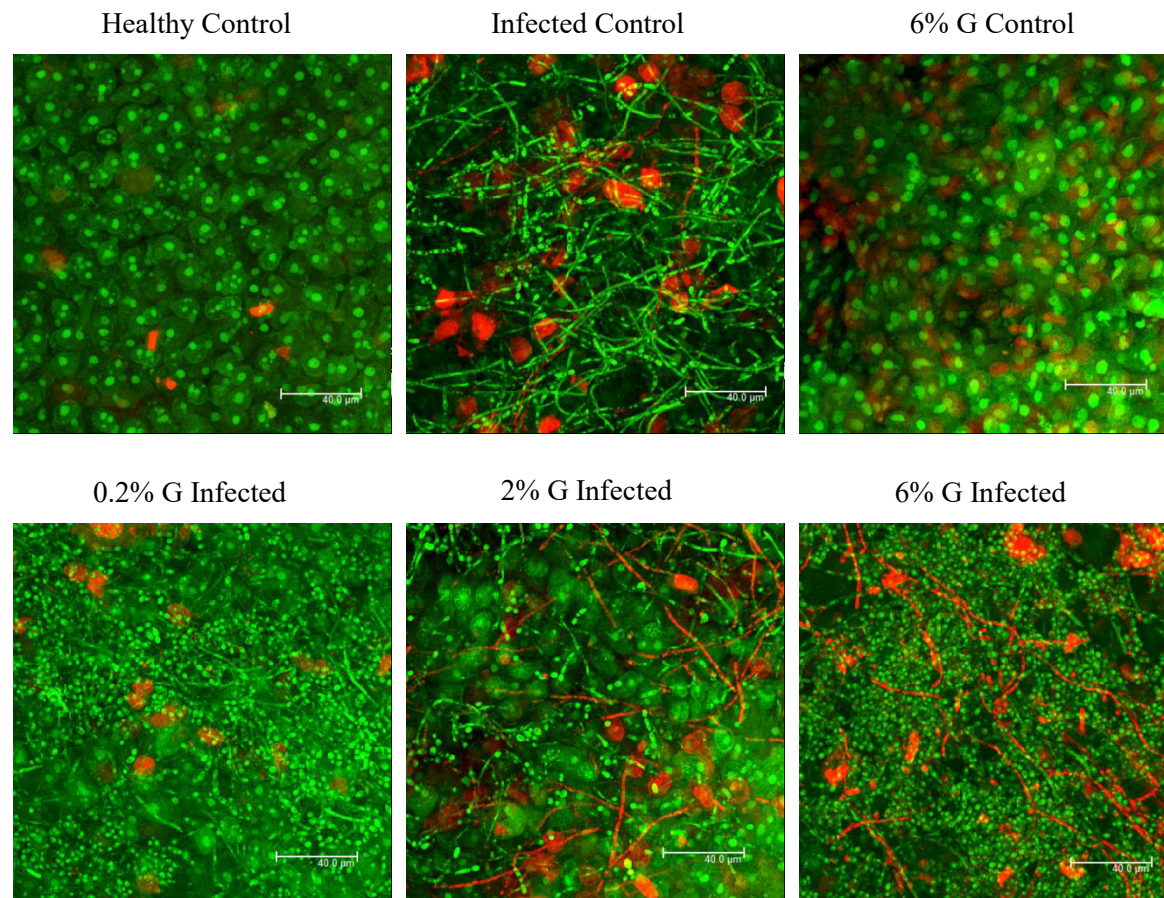


Fig 6.13: LIVE/DEAD[®] CLSM images of RHE samples infected with *C. albicans* ATCC 90028 for 12 h.

6.5 Discussion

Previous studies have shown the effectiveness of OligoG in the disruption of pseudomonal biofilms (Powell et al., 2014, Powell et al., 2013, Khan et al., 2012, Roberts et al., 2013). These studies sought to determine the effect of OligoG on fungal pathogens. Earlier experiments characterised the growth of *Candida* (n=12) and *Aspergillus* (n=3) strains in RPMI medium and Mueller-Hinton (MH) broth (Tøndervik et al., 2014). Addition of OligoG to MH and RPMI broth reduced the growth of all fungal strains tested in a concentration dependent manner (**Appendix III, Fig III.ii-iii**). The effect was most pronounced with 10% OligoG, leading to a 15-50% reduction in cell density after 48 h incubation. Analysis of the growth kinetics showed that the specific growth rate (μ) in MH broth was only slightly reduced by the addition of OligoG. Typically for *C. tropicalis* 519468, growth rates of $\mu=0.22/t$ (without OligoG) and $\mu=0.19-0.2/t$ (with 10% OligoG) were observed.

This current study showed a dose-dependent response to OligoG treatment demonstrated by biofilm disruption of the most common fungal pathogen *C. albicans*, as well as of the increasingly common *C. tropicalis*. These *in vitro* experiments showed the ability of OligoG to modulate both fungal growth and fungal biofilm formation. Treatment with OligoG demonstrated altered growth characteristics of the candidal biofilms, which was associated with concentration-dependent biofilm disruption, increased cell and hyphal death, and a less dense biofilm. Fundamentally, OligoG effectively reduced the capacity of the *Candida* species to form a strong, stable biofilm structure. Although there was no significant difference in surface roughness (Ra) measurements between the control and 2% OligoG treated samples ($P>0.05$). There was however a significant increase in Ra for both the combined fluconazole and 2% OligoG, and fluconazole alone treatments ($P<0.001$) compared to the control (**Appendix III, Fig III.iv**; Tøndervik et al., 2014). The distinct morphological changes observed here included cell “flattening”, which could be the result of non-optimal growth conditions leading to cellular dehydration.

A key feature of *Candida* species is the ability of certain species to form yeast, pseudohyphae and hyphae. Hyphae have an important role in causing disease as they invade epithelial cells and lead to tissue damage (Sudbery, 2011). Further functions of hyphae include directional translocation between host environments, consolidation

of the colony, nutrient acquisition and support for three-dimensional matrix formation (Brand, 2012). Light micrographs obtained from the germ tube assay demonstrated that OligoG markedly inhibited the hyphal growth phase of *C. albicans* and demonstrated a reduction in the number of cells producing hyphae following OligoG treatment (**Appendix III, Fig III.v**; Tøndervik et al., 2014). The concentration of OligoG required to produce an effect however, was species-dependent. An increase in non-vital filaments was seen in the CLSM imaging of the RHE model, with a statistically significant reduction in hyphal infiltration at 0.2% OligoG seen following PAS staining (**Appendix III, Fig III.vi**). These earlier observations support the current findings that OligoG has a direct effect on the invasive hyphal growth phase of *Candida* species. OligoG may reduce tissue invasion, leading to a lower chance of dysplastic cells forming (Sitheeque and Samaranyake, 2003). In this way, OligoG could also work synergistically with antifungal agents such as fluconazole.

In comparison to *C. tropicalis* and *C. albicans*, *C. glabrata* is not dimorphic and produces only blastoconidia (yeast). It can be found as a commensal and as a pathogen under a range of conditions. In contrast to other *Candida* species, only a limited amount of research has been conducted on *C. glabrata* and very little is known about its virulence. *C. glabrata* blastoconidia are smaller than those of *C. albicans* (1-4 μm compared to 4-6 μm respectively) and it is the only pathogenic *Candida* species that does not express pseudohyphae. An important distinguishing feature is the diploid genome of *C. albicans* and several other non-*albicans* *Candida* species compared to the haploid genome of *C. glabrata* (Fidel et al., 1999). In keeping with the importance of the hyphal inhibition effect of OligoG was the finding that the anti-biofilm effect was markedly reduced in *C. glabrata*. This reduced effect may potentially be due to their lack of hyphal growth, thereby indirectly implicating a possible mode of action for OligoG on filament formation.

Resistance to antifungal agents is increasingly common (Odds, 2009). *C. glabrata* is difficult to treat and often resistant to azole antifungals (Fidel et al., 1999). The biofilm forming ability of *C. glabrata* is a major contributing factor to its higher antifungal resistance, and it has been shown to possess both innate and acquired resistance to antifungals. *C. glabrata* can modify ergosterol biosynthesis, mitochondrial function or antifungal efflux, and has been found to be less susceptible

to clinical biocides (Seneviratne et al., 2010). Up-regulation of stress response proteins has also been found in the *C. glabrata* biofilm proteome (Seneviratne et al., 2010). Interestingly whilst *C. glabrata* has been shown to be unable to invade RHE tissues when on its own, in a mixed species infection, *C. albicans* caused disruption of the keratinocyte layers allowing penetration of *C. glabrata*, causing increased tissue damage (Silva et al., 2011a).

Morphological changes in *Candida* species biofilms were less evident when an established biofilm was treated with OligoG, however, some disruption of biofilm structure was demonstrated. *Candida* species biofilms are composed of a three-dimensional network with extensive spatial heterogeneity (to facilitate the influx of nutrients), microcolonies with ramifying water channels, the disposal of waste products and establishment of “micro-niches” throughout the biofilm (Ramage et al., 2005). These studies clearly showed disruption and these effects on biofilm homeostasis and architecture by OligoG may impair further biofilm development, as well as increase the effectiveness of antifungal agents. Previous studies on pseudomonal biofilms have shown the disruption in biofilm homeostasis caused by OligoG, resulting in disruption under hydrodynamic shear (Powell et al., 2013).

OligoG was able to potentiate the effect of selected antifungal agents commonly used to treat fungal infections. All *Candida* strains used showed potentiation with nystatin (up to 16-fold with *C. parapsilosis*) and fluconazole (up to 8-fold with four strains; **Appendix III, Table III.i**). This result was confirmed using SEM and AFM imaging showing the ability of OligoG to potentiate the activity of fluconazole, leading to a more “flattened” cell structure present in the disrupted biofilm. A large variation in susceptibility towards terbinafine among different clinical *Candida* isolates has previously been described (Ryder et al., 1998). Significant correlation was found between terbinafine and azole MICs which supports the hypothesis that a common mechanism regulates both azole and terbinafine resistance among many isolates (Odds, 2009). CDR2 and MDR1 homologs are over-expressed in *C. tropicalis* leading to development of resistance to azoles and terbinafine, although the genes and encoded efflux pumps involved are not yet fully characterised (Morschhauser, 2010). There may be further scope to study combination therapy of OligoG with other classes of antifungals. In addition,

an insight into its particular mode of action mechanistic may be gained by using a future molecular or protein expression profiling approach.

AFM is increasingly used to study the cell surface, (Khan et al., 2012, Powell et al., 2013) and has recently been used to assess the binding of OligoG to the cell surface of the pathogenic bacteria *P. aeruginosa*, which remained bound even after hydrodynamic shear (Powell et al., 2014). Perhaps unsurprisingly given the contrasting differences in cell wall structure and charge between the candidal and pseudomonal cell wall there was no apparent similarity in the binding of OligoG to the fungal cell wall. The candidal cell wall is composed of β -glucans, chitin and mannoproteins (Aguilar-Uscanga and Francois, 2003). A prominent component in the pseudomonal cell wall is LPS (Vaara, 1992). Nevertheless, morphological changes were clearly evident when *Candida* was exposed to OligoG. While these studies are not directly comparable (organisms were in different growth states, planktonic versus biofilm), it would suggest that different mechanisms of action may be involved in the antimicrobial effects observed in bacterial and fungal pathogens (Aguilar-Uscanga and Francois, 2003).

Microbial cell surface charge is a dominant physicochemical surface property involved in the adhesion of bacteria and fungi to cells and material surfaces, and is of pivotal importance (Busscher et al., 1997). The initial colonisation of a surface by candidal cells during biofilm formation is due to nonspecific factors such as cell surface hydrophobicity and electrostatic interactions (Williams et al., 2013). Specific adhesins on the fungal surface recognise ligands on the surface structure e.g. serum proteins. Following initial attachment, the cells quickly divide, proliferate and the biofilm matures (Ramage et al., 2005). Analysis of the surface charge of candidal cells demonstrated species-specific heterogeneity which had been observed previously during the imaging studies with *C. albicans*, which was found to have a more negative charge compared to *C. tropicalis*, in keeping with previous studies across pH 2.0 to 6.8 (Busscher et al., 1997). Busscher et al. (1997) demonstrated that the increased negative zeta potential of *C. tropicalis* was associated with less rapid adherence to negatively-charged material surfaces; concluding the more negative zeta potential slowed down adherence by electrostatic repulsion (Busscher et al., 1997). The reduced biofilm formation observed following OligoG treatment could be postulated to reflect OligoG-binding (which is also negatively charged) inducing

repulsion and hence reducing biofilm formation. Previous work (see **Chapter 1**) has demonstrated that in *P. aeruginosa*, OligoG binding significantly lowers the negative charge of this bacteria and this lower negative charge was maintained even after washing (Powell et al., 2014). In these studies with fungi, no change in surface charge was seen with either of the two *Candida* species at 0.01 M NaCl, pH 5-9, inferring that a different mechanism of action may be involved in the disruption of fungal biofilms. No change in surface charge was evident, even at lower concentrations ($\leq 0.2\%$ OligoG) where any possible masking effects of OligoG were negligible.

The fungal cell wall is highly elastic and provides both physical protection and osmotic support. As a means of combating potential cell lysis, the composition of the cell wall can be altered using a ‘compensatory mechanism’ when it is activated in response to changes in the immediate environment such as contact with cell wall perturbing agents or mutagens, thereby allowing the cell wall to be remodeled (Klis et al., 2002). Cell wall damage due to mutations of cell wall-related genes trigger a compensatory mechanism resulting in hyper-accumulation of chitin, which can ultimately reach 20% of the cell wall mass (Lagorce et al., 2002). The response to such cues can effectively direct changes in fungal growth, cell wall mass, ultra-structure, elasticity and adhesion, enzyme production and pathogenicity (Ene et al., 2012). While it is not known whether OligoG induces this kind of re-modelling effect, it is a charged molecule and so could influence, or be influenced by, molecular changes in the cell wall composition.

In healthy individuals, it is common to find asymptomatic colonisation of mixed bacteria-fungal populations on the skin, in the oral cavity, the GI tract and the lower female reproductive tract. Recently however, an increase has been seen in the frequency of mixed bacterial-fungal infections found in humans, with *C. albicans* being the most frequently isolated fungal species from such infections. Co-infection of bacteria and fungi such as *C. albicans* and *Staphylococcus aureus* has been well established. Both organisms are commonly isolated bloodstream pathogens, often found as co-infecting agents. They are also both capable of forming biofilms, and show increasing evidence of antimicrobial resistance, thereby representing a significant and growing problem in the management of poly-microbial infections. *Candida* species have been found to co-aggregate with and/or bind to bacteria

(Ramage et al., 2005). Specific binding of *S. aureus* to the hyphae of co-cultured *C. albicans* (via Als3p binding) has been shown to enable tissue infiltration and subsequent deep tissue infection by *S. aureus* (Peters et al., 2012). OligoG has been shown to have an antimicrobial effect on MDR bacterial strains (Khan et al., 2012) and has now also shown to potentially alter the pathogenicity of *Candida* species. The potential of antimicrobials capable of targeting both bacteria and yeasts, such as OligoG, have a distinct advantage for such poly-microbial infections.

Colonisation of the respiratory tract by bacteria and fungi are common in those with chronic lung disease (Peleg et al., 2010). *Candida* and *Pseudomonas* species have been co-isolated from the CF lung, but the understanding of how they communicate is largely unknown (Holcombe et al., 2010). This relationship can be directly and indirectly influenced by the other species. Bacterial and fungal factors can influence one another's growth behaviour and survival. Secreted molecules can mediate many types of interactions between bacteria and fungi. These extracellular signalling molecules, such as homoserine lactones, mediate quorum sensing (QS) in single species communities, often in response to population density (Peleg et al., 2010). The analysis of gene expression changes in *Candida* species in response to *P. aeruginosa* revealed an increase in the genes related to drug or toxin efflux and a decrease in expression of genes associated with adhesion and biofilms formation (Holcombe et al., 2010).

Studies have found that bacterial toxins can also be antifungal in nature. Collaborative relationships also exist whereby the species provide protection for each other against the attacking immune response and/or antimicrobial agents. For example, colonisation of the respiratory tract with *Candida* species may increase the risk of pseudomonal ventilator associated pneumonia (Azoulay et al., 2006). Animal studies have also shown that a mixed species infection leads to changes in microbial burden at the primary site of infection as well as the rate of dissemination of the infection from this site, all of which have a long-term effect on host survival (Peleg et al., 2010).

The decision to treat candidal wound and dental infections depends on several factors such as the immune status of the host, clinical and radiological signs of infection as well as the result of microbiological testing (De Pauw et al., 2008). Resistance, cost and toxicity are key issues around the use of antifungals. Lowering

the MIC of standard antifungals may increase their efficacy and overcome resistance, particularly in triazoles. The ability of OligoG to potentiate the disruption of *Candida* species biofilms in combined therapies could lead to a lower risk of drug toxicity *in vitro* and an opportunity to increase treatment options in the management of fungal lung infections. The potentiating activity observed in this study represents considerable promise for the clinical utility of OligoG in the treatment and management of fungal infection and reduction of antifungal toxicity in clinical practice. This is supported by similar observations for OligoG in potentiating the activity of antibiotics against MDR Gram-negative bacteria (Khan et al., 2012).

6.6 Conclusion

From this study, the synergistic activity of OligoG in disrupting the biofilm architecture could potentially permit: a) better access for antifungal agents and/or host innate defenses to biofilm-embedded organisms and, b) previously dormant (drug-tolerant) cells to move into a more drug-susceptible phase of growth. The current *in vitro* observations would appear to support some of these hypotheses, but will need to be tested with appropriate *in vivo* models. Although the precise mechanism of action of OligoG against fungi has yet to be established, it does not now appear to involve altering the surface charge.

7.1 General discussion

This thesis has studied the mechanisms by which a newly-described mode of therapy may be utilised to treat biofilm infections and meet the global healthcare challenge of emerging antibiotic resistance, with estimated direct and indirect annual healthcare costs of \$20 and \$35 billion respectively in the US (Smith and Coast, 2013). Although interventions are in place to reduce excessive antibiotic prescribing for hospital inpatients to decrease antibiotic resistance and the incidence of hospital acquired infections (Davey et al., 2013, Ashiru-Oredope et al., 2012), the apparently inexorable emergence of new, multi-drug resistant (MDR) strains (CDC, 2014) will undoubtedly require novel therapeutic approaches (Carlet et al., 2014).

Due to the limited “commercial lifespan” of novel antibiotics, commercial interest in antibiotic development has waned (Bragginton and Piddock, 2014). Consequently, whilst between 1940 and 1962, >20 new “classes” of antibiotics were marketed, in the intervening 50 years, only 2 new classes have reached the market (Conly and Johnston, 2005). In addition, the number of antibacterial agents receiving approval by the US Food and Drug Administration (FDA) has decreased by almost 60% in the period between 1983 and 2002 (Conly and Johnston, 2005). There is a huge, unmet demand for therapies for MDR Gram-negative bacteria. The Infectious Disease Society of America has estimated that at least 10 new antibiotics active against “superbugs” are required in the market to meet current needs (Coates et al., 2011).

Colonisation by MDR bacteria represents particular problems in chronic “antibiotic-exposed” populations such as those found in cystic fibrosis (CF) patients. Whilst macrolides, e.g. azithromycin, have been shown to improve respiratory function, the emergence of macrolide resistance is now evident (Southern, 2012). The clinical prescribing difficulties are nowhere more apparent than in CF, but there appears to be conflicting evidence regarding antibiotic prescribing. Studies have shown a significant clinical benefit to early long-term antibiotic administration (Smyth and Walters, 2012). However, no clear evidence was found supporting the benefits for the prevention of lung deterioration of regular, elective intra-venous antibiotics against chronic *P. aeruginosa* compared to treatment only at exacerbations (Breen and Aswani, 2012).

OligoG has been shown to disrupt the growth of MDR Gram-negative bacteria (Khan et al., 2012) *P. aeruginosa* and *B. cepacia*. OligoG treatment was also found to reduce the MICs for a range of antibiotics (by up to 512-fold), including macrolides (azithromycin, erythromycin, apicomycin and ciprofloxacin), aztreonam, ceftazidime, oxytetracycline and ciprofloxacin against bacteria such as *Pseudomonas*, *Acinetobacter* and *Burkholderia* species. Similar synergy or potentiation (but to a lesser extent) was seen with Gram-positive bacteria (*Staph aureus*). This potentiation effect was selective and not seen for every combination tested, with none seen with the aminoglycosides (tobramycin and amikacin).

OligoG was shown to decrease bacterial proliferation in liquid culture, in a dose dependent manner (Khan et al., 2012). The results were particularly striking in Gram-negative bacteria *P. aeruginosa*, *A. baumannii*, *Burkholderia* species and Enterobacteriaceae. When grown as a biofilm, *P. aeruginosa* PAO1 cells showed cell damage, cell death and a decreased biofilm cell density, with alterations in the structural organisation of the cells in the biofilm apparent when imaged using CLSM and SEM. Mechanical disruption of *P. aeruginosa* biofilms by OligoG has also been reported employing AFM and shear rheology analysis (Powell et al., 2013) which demonstrated a lower Young's modulus, decreased resistance to hydrodynamic shear and increased surface irregularity when compared to untreated biofilms. The precise mode of action of OligoG remains unresolved. Previous studies showed that there was no increase in cellular permeability of Gram-negative bacteria when grown in OligoG (Khan et al., 2012). This is reassuring since a number of "permeabilising" antimicrobial agents have been hindered in clinical trials by nonspecific permeabilisation-toxicity concerns (Hancock and Sahl, 2006). Studies employing *P. aeruginosa* PAO1 MexAB-OrpM mutants demonstrated that the effect of OligoG was not mediated by interaction with this efflux pump (Khan et al., 2012).

Charge interactions play a key role in the initiation and development of a biofilm. Alginates such as OligoG are poly-anionic in nature, exhibiting compositional heterogeneity and poly-dispersity (Andersen et al., 2012). The homogeneous OligoG studied here, was shown to interact strongly with the bacterial surface of *Pseudomonas* (**Chapter 2**) and also a range of bacteria from other biofilm-related infections (Roberts et al., 2013, Khan et al., 2012, Powell et al., 2013). The detailed studies in PAO1 confirmed its interaction with OligoG, which was

maintained even after rigorous washing (Powell et al., 2014). Of clinical importance, OligoG had a similar effect on PAO1 populations whether it was present during or after the growth phase, and this was apparent with concentrations as low as 0.2% (Powell et al., 2014). Initial stages of biofilm development involve a reversible “adhesion stage” (Garrett et al., 2008). Decreasing zeta potential overcomes the net repulsion between bacterial surfaces (Powell et al., 2014) resulting in bacterial aggregation which was evident in both the DLS and AFM studies of OligoG-treated PAO1, with the OligoG appearing to “stick” onto the bacterial cells and flagella (**Chapter 2**).

Interestingly, motility test agar stabs showed that 6% OligoG inhibited motility of *P. aeruginosa*, as well as *Escherichia coli* and *Proteus mirabilis* (Khan et al., 2012). Motility of *P. aeruginosa* has been shown to be required for bacterial penetration into hypoxic zones within stationary mucus masses (Worlitzsch et al., 2002). OligoG at higher concentrations also increases the viscosity of liquid media (BioPolymer, 2014). Previous studies have shown how decreased flagellar motility occurs as surrounding viscosity increases in bacteria such as *Vibrio alginolyticus* (Atsumi et al., 1996). As ambient medium viscosity increased, it led to a decrease in the swim-speed of bacteria such as *Prorocentrum minimum* (Sohn et al., 2013). Possession of such a property may potentially add to OligoG’s antibiofilm effect. However, changes were apparent in biofilm formation at concentrations as low as 0.2% OligoG, where media viscosity undergoes minimal change compared to the control (BioPolymer, 2014), therefore a different antibiofilm mechanistic effect must also be present.

Alginate G-subunits are known to preferentially bind to cations such as Ca^{2+} , however not all cations utilise the G subunit binding sites (Lattner et al., 2003). Imaging results showed that OligoG clearly altered the bacterial membrane, and further research into its interaction with divalent cations may aid our understanding of how OligoG potentiates antibiotics.

During the course of infection, *P. aeruginosa* undergoes a phenotypic switch to a mucoid form, characterised by overproduction of exopolysaccharide alginate, which is thought to protect the biofilm from the harsh environment of the CF lung. In a non-mucoidal strain, such as PAO1, alginate biosynthesis genes are not expressed (Wozniak et al., 2003) and therefore can only be used to understand the

implications of early events in the infected CF airway when non-mucoid strains predominate. An obvious criticism of any *in vitro* study is that the situation bears no resemblance to the *in vivo* model. In the initial studies, PAO1 was employed which is a clinical isolate originally derived over 40 years ago (Bruinsma et al., 2001), see **Chapter 2**, and is deemed a useful reference strain for initial biofilm characterisation. The latter part of this study (**Chapter 3**) employed a human CF sputum mucoid *P. aeruginosa* isolate (NH57388A) to assess the biofilm inhibition and disruption properties of OligoG. The nutritionally-depleted AS medium was employed in later experiments which has recently been describe with NH53788 to establish three-dimensional bacterial structures, in an attempt to mimic the micro-colonies of the “infected” CF lung. However, the biofilm model was only run for a maximum of 24 h, meaning that the response to chronic multi-organism biofilms present in the lung for several years could not be evaluated. Also the conditions of growth within the lung cannot be directly accounted for *in vivo*.

Mucoid *P. aeruginosa* secrete alginates consisting of the uronic acid residues β -D-mannuronate and α -L-guluronate, making it a polyelectrolyte. Binding in extracellular polymeric substance (EPS) is conferred by electrostatic interactions between divalent Ca^{2+} and the COO^- groups of the polysaccharide. The extent of this binding will vary depending on the MW and ratios of G- and M-oligomers in the molecule, both of which contribute to the rheological properties of the network of EPS macromolecules (Wloka et al., 2004). Previous studies (employing AFM) suggested that OligoG, being composed of G-residues, may compete for these cross-links within the EPS (Sletmoen et al., 2012) and prevent tight EPS formation. Comparable properties were seen in the ability of OligoG to disrupt biofilm development of the highly mucoid strain NH53788 (evident in **Chapter 3**) and its ability to disrupt the EPS “network” both of which support the potential application of OligoG in both biofilm disruption and mucolysis in respiratory disease.

Several recent antibiofilm research studies have focused on facilitating penetration of the EPS biofilm layer, an important step that appears to be a prerequisite for biofilm disruption. For example, cellulase has been used to aid degradation of EPS formed by *P. aeruginosa* and whilst not totally inhibiting biofilm formation, it was highlighted as a combination treatment with other therapeutics (Loiselle and Anderson, 2003). Bacteriophages have also shown the ability to

diffuse through the alginate EPS of *P. aeruginosa* to reach the bacterial surface, reducing both bacterial cell numbers and the viscosity of alginates, which could assist penetration of the biofilm (Hanlon et al., 2001). A notable finding of the CF lung is the dense bacterial spheres formed in the excised lungs of CF patients infected with *P. aeruginosa* following transplantation (Worlitzsch et al., 2002). These bacterial spheres were estimated to be >100 µm in size, and interestingly may be synonymous with the “unattached” *in vitro* spheres observed in the AS medium studies (**Chapter 3**). Several genes such as the extracellular polysaccharide alginate (*algD*) and type IV pili (*pilB*) were found to be necessary for tight microcolony formation (Sriramulu et al., 2005). Intriguingly, Worlitzsch et al. (2002) also found that up to 94.5% of the lung bacteria were within the airway lumen, around 5-17 µm from the epithelial cell surface. None were in fact found to be in direct contact with the epithelial surface. This was confirmed *in vitro*, where the bacteria were found to selectively bind to mucus rather than airway epithelial cells. Similarly in this current research, the biofilms did not form on the surface of the well plates, and reflected the spherical structures recorded in the literature. Whilst these studies have focused on *P. aeruginosa*, *S. aureus* is another prominent bacterium affecting CF patients with chronic colonisation peaking between 20-23 years of age. It is also known to form biofilms *in vitro*. In addition, *S. aureus* has also been found to form biofilm-like structures when grown in AS medium (Haley et al., 2012). Hence, it would be interesting to see if OligoG affects this early onset bacterium *in vivo* in CF patients. The importance of targeting antibiofilm strategies to these tight complex structures cannot be underestimated.

Previous reduction studies using AS medium have been performed, showing that all the components are vital for microcolony (sphere) formation (Sriramulu et al., 2005). For example, when mucin was completely eliminated, there was little growth (and only as conventional biofilm) with significant adherence of *P. aeruginosa* to the walls of the polystyrene wells. Poor growth in the absence of mucin suggested its use as a major energy/carbon source for *P. aeruginosa* in this medium (Sriramulu et al., 2005). In addition, DNA concentration was also proven to be important (Haley et al., 2012). eDNA patterns within *P. aeruginosa* biofilms alter with biofilm age, with young biofilms forming grid-like structures in the substratum. As the biofilm develops, a high concentration of eDNA is found at the

surface of the microcolonies where it predominates in the stalk portion of the mushroom-shaped structures. At this point, the highest eDNA concentration is found on the outer part of the stalks, creating a border between the stalk subpopulation and the cap subpopulation. As the biofilm gets older eDNA is throughout the mushroom shaped structures with high concentrations found in discrete layers (Allesen-Holm et al., 2006). In the CF patient, the reduction in microcolony formation might be contributed by rhDNase I treatment, as it facilitates eradication of bacteria and in particular high MW eDNA (Sriramulu et al., 2005). These differential targets may help to explain the synergistic effect seen in our study between OligoG and rhDNase I in sputum in **Chapter 5**.

Whilst OligoG was shown to potentiate antibiotics (Khan et al., 2012), alter bacterial surface charge and change actual biofilm structure, its location within a biofilm was unknown. Imaging the distribution of OligoG within the biofilms could clearly improve our understanding of its mechanism of action. Previous studies had investigated lectin binding to polysaccharides to localise production by mucoid *P. aeruginosa*. Since non-specific binding between EPS and OligoG was likely to occur (Strathmann et al., 2002), specific covalent fluorescent labelling with TxRd cadaverine to OligoG was undertaken. Importantly, the conjugate exhibited similar biofilm inhibition and disruption properties as un-labelled OligoG. Unfortunately, the fluorophore appeared to interact with the bacterial cell wall giving inconclusive mechanistic data (**Chapter 3**). Future studies could incorporate a wash step before imaging to see if TxRd-OligoG could be dissociated from the bacterial biofilm. However, there is a danger that such a procedure may disrupt the biofilm structure or wash away important structural components. Furthermore, since TxRd cadaverine has a positively charged amino end group, it is possible that this may be responsible for the interactions with bacterial membranes. This could be confirmed by employing a TxRd succinimidyl ester as the “free” TxRd form, thereby reducing interaction with the negatively charged bacterial cell membrane.

As mucins are a key component of CF sputum, studying their interaction with OligoG is of vital importance. Similar to the lack of clinical relevance discussed for the *P. aeruginosa* (PAO1), a similar criticism could be levelled at the use of PGM for these studies. Although the protein backbone of PGM shows high similarity to human mucin in the amide I and amide II region, its viscosity varies greatly as a

result of variation in the degree of glycosidic bonding (Teubl et al., 2013a). PGM shows only 68% homology to its human equivalent at the protein level. Simple and direct extrapolation of the results obtained here with PGM should be related to human respiratory mucin with caution (Teubl et al., 2013a). The initial imaging studies, employing SEM and AFM, confirmed OligoG disruption of the tight mucin aggregates leading to a more “open” structure, with reduced inter-linking networks. This resembled the disrupted biofilm pattern seen when treated with OligoG, which led to bacterial clumping (**Chapter 3**). This observed disruption was evident in both direct imaging and was reflected in ELS analysis, where PGM became more negative when treated with OligoG.

Mucins have extensive diversity of oligosaccharide structures which are important in mediating interactions with other proteins, cells and pathogens. The exact disease-related changes in glycosylation associated with CF remain unclear and may vary with infection/inflammation status, which may even affect patients in early childhood (Schulz et al., 2007). Clear differences include a decreased mean carbohydrate dry weight of non-diseased individuals (59%) compared to CF patients (76%). Furthermore, the majority of the *O*-glycans in non-diseased mucin are “neutral”, whereas a majority of *O*-glycan from CF patients are anionic (~63%), containing both sialylated and/or sulfated species (Xia et al., 2005). *P. aeruginosa* colonisation is established in the respiratory epithelium via adhesion to these specific mucins. These studies (**Chapter 4**) showed how mucin became more negative when combined with OligoG, which might effectively alter its ability to establish ‘typical’ biofilms, and hinder the bacterial growth environment (Robinson et al., 2012).

In vivo binding of mucin in the CF lung is complex. In the diseased state, CFTR is not expressed in the goblet cells and mucous glands of acinar cells, which synthesise respiratory mucins. As a consequence of CFTR mutation, differential mucin glycosylation and sulfation may be a secondary effect of the mutation such as chronic infection and inflammation (Xia et al., 2005). Sulfation may be a result of the underlying inflammation, along with defects in the cell surface CFTR, which may be a receptor for *P. aeruginosa*. Inflammation in CF individuals may precede further bacterial colonisation, being a major factor and cause of this altered glycosylation and sulfation of mucins (Xia et al., 2005).

Isolates from the CF lung are able to utilise human respiratory mucin as a source of sulfate for growth, compared to non-clinical species of the genus *Pseudomonas* which cannot (Robinson et al., 2012). A possibility is to speculate and suggest that the interaction of OligoG with free sulfate (SO_4^{2-}) may reduce the energy sources available for bacterial growth in sputum, and thereby hinder biofilm development. However, as inorganic sulfate for growth in sputum is plentiful, mucin de-sulfation is unlikely to be a limiting energy source. It has been postulated that it has an alternative, as yet unknown, purpose in the CF lung (Robinson et al., 2012). A reduction in sulfation has been associated with improved pulmonary function in CF subjects. Although a CF patients general health may improve after exacerbation, their lung biochemistry remains fundamentally in a worse state than that of healthy non-CF individuals (Schulz et al., 2007). The interaction between OligoG and the sulfate moiety (SO_4^{2-}) may lead to improved pulmonary function, and could be sustained during periods of remission (**Chapter 4**). To confirm the validity of the mucins used in this study, a comparison of mucin MUC5AC (extracted from CF sputum samples and cell lines) with freshly cleaved PGM and commercial PGM would be highly beneficial. This would be novel research and would also add valuable data to the published literature. It was postulated in this study that OligoG may be interacting with MUC5AC (**Chapter 4**), leading to the hypothesis that this opened the mucin network via hydrogen bonding.

Unfortunately dynamic light scattering (DLS) analysis of sizing measurements could not be performed with mucin in this study, as the maximum size that could be analysed was 10 μm . Since mucins are likely to form rod-like aggregates due to electrostatic repulsion, any aggregates formed will have been considerably larger, being at least one order of magnitude greater than its “native” mucin biopolymer (Bhaskar et al., 1991). Electron microscopy of intact MUC5AC mucin has shown its poly-disperse nature, with filamentous threads, many in excess of 10 μm in length (Sheehan et al., 2000). As mucin samples have a tendency to “clump”, results may be missed if they were out of range. Future research could possibly measure mucin particle size using a homodyne DLS instrument (Chen et al., 2012).

The use of FTIR in this study proved challenging due to the heterogeneous nature of the samples used (Lewis et al., 2013a). Also as this study, had a focus of testing only non-induced sputum, there were difficulties in obtaining large numbers

of patient specimens (**Chapter 4**). Although induced sputum is known to provide samples with higher cell viability, sputum induction requires saline inhalation and therefore leads to an increased osmolarity of the airway lining (Paggiaro et al., 2002). This would directly affect the rheology of the sample and the chemical bonds found in FTIR. An induced sample may also have more nasal and pharyngeal contamination (Paggiaro et al., 2002). Despite this, the data generated was promising in analysing the sputum/OligoG interactions, and will contribute to future research studies. In the first instance, a larger study sample is required, as 9 patients were insufficient to obtain definitive statistical results. Also, as *in vivo* studies with OligoG are now underway, it would be highly preferable if new samples could be obtained from these studies, where OligoG treatment is given *in vivo* prior to FTIR analysis. The DNA concentration between sputum samples can vary greatly, for example, in a study of 167 CF patient sputum, the level of DNA ranged from 0.3 – 9.5 mg/ml (Haley et al., 2012). A greater understanding of the interaction of OligoG with DNA is also required.

The rheological properties of biofilms determine the shape and mechanical stability of a biofilm structure, which in turn affects mass-transfer and detachment processes. In the diseased lung, the EPS can aggregate due to hydrogen bonding, to form highly hydrated viscoelastic gels (Stoodley et al., 2002), contributing to an ineffective cough and airway clearance. Progressive airway obstruction by “thickened sputum” leads to chronic bacterial infection and inflammation, and production of more sputum. Mucin is an important component of sputum and studies have shown that a significant correlation exists between mucin content and rheological moduli, elastic and viscous responses (Sanders et al., 2000). The co-delivery of inhaled antibiotics with mucolytics to decrease sputum viscoelasticity is perceived to improve antibiotic penetration into the sputum, leading to an increased antibacterial potency and reduction of the dose required for clinical benefit (Yang et al., 2010). OligoG has been suggested to potentially alter sputum viscoelasticity (Nordgard and Draget, 2011) as well as enhancing antimicrobial therapy (Khan et al., 2012), suggesting that it might have *in vivo* therapeutic benefit.

The use of extensional rheology on these sputum samples would have conferred considerable advantage in the small sample sizes required to perform the test. The heterogeneity of the untreated samples is considerable, thereby skewing

any readings obtained. Interestingly, this heterogeneity was markedly reduced following treatment with 2% OligoG (**Chapter 5**). Subsequent testing was carried out using bulk shear rheology which had been extensively used in previous sputum studies (Nordgard and Draget, 2011, Henke and Ratjen, 2007, Hoffer-Schaefer et al., 2014, Nielsen et al., 2004). These studies demonstrated a significant decrease in elastic and viscous response following OligoG treatment.

The longitudinal study on CF sputum from a single patient demonstrated the synergistic effects of OligoG with rhDNase I, further amplifying the possible *in vivo* benefits of OligoG treatment. Surprisingly in the longitudinal study, large intra-patient variation was seen in sputum samples, even within 24 h of sample collection. Importantly, this was not associated with exacerbation, FEV₁, duration of intravenous antibiotics or length of hospital admission.

OligoG appears to target the mucin component of sputum (Sletmoen et al., 2012), whilst rhDNase I targets the eDNA (Sanders et al., 2006, Visick and Fuqua, 2005), both of which act to significantly reduce the viscoelasticity of CF sputum. These results were in keeping with preliminary FTIR data (showing changes to the sulfated moiety of mucin in OligoG treated-CF sputum), suggesting that OligoG can effectively ‘open-up’ or ‘unravel’ the sputum structure and alter the viscoelasticity of sputum.

A range of mucolytic drug delivery approaches, including use of nanoparticles and nanocarrier-based systems have been evaluated, some of which have been demonstrated, *in vitro*, to disrupt the structure of mucus and sputum (Chen et al., 2012) and to facilitate drug delivery (Cartiera et al., 2010, Tang et al., 2009). These studies investigated diseased sputum/mucus, as mucus from healthy individuals is not spontaneously expectorated and therefore difficult to obtain. A greater understanding of the behaviour of healthy mucus could considerably increase our knowledge of the effects of OligoG in enhancing permeability of mucus gel. For example, healthy mucus could be collected from the endotracheal tubes of patients without respiratory co-morbidities, such as patients undergoing elective non-cardiothoracic surgery. However, mucus collected from endotracheal tubes may be altered compared to the mucus gel layer *in vivo*, since endotracheal tubes are connected to a passive heat and moisture exchanger to humidify the ventilated air.

This means of sample collection is nevertheless preferable to bronchial lavages, as it minimises sample dilution and salivary contamination (Schuster et al., 2013).

Current conventional antifungals consist of azoles (with fluconazole being the most potent), polyenes (such as nystatin) and echinocandins (Denning, 2002). Combining antifungal drugs has been recommended to enhance efficacy against invasive fungal infections. The aim of a combined therapy is to widen the spectrum and potency of drug activity, provide a rapid synergistic effect, reduce toxicity and the risk of resistance. Echinocandins are one of the newer class of antifungals, with less drug interactions compared to azoles (Denning, 2002). However, resistance to echinocandins has already been reported (Cappelletty and Eiselstein-McKittrick, 2007). A case-study found caspofungin treatment-failure of oral candidosis and oesophagitis due to a mutation in the candidal gene encoding 1-3- β -D-glycan synthase, thereby reducing susceptibility to echinocandins (Baixench et al., 2007). This may be an area where, if synergy with OligoG could be shown, applications to treat yeast infections associated with echinocandin resistance could be undertaken.

Physical studies of OligoG interactions with the fungal cell surface showed significant differences to those obtained from the bacterial studies. There were no changes in zeta potential for *Candida* species treated with OligoG (**Chapter 6**), in contrast to that observed for *P. aeruginosa* (PAO1; **Chapter 2**).

Candida cell walls are essentially highly glycosylated polypeptides, consisting of several *N*-linked glycans with outer side chains of mannose units. The anionic surface charge of yeasts and their hydrophobicity is linked to phosphorylation of these mannosyl side chains. These “mannoproteins” are mainly on the outside of the *Candida* cell wall, and are responsible for initial biofilm establishment. Their anionic charge is thought to repel COO⁻ groups (Park et al., 2003) and may, in part, explain the failure of polyanionic OligoG to “bind” with the cell wall, which instead appeared to keep the cells apart, via repulsion of the two carboxylic acid moieties on both the cell wall and OligoG.

Whilst studies of *P. aeruginosa*, *B. cepacia* and *Achromobacter* species (due to their disease association and mortality respectively in CF) are frequent, *Candida* species are often overlooked in CF patients. Of the *Candida* species found in CF patients, 95% have been identified as *C. albicans*, with the remaining isolates being *C. glabrata*, *C. parapsilosis*, *C. krusei* and *C. dubliniensis*. Confounding factors that

make CF patients at higher risk of colonisation with *Candida* species include xerostomia from diabetes-related CF, inhaled corticosteroids and prolonged antibiotic use (Chotirmall et al., 2010). There has also been an improvement in species identification leading to a greater understanding of the lung microorganisms isolated (Peltroche-Llacsahuanga et al., 2002). A large-scale study from the European Epidemiologic Registry of Cystic Fibrosis found that fungal colonisation was associated with differences in FEV₁ (Navarro et al., 2001). Navarro et al., 2011 found that *Aspergillus* species and *Candida* species colonisation were associated with a significant decrease in FEV₁ in all age groups. Interestingly, 33.5% of all patients in the study were colonised with *Candida* species and 16.9% with *Aspergillus* species (Navarro et al., 2001). It has been shown that antibiotic therapy with amoxicillin, azithromycin, third generation cephalosporins and oral vancomycin all increased the rate and load of *Candida* species colonisation in CF children (Gammelsrud et al., 2011).

Initial OligoG candidal studies were carried out by the Department of Bioprocess Technology, SINTEF Materials and Chemistry, N-7465 Trondheim, Norway (see **Appendix III**). High-throughput robotic MIC screening demonstrated the potentiating effects of OligoG (2, 6 and 10%) with several classes of antifungal agents including fluconazole with strains tested. In addition, RHE work demonstrated a statistically significant reduction in candidal hyphal infiltration at a low concentration of 0.2% OligoG (see **Appendix III**). This precipitated further investigation of OligoG as an antifungal. Importantly, development of OligoG as an inhalation therapy (with no known antimicrobial resistance) has the potential to lower the bacterial load within the lung, which in turn could reduce fungal pathogenicity.

As OligoG has moved towards clinical use, Phase I clinical studies of the safety and toxicology of OligoG have been undertaken using a working concentration between 2-10% (www.clinicaltrials.gov [identifier NCT00970346]). Concomitant research studies focused on the same principal concentrations 2, 6 and 10% OligoG (Khan et al., 2012, Roberts et al., 2013, Powell et al., 2013). In the subsequent human patient clinical trial, in 2012, studies employed a 6% inhaled solution of OligoG (www.clinicaltrials.gov [identifier NCT01465529]). From this

study, it was estimated that only 20% of the nebulised OligoG actually entered the lung (i.e. giving an actual dose of 1.2%). This led to a reassessment of the actual experimental concentrations that should be used in the *in vitro* studies. Therefore, to analyse the interaction between OligoG and bacteria, using nanoscale imaging, the concentrations of OligoG used in later experiments were lowered to 0.2-0.5% OligoG (Powell et al., 2014, Roberts et al., 2013). To get a more accurate picture of the actual dose reaching the lung, an open labelled, randomised, two-way crossover scintigraphic study will investigate lung deposition of radiolabelled OligoG delivered as a dry powder and as a nebulised solution in CF patients. This will determine the ratio of OligoG in the central airways compared to the peripheral region, as well as characterise the extra-pulmonary deposition (i.e. in the oesophagus and stomach) and estimate retention of OligoG in the nebuliser or inhaler. Further information regarding animal and human inhalation OligoG studies can be found in **Appendix IV**.

OligoG contains sodium salts (12.4% w/w sodium salt) and this may affect the osmolarity of the suspending medium. In bacterial environments where salt concentrations are higher, such as the skin, osmotic pressure did not appear to affect the growth rate and extent of *Staphylococcus epidermis* at NaCl concentrations ≤ 1 M (Linnes et al., 2013). Other bacterial genera however have shown activation of biofilm genes, such as the *bdm* (biofilm dependent modulation) gene in *E. coli* during osmotic shock at 0.5 M NaCl (Francez-Charlot et al., 2005). Interestingly in CF patients, high salinity in the lung is often encountered and osmo-adaptation is therefore crucial for survival of *P. aeruginosa* in this habitat (Aspedon et al., 2006). In another study, hyperosmotic stress (0.5 M NaCl) applied to exponentially growing *P. aeruginosa* (PAO1), interrupted rhamnolipid synthesis (Bazire et al., 2005) which is also involved in biofilm formation. Furthermore, a *MucA* mutant (leading to a mucoid phenotype) was found to be more susceptible to osmotic stress than the wild type, with no increase in alginate synthesis seen under chronic osmotic stress (Behrends et al., 2010). These findings may be advantageous for OligoG in aiding disruption of biofilm formation, as well as further altering sputum viscoelasticity. Interestingly, the *C. tropicalis* AFM images (**Chapter 6**) demonstrated cell flattening when treated with OligoG, which could be partly explained by osmotic stress caused by the actual salt levels found in OligoG itself.

Identification of natural strategies that interfere with intra- and inter-species cell-cell communication is promising and could provide new treatments for bacterial disease (Federle and Bassler, 2003). A new school of thought has emerged to target QS, hydrophobicity and EPS as a means of preventing biofilm formation. Marine bacterial extracts have been shown to have antibiofilm properties against *P. aeruginosa* (PAO1), including QS inhibition and reduction of EPS production. These effects caused biofilm dispersion and disruption, and a reduced hydrophobicity index (Nithya et al., 2010). QS signals of pathogens can regulate expression of virulence factors, and recently they have become targets for novel therapies. The development of QS inhibitors has been shown to make biofilms more susceptible to antimicrobial treatments. This in turn, may lead to a reduction in bacterial virulence and patient mortality (Rasmussen and Givskov, 2006). Coral-associated bacteria have also been shown to possess antibiofilm activity against biofilm formation in *Streptococcus pyogenes* due to QS inhibition properties (Thenmozhi et al., 2009). What is still needed for all these antimicrobials is that they have to make the “giant leap” from the laboratory to the patient. Many problems exist in this transition including toxicity in chronic usage and those of safe, commercial scale-up. As for OligoG, this step is already underway.

7.2 The future

Important direct physical changes with OligoG that alter bacterial electrostatic interactions, aggregation, biofilm formation, and mucin assembly have been demonstrated. However, much work remains to be done to understand OligoG's precise mode of action. Also, its exact role in the potentiation of antibiotics remains unresolved with important targets e.g. QS and cell-surface hydrophobicity, needing still to be studied at a molecular and functional level. Importantly, no build-up of resistance to OligoG has been noted *in vitro* even following prolonged serial sub-culture using escalating OligoG concentrations (Khan et al., 2012).

In addition to mechanistic and structural studies, the ability of OligoG to alter the viscoelasticity of sputum and its antibiofilm effects are both highly promising features for other respiratory diseases such as COPD. These areas represent research avenues that could also be pursued in the future. There are a number of other

potential new applications for OligoG, including its topical application for chronic wounds and burns, as well as in dental products.

Production of alginates with specific physical properties can be affected by a number of factors including the species of seaweed used, source and water temperature. Alginates isolated from bacteria and algae are usually of high MW (typically 10^5 to 10^6 Da), corresponding to about 500-5000 residue per chain (Andersen et al., 2012). The ability to produce alginates reproducibly and efficiently is vital for therapeutic products, whilst still maintaining the maximum therapeutic effect. Complying with economic and environmental challenges, whilst keeping up with demand for production of OligoG, is also of vital importance. Lower MW alginates are obtained by partial degradation, for example, by acid hydrolysis (Andersen et al., 2012) or epimerase activity (Gimmestad et al 2003). Whilst it is known that OligoMG and OligoM oligomers (of similar MW profile to OligoG) do not have as strong a potentiation effect as OligoG (Khan et al., 2012), we know little of the structure-function relationship. The techniques described in this thesis could therefore be valuable in future screening for potential new agents.

7.3 Conclusion

This thesis describes the interaction of OligoG with bacteria and disruption of biofilms of MDR and pan-drug resistant bacteria. OligoG has been shown to inhibit and disrupt pseudomonal biofilms, leading to changes in surface charge and sizing. These bacteria-polysaccharide interactions were not easily disrupted on washing. AFM, SEM and CLSM were used to visualise cellular changes, as well as using a fluorescently-labelled OligoG conjugate to highlight distribution of OligoG within the biofilm. OligoG has also been shown to decrease filament formation in *Candida*, working synergistically with fluconazole.

The complex interaction of OligoG with mucin was further investigated, showing that OligoG caused a change in mucin conformation, which may also play a role in hindering biofilm formation. Extensional and shear rheological analysis confirmed that OligoG reduced both viscous and elastic parameters of sputum, as well as working synergistically with rhDNase I. These alterations, as well as its antibiofilm properties, are positive features for improving pulmonary function in CF

patients. Promisingly, the clinical trials for OligoG are currently at the Phase IIb stage in CF patients, with a significant prospect that this translational research will make the exciting journey from laboratory to clinical therapy.

7.4 Papers published from thesis to date

Published-

- TØNDERVIK, A., SLETTA, H., KLINKENBERG, G., EMANUEL, C., POWELL, L. C., PRITCHARD, M. F., KHAN, S., CRAINE, K. M., ONSOYEN, E., RYE, P. D., WRIGHT, C., THOMAS, D. W. & HILL, K. E. 2014. Alginate oligosaccharides inhibit fungal cell growth and potentiate the activity of antifungals against *Candida* and *Aspergillus* spp. *Plos One*, 9 (11) e112518.
- POWELL, L. C., PRITCHARD, M. F., EMANUEL, C., ONSOYEN, E., RYE, P. D., WRIGHT, C. J., HILL, K. E. & THOMAS, D. W. 2014. A nanoscale characterization of the interaction of a novel alginate oligomer with the cell surface and motility of *Pseudomonas aeruginosa*. *American Journal of Respiratory Cell and Molecular Biology*, 50, 483-492.
- ROBERTS, J. L., KHAN, S., EMANUEL, C., POWELL, L. C., PRITCHARD, M. F., ONSOYEN, E., MYRVOLD, R., THOMAS, D. W. & HILL, K. E. 2013. An *in vitro* study of alginate oligomer therapies on oral biofilms. *Journal of Dentistry*, 41, 892-899.

Bibliography

- AGGARWAL, S. & HOZALSKI, R. M. 2010. Determination of biofilm mechanical properties from tensile tests performed using a micro-cantilever method. *Biofouling*, 26, 479-486.
- AGUILAR-USCANGA, B. & FRANCOIS, J. M. 2003. A study of the yeast cell wall composition and structure in response to growth conditions and mode of cultivation. *Letters in Applied Microbiology*, 37, 268-274.
- AHIMOU, F., DENIS, F. A., TOUHAMI, A. & DUFRENE, Y. F. 2002. Probing microbial cell surface charges by atomic force microscopy. *Langmuir*, 18, 9937-9941.
- AITKEN, M. L., BELLON, G., DE BOECK, K., FLUME, P. A., FOX, H. G., GELLER, D. E., HAARMAN, E. G., HEBESTREIT, H. U., LAPEY, A., SCHOU, I. M., ZUCKERMAN, J. B., CHARLTON, B. & INVESTIGATORS, C. F. 2012. Long-term inhaled dry powder mannitol in cystic fibrosis an international randomized study. *American Journal of Respiratory and Critical Care Medicine*, 185, 645-652.
- AL-FATTANI, M. A. & DOUGLAS, L. J. 2006. Biofilm matrix of *Candida albicans* and *Candida tropicalis*: chemical composition and role in drug resistance. *Journal of Medical Microbiology*, 55, 999-1008.
- ALAVI, M. R., STOJADINOVIC, A. & IZADJOO, M. J. 2012. An overview of biofilm and its detection in clinical samples. *Journal of Wound Care*, 21, 376-383.
- ALGIPHARMA. 2014. *OligoG technology* [Online]. Available: <http://www.algipharma.com/en/Products.aspx> [Accessed 23/06/2014].
- ALI, I., SHARMA, P., SURI, K. A., SATTI, N. K., DUTT, P., AFRIN, F. & KHAN, I. A. 2011. *In vitro* antifungal activities of amphotericin B in combination with acteoside, a phenylethanoid glycoside from *Colebrookea oppositifolia*. *Journal of Medical Microbiology*, 60, 1326-1336.
- ALIPOUR, M., SUNTRES, Z. E. & OMRI, A. 2009. Importance of DNase and alginate lyase for enhancing free and liposome encapsulated aminoglycoside activity against *Pseudomonas aeruginosa*. *Journal of Antimicrobial Chemotherapy*, 64, 317-325.
- ALKAWASH, M. A., SOOTHILL, J. S. & SCHILLER, N. L. 2006. Alginate lyase enhances antibiotic killing of mucoid *Pseudomonas aeruginosa* in biofilms. *Apmis*, 114, 131-138.
- ALLESEN-HOLM, M., BARKEN, K. B., YANG, L., KLAUSEN, M., WEBB, J. S., KJELLEBERG, S., MOLIN, S., GIVSKOV, M. & TOLKER-NIELSEN, T. 2006. A characterization of DNA release in *Pseudomonas aeruginosa* cultures and biofilms. *Molecular Microbiology*, 59, 1114-1128.
- ALVES, C. S., MELO, M. N., FRANQUELIM, H. G., FERRE, R., PLANAS, M., FELIU, L., BARDAJI, E., KOWALCZYK, W., ANDREU, D., SANTOS, N. C., FERNANDES, M. X. & CASTANHO, M. A. R. B. 2010. *Escherichia coli* cell surface perturbation and disruption induced by antimicrobial peptides BP100 and pepR. *Journal of Biological Chemistry*, 285, 27536-27544.
- ANDERSEN, T., STRAND, B. L., FORMO, K., ALSBERG, E. & CHRISTENSEN, B. E. 2012. Alginates as biomaterials in tissue engineering. *Carbohydrate Chemistry*, 37, 227-258.

- ANEES, M. 1996. Location of tumour cells in colon tissue by Texas red labelled pentosan polysulphate, an inhibitor of a cell surface protease. *Journal of Enzyme Inhibition*, 10, 203-214.
- APERIS, G., MYRIOUNIS, N., SPANAKIS, E. K. & MYLONAKIS, E. 2006. Developments in the treatment of candidiasis: more choices and new challenges. *Expert Opinion on Investigational Drugs*, 15, 1319-1336.
- ASHIRU-OREDOPE, D., SHARLAND, M., CHARANI, E., MCNULTY, C., COOKE, J. & GR, A. A. S. 2012. Improving the quality of antibiotic prescribing in the NHS by developing a new Antimicrobial Stewardship Programme: Start Smart-Then Focus. *Journal of Antimicrobial Chemotherapy*, 67, I51-I63.
- ASPEDON, A., PALMER, K. & WHITELEY, M. 2006. Microarray analysis of the osmotic stress response in *Pseudomonas aeruginosa*. *Journal of Bacteriology*, 188, 2721-2725.
- ATSUMI, T., MAEKAWA, Y., YAMADA, T., KAWAGISHI, I., IMAE, Y. & HOMMA, M. 1996. Effect of viscosity on swimming by the lateral and polar flagella of *Vibrio alginolyticus*. *Journal of Bacteriology*, 178, 5024-5026.
- ATTWOOD, A. I. 1989. Calcium alginate dressing accelerates split skin-graft donor site healing. *British Journal of Plastic Surgery*, 42, 373-379.
- AZOULAY, E., TIMSIT, J. F., TAFFLET, M., DE LASSENCE, A., DARMON, M., ZAHAR, J. R., ADRIE, C., GARROUSTE-ORGEAS, M., COHEN, Y., MOURVILLIER, B., SCHLEMMER, B. & OUTCOMEREA STUDY, G. 2006. Candida colonization of the respiratory tract and subsequent pseudomonas ventilator-associated pneumonia. *Chest*, 129, 110-117.
- BAILLIE, G. S. & DOUGLAS, L. J. 2000. Matrix polymers of Candida biofilms and their possible role in biofilm resistance to antifungal agents. *Journal of Antimicrobial Chemotherapy*, 46, 397-403.
- BAIXENCH, M.-T., AOUN, N., DESNOS-OLLIVIER, M., GARCIA-HERMOSO, D., BRETAGNE, S., RAMIRES, S., PIKETTY, C. & DANNAOUI, E. 2007. Acquired resistance to echinocandins in *Candida albicans*: case report and review. *Journal of Antimicrobial Chemotherapy*, 59, 1076-1083.
- BANSIL, R., STANLEY, H. E. & LAMONT, J. T. 1995. Mucin Biophysics. *Annual Review of Physiology*, 57, 635-657.
- BANSIL, R. & TURNER, B. S. 2006. Mucin structure, aggregation, physiological functions and biomedical applications. *Current Opinion in Colloid & Interface Science*, 11, 164-170.
- BARNES, H. A. 2000. *A handbook of elementary rheology*, Aberystwyth, The University of Wales Institute of Non-Newtonian Fluid Mechanics.
- BARTIE, K. L., WILLIAMS, D. W., WILSON, M. J., POTTS, A. J. C. & LEWIS, M. A. O. 2004. Differential invasion of *Candida albicans* isolates in an *in vitro* model of oral candidosis. *Oral Microbiology and Immunology*, 19, 293-296.
- BAYER, M. E. & SLOYER, J. L. 1990. The electrophoretic mobility of gram-negative and gram-positive bacteria- an electrokinetic analysis. *Journal of General Microbiology*, 136, 867-874.
- BAZIRE, A., DHEILLY, A., DIAB, F., MORIN, D., JEBBAR, M., HARAS, D. & DUFOUR, A. 2005. Osmotic stress and phosphate limitation alter production of cell-to-cell signal molecules and rhamnolipid biosurfactant by *Pseudomonas aeruginosa*. *Fems Microbiology Letters*, 253, 125-131.

- BEECH, I. B., SMITH, J. R., STEELE, A. A., PENEGAR, I. & CAMPBELL, S. A. 2002. The use of atomic force microscopy for studying interactions of bacterial biofilms with surfaces. *Colloids and Surfaces B: Biointerfaces*, 23, 231-247.
- BEHRENDTS, V., RYALL, B., WANG, X., BUNDY, J. G. & WILLIAMS, H. D. 2010. Metabolic profiling of *Pseudomonas aeruginosa* demonstrates that the anti-sigma factor MucA modulates osmotic stress tolerance. *Molecular Biosystems*, 6, 562-569.
- BEKIR, K., NOUMI, E., ABID, N. B. S. & BAKHROUF, A. 2014. Adhesive properties to materials used in unit care by *Staphylococcus aureus* strains incubated in seawater microcosms. *Journal of Industrial and Engineering Chemistry*, 20, 2447-2451.
- BERNE, B. J. & PECORA, R. 2000. Dynamic Light Scattering: with Applications to Chemistry, Biology, and Physics. *Courier Dover Publications*
- BESINIS, A., DE PERALTA, T. & HANDY, R. D. 2014. Inhibition of biofilm formation and antibacterial properties of a silver nano-coating on human dentine. *Nanotoxicology*, 8, 745-754.
- BHASKAR, K. R., GONG, D., BANSIL, R., PAJEVIC, S., HAMILTON, J. A., TURNER, B. S. & LAMONT, J. T. 1991. Profound increase in viscosity and aggregation of pig gastric mucin at low pH. *American Journal of Physiology*, 261, G827-G833.
- BHAT, P. G., FLANAGAN, D. R. & DONOVAN, M. D. 1996. Drug diffusion through cystic fibrotic mucus: Steady-state permeation, rheologic properties, and glycoprotein morphology. *Journal of Pharmaceutical Sciences*, 85, 624-630.
- BILTON, D. & OSMOND, J. 2010. Cystic Fibrosis Trust Annual data report 2010. *UK CF registry: Cystic Fibrosis Trust*. London: Cystic Fibrosis Trust.
- BILTON, D., ROBINSON, P., COOPER, P., GALLAGHER, C. G., KOLBE, J., FOX, H., JAQUES, A., CHARLTON, B. & INVESTIGATORS, C. F. S. 2011. Inhaled dry powder mannitol in cystic fibrosis: an efficacy and safety study. *European Respiratory Journal*, 38, 1071-1080.
- BINGOEL, A. O., LOHMANN, D., PUESCHEL, K. & KULICKE, W. M. 2010. Characterization and comparison of shear and extensional flow of sodium hyaluronate and human synovial fluid. *Biorheology*, 47, 205-224.
- BIOPOLYMER, F. 2014. *Alginates / PGA / Functionality and Rheology* [Online]. Available: <http://www.fmcbiopolymer.com/Food/Ingredients/AlginatesPGA/FunctionalityandRheology.aspx> [Accessed 01/09/2014].
- BITTAR, F. & ROLAIN, J. M. 2010. Detection and accurate identification of new or emerging bacteria in cystic fibrosis patients. *Clinical Microbiology and Infection*, 16, 809-820.
- BOATENG, J. S., MATTHEWS, K. H., STEVENS, H. N. E. & ECCLESTON, G. M. 2008. Wound healing dressings and drug delivery systems: A review. *Journal of Pharmaceutical Sciences*, 97, 2892-2923.
- BOSCH, A., MINAN, A., VESCINA, C., DEGROSSI, J., GATTI, B., MONTANARO, P., MESSINA, M., FRANCO, M., VAY, C., SCHMITT, J., NAUMANN, D. & YANTORNO, O. 2008. Fourier transform infrared spectroscopy for rapid identification of nonfermenting gram-negative bacteria

- isolated from sputum samples from cystic fibrosis patients. *Journal of Clinical Microbiology*, 46, 2535-2546.
- BOWEN, W. R., FENTON, A. S., LOVITT, R. W. & WRIGHT, C. J. 2002. The measurement of *Bacillus mycoides* spore adhesion using atomic force microscopy, simple counting methods, and a spinning disk technique. *Biotechnology and Bioengineering*, 79, 170-179.
- BOYCE, J. R. & MILLER, R. V. 1982. Selection of non-mucoid derivatives of mucoid *Pseudomonas aeruginosa* is strongly influenced by the level of iron in the culture medium. *Infection and Immunity*, 37, 695-701.
- BOYLE, M. P. & DE BOECK, K. 2013. A new era in the treatment of cystic fibrosis: correction of the underlying CFTR defect. *Lancet Respiratory Medicine*, 1, 158-163.
- BRADFORD, P. A. 2001. Extended-spectrum beta-lactamases in the 21st century: Characterization, epidemiology, and detection of this important resistance threat. *Clinical Microbiology Reviews*, 14, 933-951.
- BRAGA, P. C. & RICCI, D. 1998. Atomic force microscopy: Application to investigation of *Escherichia coli* morphology before and after exposure to cefodizime. *Antimicrobial Agents and Chemotherapy*, 42, 18-22.
- BRAGGINTON, E. C. & PIDDOCK, L. J. V. 2014. UK and European Union public and charitable funding from 2008 to 2013 for bacteriology and antibiotic research in the UK: an observational study. *The Lancet Infectious Diseases*, 14, 857-868.
- BRAND, A. 2012. Hyphal growth in human fungal pathogens and its role in virulence. *International journal of microbiology*, 2012, doi:10.1155/2012/517529.
- BREEN, L. & ASWANI, N. 2012. Elective versus symptomatic intravenous antibiotic therapy for cystic fibrosis. *Cochrane Database of Systematic Reviews*, 7, CD002767.
- BROOUN, A., LIU, S. H. & LEWIS, K. 2000. A dose-response study of antibiotic resistance in *Pseudomonas aeruginosa* biofilms. *Antimicrobial Agents and Chemotherapy*, 44, 640-646.
- BRUINSMA, G. M., RUSTEMA-ABBING, M., VAN DER MEI, H. C. & BUSSCHER, H. J. 2001. Effects of cell surface damage on surface properties and adhesion of *Pseudomonas aeruginosa*. *Journal of Microbiological Methods*, 45, 95-101.
- BRUINSMA, G. M., RUSTEMA-ABBING, M., VAN DER MEI, H. C., LAKKIS, C. & BUSSCHER, H. J. 2006. Resistance to a polyquaternium-1 lens care solution and isoelectric points of *Pseudomonas aeruginosa* strains. *Journal of Antimicrobial Chemotherapy*, 57, 764-766.
- BRUTON, J., TAVI, P., AYDIN, J., WESTERBLAD, H. & LANNERGREN, J. 2003. Mitochondrial and myoplasmic Ca²⁺ in single fibres from mouse limb muscles during repeated tetanic contractions. *Journal of Physiology-London*, 551, 179-190.
- BUCKI, R., BYFIELD, F. J. & JANMEY, P. A. 2007. Release of the antimicrobial peptide LL-37 from DNA/F-actin bundles in cystic fibrosis sputum. *European Respiratory Journal*, 29, 624-632.
- BUGLI, F., POSTERARO, B., PAPI, M., TORELLI, R., MAIORANA, A., STERBINI, F. P., POSTERARO, P., SANGUINETTI, M. & DE SPIRITO, M. 2013. *In vitro* Interaction between Alginate Lyase and Amphotericin B

- against *Aspergillus fumigatus* Biofilm Determined by Different Methods. *Antimicrobial Agents and Chemotherapy*, 57, 1275-1282.
- BUSSCHER, H. J., GEERTSEMADOORNBUSCH, G. I. & VANDERMEI, H. C. 1997. Adhesion to silicone rubber of yeasts and bacteria isolated from voice prostheses: Influence of salivary conditioning films. *Journal of Biomedical Materials Research*, 34, 201-209.
- BUSSIERE, D. E., MUCHMORE, S. W., DEALWIS, C. G., SCHLUCKEBIER, G., NIENABER, V. L., EDALJI, R. P., WALTER, K. A., LADROR, U. S., HOLZMAN, T. F. & ABAD-ZAPATERO, C. 1998. Crystal structure of ErmC', an rRNA methyltransferase which mediates antibiotic resistance in bacteria. *Biochemistry*, 37, 7103-7112.
- BUTLER, M. T., WANG, Q. & HARSHEY, R. M. 2010. Cell density and mobility protect swarming bacteria against antibiotics. *Proceedings of the National Academy of Sciences of the United States of America*, 107, 3776-3781.
- CAIAZZA, N. C., SHANKS, R. M. Q. & O'TOOLE, G. A. 2005. Rhamnolipids modulate swarming motility patterns of *Pseudomonas aeruginosa*. *Journal of Bacteriology*, 187, 7351-7361.
- CAO, X. X., BANSIL, R., BHASKAR, K. R., TURNER, B. S., LAMONT, J. T., NIU, N. & AFDHAL, N. H. 1999. pH-dependent conformational change of gastric mucin leads to sol-gel transition. *Biophysical Journal*, 76, 1250-1258.
- CAPPELLETTY, D. & EISELSTEIN-MCKITRICK, K. 2007. The echinocandins. *Pharmacotherapy*, 27, 369-388.
- CARLET, J., PULCINI, C. & PIDDOCK, L. J. 2014. Antibiotic resistance: A geopolitical issue. *Clinical microbiology and infection*, doi: 10.1111/1469-0691.12767.
- CARTIERA, M. S., FERREIRA, E. C., CAPUTO, C., EGAN, M. E., CAPLAN, M. J. & SALTZMAN, W. M. 2010. Partial correction of cystic fibrosis defects with PLGA nanoparticles encapsulating curcumin. *Molecular Pharmaceutics*, 7, 86-93.
- CDC. 2014. *Threat Report 2013* [Online]. Available: <http://www.cdc.gov/drugresistance/threat-report-2013/index.html> [Accessed 08/08/2014].
- CHAMILOS, G., LEWIS, R. E., ALBERT, N. & KONTOYIANNIS, D. P. 2007. Paradoxical effect of echinocandins across *Candida* species *in vitro*: Evidence for echinocandin-specific and *Candida* species-related differences. *Antimicrobial Agents and Chemotherapy*, 51, 2257-2259.
- CHEN, E. Y., DALEY, D., WANG, Y.-C., GARNICA, M., CHEN, C.-S. & CHIN, W.-C. 2012. Functionalized carboxyl nanoparticles enhance mucus dispersion and hydration. *Scientific Reports*, 2, 1-5.
- CHEN, E. Y. T., WANG, Y. C., CHEN, C. S. & CHIN, W. C. 2010. Functionalized positive nanoparticles reduce mucin swelling and dispersion. *Plos One*, 5(11): e15434. doi: 10.1371/journal.pone.0015434.
- CHOTIRMALL, S. H., O'DONOGHUE, E., BENNETT, K., GUNARATNAM, C., O'NEILL, S. J. & MCELVANEY, N. G. 2010. Sputum *Candida albicans* presages FEV₁ decline and hospital-treated exacerbations in cystic fibrosis. *Chest*, 138, 1186-1195.
- CHVATAL, S. A., KIM, Y.-T., BRATT-LEAL, A. M., LEE, H. & BELLAMKONDA, R. V. 2008. Spatial distribution and acute anti-

- inflammatory effects of Methylprednisolone after sustained local delivery to the contused spinal cord. *Biomaterials*, 29, 1967-1975.
- COATES, A. R. M., HALLS, G. & HU, Y. 2011. Novel classes of antibiotics or more of the same? *British Journal of Pharmacology*, 163, 184-194.
- COHEN-CYMBERKNOH, M., SHOSEYOV, D. & KEREM, E. 2011. Managing cystic fibrosis strategies that increase life expectancy and improve quality of life. *American Journal of Respiratory and Critical Care Medicine*, 183, 1463-1471.
- COLLINS, T. J., BERRIDGE, M. J., LIPP, P. & BOOTMAN, M. D. 2002. Mitochondria are morphologically and functionally heterogeneous within cells. *Embo Journal*, 21, 1616-1627.
- CONE, R. A. 2009. Barrier properties of mucus. *Advanced Drug Delivery Reviews*, 61, 75-85.
- CONLY, J. & JOHNSTON, B. 2005. Where are all the new antibiotics? The new antibiotic paradox. *The Canadian journal of infectious diseases and medical microbiology* 16, 159-60.
- COSTERTON, J. W., STEWART, P. S. & GREENBERG, E. P. 1999. Bacterial biofilms: A common cause of persistent infections. *Science*, 284, 1318-1322.
- COWAN, M. M., VANDERMEI, H. C., STOKROOS, I. & BUSSCHER, H. J. 1992. Heterogeneity of surfaces of subgingival bacteria as detected by zeta potential measurements. *Journal of Dental Research*, 71, 1803-1806.
- CRATER, J. S. & CARRIER, R. L. 2010. Barrier properties of gastrointestinal mucus to nanoparticle transport. *Macromolecular Bioscience*, 10, 1473-1483.
- DA SILVA, C. R., NETO, J. B. D., SIDRIM, J. J. C., ANGELO, M. R. F., MAGALHAES, H. I. F., CAVALCANTI, B. C., BRILHANTE, R. S. N., MACEDO, D. S., DE MORAES, M. O., LOBO, M. D. P., GRANGEIRO, T. B. & NOBRE, H. V. 2013. Synergistic effects of amiodarone and fluconazole on *Candida tropicalis* resistant to fluconazole. *Antimicrobial Agents and Chemotherapy*, 57, 1691-1700.
- DASGUPTA, B., BROWN, N. E. & KING, M. 1998. Effects of sputum oscillations and rhDNase *in vitro*: A combined approach to treat cystic fibrosis lung disease. *Pediatric Pulmonology*, 26, 250-255.
- DAVEY, P., BROWN, E., CHARANI, E., FENELON, L., GOULD, I. M., HOLMES, A., RAMSAY, C. R., WIFFEN, P. J. & WILCOX, M. 2013. Interventions to improve antibiotic prescribing practices for hospital inpatients. *Cochrane Database of Systematic Reviews*, 1-208.
- DAVIES, D. 2003. Understanding biofilm resistance to antibacterial agents. *Nature Reviews Drug Discovery*, 2, 114-122.
- DAVRIL, M., DEGROOTE, S., HUMBERT, P., GALABERT, C., DUMUR, V., LAFITTE, J. J., LAMBLIN, G. & ROUSSEL, P. 1999. The sialylation of bronchial mucins secreted by patients suffering from cystic fibrosis or from chronic bronchitis is related to the severity of airway infection. *Glycobiology*, 9, 311-321.
- DE LA FUENTE-NUNEZ, C., KOROLIK, V., BAINS, M., UYEN, N., BREIDENSTEIN, E. B. M., HORSMAN, S., LEWENZA, S., BURROWS, L. & HANCOCK, R. E. W. 2012. Inhibition of bacterial biofilm formation and swarming motility by a small synthetic cationic peptide. *Antimicrobial Agents and Chemotherapy*, 56, 2696-2704.

- DE PAUW, B., WALSH, T. J., DONNELLY, J. P., STEVENS, D. A., EDWARDS, J. E., CALANDRA, T., PAPPAS, P. G., MAERTENS, J., LORTHOLARY, O., KAUFFMAN, C. A., DENNING, D. W., PATTERSON, T. F., MASCHMEYER, G., BILLE, J., DISMUKES, W. E., HERBRECHT, R., HOPE, W. W., KIBBLER, C. C., KULLBERG, B. J., MARR, K. A., MUNOZ, P., ODDS, F. C., PERFECT, J. R., RESTREPO, A., RUHNKE, M., SEGAL, B. H., SOBEL, J. D., SORRELL, T. C., VISCOLI, C., WINGARD, J. R., ZAOUTIS, T. & BENNETT, J. E. 2008. Revised definitions of invasive fungal disease from the European organization for research and treatment of cancer/invasive fungal infections cooperative group and the national institute of allergy and infectious diseases mycoses study group (EORTC/MSG) Consensus Group. *Clinical Infectious Diseases*, 46, 1813-1821.
- DE SORDI, L. & MUHLSCHLEGEL, F. A. 2009. Quorum sensing and fungal-bacterial interactions in *Candida albicans*: a communicative network regulating microbial coexistence and virulence. *Fems Yeast Research*, 9, 990-999.
- DEACON, M. P., MCGURK, S., ROBERTS, C. J., WILLIAMS, P. M., TENDLER, S. J. B., DAVIES, M. C., DAVIS, S. S. & HARDING, S. E. 2000. Atomic force microscopy of gastric mucin and chitosan mucoadhesive systems. *Biochemical Journal*, 348, 557-563.
- DEDINAITE, A. 2012. Biomimetic lubrication. *Soft Matter*, 8, 273-284.
- DEGROOTE, S., DUCOUROUBLE, M. P., ROUSSEL, P. & LAMBLIN, G. 1999. Sequential biosynthesis of sulfated and/or sialylated Lewis x determinants by transferases of the human bronchial mucosa. *Glycobiology*, 9, 1199-1211.
- DEGROOTE, S., MAES, E., HUMBERT, P., DELMOTTE, P., LAMBLIN, G. & ROUSSEL, P. 2003. Sulfated oligosaccharides isolated from the respiratory mucins of a secretor patient suffering from chronic bronchitis. *Biochimie*, 85, 369-379.
- DELMOTTE, P., DEGROOTE, S., LAFITTE, J. J., LAMBLIN, G., PERINI, J. M. & ROUSSEL, P. 2002. Tumor necrosis factor alpha increases the expression of glycosyltransferases and sulfotransferases responsible for the biosynthesis of sialylated and/or sulfated Lewis x epitopes in the human bronchial mucosa. *Journal of Biological Chemistry*, 277, 424-431.
- DENNING, D. W. 2002. Echinocandins: a new class of antifungal. *Journal of Antimicrobial Chemotherapy*, 49, 889-891.
- DES CHAMPS-BRO, B., LEROY-COTTEAU, A., MAZINGUE, F., PASQUIER, F., FRANCOIS, N., LEMAITRE, L., POULAIN, D., YAKOUB-AGHA, I., ALFANDARI, S. & SENDID, B. 2011. Invasive fungal infections: epidemiology and analysis of antifungal prescriptions in onco-haematology. *Journal of Clinical Pharmacy and Therapeutics*, 36, 152-160.
- DISMUKES, W. E. 2000. Introduction to antifungal drugs. *Clinical Infectious Diseases*, 30, 653-657.
- DONG, A., HUANG, P. & CAUGHEY, W. S. 1992. Redox-dependent changes in beta-extended chain and turn structures of cytochrome-c in water solution determined by 2nd derivative amide-I infrared-spectra. *Biochemistry*, 31, 182-189.
- DONLAN, R. M. 2002. Biofilms: Microbial life on surfaces. *Emerging Infectious Diseases*, 8, 881-890.

- DOROBANTU, L. S. & GRAY, M. R. 2010. Application of Atomic Force Microscopy in Bacterial Research. *Scanning*, 32, 74-96.
- DRAGET, K. I. & TAYLOR, C. 2011. Chemical, physical and biological properties of alginates and their biomedical implications. *Food Hydrocolloids*, 25, 251-256.
- DUFRENE, Y. F. 2002. Atomic force microscopy, a powerful tool in microbiology. *Journal of Bacteriology*, 184, 5205-5213.
- DUNNE, W. M. 2002. Bacterial adhesion: Seen any good biofilms lately? *Clinical Microbiology Reviews*, 15, 155-166.
- EASTY, G. C., HAEMMERLI, G., EASTY, D. M. & STRAULI, P. 1982. Interactions between normal epithelial and squamous carcinoma cells in monolayer culture. *Cancer Research*, 42, 4248-4255.
- ELKINS, M. R. & BYE, P. T. P. 2006. Inhaled hypertonic saline as a therapy for cystic fibrosis. *Current Opinion in Pulmonary Medicine*, 12, 445-452.
- EMERSON, J., ROSENFELD, M., MCNAMARA, S., RAMSEY, B. & GIBSON, R. L. 2002. *Pseudomonas aeruginosa* and other predictors of mortality and morbidity in young children with cystic fibrosis. *Pediatric Pulmonology*, 34, 91-100.
- ENE, I. V., ADYA, A. K., WEHMEIER, S., BRAND, A. C., MACCALLUM, D. M., GOW, N. A. R. & BROWN, A. J. P. 2012. Host carbon sources modulate cell wall architecture, drug resistance and virulence in a fungal pathogen. *Cellular Microbiology*, 14, 1319-1335.
- ERNST, R. K., YI, E. C., GUO, L., LIM, K. B., BURNS, J. L., HACKETT, M. & MILLER, S. I. 1999. Specific lipopolysaccharide found in cystic fibrosis airway *Pseudomonas aeruginosa*. *Science*, 286, 1561-1565.
- ESTRELA, A. B., HECK, M. G. & ABRAHAM, W.-R. 2009. Novel Approaches to Control Biofilm Infections. *Current Medicinal Chemistry*, 16, 1512-1530.
- FEDERLE, M. J. & BASSLER, B. L. 2003. Interspecies communication in bacteria. *Journal of Clinical Investigation*, 112, 1291-1299.
- FELGENTREFF, K., BEISSWENGER, C., GRIESE, M., GULDER, T., BRINGMANN, G. & BALS, R. 2006. The antimicrobial peptide cathelicidin interacts with airway mucus. *Peptides*, 27, 3100-3106.
- FENG, W., GARRETT, H., SPEERT, D. P. & KING, M. 1998. Improved clearability of cystic fibrosis sputum with dextran treatment *in vitro*. *American Journal of Respiratory and Critical Care Medicine*, 157, 710-714.
- FENG, W., NAKAMURA, S., SUDO, E., LEE, M. M., SHAO, A. & KING, M. 1999. Effects of dextran on tracheal mucociliary velocity in dogs *in vivo*. *Pulmonary Pharmacology & Therapeutics*, 12, 35-41.
- FERGUSON, E. L. & DUNCAN, R. 2009. Dextrin-Phospholipase A2: Synthesis and Evaluation as a Bioresponsive Anticancer Conjugate. *Biomacromolecules*, 10, 1358-1364.
- FERGUSON, E. L., RICHARDSON, S. C. W. & DUNCAN, R. 2010. Studies on the mechanism of action of dextrin-phospholipase A(2) and its suitability for use in combination therapy. *Molecular Pharmaceutics*, 7, 510-521.
- FERRARI, S. 1997. Approaches to gene therapy of cystic fibrosis. *Minerva Biotecnologica*, 9, 242-253.
- FIDEL, P. L., VAZQUEZ, J. A. & SOBEL, J. D. 1999. *Candida glabrata*: Review of epidemiology, pathogenesis, and clinical disease with comparison to *Candida albicans*. *Clinical Microbiology Reviews*, 12, 80-96.

- FISCHER, H. & WIDDICOMBE, J. H. 2006. Mechanisms of acid and base secretion by the airway epithelium. *Journal of Membrane Biology*, 211, 139-150.
- FLEMMING, H.-C., NEU, T. R. & WOZNIAK, D. J. 2007. The EPS matrix: The "House of Biofilm cells". *Journal of Bacteriology*, 189, 7945-7947.
- FOGG, F. J. J., HUTTON, D. A., JUMEL, K., PEARSON, J. P., HARDING, S. E. & ALLEN, A. 1996. Characterization of pig colonic mucins. *Biochemical Journal*, 316, 937-942.
- FOLADORI, P., QUARANTA, A. & ZIGLIO, G. 2008. Use of silica microspheres having refractive index similar to bacteria for conversion of flow cytometric forward light scatter into biovolume. *Water Research*, 42, 3757-3766.
- FRANCEZ-CHARLOT, A., CASTANIE-CORNET, M. P., GUTIERREZ, C. & CAM, K. 2005. Osmotic regulation of the *Escherichia coli* bdm (biofilm-dependent modulation) gene by the RcsCDB His-Asp phosphorelay. *Journal of Bacteriology*, 187, 3873-3877.
- FRANCOLINI, I., NORRIS, P., PIOZZI, A., DONELLI, G. & STOODLEY, P. 2004. Usnic acid, a natural antimicrobial agent able to inhibit bacterial biofilm formation on polymer surfaces. *Antimicrobial Agents and Chemotherapy*, 48, 4360-4365.
- FRATESI, S. E., LYNCH, F. L., KIRKLAND, B. L. & BROWN, L. R. 2004. Effects of SEM preparation techniques on the appearance of bacteria and biofilms in the carter sandstone. *Journal of Sedimentary Research*, 74, 858-867.
- FREIFELDER, D. 1982. *Physical Biochemistry*, New York, W. H. Freeman and Co.
- FUCHS, H. J., BOROWITZ, D. S., CHRISTIANSEN, D. H., MORRIS, E. M., NASH, M. L., RAMSEY, B. W., ROSENSTEIN, B. J., SMITH, A. L. & WOHL, M. E. 1994. Effect of aerosolized recombinant human DNase on exacerbations of respiratory symptoms and on pulmonary function in patients with cystic fibrosis. *New England Journal of Medicine*, 331, 637-642.
- FUKUDA, T., HASEGAWA, Y., SAKABE, Y., TOMODA, H. & OMURA, S. 2008. Citrinamides, new potentiators of antifungal miconazole activity, produced by *Penicillium* sp FKI-1938. *Journal of Antibiotics*, 61, 550-555.
- FUKUYAMA, Y., YOSHIDA, S., YANAGISAWA, S. & SHIMIZU, M. 1999. A study on the differences between oral squamous cell carcinomas and normal oral mucosas measured by Fourier transform infrared spectroscopy. *Biospectroscopy*, 5, 117-126.
- FUNG, C., NAUGHTON, S., TURNBULL, L., TINGPEJ, P., ROSE, B., ARTHUR, J., HU, H., HARMER, C., HARBOUR, C., HASSETT, D. J., WHITCHURCH, C. B. & MANOS, J. 2010. Gene expression of *Pseudomonas aeruginosa* in a mucin-containing synthetic growth medium mimicking cystic fibrosis lung sputum. *Journal of Medical Microbiology*, 59, 1089-1100.
- FUONGFUCHAT, A., JAMIESON, A. M., BLACKWELL, J. & GERKEN, T. A. 1996. Rheological studies of the interaction of mucins with alginate and polyacrylate. *Carbohydrate Research*, 284, 85-99.
- GALINDO, E., PENA, C., NUNEZ, C., SEGURA, D. & ESPIN, G. 2007. Molecular and bioengineering strategies to improve alginate and polyhydroxyalkanoate production by *Azotobacter vinelandii*. *Microbial Cell Factories*, 6.
- GAMMELSRUD, K. W., SANDVEN, P., HØIBY, E. A., SANDVIK, L., BRANDTZAEG, P. & GAUSTAD, P. 2011. Colonization by *Candida* in

- children with cancer, children with cystic fibrosis, and healthy controls. *Clinical Microbiology and Infection*, 17, 1875-1881.
- GARRETT, T. R., BHAKOO, M. & ZHANG, Z. 2008. Bacterial adhesion and biofilms on surfaces. *Progress in Natural Science-Materials International*, 18, 1049-1056.
- GEORGE, P. M., BANYA, W., PAREEK, N., BILTON, D., CULLINAN, P., HODSON, M. E. & SIMMONDS, N. J. 2011. Improved survival at low lung function in cystic fibrosis: cohort study from 1990 to 2007. *British Medical Journal*, 342, 342: d1008.
- GHOSH, M., SONG, X. Y., MOUNEIMNE, G., SIDANI, M., LAWRENCE, D. S. & CONDEELIS, J. S. 2004. Cofilin promotes actin polymerization and defines the direction of cell motility. *Science*, 304, 743-746.
- GIANNOLA, L. I., DE CARO, V., GIANDALIA, G., SIRAGUSA, M. G., CAMPISI, G., FLORENA, A. M. & CIACH, T. 2007. Diffusion of naltrexone across reconstituted human oral epithelium and histomorphological features. *European Journal of Pharmaceutics and Biopharmaceutics*, 65, 238-246.
- GIBSON, R. L., BURNS, J. L. & RAMSEY, B. W. 2003. Pathophysiology and management of pulmonary infections in cystic fibrosis. *American Journal of Respiratory and Critical Care Medicine*, 168, 918-951.
- GILLJAM, H., ELLIN, A. & STRANDVIK, B. 1989. Increased bronchial chloride concentration in cystic fibrosis. *Scandinavian Journal of Clinical & Laboratory Investigation*, 49, 121-124.
- GIMMESTAD, M., SLETTA, H., ERTESVAG, H., BAKKEVIG, K., JAIN, S., SUH, S., SKJAK-BRAEK, G., ELLINGSEN, T. E., OHMAN, D. E. & VALLA, S. 2003. The *Pseudomonas fluorescens* AlgG protein, but not its mannuronan C-5-epimerase activity, is needed for alginate polymer formation. *Journal of Bacteriology*, 185, 3515-3523.
- GIORDANI, R., REGLI, P., KALOUSTIAN, J., MIKAIL, C., ABOU, L. & PORTUGAL, H. 2004. Antifungal effect of various essential oils against *Candida albicans*. Potentiation of antifungal action of amphotericin B by essential oil from *Thymus vulgaris*. *Phytotherapy Research*, 18, 990-995.
- GIORDANI, R., REGLI, P., KALOUSTIAN, J. & PORTUGAL, H. 2006. Potentiation of antifungal activity of amphotericin B by essential oil from *Cinnamomum cassia*. *Phytotherapy Research*, 20, 58-61.
- GOMPERTS, B., LANTELME, F. & STOCK, R. 1970. Ion association reactions with biological membranes, studied with fluorescent dye 1-anilino-8-naphthalensulfonate. *Journal of Membrane Biology*, 3, 241-266.
- GOVAN, J. R. W. & DERETIC, V. 1996. Microbial pathogenesis in cystic fibrosis: Mucoid *Pseudomonas aeruginosa* and *Burkholderia cepacia*. *Microbiological Reviews*, 60, 539-574.
- GREENWOOD, D., SLACK, R., PEUTHERER, J. & BARER, M. 2007. *Medical Microbiology*, Elsevier Limited.
- GROSS, M., CRAMTON, S. E., GOTZ, F. & PESCHEL, A. 2001. Key role of teichoic acid net charge in *Staphylococcus aureus* colonization of artificial surfaces. *Infection and Immunity*, 69, 3423-3426.
- GROUX-DEGROOTE, S., KRZEWINSKI-RECCHI, M.-A., CAZET, A., VINCENT, A., LEHOUX, S., LAFITTE, J.-J., VAN SEUNINGEN, I. & DELANNOY, P. 2008. IL-6 and IL-8 increase the expression of

- glycosyltransferases and sulfotransferases involved in the biosynthesis of sialylated and/or sulfated Lewis(x) epitopes in the human bronchial mucosa. *Biochemical Journal*, 410, 213-223.
- GUIOT, E., GEORGES, P., BRUN, A., FONTAINE-AUPART, M. P., BELLON-FONTAINE, M. N. & BRIANDET, R. 2002. Heterogeneity of diffusion inside microbial biofilms determined by fluorescence correlation spectroscopy under two-photon excitation. *Photochemistry and Photobiology*, 75, 570-578.
- HALEY, C. L., COLMER-HAMOOD, J. A. & HAMOOD, A. N. 2012. Characterization of biofilm-like structures formed by *Pseudomonas aeruginosa* in a synthetic mucus medium. *Bmc Microbiology*, 12, 2-20.
- HALL-STOODLEY, L. & STOODLEY, P. 2002. Developmental regulation of microbial biofilms. *Current Opinion in Biotechnology*, 13, 228-233.
- HANCOCK, R. E. W. & SAHL, H.-G. 2006. Antimicrobial and host-defense peptides as new anti-infective therapeutic strategies. *Nature Biotechnology*, 24, 1551-1557.
- HANCOCK, R. E. W., SIEHNEL, R. & MARTIN, N. 1990. Outer membrane proteins of *Pseudomonas*. *Molecular Microbiology*, 4, 1069-1075.
- HANLON, G. W., DENYER, S. P., OLLIFF, C. J. & IBRAHIM, L. J. 2001. Reduction in exopolysaccharide viscosity as an aid to bacteriophage penetration through *Pseudomonas aeruginosa* biofilms. *Applied and Environmental Microbiology*, 67, 2746-2753.
- HARRIS, M. R. & COOTE, P. J. 2010. Combination of caspofungin or anidulafungin with antimicrobial peptides results in potent synergistic killing of *Candida albicans* and *Candida glabrata* *in vitro*. *International Journal of Antimicrobial Agents*, 35, 347-356.
- HARSHEY, R. M. 1994. Bees aren't the only ones- swarming in Gram-negative bacteria. *Molecular Microbiology*, 13, 389-394.
- HARTMANN, M., DENTINI, M., DRAGET, K. I. & SKJAK-BRAEK, G. 2006. Enzymatic modification of alginates with the mannuronan C-5 epimerase AlgE4 enhances their solubility at low pH. *Carbohydrate Polymers*, 63, 257-262.
- HASSETT, D. J., KORFHAGEN, T. R., IRVIN, R. T., SCHURR, M. J., SAUER, K., LAU, G. W., SUTTON, M. D., YU, H. & HØIBY, N. 2010. *Pseudomonas aeruginosa* biofilm infections in cystic fibrosis: insights into pathogenic processes and treatment strategies. *Expert Opinion on Therapeutic Targets*, 14, 117-130.
- HAWARD, S. J., ODELL, J. A., BERRY, M. & HALL, T. 2011. Extensional rheology of human saliva. *Rheologica Acta*, 50, 869-879.
- HELGERSON, S. L. & CRAMER, W. A. 1977. Changes in *Escherichia coli* cell envelope structure and sites of fluorescence probe binding caused by carbonyl cyanide para-trifluoromethoxyphenylhydrazone. *Biochemistry*, 16, 4109-4117.
- HENKE, M. O., JOHN, G., GERMAN, M., LINDEMANN, H. & RUBIN, B. K. 2007. MUC5AC and MUC5B Mucins increase in cystic fibrosis airway secretions during pulmonary exacerbation. *American Journal of Respiratory and Critical Care Medicine*, 175, 816-821.

- HENKE, M. O., JOHN, G., RHEINECK, C., CHILLAPPAGARI, S., NAEHRLICH, L. & RUBIN, B. K. 2011. Serine proteases degrade airway mucins in cystic fibrosis. *Infection and Immunity*, 79, 3438-3444.
- HENKE, M. O. & RATJEN, F. 2007. Mucolytics in cystic fibrosis. *Paediatric Respiratory Reviews*, 8, 24-29.
- HENKE, M. O., RENNER, A., HUBER, R. M., SEEDS, M. C. & RUBIN, B. K. 2004. MUC5AC and MUC5B Mucins are decreased in cystic fibrosis airway secretions. *American Journal of Respiratory Cell and Molecular Biology*, 31, 86-91.
- HERMANSSON, M. 1999. The DLVO theory in microbial adhesion. *Colloids and Surfaces B: Biointerfaces*, 14, 105-119.
- HOFFER-SCHAEFER, A., ROZYCKI, H. J., YOPP, M. A. & RUBIN, B. K. 2014. Guaifenesin has no effect on sputum volume or sputum properties in adolescents and adults with acute respiratory tract infections. *Respiratory care*, 59, 631-6.
- HØIBY, N., CIOFU, O. & BJARNSHOLT, T. 2010. *Pseudomonas aeruginosa* biofilms in cystic fibrosis. *Future Microbiology*, 5, 1663-1674.
- HOLCOMBE, L. J., MCALESTER, G., MUNRO, C. A., ENJALBERT, B., BROWN, A. J. P., GOW, N. A. R., DING, C., BUTLER, G., O'GARA, F. & MORRISSEY, J. P. 2010. *Pseudomonas aeruginosa* secreted factors impair biofilm development in *Candida albicans*. *Microbiology*, 156, 1476-1486.
- HOLLENBECK, P. J. 1993. Products of endocytosis and autophagy are retrieved from axons by regulated retrograde organelle transport. *Journal of Cell Biology*, 121, 305-315.
- HONG, Z. N., CHASAN, B., BANSIL, R., TURNER, B. S., BHASKAR, K. R. & AFDHAL, N. H. 2005. Atomic force microscopy reveals aggregation of gastric mucin at low pH. *Biomacromolecules*, 6, 3458-3466.
- HOPE, C. K. & WILSON, M. 2004. Analysis of the effects of chlorhexidine on oral biofilm vitality and structure based on viability profiling and an indicator of membrane integrity. *Antimicrobial Agents and Chemotherapy*, 48, 1461-1468.
- HORSLEY, A., ROUSSEAU, K., RIDLEY, C., FLIGHT, W., JONES, A., WAIGH, T. A. & THORNTON, D. J. 2014. Reassessment of the importance of mucins in determining sputum properties in cystic fibrosis. *Journal of Cystic Fibrosis*, 13, 260-266.
- HORSLEY, A. R., DAVIES, J. C., GRAY, R. D., MACLEOD, K. A., DONOVAN, J., AZIZ, Z. A., BELL, N. J., RAINER, M., MT-ISA, S., VOASE, N., DEWAR, M. H., SAUNDERS, C., GIBSON, J. S., PARRA-LEITON, J., LARSEN, M. D., JESWIET, S., SOUSSI, S., BAKAR, Y., MEISTER, M. G., TYLER, P., DOHERTY, A., HANSELL, D. M., ASHBY, D., HYDE, S. C., GILL, D. R., GREENING, A. P., PORTEOUS, D. J., INNES, J. A., BOYD, A. C., GRIESENBACH, U., CUNNINGHAM, S. & ALTON, E. 2013. Changes in physiological, functional and structural markers of cystic fibrosis lung disease with treatment of a pulmonary exacerbation. *Thorax*, 68, 532-539.
- HORST, A. M., NEAL, A. C., MIELKE, R. E., SISLIAN, P. R., SUH, W. H., MADLER, L., STUCKY, G. D. & HOLDEN, P. A. 2010. Dispersion of TiO₂ Nanoparticle Agglomerates by *Pseudomonas aeruginosa*. *Applied and Environmental Microbiology*, 76, 7292-7298.

- HOUNSELL, E. F. 1994. Physicochemical analyses of oligosaccharide determinants of glycoproteins. *Advances in Carbohydrate Chemistry and Biochemistry*, Vol 50, 50, 311-350.
- HUGHES, L. D., RAWLE, R. J. & BOXER, S. G. 2014. Choose your label wisely: Water-soluble fluorophores often interact with lipid bilayers. *Plos One*, 9(2): e87649. doi: 10.1371/journal.pone.0087649.
- HURDLE, J. G., O'NEILL, A. J., CHOPRA, I. & LEE, R. E. 2011. Targeting bacterial membrane function: an underexploited mechanism for treating persistent infections. *Nature Reviews Microbiology*, 9, 62-75.
- HWANG, G., KANG, S., EI-DIN, M. G. & LIU, Y. 2012. Impact of conditioning films on the initial adhesion of *Burkholderia cepacia*. *Colloids and Surfaces B: Biointerfaces*, 91, 181-188.
- JACOBSEN, J., NIELSEN, E. B., BRONDUM-NIELSEN, K., CHRISTENSEN, M. E., OLIN, H. B. D., TOMMERUP, N. & RASSING, M. R. 1999. Filter-grown TR146 cells as an *in vitro* model of human buccal epithelial permeability. *European Journal of Oral Sciences*, 107, 138-146.
- JANA, S. & DEB, J. K. 2006. Molecular understanding of aminoglycoside action and resistance. *Applied Microbiology and Biotechnology*, 70, 140-150.
- JAYARAMAN, S., SONG, Y. L., VETRIVEL, L., SHANKAR, L. & VERKMAN, A. S. 2001. Noninvasive *in vivo* fluorescence measurement of airway-surface liquid depth, salt concentration, and pH. *Journal of Clinical Investigation*, 107, 317-324.
- JAYATILAKE, J., SAMARANAYAKE, Y. H. & SAMARANAYAKE, L. P. 2005. An ultrastructural and a cytochemical study of candidal invasion of reconstituted human oral epithelium. *Journal of Oral Pathology & Medicine*, 34, 240-246.
- JENKINS, A. T. A., BUCKLING, A., MCGHEE, M. & FFRENCH-CONSTANT, R. H. 2005. Surface plasmon resonance shows that type IV pili are important in surface attachment by *Pseudomonas aeruginosa*. *Journal of the Royal Society Interface*, 2, 255-259.
- JESAITIS, A. J., FRANKLIN, M. J., BERGLUND, D., SASAKI, M., LORD, C. I., BLEAZARD, J. B., DUFFY, J. E., BEYENAL, H. & LEWANDOWSKI, Z. 2003. Compromised host defense on *Pseudomonas aeruginosa* biofilms: Characterization of neutrophil and biofilm interactions. *Journal of Immunology*, 171, 4329-4339.
- JIANG, P., LI, J., HAN, F., DUAN, G., LU, X., GU, Y. & YU, W. 2011. Antibiofilm activity of an exopolysaccharide from marine *Bacterium vibrio* sp QY101. *Plos One*, 6(4): e18514. doi: 10.1371/journal.pone.0018514.
- JOHANSEN, C., GILL, T. & GRAM, L. 1996. Changes in cell morphology of *Listeria monocytogenes* and *Shewanella putrefaciens* resulting from the action of protamine. *Applied and Environmental Microbiology*, 62, 1058-1064.
- JOHNSON, A. R., HAUSNER, M., SCHNELL, A. & WUERTZ, S. 2000. Evaluation of fluorescently labeled lectins for noninvasive localization of extracellular polymeric substances in *Sphingomonas* biofilms. *Applied and Environmental Microbiology*, 66, 3487-3491.
- JONCKHEERE, N. & VAN SEUNINGEN, I. 2008. The membrane-bound mucins: How large O-glycoproteins play key roles in epithelial cancers and hold

- promise as biological tools for gene-based and immunotherapies. *Critical Reviews in Oncogenesis*, 14, 177-196.
- JONES, A. P. & WALLIS, C. 2010. Dornase alfa for cystic fibrosis. *Cochrane Database of Systematic Reviews*, 1-66.
- JORIS, L., DAB, I. & QUINTON, P. M. 1993. Elemental composition of human airway surface fluid in healthy and diseased airways. *American Review of Respiratory Disease*, 148, 1633-1637.
- KACURAKOVA, M. & MATHLOUTHI, M. 1996. FTIR and laser-Raman spectra of oligosaccharides in water: Characterization of the glycosidic bond. *Carbohydrate Research*, 284, 145-157.
- KAGNOFF, M. F. & ECKMANN, L. 1997. Epithelial cells as sensors for microbial infection. *Journal of Clinical Investigation*, 100, 6-10.
- KALKANCI, A., DIZBAY, M., SARI, N., YALCIN, B., FIDAN, I., ARMAN, D. & KUSTIMUR, S. 2010. Fluconazole, caspofungin, voriconazole in combination with amphotericin B. *Central European Journal of Medicine*, 5, 194-197.
- KAMYSZ, W., NADOLSKI, P., KEDZIA, A., CIRIONI, O., BARCHIESI, F., GIACOMETTI, A., SCALISE, G., LUKASIAK, J. & OKROJ, M. 2006. *In vitro* activity of synthetic antimicrobial peptides against *Candida*. *Polish Journal of Microbiology*, 55, 303-307.
- KASAS, S., FELLAY, B. & CARGNELLO, R. 1994. Observation of the action of penicillin on *Bacillus subtilis* using atomic force microscopy- technique for the preparation of bacteria. *Surface and Interface Analysis*, 21, 400-401.
- KATER, A., HENKE, M. O. & RUBIN, B. K. 2007. The role of DNA and actin polymers on the polymer structure and rheology of cystic fibrosis sputum and depolymerization by gelsolin or thymosin beta 4. In: GOLDSTEIN, A. L. & GARACI, E. (eds.) *Thymosins in Health and Disease: First International Symposium*.
- KAVITA, K., SINGH, V. K., MISHRA, A. & JHA, B. 2014. Characterisation and anti-biofilm activity of extracellular polymeric substances from *Oceanobacillus iheyensis*. *Carbohydrate Polymers*, 101, 29-35.
- KHAJEHPUR, M., DASHNAU, J. L. & VANDERKOOI, J. M. 2006. Infrared spectroscopy used to evaluate glycosylation of proteins. *Analytical Biochemistry*, 348, 40-48.
- KHAN, S., TONDERVIK, A., SLETTA, H., KLINKENBERG, G., EMANUEL, C., ONSOYEN, E., MYRVOLD, R., HOWE, R. A., WALSH, T. R., HILL, K. E. & THOMAS, D. W. 2012. Overcoming drug resistance with alginate oligosaccharides able to potentiate the action of selected antibiotics. *Antimicrobial Agents and Chemotherapy*, 56, 5134-5141.
- KIM, J. S., HACKLEY, G. H., OKAMOTO, K. & RUBIN, B. K. 2001. Sputum processing for evaluation of inflammatory mediators. *Pediatric Pulmonology*, 32, 152-158.
- KIM, J. S., OKAMOTO, K. & RUBIN, B. K. 2006. Pulmonary function is negatively correlated with sputum inflammatory markers and cough clearability in subjects with cystic fibrosis but not those with chronic bronchitis. *Chest*, 129, 1148-1154.
- KIM, W., KILLAM, T., SOOD, V. & SURETTE, M. G. 2003. Swarm-cell differentiation in *Salmonella enterica* serovar typhimurium results in elevated resistance to multiple antibiotics. *Journal of Bacteriology*, 185, 3111-3117.

- KING, M. 1980. Relationship between mucus viscoelasticity and ciliary transport in guaran gel-frog palate model system. *Biorheology*, 17, 249-254.
- KING, M. 1987. The role of mucus viscoelasticity in cough clearance. *Biorheology*, 24, 589-597.
- KING, M. 1998. Experimental models for studying mucociliary clearance. *European Respiratory Journal*, 11, 222-228.
- KING, M. 2005. *Mucus and its role in airway clearance and cytoprotection*, Hamilton, Ontario, Canada, BC Decker.
- KING, M., BROCK, G. & LUNDELL, C. 1985. Clearance of mucus by stimulated cough. *Journal of Applied Physiology*, 58, 1776-1782.
- KING, M., DASGUPTA, B., TOMKIEWICZ, R. P. & BROWN, N. E. 1997. Rheology of cystic fibrosis sputum after *in vitro* treatment with hypertonic saline alone and in combination with recombinant human deoxyribonuclease I. *American Journal of Respiratory and Critical Care Medicine*, 156, 173-177.
- KING, M. & RUBIN, B. K. 2002. Pharmacological approaches to discovery and development of new mucolytic agents. *Advanced Drug Delivery Reviews*, 54, 1475-1490.
- KING, M., ZAHM, J. M., PIERROT, D., VAQUEZGIROD, S. & PUCHELLE, E. 1989. The role of mucus gel viscosity, spinnability, and adhesive properties in clearance by stimulated cough. *Biorheology*, 26, 737-745.
- KIPNIS, E., SAWA, T. & WIENER-KRONISH, J. 2006. Targeting mechanisms of *Pseudomonas aeruginosa* pathogenesis. *Medecine Et Maladies Infectieuses*, 36, 78-91.
- KIRCHNER, S., FOTHERGILL, J. L., WRIGHT, E. A., JAMES, C. E., MOWAT, E. & WINSTANLEY, C. 2012. Use of artificial sputum medium to test antibiotic efficacy against *Pseudomonas aeruginosa* in conditions more relevant to the cystic fibrosis lung. *Journal of visualized experiments*, e3857-e3857.
- KIRKHAM, S., KOLSUM, U., ROUSSEAU, K., SINGH, D., VESTBO, J. & THORNTON, D. 2008. MUC5B Is the Major Mucin in the Gel Phase of Sputum in Chronic Obstructive Pulmonary Disease. *American Journal of Respiratory and Critical Care Medicine*, 178, 1033-1039.
- KLEMETSrud, T., JONASSEN, H., HIORTH, M., KJONIKSEN, A.-L. & SMISTAD, G. 2013. Studies on pectin-coated liposomes and their interaction with mucin. *Colloids and Surfaces B: Biointerfaces*, 103, 158-165.
- KLIS, F. M., MOL, P., HELLINGWERF, K. & BRUL, S. 2002. Dynamics of cell wall structure in *Saccharomyces cerevisiae*. *Fems Microbiology Reviews*, 26, 239-256.
- KLODZINSKA, E., SZUMSKI, M., DZIUBAKIEWICZ, E., HRYNKIEWICZ, K., SKWAREK, E., JANUSZ, W. & BUSZEWSKI, B. 2010. Effect of zeta potential value on bacterial behavior during electrophoretic separation. *Electrophoresis*, 31, 1590-1596.
- KNOWLES, M. R. & DURIE, P. R. 2002. What is cystic fibrosis? *New England Journal of Medicine*, 347, 439-442.
- KOCEVARNARED, J., KRISTL, J. & SMIDKORBAR, J. 1997. Comparative rheological investigation of crude gastric mucin and natural gastric mucus. *Biomaterials*, 18, 677-681.

- KOHRI, K., UEKI, I. F., SHIM, J. J., BURGEL, P. R., OH, Y. M., TAM, D. C., DAO-PICK, T. & NADEL, J. A. 2002. *Pseudomonas aeruginosa* induces MUC5AC production via epidermal growth factor receptor. *European Respiratory Journal*, 20, 1263-1270.
- KONSTAN, M. W. 2008. Dornase alfa and progression of lung disease in cystic fibrosis. *Pediatric Pulmonology*, 43, S24-S28.
- KONSTAN, M. W. & RATJEN, F. 2012. Effect of dornase alfa on inflammation and lung function: Potential role in the early treatment of cystic fibrosis. *Journal of Cystic Fibrosis*, 11, 78-83.
- KOZLOVA, I., VANTHANOUVONG, V., JOHANNESSON, M. & ROOMANS, G. M. 2006. Composition of airway surface liquid determined by x-ray microanalysis. *Upsala Journal of Medical Sciences*, 111, 137-153.
- LAGORCE, A., LE BERRE-ANTON, V., AGUILAR-USCANGA, B., MARTIN-YKEN, H., DAGKESSAMANSKAIA, A. & FRANCOIS, J. 2002. Involvement of GFA1, which encodes glutamine-fructose-6-phosphate amidotransferase, in the activation of the chitin synthesis pathway in response to cell-wall defects in *Saccharomyces cerevisiae*. *European Journal of Biochemistry*, 269, 1697-1707.
- LAI, S. K., WANG, Y.-Y. & HANES, J. 2009a. Mucus-penetrating nanoparticles for drug and gene delivery to mucosal tissues. *Advanced Drug Delivery Reviews*, 61, 158-171.
- LAI, S. K., WANG, Y. Y., WIRTZ, D. & HANES, J. 2009b. Micro- and macrorheology of mucus. *Advanced Drug Delivery Reviews*, 61, 86-100.
- LAM, J., CHAN, R., LAM, K. & COSTERTON, J. W. 1980. Production of mucoid micro-colonies by *Pseudomonas aeruginosa* within infected lungs in cystic fibrosis. *Infection and Immunity*, 28, 546-556.
- LAMBIASE, A., RAI, V., DEL PEZZO, M., SEPE, A., CARNOVALE, V. & ROSSANO, F. 2006. Microbiology of airway disease in a cohort of patients with Cystic Fibrosis. *BMC Infectious Diseases*, 6.
- LAMBLIN, G., DEGROOTE, S., PERINI, J. M., DELMOTTE, P., SCHARFMAN, A. E., DAVRIL, M., LO-GUIDICE, J. M., HOUDRET, N., DUMUR, V., KLEIN, A. & ROUSSEL, P. 2001. Human airway mucin glycosylation: A combinatorial of carbohydrate determinants which vary in cystic fibrosis. *Glycoconjugate Journal*, 18, 661-684.
- LANDRY, R. M., AN, D. D., HUPP, J. T., SINGH, P. K. & PARSEK, M. R. 2006. Mucin-*Pseudomonas aeruginosa* interactions promote biofilm formation and antibiotic resistance. *Molecular Microbiology*, 59, 142-151.
- LASS-FLOERL, C. 2009. The changing face of epidemiology of invasive fungal disease in Europe. *Mycoses*, 52, 197-205.
- LATTNER, D., FLEMMING, H. C. & MAYER, C. 2003. (13)C-NMR study of the interaction of bacterial alginate with bivalent cations. *International Journal of Biological Macromolecules*, 33, 81-88.
- LEE, S., MULLER, M., REZWAN, K. & SPENCER, N. D. 2005. Porcine gastric mucin (PGM) at the water/poly(dimethylsiloxane) (PDMS) interface: Influence of pH and ionic strength on its conformation, adsorption, and aqueous lubrication properties. *Langmuir*, 21, 8344-8353.
- LETHEM, M. I., JAMES, S. L., MARRIOTT, C. & BURKE, J. F. 1990. The origin of DNA associated with mucus glycoproteins in cystic fibrosis sputum. *European Respiratory Journal*, 3, 19-23.

- LEWIS, A. T., JONES, K., LEWIS, K. E., JONES, S. & LEWIS, P. D. 2013a. Detection of Lewis antigen structural change by FTIR spectroscopy. *Carbohydrate Polymers*, 92, 1294-1301.
- LEWIS, K. 2010. Persister Cells. In: GOTTESMAN, S. & HARWOOD, C. S. (eds.) *Annual Review of Microbiology*.
- LEWIS, P. D., LEWIS, K. E., GHOSAL, R., BAYLISS, S., LLOYD, A. J., WILLS, J., GODFREY, R., KLOER, P. & MUR, L. A. J. 2010. Evaluation of FTIR Spectroscopy as a diagnostic tool for lung cancer using sputum. *Bmc Cancer*, doi: 10.1186/1471-2407-10-640
- LEWIS, R. E. 2011. Current Concepts in Antifungal Pharmacology. *Mayo Clinic Proceedings*, 86, 805-817.
- LEWIS, S. P., LEWIS, A. T. & LEWIS, P. D. 2013b. Prediction of glycoprotein secondary structure using ATR-FTIR. *Vibrational Spectroscopy*, 69, 21-29.
- LI, A., LEE, P. Y., HO, B., DING, J. L. & LIM, C. T. 2007. Atomic force microscopy study of the antimicrobial action of Sushi peptides on Gram negative bacteria. *Biochimica Et Biophysica Acta-Biomembranes*, 1768, 411-418.
- LI, F., YU, J., YANG, H., WAN, Z. & BAI, D. 2008. Effects of ambroxol on alginate of mature *Pseudomonas aeruginosa* biofilms. *Current Microbiology*, 57, 1-7.
- LIN, M. Y., CARMELI, Y., ZUMSTEG, J., FLORES, E. L., TOLENTINO, J., SREERAMOJU, P. & WEBER, S. G. 2005. Prior antimicrobial therapy and risk for hospital-acquired *Candida glabrata* and *Candida krusei* fungemia: a case-case-control study. *Antimicrobial Agents and Chemotherapy*, 49, 4555-4560.
- LINDEN, S. K., SUTTON, P., KARLSSON, N. G., KOROLIK, V. & MCGUCKIN, M. A. 2008. Mucins in the mucosal barrier to infection. *Mucosal Immunology*, 1, 183-197.
- LINNES, J. C., MA, H. & BRYERS, J. D. 2013. Giant Extracellular Matrix Binding Protein Expression in *Staphylococcus epidermidis* is Regulated by Biofilm Formation and Osmotic Pressure. *Current Microbiology*, 66, 627-633.
- LIPIEC, E., KOWALSKA, J., LEKKI, J., WIECHEC, A. & KWIATEK, W. M. 2012. FTIR microspectroscopy in studies of DNA damage induced by proton microbeam in single PC-3 cells. *Acta Physica Polonica A*, 121, 506-509.
- LIVRAGHI-BUTRICO, A., KELLY, E. J., KLEM, E. R., DANG, H., WOLFGANG, M. C., BOUCHER, R. C., RANDELL, S. H. & O'NEAL, W. K. 2012. Mucus clearance, MyD88-dependent and MyD88-independent immunity modulate lung susceptibility to spontaneous bacterial infection and inflammation. *Mucosal Immunology*, 5, 397-408.
- LOH, B., GRANT, C. & HANCOCK, R. E. W. 1984. Use of fluorescent probe 1-N-phenyl-naphthylamine to study the interactions of aminoglycoside antibiotics with the outer membrane of *Pseudomonas aeruginosa*. *Antimicrobial Agents and Chemotherapy*, 26, 546-551.
- LOISELLE, M. & ANDERSON, K. W. 2003. The use of cellulase in inhibiting biofilm formation from organisms commonly found on medical implants. *Biofouling*, 19, 77-85.
- LOWMAN, D. W., ENSLEY, H. E., GREENE, R. R., KNAGGE, K. J., WILLIAMS, D. L. & KRUPPA, M. D. 2011. Mannan structural complexity

- is decreased when *Candida albicans* is cultivated in blood or serum at physiological temperature. *Carbohydrate Research*, 346, 2752-2759.
- LUCA, V., STRINGARO, A., COLONE, M., PINI, A. & MANGONI, M. L. 2013. Esculentin(1-21), an amphibian skin membrane-active peptide with potent activity on both planktonic and biofilm cells of the bacterial pathogen *Pseudomonas aeruginosa*. *Cellular and Molecular Life Sciences*, 70, 2773-2786.
- LUIS MARTINEZ, J., FAJARDO, A., GARMENDIA, L., HERNANDEZ, A., FRANCISCO LINARES, J., MARTINEZ-SOLANO, L. & BLANCA SANCHEZ, M. 2009. A global view of antibiotic resistance. *Fems Microbiology Reviews*, 33, 44-65.
- LYCZAK, J. B., CANNON, C. L. & PIER, G. B. 2000. Establishment of *Pseudomonas aeruginosa* infection: lessons from a versatile opportunist. *Microbes and Infection*, 2, 1051-1060.
- MADEIRA, V. M. & ANTUNESM-MADEIRA, M. C. 1973. Interaction of Ca^{2+} and Mg^{2+} with synaptic plasma membranes. *Biochimica Et Biophysica Acta*, 323, 396-407.
- MAH, T. F., PITTS, B., PELLOCK, B., WALKER, G. C., STEWART, P. S. & O'TOOLE, G. A. 2003. A genetic basis for *Pseudomonas aeruginosa* biofilm antibiotic resistance. *Nature*, 426, 306-310.
- MAH, T. F. C. & O'TOOLE, G. A. 2001. Mechanisms of biofilm resistance to antimicrobial agents. *Trends in Microbiology*, 9, 34-39.
- MAKIN, S. A. & BEVERIDGE, T. J. 1996. The influence of A-band and B-band lipopolysaccharide on the surface characteristics and adhesion of *Pseudomonas aeruginosa* to surfaces. *Microbiology*, 142, 299-307.
- MALEKI, A., LAFITTE, G., KJONIKSEN, A.-L., THURESSON, K. & NYSTROM, B. 2008. Effect of pH on the association behavior in aqueous solutions of pig gastric mucin. *Carbohydrate Research*, 343, 328-340.
- MALIC, S., HILL, K. E., RALPHS, J. R., HAYES, A., THOMAS, D. W., POTTS, A. J. & WILLIAMS, D. W. 2007. Characterization of *Candida albicans* infection of an *in vitro* oral epithelial model using confocal laser scanning microscopy. *Oral Microbiology and Immunology*, 22, 188-194.
- MALVERN. 2014a. *Application of Dynamic Light Scattering (DLS) to Protein Therapeutic Formulations: Principles, Measurements and Analysis - 1. Basic Principles (Version 12 Whitepaper)* [Online]. Available: <http://www.malvern.com/en/support/resource-center/Whitepapers/WP140207ApplicDLSprotein1.aspx> [Accessed 22/05/2014 2014].
- MALVERN. 2014b. *Application of Dynamic Light Scattering (DLS) to Protein Therapeutic Formulations: Principles, Measurements and Analysis - 2. Concentration Effects and Particle Interactions (Version 8 Whitepaper)* [Online]. Available: <http://www.malvern.com/en/support/resource-center/Whitepapers/WP140207ApplicDLSprotein2.aspx> [Accessed 22/05/2014 2014].
- MANZENREITER, R., KIENBERGER, F., MARCOS, V., SCHILCHER, K., KRAUTGARTNER, W. D., OBERMAYER, A., HUML, M., STOIBER, W., HECTOR, A., GRIESE, M., HANNIG, M., STUDNICKA, M., VITKOV, L. & HART, D. 2012. Ultrastructural characterization of cystic fibrosis sputum

- using atomic force and scanning electron microscopy. *Journal of Cystic Fibrosis*, 11, 84-92.
- MARAGAKIS, L. L., PERENCEVICH, E. N. & COSGROVE, S. E. 2008. Clinical and economic burden of antimicrobial resistance. *Expert Review of Anti-Infective Therapy*, 6, 751-763.
- MARSHALL, K. C., STOUT, R. & MITCHELL, R. 1971. Mechanism of initial events in sorption of marine bacteria to surfaces. *Journal of General Microbiology*, 68, 337-348.
- MAYER, C., MORITZ, R., KIRSCHNER, C., BORCHARD, W., MAIBAUM, R., WINGENDER, J. & FLEMMING, H. C. 1999. The role of intermolecular interactions: studies on model systems for bacterial biofilms. *International Journal of Biological Macromolecules*, 26, 3-16.
- MCMASTER, T. J., BERRY, M., CORFIELD, A. P. & MILES, M. J. 1999. Atomic force microscopy of the submolecular architecture of hydrated ocular mucins. *Biophysical Journal*, 77, 533-541.
- MCSHANE, D., DAVIES, J. C., DAVIES, M. G., BUSH, A., GEDDES, D. M. & ALTON, E. 2003. Airway surface pH in subjects with cystic fibrosis. *European Respiratory Journal*, 21, 37-42.
- MENDICINO, J. & SANGADALA, S. 1999. Synthesis of sulfated oligosaccharides by cystic fibrosis trachea epithelial cells. *Molecular and Cellular Biochemistry*, 201, 141-149.
- MENZIES, G. E., FOX, H. R., MARNANE, C., POPE, L., PRABHU, V., WINTER, S., DERRICK, A. V. & LEWIS, P. D. 2014. Fourier transform infrared for noninvasive optical diagnosis of oral, oropharyngeal, and laryngeal cancer. *Translational Research*, 163, 19-26.
- MILLAR, T. J., PAPAS, E. B., OZKAN, J., JALBERT, I. & BALL, M. 2003. Clinical appearance and microscopic analysis of mucin balls associated with contact lens wear. *Cornea*, 22, 740-745.
- MILLER, M. B. & BASSLER, B. L. 2001. Quorum sensing in bacteria. *Annual Review of Microbiology*, 55, 165-199.
- MINASIAN, C., WALLIS, C., METCALFE, C. & BUSH, A. 2010. Comparison of inhaled mannitol, daily rhDNase and a combination of both in children with cystic fibrosis: a randomised trial. *Thorax*, 65, 51-56.
- MOLLER, C., ALLEN, M., ELINGS, V., ENGEL, A. & MULLER, D. J. 1999. Tapping-mode atomic force microscopy produces faithful high-resolution images of protein surfaces. *Biophysical Journal*, 77, 1150-1158.
- MONROE, D. 2007. Looking for chinks in the armor of bacterial biofilms. *Plos Biology*, 5(11): e307. doi: 10.1371/journal.pone.0050307.
- MOORE, R. A., BATES, N. C. & HANCOCK, R. E. W. 1986. Interaction of polycationic antibiotics with *Pseudomonas aeruginosa* lipopolysaccharide and lipid A studied by using dansyl polymyxin. *Antimicrobial Agents and Chemotherapy*, 29, 496-500.
- MOREAU-MARQUIS, S., STANTON, B. A. & O'TOOLE, G. A. 2008. *Pseudomonas aeruginosa* biofilm formation in the cystic fibrosis airway. *Pulmonary Pharmacology & Therapeutics*, 21, 595-599.
- MORSCHHAUSER, J. 2010. Regulation of multidrug resistance in pathogenic fungi. *Fungal Genetics and Biology*, 47, 94-106.
- MOSSIALOS, E., MOREL, C. M., EDWARDS, S., BERENSON, J., GEMMILL-TOYAMA, M. & BROGAN, D. 2010. *Policies and incentives for promoting*

- innovation in antibiotic research*, The European Observatory on Health Systems and Policies.
- MOTHEY, D., BUTTARO, B. A. & PIGGOT, P. J. 2014. Mucin can enhance growth, biofilm formation, and survival of *Streptococcus mutans*. *Fems Microbiology Letters*, 350, 161-167.
- MULCAHY, L. R., BURNS, J. L., LORY, S. & LEWIS, K. 2010. Emergence of *Pseudomonas aeruginosa* strains producing high levels of persister cells in patients with cystic fibrosis. *Journal of Bacteriology*, 192, 6191-6199.
- MURASCHI, T. F., BOLLES, D. M., MOCZULSKA & LINDSAY, M. 1966. Serologic types of *Pseudomonas aeruginosa* based on heat-stable O antigens—correlation of Habs' (European) and Verder and Evans' (North American) classifications. *Journal of Infectious Diseases*, 116, 84-88.
- MURILLO, L. A., NEWPORT, G., LAN, C. Y., HABELITZ, S., DUNGAN, J. & AGABIAN, N. M. 2005. Genome-wide transcription profiling of the early phase of biofilm formation by *Candida albicans*. *Eukaryotic Cell*, 4, 1562-1573.
- MUTER, O., PATMALNIEKS, A. & RAPOPORT, A. 2001. Interrelations of the yeast *Candida utilis* and Cr(VI): metal reduction and its distribution in the cell and medium. *Process Biochemistry*, 36, 963-970.
- NAGANT, C., FENG, Y., LUCAS, B., BRAECKMANS, K., SAVAGE, P. & DEHAYE, J. P. 2011. Effect of a low concentration of a cationic steroid antibiotic (CSA-13) on the formation of a biofilm by *Pseudomonas aeruginosa*. *Journal of Applied Microbiology*, 111, 763-772.
- NAVARRO, J., RAINISIO, M., HARMS, H. K., HODSON, M. E., KOCH, C., MASTELLA, G., STRANDVIK, B., MCKENZIE, S. G. & INVESTIGATORS EUROPEAN, E. 2001. Factors associated with poor pulmonary function: cross-sectional analysis of data from the ERCF. *European Respiratory Journal*, 18, 298-305.
- NEWPORT, S., AMIN, N. & DOZOR, A. J. 2009. Exhaled breath condensate pH and ammonia in cystic fibrosis and response to treatment of acute pulmonary exacerbations. *Pediatric Pulmonology*, 44, 866-872.
- NIELSEN, H., HVIDT, S., SHELLS, C. A. & JANMEY, P. A. 2004. Elastic contributions dominate the viscoelastic properties of sputum from cystic fibrosis patients. *Biophysical Chemistry*, 112, 193-200.
- NIJLAND, R., HALL, M. J. & BURGESS, J. G. 2010. Dispersal of biofilms by secreted, matrix degrading, bacterial DNase. *Plos One*, 5(12): e15668. doi: 10.1371/journal.pone.0015668.
- NITHYA, C., BEGUM, M. F. & PANDIAN, S. K. 2010. Marine bacterial isolates inhibit biofilm formation and disrupt mature biofilms of *Pseudomonas aeruginosa* PAO1. *Applied Microbiology and Biotechnology*, 88, 341-358.
- NOBILE, C. J., NETT, J. E., ANDES, D. R. & MITCHELL, A. P. 2006. Function of *Candida albicans* adhesin Hwp1 in biofilm formation. *Eukaryotic Cell*, 5, 1604-1610.
- NOBILE, C. J., SOLIS, N., MYERS, C. L., FAY, A. J., DENEALD, J.-S., NANTEL, A., MITCHELL, A. P. & FILLER, S. G. 2008. *Candida albicans* transcription factor Rim101 mediates pathogenic interactions through cell wall functions. *Cellular Microbiology*, 10, 2180-2196.
- NORDGARD, C. T. & DRAGET, K. I. 2011. Oligosaccharides as modulators of rheology in complex mucous systems. *Biomacromolecules*, 12, 3084-3090.

- NORDGARD, C. T., NONSTAD, U., OLDEROY, M. O., ESPEVIK, T. & DRAGET, K. I. 2014. Alterations in mucus barrier function and matrix structure induced by guluronate oligomers. *Biomacromolecules*, 15, 2294-2300.
- NORICE, C. T., SMITH, F. J., JR., SOLIS, N., FILLER, S. G. & MITCHELL, A. P. 2007. Requirement for *Candida albicans* sun41 in biofilm formation and virulence. *Eukaryotic Cell*, 6, 2046-2055.
- NORMARK, B. H. & NORMARK, S. 2002. Evolution and spread of antibiotic resistance. *Journal of Internal Medicine*, 252, 91-106.
- O'MAY, C. Y., SANDERSON, K., RODDAM, L. F., KIROV, S. M. & REID, D. W. 2009. Iron-binding compounds impair *Pseudomonas aeruginosa* biofilm formation, especially under anaerobic conditions. *Journal of Medical Microbiology*, 58, 765-773.
- ODA, D., SAVARD, C. E., ENG, L., SEKIJIMA, J., HAIGH, G. & LEE, S. P. 1998. Reconstituted human oral and esophageal mucosa in culture. *In vitro Cellular & Developmental Biology-Animal*, 34, 46-52.
- ODDS, F. C. 2009. In *Candida albicans*, resistance to flucytosine and terbinafine is linked to MAT locus homozygosity and multilocus sequence typing clade 1. *Fems Yeast Research*, 9, 1091-1101.
- OPARKA, K. J., PRIOR, D. A. M., SANTACRUZ, S., PADGETT, H. S. & BEACHY, R. N. 1997. Gating of epidermal plasmodesmata is restricted to the leading edge of expanding infection sites of tobacco mosaic virus (TMV). *Plant Journal*, 12, 781-789.
- OVERHAGE, J., BAINS, M., BRAZAS, M. D. & HANCOCK, R. E. W. 2008. Swarming of *Pseudomonas aeruginosa* is a complex adaptation leading to increased production of virulence factors and antibiotic resistance. *Journal of Bacteriology*, 190, 2671-2679.
- PAGGIARO, P. L., CHANEZ, P., HOLZ, O., IND, P. W., DJUKANOVIC, R., MAESTRELLI, P. & STERK, P. J. 2002. Sputum induction. *The European respiratory journal. Supplement*, 37, 3-8.
- PAIXAO, V. A., BARROS, T. F., MOTA, C. M. C., MOREIRA, T. F., SANTANA, M. A. & REIS, J. N. 2010. Prevalence and antimicrobial susceptibility of respiratory pathogens in patients with cystic fibrosis. *Brazilian Journal of Infectious Diseases*, 14, 406-409.
- PALLUA, J. D., PEZZEI, C., ZELGER, B., SCHAEFER, G., BITTNER, L. K., HUCK-PEZZEI, V. A., SCHOENBICHLER, S. A., HAHN, H., KLOSS-BRANDSTAETTER, A., KLOSS, F., BONN, G. K. & HUCK, C. W. 2012. Fourier transform infrared imaging analysis in discrimination studies of squamous cell carcinoma. *Analyst*, 137, 3965-3974.
- PALMER, J., FLINT, S. & BROOKS, J. 2007a. Bacterial cell attachment, the beginning of a biofilm. *Journal of Industrial Microbiology & Biotechnology*, 34, 577-588.
- PALMER, K. L., AYE, L. A. & WHITELEY, M. 2007b. Nutritional cues control *Pseudomonas aeruginosa* multicellular Behavior in cystic fibrosis sputum. *Journal of Bacteriology*, 189, 8079-8087.
- PARK, S. E., PERIATHAMBY, A. R. & LOZA, J. C. 2003. Effect of surface-charged poly(methyl methacrylate) on the adhesion of *Candida albicans*. *Journal of prosthodontics: official journal of the American College of Prosthodontists*, 12, 249-54.

- PAROT, P., DUFRENE, Y. F., HINTERDORFER, P., LE GRIMELLE, C., NAVAJAS, D., PELLEQUER, J.-L. & SCHEURING, S. 2007. Past, present and future of atomic force microscopy in life sciences and medicine. *Journal of Molecular Recognition*, 20, 418-431.
- PAULSEN, I. T., BROWN, M. H. & SKURRAY, R. A. 1996. Proton-dependent multidrug efflux systems. *Microbiological Reviews*, 60, 575-608.
- PEARSON, H. 2007. The good, the bad and the ugly. *Nature*, 447, 138-140.
- PELEG, A. Y., HOGAN, D. A. & MYLONAKIS, E. 2010. Medically important bacterial-fungal interactions. *Nature Reviews Microbiology*, 8, 340-349.
- PELTROCHE-LLACSAHUANGA, H., DOHMEN, H. & HAASE, G. 2002. Recovery of *Candida dubliniensis* from sputum of cystic fibrosis patients. *Mycoses*, 45, 15-18.
- PENA, C., MIRANDA, L., SEGURA, D., NUNEZ, C., ESPIN, G. & GALINDO, E. 2002. Alginate production by *Azotobacter vinelandii* mutants altered in poly-beta-hydroxybutyrate and alginate biosynthesis. *Journal of Industrial Microbiology & Biotechnology*, 29, 209-213.
- PERCIVAL, S. L., HILL, K. E., MALIC, S., THOMAS, D. W. & WILLIAMS, D. W. 2011. Antimicrobial tolerance and the significance of persister cells in recalcitrant chronic wound biofilms. *Wound Repair and Regeneration*, 19, 1-9.
- PERKS, B. & SHUTE, J. K. 2000. DNA and actin bind and inhibit interleukin-8 function in cystic fibrosis sputa - *In vitro* effects of mucolytics. *American Journal of Respiratory and Critical Care Medicine*, 162, 1767-1772.
- PERNI, S., PREEDY, E. C. & PROKOPOVICH, P. 2014. Success and failure of colloidal approaches in adhesion of microorganisms to surfaces. *Advances in Colloid and Interface Science*, 206, 265-274.
- PETERS, B. M., OVCHINNIKOVA, E. S., KROM, B. P., SCHLECHT, L. M., ZHOU, H., HOYER, L. L., BUSSCHER, H. J., VAN DER MEI, H. C., JABRA-RIZK, M. A. & SHIRTLIFF, M. E. 2012. *Staphylococcus aureus* adherence to *Candida albicans* hyphae is mediated by the hyphal adhesin Als3p. *Microbiology-Sgm*, 158, 2975-2986.
- PHILLIPS, J. E., CASE, N. R., CELLY, C., CHAPMAN, R. W., HEY, J. A. & MINNICOZZI, M. 2006. An enzyme-linked immunosorbent assay (ELISA) for the determination of mucin levels in bronchoalveolar lavage fluid. *Journal of Pharmacological and Toxicological Methods*, 53, 160-167.
- PICOT, R., DAS, I. & REID, L. 1978. Pus, deoxyribonucleic-acid, and sputum viscosity. *Thorax*, 33, 235-242.
- PINTO-ALPHANDARY, H., ANDREMONT, A. & COUVREUR, P. 2000. Targeted delivery of antibiotics using liposomes and nanoparticles: research and applications. *International Journal of Antimicrobial Agents*, 13, 155-168.
- POOLE, K. 2004. Resistance to beta-lactam antibiotics. *Cellular and Molecular Life Sciences*, 61, 2200-2223.
- POORTINGA, A. T., BOS, R., NORDE, W. & BUSSCHER, H. J. 2002. Electric double layer interactions in bacterial adhesion to surfaces. *Surface science report*, 47, 1-32.
- POTAPENKO, I. O., HAAKENSEN, V. D., LUDERS, T., HELLAND, A., BUKHOLM, I., SORLIE, T., KRISTENSEN, V. N., LINGJAERDE, O. C. & BORRESEN-DALE, A. L. 2010a. Glycan gene expression signatures in

- normal and malignant breast tissue; possible role in diagnosis and progression. *Molecular Oncology*, 4, 98-118.
- POTAPENKO, I. O., HAAKENSEN, V. D., LUDERS, T., HELLAND, A., BUKHOLM, I., SORLIE, T., KRISTENSEN, V. N., LINGJAERDE, O. C. & BORRESEN-DALE, A. L. 2010b. Glycan gene expression signatures distinguish normal and malignant breast tissue; possible role in diagnosis and progression. *Ejc Supplements*, 8, 102-102.
- POWELL, D. A., TURULA, V., DEHASETH, J. A., VANHALBEEK, H. & MEYER, B. 1994. Sulfate detection in glycoprotein derived oligosaccharides by artificial neural network analysis Fourier Transform Infrared Spectra. *Analytical Biochemistry*, 220, 20-27.
- POWELL, L. C., PRITCHARD, M. F., EMANUEL, C., ONSOYEN, E., RYE, P. D., WRIGHT, C. J., HILL, K. E. & THOMAS, D. W. 2014. A Nanoscale Characterization of the Interaction of a Novel Alginate Oligomer with the Cell Surface and Motility of *Pseudomonas aeruginosa*. *American Journal of Respiratory Cell and Molecular Biology*, 50, 483-492.
- POWELL, L. C., SOWEDAN, A., KHAN, S., WRIGHT, C. J., HAWKINS, K., ONSOYEN, E., MYRVOLD, R., HILL, K. E. & THOMAS, D. W. 2013. The effect of alginate oligosaccharides on the mechanical properties of Gram-negative biofilms. *Biofouling*, 29, 413-21.
- PRASAD, P. A., COFFIN, S. E., LECKERMAN, K. H., WALSH, T. J. & ZAOUTIS, T. E. 2008. Pediatric Antifungal Utilization New Drugs, New Trends. *Pediatric Infectious Disease Journal*, 27, 1083-1088.
- PRITT, B., O'BRIEN, L. & WINN, W. 2007. Mucoid *Pseudomonas* in cystic fibrosis. *American Journal of Clinical Pathology*, 128, 32-34.
- PRUDEN, A., LARSSON, D. G. J., AMEZQUITA, A., COLLIGNON, P., BRANDT, K. K., GRAHAM, D. W., LAZORCHAK, J. M., SUZUKI, S., SILLEY, P., SNAPE, J. R., TOPP, E., ZHANG, T. & ZHU, Y.-G. 2013. Management options for reducing the release of antibiotics and antibiotic resistance genes to the environment. *Environmental Health Perspectives*, 121, 878-885.
- PUGH, D. & CAWSON, R. A. 1975. Cytochemical-localization of phospholipase A and lysophospholipase in *Candida albicans*. *Sabouraudia-Journal of Medical and Veterinary Mycology*, 13, 110-115.
- QIN, Y. 2008. Alginate fibres: an overview of the production processes and applications in wound management. *Polymer International*, 57, 171-180.
- RAFF, H. & LEVITZKY, M. 2011. *Medical physiology*, New York McGraw-Hill Medical.
- RAMAGE, G., MARTINEZ, J. P. & LOPEZ-RIBOT, J. L. 2006. *Candida* biofilms on implanted biomaterials: a clinically significant problem. *Fems Yeast Research*, 6, 979-986.
- RAMAGE, G., SAVILLE, S. P., THOMAS, D. P. & LOPEZ-RIBOT, J. L. 2005. *Candida* biofilms: an update. *Eukaryotic Cell*, 4, 633-638.
- RAMPHAL, R. & ARORA, S. K. 2001. Recognition of mucin components by *Pseudomonas aeruginosa*. *Glycoconjugate Journal*, 18, 709-713.
- RASMUSSEN, T. B. & GIVSKOV, M. 2006. Quorum-sensing inhibitors as anti-pathogenic drugs. *International Journal of Medical Microbiology*, 296, 149-161.

- REICHART, P. A., PHILIPSEN, H. P., SCHMIDTWESTHAUSEN, A. & SAMARANAYAKE, L. P. 1995. Pseudomembranous oral candidiasis in HIV infection: ultrastructure findings. *Journal of Oral Pathology & Medicine*, 24, 276-281.
- RICHARDSON, S. C. W., WALLOM, K.-L., FERGUSON, E. L., DEACON, S. P. E., DAVIES, M. W., POWELL, A. J., PIPER, R. C. & DUNCAN, R. 2008. The use of fluorescence microscopy to define polymer localisation to the late endocytic compartments in cells that are targets for drug delivery. *Journal of Controlled Release*, 127, 1-11.
- RITZOULIS, C., SIASIOS, S., MELIKIDOU, K. D., KOUKIOTIS, C., VASILIADOU, C. & LOLAKOS, S. 2012. Interactions between pig gastric mucin and sodium caseinate in solutions and in emulsions. *Food Hydrocolloids*, 29, 382-388.
- ROBERTS, A. G., CRUZ, S. S., ROBERTS, I. M., PRIOR, D. A. M., TURGEON, R. & OPARKA, K. J. 1997. Phloem unloading in sink leaves of *Nicotiana benthamiana*: Comparison of a fluorescent solute with a fluorescent virus. *Plant Cell*, 9, 1381-1396.
- ROBERTS, J. L., KHAN, S., EMANUEL, C., POWELL, L. C., PRITCHARD, M. F., ONSOYEN, E., MYRVOLD, R., THOMAS, D. W. & HILL, K. E. 2013. An *in vitro* study of alginate oligomer therapies on oral biofilms. *Journal of Dentistry*, 41, 892-899.
- ROBINSON, C. V., ELKINS, M. R., BIALKOWSKI, K. M., THORNTON, D. J. & KERTESZ, M. A. 2012. Desulfurization of mucin by *Pseudomonas aeruginosa*: influence of sulfate in the lungs of cystic fibrosis patients. *Journal of Medical Microbiology*, 61, 1644-1653.
- ROBINSON, M., HEMMING, A. L., REGNIS, J. A., WONG, A. G., BAILEY, D. L., BAUTOVICH, G. J., KING, M. & BYE, P. T. P. 1997. Effect of increasing doses of hypertonic saline on mucociliary clearance in patients with cystic fibrosis. *Thorax*, 52, 900-903.
- RODRIGUEZ-TUDELA, J. L., ARENDRUP, M. C., BARCHIESI, F., BILLE, J., CHRYSANTHOU, E., CUENCA-ESTRELLA, M., DANNAOUI, E., DENNING, D. W., DONNELLY, J. P., DROMER, F., FEGELER, W., LASS-FLOERL, C., MOORE, C., RICHARDSON, M., SANDVEN, P., VELEGRAKI, A., VERWEIJ, P., SUBCOMMITTEE ANTIFUNGAL, S. & ESCMID, E. 2008. EUCAST Definitive Document EDef 7.1: method for the determination of broth dilution MICs of antifungal agents for fermentative yeasts. *Clinical Microbiology and Infection*, 14, 398-405.
- ROOSJEN, A., BUSSCHER, H. J., NORDEL, W. & VAN DER MEI, H. C. 2006. Bacterial factors influencing adhesion of *Pseudomonas aeruginosa* strains to a poly(ethylene oxide) brush. *Microbiology-Sgm*, 152, 2673-2682.
- ROSE, M. C. & VOYNOW, J. A. 2006. Respiratory tract mucin genes and mucin glycoproteins in health and disease. *Physiological Reviews*, 86, 245-278.
- ROSSETTO, G., BERGESE, P., COLOMBI, P., DEPERO, L. E., GIULIANI, A., NICOLETTO, S. F. & PIRRI, G. 2007. Atomic force microscopy evaluation of the effects of a novel antimicrobial multimeric peptide on *Pseudomonas aeruginosa*. *Nanomedicine: Nanotechnology Biology and Medicine*, 3, 198-207.
- ROUND, A. N., BERRY, M., MCMASTER, T. J., CORFIELD, A. P. & MILES, M. J. 2004. Glycopolymer charge density determines conformation in human

- ocular mucin gene products: an atomic force microscope study. *Journal of Structural Biology*, 145, 246-253.
- ROUND, A. N., BERRY, M., MCMASTER, T. J., STOLL, S., GOWERS, D., CORFIELD, A. P. & MILES, M. J. 2002. Heterogeneity and persistence length in human ocular mucins. *Biophysical Journal*, 83, 1661-1670.
- ROWLAND, R. E. & NICKLESS, E. M. 2000. Confocal microscopy opens the door to 3-dimensional analysis of cells *Bioscene*, 26, 3-7.
- RUBIN, B. K. 2007. Mucus structure and properties in cystic fibrosis. *Paediatric Respiratory Reviews*, 8, 4-7.
- RUSSO, P., STIGLIANI, M., PROTA, L., AURIEMMA, G., CRESCENZI, C., PORTA, A. & AQUINO, R. P. 2013. Gentamicin and leucine inhalable powder: What about antipseudomonal activity and permeation through cystic fibrosis mucus? *International Journal of Pharmaceutics*, 440, 250-255.
- RYDER, N. S., WAGNER, S. & LEITNER, I. 1998. *In vitro* activities of terbinafine against cutaneous isolates of *Candida albicans* and other pathogenic yeasts. *Antimicrobial Agents and Chemotherapy*, 42, 1057-1061.
- SANDERS, N. N., DE SMEDT, S. C., VAN ROMPAEY, E., SIMOENS, P., DE BAETS, F. & DEMEESTER, J. 2000. Cystic fibrosis sputum - A barrier to the transport of nanospheres. *American Journal of Respiratory and Critical Care Medicine*, 162, 1905-1911.
- SANDERS, N. N., FRANCKX, H., DE BOECK, K., HAUSTRAETE, J., DE SMEDT, S. C. & DEMEESTER, J. 2006. Role of magnesium in the failure of rhDNase therapy in patients with cystic fibrosis. *Thorax*, 61, 962-968.
- SANFORD, B. A., DEFEIJTER, A. W., WADE, M. H. & THOMAS, V. L. 1996. A dual fluorescence technique for visualization of *Staphylococcus epidermidis* biofilm using scanning confocal laser microscopy. *Journal of Industrial Microbiology*, 16, 48-56.
- SCHALLER, M., JANUSCHKE, E., SCHACKERT, C., WOERLE, B. & KORTING, H. C. 2001. Different isoforms of secreted aspartyl proteinases (Sap) are expressed by *Candida albicans* during oral and cutaneous candidosis *in vivo*. *Journal of Medical Microbiology*, 50, 743-747.
- SCHALLER, M., KORTING, H. C., BORELLI, C., HAMM, G. & HUBE, B. 2005. *Candida albicans*-secreted aspartic proteinases modify the epithelial cytokine response in an *in vitro* model of vaginal candidiasis. *Infection and Immunity*, 73, 2758-2765.
- SCHALLER, M., KORTING, H. C., SCHAFFER, W., BASTERT, J., CHEN, W. C. & HUBE, B. 1999. Secreted aspartic proteinase (Sap) activity contributes to tissue damage in a model of human oral candidosis. *Molecular Microbiology*, 34, 169-180.
- SCHALLER, M., SCHAFFER, W., KORTING, H. C. & HUBE, B. 1998. Differential expression of secreted aspartyl proteinases in a model of human oral candidosis and in patient samples from the oral cavity. *Molecular Microbiology*, 29, 605-615.
- SCHATZEL, K. 1991. Suppression of multiple-scattering by photon cross-correlation techniques. *Journal of Modern Optics*, 38, 1849-1865.
- SCHINDELIN, J., ARGANDA-CARRERAS, I., FRISE, E., KAYNIG, V., LONGAIR, M., PIETZSCH, T., PREIBISCH, S., RUEDEN, C., SAALFELD, S., SCHMID, B., TINEVEZ, J. Y., WHITE, D. J., HARTENSTEIN, V., ELICEIRI, K., TOMANCAK, P. & CARDONA, A.

2012. Fiji: an open-source platform for biological-image analysis. *Nature Methods*, 9, 676-682.
- SCHULTZ, C. P., LIU, K. Z., KERR, P. D. & MANTSCH, H. M. 1998. *In situ* infrared histopathology of keratinization in human oral/oropharyngeal squamous cell carcinoma. *Oncology Research*, 10, 277-286.
- SCHULZ, B. L., SLOANE, A. J., ROBINSON, L. J., PRASAD, S. S., LINDNER, R. A., ROBINSON, M., BYE, P. T., NIELSON, D. W., HARRY, J. L., PACKER, N. H. & KARLSSON, N. G. 2007. Glycosylation of sputum mucins is altered in cystic brosis patients. *Glycobiology*, 17, 698-712.
- SCHUSTER, B. S., SUK, J. S., WOODWORTH, G. F. & HANES, J. 2013. Nanoparticle diffusion in respiratory mucus from humans without lung disease. *Biomaterials*, 34, 3439-3446.
- SEIB, F. P., JONES, A. T. & DUNCAN, R. 2006. Establishment of subcellular fractionation techniques to monitor the intracellular fate of polymer therapeutics I. Differential centrifugation fractionation B16F10 cells and use to study the intracellular fate of HPMA copolymer-doxorubicin. *Journal of Drug Targeting*, 14, 375-390.
- SEIB, F. P., JONES, A. T. & DUNCAN, R. 2007. Comparison of the endocytic properties of linear and branched PEIs, and cationic PAMAM dendrimers in B16f10 melanoma cells. *Journal of Controlled Release*, 117, 291-300.
- SENEVIRATNE, C. J., WANG, Y., JIN, L., ABIKO, Y. & SAMARANAYAKE, L. P. 2010. Proteomics of drug resistance in *Candida glabrata* biofilms. *Proteomics*, 10, 1444-1454.
- SERISIER, D. J., CARROLL, M. P., SHUTE, J. K. & YOUNG, S. A. 2009. Macrorheology of cystic fibrosis, chronic obstructive pulmonary disease & normal sputum. *Respiratory Research*, 10, doi:10.1186/1465-9921-10-63.
- SERVERA, E., SANCHO, J. & ZAFRA, M. J. 2003. Cough and neuromuscular diseases. Noninvasive airway secretion management. *Archivos De Bronconeumologia*, 39, 420-427.
- SHAH, P. L., SCOTT, S. F., FUCHS, H. J., GEDDES, D. M. & HODSON, M. E. 1995. Medium term treatment of stable stage cystic fibrosis with recombinant human DNase I. *Thorax*, 50, 333-338.
- SHAH, P. L., SCOTT, S. F., KNIGHT, R. A., MARRIOTT, C., RANASINHA, C. & HODSON, M. E. 1996. *In vivo* effects of recombinant human DNase I on sputum in patients with cystic fibrosis. *Thorax*, 51, 119-125.
- SHAKIR, A., ELBADAWAY, M. R., SHIELDS, R. C., JAKUBOVICS, N. S. & BURGESS, J. G. 2012. Removal of Biofilms from Tracheoesophageal Speech Valves Using a Novel Marine Microbial Deoxyribonuclease. *Otolaryngology-Head and Neck Surgery*, 147, 509-514.
- SHARP, K. 2014. *Section 2- Confocal laser scanning microscopy*, Biofouling Methods, ed. S.W. Dobretsov, D. and J. Thomason: Wiley-Blackwell.
- SHEEHAN, J. K., BRAZEAU, C., KUTAY, S., PIGEON, H., KIRKHAM, S., HOWARD, M. & THORNTON, D. J. 2000. Physical characterization of the MUC5AC mucin: a highly oligomeric glycoprotein whether isolated from cell culture or *in vivo* from respiratory mucous secretions. *Biochemical Journal*, 347, 37-44.
- SHEPHARD, J., MCQUILLAN, A. J. & BREMER, P. J. 2008. Mechanisms of cation exchange by *Pseudomonas aeruginosa* PAO1 and PAO1 wbpL, a

- strain with a truncated lipopolysaccharide. *Applied and Environmental Microbiology*, 74, 6980-6986.
- SHEPHARD, J. J., SAVORY, D. M., BREMER, P. J. & MCQUILLAN, A. J. 2010. Salt modulates bacterial hydrophobicity and charge properties influencing adhesion of *Pseudomonas aeruginosa* (PA01) in aqueous suspensions. *Langmuir*, 26, 8659-8665.
- SHEU, B. C., LIN, C. C., FU, Y. H., LEE, S. Y., LAI, H. C., WU, R. S., LIU, C. H., TSAI, J. C. & LIN, S. M. 2010. Unraveling the Role of the rscC Gene of *Serratia marcescens* by Atomic Force Microscopy. *Microscopy and Microanalysis*, 16, 755-763.
- SHIMIZU, M. T., ALMEIDA, N. Q., FANTINATO, V. & UNTERKIRCHER, C. S. 1996. Studies on hyaluronidase, chondroitin sulphatase, proteinase and phospholipase secreted by *Candida* species. *Mycoses*, 39, 161-167.
- SILVA, S., HENRIQUES, M., HAYES, A., OLIVEIRA, R., AZEREDO, J. & WILLIAMS, D. W. 2011a. *Candida glabrata* and *Candida albicans* co-infection of an *in vitro* oral epithelium. *Journal of Oral Pathology & Medicine*, 40, 421-427.
- SILVA, S., HOOPER, S. J., HENRIQUES, M., OLIVEIRA, R., AZEREDO, J. & WILLIAMS, D. W. 2011b. The role of secreted aspartyl proteinases in *Candida tropicalis* invasion and damage of oral mucosa. *Clinical Microbiology and Infection*, 17, 264-272.
- SILVA, S., NEGRI, M., HENRIQUES, M., OLIVEIRA, R., WILLIAMS, D. W. & AZEREDO, J. 2012. *Candida glabrata*, *Candida parapsilosis* and *Candida tropicalis*: biology, epidemiology, pathogenicity and antifungal resistance. *Fems Microbiology Reviews*, 36, 288-305.
- SINAI, A. P., HAYES, S. F., SMALL, P. L. C. & BAVOIL, P. M. 1995. Low efficiency macro-pinocytic internalization of nonpathogenic *Escherichia coli* into HEP-2 cells. *Research in Microbiology*, 146, 617-631.
- SINGH, P. K., SCHAEFER, A. L., PARSEK, M. R., MONINGER, T. O., WELSH, M. J. & GREENBERG, E. P. 2000. Quorum-sensing signals indicate that cystic fibrosis lungs are infected with bacterial biofilms. *Nature*, 407, 762-764.
- SITHEEQUE, M. A. M. & SAMARANAYAKE, L. P. 2003. Chronic hyperplastic candidosis/candidiasis (Candidal leukoplakia). *Critical Reviews in Oral Biology & Medicine*, 14, 253-267.
- SKAUG, M. J., LONGO, M. L. & FALLER, R. 2011. The impact of Texas Red on lipid bilayer properties. *Journal of Physical Chemistry B*, 115, 8500-8505.
- SLETMOEN, M., MAURSTAD, G., NORDGARD, C. T., DRAGET, K. I. & STOKKE, B. T. 2012. Oligoguluronate induced competitive displacement of mucin-alginate interactions: relevance for mucolytic function. *Soft Matter*, 8, 8413-8421.
- SMITH, A. W. 2005. Biofilms and antibiotic therapy: Is there a role for combating bacterial resistance by the use of novel drug delivery systems? *Advanced Drug Delivery Reviews*, 57, 1539-1550.
- SMITH, J. J., TRAVIS, S. M., GREENBERG, E. P. & WELSH, M. J. 1996. Cystic fibrosis airway epithelia fail to kill bacteria because of abnormal airway surface fluid. *Cell*, 85, 229-236.
- SMITH, R. & COAST, J. 2013. The true cost of antimicrobial resistance. *British Medical Journal*, 346, f1493

- SMYTH, A. R. & WALTERS, S. 2012. Prophylactic anti-staphylococcal antibiotics for cystic fibrosis. *Cochrane Database of Systematic Reviews*.
- SOHN, M. H., LIM, S., SEO, K. W. & LEE, S. J. 2013. Effect of ambient medium viscosity on the motility and flagella motion of *Prorocentrum minimum* (Dinophyceae). *Journal of Plankton Research*, 35, 1294-1304.
- SONG, Y. L., THIAGARAJAH, J. & VERKMAN, A. S. 2003. Sodium and chloride concentrations, pH, and depth of airway surface liquid in distal airways. *Journal of General Physiology*, 122, 511-519.
- SONI, K. A., BALASUBRAMANIAN, A. K., BESKOK, A. & PILLAI, S. D. 2008. Zeta potential of selected bacteria in drinking water when dead, starved, or exposed to minimal and rich culture media. *Current Microbiology*, 56, 93-97.
- SOON, R. L., NATION, R. L., COCKRAM, S., MOFFATT, J. H., HARPER, M., ADLER, B., BOYCE, J. D., LARSON, I. & LI, J. 2011. Different surface charge of colistin-susceptible and -resistant *Acinetobacter baumannii* cells measured with zeta potential as a function of growth phase and colistin treatment. *Journal of Antimicrobial Chemotherapy*, 66, 126-133.
- SOON, R. L., NATION, R. L., HARTLEY, P. G., LARSON, I. & LI, J. 2009. Atomic force microscopy investigation of the morphology and topography of colistin-heteroresistant *Acinetobacter baumannii* strains as a function of growth phase and in response to colistin treatment. *Antimicrobial Agents and Chemotherapy*, 53, 4979-4986.
- SOSINSKA, G. J., DE KONING, L. J., DE GROOT, P. W. J., MANDERS, E. M. M., DEKKER, H. L., HELLINGWERF, K. J., DE KOSTER, C. G. & KLIS, F. M. 2011. Mass spectrometric quantification of the adaptations in the wall proteome of *Candida albicans* in response to ambient pH. *Microbiology-Sgm*, 157, 136-146.
- SOUSA, P. C., PINHO, F. T., OLIVEIRA, M. S. N. & ALVES, M. A. 2011. Extensional flow of blood analog solutions in microfluidic devices. *Biomicrofluidics*, 5, 014108
- SOUTHERN, K. W. 2012. Macrolide antibiotics for cystic fibrosis. *Paediatric Respiratory Reviews*, 13, 228-229.
- SRIRAMULU, D. D., LUNSDORF, H., LAM, J. S. & ROMLING, U. 2005. Microcolony formation: a novel biofilm model of *Pseudomonas aeruginosa* for the cystic fibrosis lung. *Journal of Medical Microbiology*, 54, 667-676.
- STANEK, A., BRAMBRINK, A. M., LATORRE, F., BENDER, B. & KLEEMANN, P. P. 1998. Effects of normobaric oxygen on ciliary beat frequency of human respiratory epithelium. *British Journal of Anaesthesia*, 80, 660-664.
- STEINBERGER, R. E., ALLEN, A. R., HANSMA, H. G. & HOLDEN, P. A. 2002. Elongation correlates with nutrient deprivation in *Pseudomonas aeruginosa*-unsaturated biofilms. *Microbial Ecology*, 43, 416-423.
- STEWART, P. S. & COSTERTON, J. W. 2001. Antibiotic resistance of bacteria in biofilms. *Lancet*, 358, 135-138.
- STOODLEY, P., DEBEER, D. & LAPPINSCOTT, H. M. 1997. Influence of electric fields and pH on biofilm structure as related to the bioelectric effect. *Antimicrobial Agents and Chemotherapy*, 41, 1876-1879.
- STOODLEY, P., SAUER, K., DAVIES, D. G. & COSTERTON, J. W. 2002. Biofilms as complex differentiated communities. *Annual Review of Microbiology*, 56, 187-209.

- STOVER, C. K., PHAM, X. Q., ERWIN, A. L., MIZOGUCHI, S. D., WARRENER, P., HICKEY, M. J., BRINKMAN, F. S. L., HUFNAGLE, W. O., KOWALIK, D. J., LAGROU, M., GARBER, R. L., GOLTRY, L., TOLENTINO, E., WESTBROCK-WADMAN, S., YUAN, Y., BRODY, L. L., COULTER, S. N., FOLGER, K. R., KAS, A., LARBIG, K., LIM, R., SMITH, K., SPENCER, D., WONG, G. K. S., WU, Z., PAULSEN, I. T., REIZER, J., SAIER, M. H., HANCOCK, R. E. W., LORY, S. & OLSON, M. V. 2000. Complete genome sequence of *Pseudomonas aeruginosa* PAO1, an opportunistic pathogen. *Nature*, 406, 959-964.
- STRATHMANN, M., WINGENDER, J. & FLEMMING, H. C. 2002. Application of fluorescently labelled lectins for the visualization and biochemical characterization of polysaccharides in biofilms of *Pseudomonas aeruginosa*. *Journal of Microbiological Methods*, 50, 237-248.
- STRESSMANN, F. A., ROGERS, G. B., MARSH, P., LILLEY, A. K., DANIELS, T. W. V., CARROLL, M. P., HOFFMAN, L. R., JONES, G., ALLEN, C. E., PATEL, N., FORBES, B., TUCK, A. & BRUCE, K. D. 2011. Does bacterial density in cystic fibrosis sputum increase prior to pulmonary exacerbation? *Journal of Cystic Fibrosis*, 10, 357-365.
- SUDBERY, P. E. 2011. Growth of *Candida albicans* hyphae. *Nature Reviews Microbiology*, 9, 737-748.
- SUN, F., ZONG, W., LIU, R., CHAI, J. & LIU, Y. 2010. Micro-environmental influences on the fluorescence of tryptophan. *Spectrochimica Acta Part A: Molecular and Biomolecular Spectroscopy*, 76, 142-145.
- SUNDQVIST, K., KULKARNI, P., HYBBINETTE, S. S., BERTOLERO, F., LIU, Y. & GRAFSTROM, R. C. 1991. Serum-free growth and karyotype analyses of cultured normal and tumorous (SQCC/Y1) human buccal epithelial cells. *Cancer Communications*, 3, 331-340.
- TAGER, A. M., WU, J. Y. & VERMEULEN, M. W. 1998. The effect of chloride concentration on human neutrophil functions: Potential relevance to cystic fibrosis. *American Journal of Respiratory Cell and Molecular Biology*, 19, 643-652.
- TAKEYAMA, K., DABBAGH, K., LEE, H. M., AGUSTI, C., LAUSIER, J. A., UEKI, I. F., GRATTAN, K. M. & NADEL, J. A. 1999. Epidermal growth factor system regulates mucin production in airways. *Proceedings of the National Academy of Sciences of the United States of America*, 96, 3081-3086.
- TANG, B. C., DAWSON, M., LAI, S. K., WANG, Y.-Y., SUK, J. S., YANG, M., ZEITLIN, P., BOYLE, M. P., FU, J. & HANES, J. 2009. Biodegradable polymer nanoparticles that rapidly penetrate the human mucus barrier. *Proceedings of the National Academy of Sciences of the United States of America*, 106, 19268-19273.
- TARRAN, R., GRUBB, B. R., PARSONS, D., PICHER, M., HIRSH, A. J., DAVIS, C. W. & BOUCHER, R. C. 2001. The CF salt controversy: *In vivo* observations and therapeutic approaches. *Molecular Cell*, 8, 149-158.
- TATE, S., MACGREGOR, G., DAVIS, M., INNES, J. A. & GREENING, A. P. 2002. Airways in cystic fibrosis are acidified: detection by exhaled breath condensate. *Thorax*, 57, 926-929.

- TAYLOR, C., DRAGET, K. I., PEARSON, J. P. & SMIDSRØD, O. 2005a. Mucous systems show a novel mechanical response to applied deformation. *Biomacromolecules*, 6, 1524-1530.
- TAYLOR, C., PEARSON, J. P., DRAGET, K. I., DETTMAR, P. W. & SMIDSRØD, O. 2005b. Rheological characterisation of mixed gels of mucin and alginate. *Carbohydrate Polymers*, 59, 189-195.
- TEPER, A., JAQUES, A., CHARLTON, B. & INVESTIGATORS, C. F. S. 2011. Inhaled mannitol in patients with cystic fibrosis: A randomised open-label dose response trial. *Journal of Cystic Fibrosis*, 10, 1-8.
- TERRY, J. M., PINA, S. E. & MATTINGLY, S. J. 1992. Role of energy metabolism in conversion of nonmucoid *Pseudomonas aeruginosa* to the mucoid phenotype. *Infection and Immunity*, 60, 1329-1335.
- TEUBL, B. J., ABSENGER, M., FROEHLICH, E., LEITINGER, G., ZIMMER, A. & ROBLEGG, E. 2013a. The oral cavity as a biological barrier system: Design of an advanced buccal *in vitro* permeability model. *European Journal of Pharmaceutics and Biopharmaceutics*, 84, 386-393.
- TEUBL, B. J., MEINDL, C., EITZLMAYR, A., ZIMMER, A., FROEHLICH, E. & ROBLEGG, E. 2013b. *In vitro* permeability of neutral polystyrene particles via buccal mucosa. *Small*, 9, 457-466.
- THENMOZHI, R., NITHYANAND, P., RATHNA, J. & PANDIAN, S. K. 2009. Antibiofilm activity of coral-associated bacteria against different clinical M serotypes of *Streptococcus pyogenes*. *Fems Immunology and Medical Microbiology*, 57, 284-294.
- THETHI, K. & DUSZYK, M. 1997. Decreased cell surface charge in cystic fibrosis epithelia. *Cell Biochemistry and Function*, 15, 35-38.
- THOMAS, V. C., THURLOW, L. R., BOYLE, D. & HANCOCK, L. E. 2008. Regulation of autolysis-dependent extracellular DNA release by *Enterococcus faecalis* extracellular proteases influences biofilm development. *Journal of Bacteriology*, 190, 5690-5698.
- THORNTON, D. J., SHEEHAN, J. K., LINDGREN, H. & CARLSTEDT, I. 1991. Mucus glycoproteins from cystic fibrotic sputum. Macromolecular properties and structural architecture. *Biochemical Journal*, 276, 667-675.
- TØNDERVIK, A., SLETTA, H., KLINKENBERG, G., EMANUEL, C., POWELL, L. C., PRITCHARD, M. F., KHAN, S., CRAINE, K. M., ONSOYEN, E., RYE, P. D., WRIGHT, C., THOMAS, D. W. & HILL, K. E. 2014. Alginate oligosaccharides inhibit fungal cell growth and potentiate the activity of antifungals against *Candida* and *Aspergillus* spp. *Plos One*, 9 (11) e112518.
- TOUTAIN-KIDD, C. M., KADIVAR, S. C., BRAMANTE, C. T., BOBIN, S. A. & ZEGANS, M. E. 2009. Polysorbate 80 inhibition of *Pseudomonas aeruginosa* biofilm formation and its cleavage by the secreted lipase LipA. *Antimicrobial Agents and Chemotherapy*, 53, 136-145.
- URATANI, Y. 1982. Dansyl chloride labelling of *Pseudomonas aeruginosa* treated with pyocin-R1- change in permeability of the cell envelope. *Journal of Bacteriology*, 149, 523-528.
- VAARA, M. 1992. Agents that increase the permeability of the outer-membrane. *Microbiological Reviews*, 56, 395-411.
- VALENZA, G., TAPPE, D., TURNWALD, D., FROSCH, M., KONIG, C., HEBESTREIT, H. & ABELE-HORN, M. 2008. Prevalence and antimicrobial

- susceptibility of microorganisms isolated from sputa of patients with cystic fibrosis. *Journal of Cystic Fibrosis*, 7, 123-127.
- VAN GENNIP, M., CHRISTENSEN, L. D., ALHEDE, M., QVORTRUP, K., JENSEN, P. O., HØIBY, N., GIVSKOV, M. & BJARNSHOLT, T. 2012. Interactions between polymorphonuclear leukocytes and *Pseudomonas aeruginosa* biofilms on silicone implants *in vivo*. *Infection and Immunity*, 80, 2601-2607.
- VAN MERODE, A. E. J., VAN DER MEI, H. C., BUSSCHER, H. J. & KROM, B. P. 2006. Influence of culture heterogeneity in cell surface charge on adhesion and biofilm formation by *Enterococcus faecalis*. *Journal of Bacteriology*, 188, 2421-2426.
- VANDERMEI, H. C., LEONARD, A. J., WEERKAMP, A. H., ROUXHET, P. G. & BUSSCHER, H. J. 1988. Properties of oral *Streptococci* relevant for adherence- zeta potential, surface free-energy and elemental composition. *Colloids and Surfaces*, 32, 297-305.
- VASCONCELLOS, C. A., ALLEN, P. G., WOHL, M. E., DRAZEN, J. M., JANMEY, P. A. & STOSSEL, T. P. 1994. Reduction in viscosity of cystic fibrosis sputum *in vitro* by gelsolin. *Science*, 263, 969-971.
- VEIGA-SANTOS, P., BARRIAS, E. S., SANTOS, J. F. C., DE BARROS MOREIRA, T. L., ULISSES DE CARVALHO, T. M., URBINA, J. A. & DE SOUZA, W. 2012. Effects of amiodarone and posaconazole on the growth and ultrastructure of *Trypanosoma cruzi*. *International Journal of Antimicrobial Agents*, 40, 61-71.
- VERNOOIJ-VAN LANGEN, A. M. M., LOEBER, J. G., ELVERS, B., TRIEPELS, R. H., GILLE, J. J. P., VAN DER PLOEG, C. P. B., REIJNTJENS, S., DOMPELING, E., DANKERT-ROELSE, J. E. & GRP, C. S. 2012. Novel strategies in newborn screening for cystic fibrosis: a prospective controlled study. *Thorax*, 67, 289-295.
- VILLENA, G. K., FUJIKAWA, T., TSUYUMU, S. & GUTIERREZ-CORREA, M. 2010. Structural analysis of biofilms and pellets of *Aspergillus niger* by confocal laser scanning microscopy and cryo scanning electron microscopy. *Bioresource Technology*, 101, 1920-1926.
- VISICK, K. L. & FUQUA, C. 2005. Decoding microbial chatter: Cell-cell communication in bacteria. *Journal of Bacteriology*, 187, 5507-5519.
- WAINE, D. J., HONEYBOURNE, D., SMITH, E. G., WHITEHOUSE, J. L. & DOWSON, C. G. 2008. Association between hypermutator phenotype, clinical variables, mucoid phenotype, and antimicrobial resistance in *Pseudomonas aeruginosa*. *Journal of Clinical Microbiology*, 46, 3491-3493.
- WALSH, C. 2000. Molecular mechanisms that confer antibacterial drug resistance. *Nature*, 406, 775-781.
- WANG, H. P., WANG, H. C. & HUANG, Y. J. 1997. Microscopic FTIR studies of lung cancer cells in pleural fluid. *Science of the Total Environment*, 204, 283-287.
- WATERS, C. M. & BASSLER, B. L. 2005. Quorum sensing: Cell-to-cell communication in bacteria. *Annual Review of Cell and Developmental Biology*.
- WATT, K., BENJAMIN, D. K., JR. & COHEN-WOLKOWIEZ, M. 2011. Pharmacokinetics of antifungal agents in children. *Early Human Development*, 87, S61-S65.

- WHITEMAN, S. C., YANG, Y., JONES, J. M. & SPITERI, M. A. 2008. FTIR spectroscopic analysis of sputum: preliminary findings on a potential novel diagnostic marker for COPD. *Therapeutic advances in respiratory disease*, 2, 23-31.
- WIDDICOMBE, J. G. 1997. Airway liquid: a barrier to drug diffusion? *European Respiratory Journal*, 10, 2194-2197.
- WILLIAMS, D. W., JORDAN, R. P. C., WEI, X.-Q., ALVES, C. T., WISE, M. P., WILSON, M. J. & LEWIS, M. A. O. 2013. Interactions of *Candida albicans* with host epithelial surfaces. *Journal of oral microbiology*, 5: 22434-
<http://dx.doi.org/10.3402/jom.v5i0.22434>
- WILLITS, R. K. & SALTZMAN, W. M. 2001. Synthetic polymers alter the structure of cervical mucus. *Biomaterials*, 22, 445-452.
- WILLS, P. J., HALL, R. L., CHAN, W. M. & COLE, P. J. 1997. Sodium chloride increases the ciliary transportability of cystic fibrosis and bronchiectasis sputum on the mucus-depleted bovine trachea. *Journal of Clinical Investigation*, 99, 9-13.
- WILSON, W. W., WADE, M. M., HOLMAN, S. C. & CHAMPLIN, F. R. 2001. Status of methods for assessing bacterial cell surface charge properties based on zeta potential measurements. *Journal of Microbiological Methods*, 43, 153-164.
- WIMPENNY, J., MANZ, W. & SZEWZYK, U. 2000. Heterogeneity in biofilms. *Fems Microbiology Reviews*, 24, 661-671.
- WLOKA, M., REHAGE, H., FLEMMING, H. C. & WINGENDER, J. 2004. Rheological properties of viscoelastic biofilm extracellular polymeric substances and comparison to the behavior of calcium alginate gels. *Colloid and Polymer Science*, 282, 1067-1076.
- WORLITZSCH, D., TARRAN, R., ULRICH, M., SCHWAB, U., CEKICI, A., MEYER, K. C., BIRRER, P., BELLON, G., BERGER, J., WEISS, T., BOTZENHART, K., YANKASKAS, J. R., RANDELL, S., BOUCHER, R. C. & DORING, G. 2002. Effects of reduced mucus oxygen concentration in airway *Pseudomonas* infections of cystic fibrosis patients. *Journal of Clinical Investigation*, 109, 317-325.
- WOZNIAK, D. J., WYCKOFF, T. J. O., STARKEY, M., KEYSER, R., AZADI, P., O'TOOLE, G. A. & PARSEK, M. R. 2003. Alginate is not a significant component of the extracellular polysaccharide matrix of PA14 and PAO1 *Pseudomonas aeruginosa* biofilms. *Proceedings of the National Academy of Sciences of the United States of America*, 100, 7907-7912.
- WRIGHT, C. J., SHAH, M. K., POWELL, L. C. & ARMSTRONG, I. 2010. Application of AFM from microbial cell to biofilm. *Scanning*, 32, 134-149.
- WRIGHT, E. A., FOTHERGILL, J. L., PATERSON, S., BROCKHURST, M. A. & WINSTANLEY, C. 2013. Sub-inhibitory concentrations of some antibiotics can drive diversification of *Pseudomonas aeruginosa* populations in artificial sputum medium. *BMC Microbiology*, 13, doi:10.1186/1471-2180-13-170.
- XABI, M., CRISTIANE DE SOUZA, C. & CLAUS-MICHAEL, L. 2014. Overcoming the pulmonary barrier: new insights to improve the efficiency of inhaled therapeutics. *European Journal of Nanomedicine*, 6, 157-169.
- XIA, B. Y., ROYALL, J. A., DAMERA, G., SACHDEV, G. P. & CUMMINGS, R. D. 2005. Altered O-glycosylation and sulfation of airway mucins associated with cystic fibrosis. *Glycobiology*, 15, 747-775.

- YANG, J. S., XIE, Y. J. & HE, W. 2011a. Research progress on chemical modification of alginate: A review. *Carbohydrate Polymers*, 84, 33-39.
- YANG, L., JELSBAK, L. & MOLIN, S. 2011b. Microbial ecology and adaptation in cystic fibrosis airways. *Environmental Microbiology*, 13, 1682-1689.
- YANG, Y., TSIFANSKY, M. D., WU, C. J., YANG, H. I., SCHMIDT, G. & YEO, Y. 2010. Inhalable antibiotic delivery using a dry powder co-delivering recombinant deoxyribonuclease and ciprofloxacin for treatment of cystic fibrosis. *Pharmaceutical Research*, 27, 151-160.
- YANO, K., OHOSHIMA, S., GOTOU, Y., KUMAIIDO, K., MORIGUCHI, T. & KATAYAMA, H. 2000. Direct measurement of human lung cancerous and noncancerous tissues by Fourier transform infrared microscopy: Can an infrared microscope be used as a clinical tool? *Analytical Biochemistry*, 287, 218-225.
- YANO, K., OHOSHIMA, S., SHIMIZU, Y., MORIGUCHI, T. & KATAYAMA, H. 1996. Evaluation of glycogen level in human lung carcinoma tissues by an infrared spectroscopic method. *Cancer Letters*, 110, 29-34.
- YEUNG, A. T. Y., PARAYNO, A. & HANCOCK, R. E. W. 2012. Mucin promotes rapid surface motility in *Pseudomonas aeruginosa*. *mBio* 3(3):e00073-12. doi:10.1128/mBio.00073-12.
- YING, S. & CHUNYANG, L. 2012. Correlation between phospholipase of *Candida albicans* and resistance to fluconazole. *Mycoses*, 55, 50-5.
- YOON, M. Y., LEE, K. M., PARK, Y. & YOON, S. S. 2011. Contribution of cell elongation to the biofilm formation of *Pseudomonas aeruginosa* during anaerobic respiration. *Plos One*, 6(1): e16105. doi: 10.1371/journal.pone.0016105.
- ZAHM, J. M., DEBENTZMANN, S. G., DENEUVILLE, E., PERROTMINNOT, C., DABADIE, A., PENNAFORTE, F., ROUSSEY, M., SHAK, S. & PUCHELLE, E. 1995. Dose-dependent *in-vitro* effect of recombinant human DNase on rheological and transport-properties of cystic fibrosis respiratory mucus. *European Respiratory Journal*, 8, 381-386.
- ZANETTI-DOMINGUES, L. C., TYNAN, C. J., ROLFE, D. J., CLARKE, D. T. & MARTIN-FERNANDEZ, M. 2013. Hydrophobic fluorescent probes introduce artifacts into single molecule tracking experiments due to non-specific binding. *Plos One*, 8(9):e74200. doi:10.1371/journal.pone.0074200.
- ZAREMBER, K. A., CRUZ, A. R., HUANG, C.-Y. & GALLIN, J. I. 2009. Antifungal activities of natural and synthetic iron chelators alone and in combination with azole and polyene antibiotics against *Aspergillus fumigatus*. *Antimicrobial Agents and Chemotherapy*, 53, 2654-2656.
- ZAYAS, J. G., MAN, G. C. W. & KING, M. 1990. Tracheal mucus rheology in patients undergoing diagnostic bronchoscopy- interrelations with smoking and cancer. *American Review of Respiratory Disease*, 141, 1107-1113.
- ZHANG, Y. L., DORANZ, B., YANKASKAS, J. R. & ENGELHARDT, J. F. 1995. Genotypic analysis of respiratory mucous sulfation defects in cystic fibrosis. *Journal of Clinical Investigation*, 96, 2997-3004.
- ZUSSMAN, E., YARIN, A. L. & NAGLER, R. M. 2007. Age- and flow-dependency of salivary viscoelasticity. *Journal of Dental Research*, 86, 281-285.

Appendix I:
Nanoscale chapter

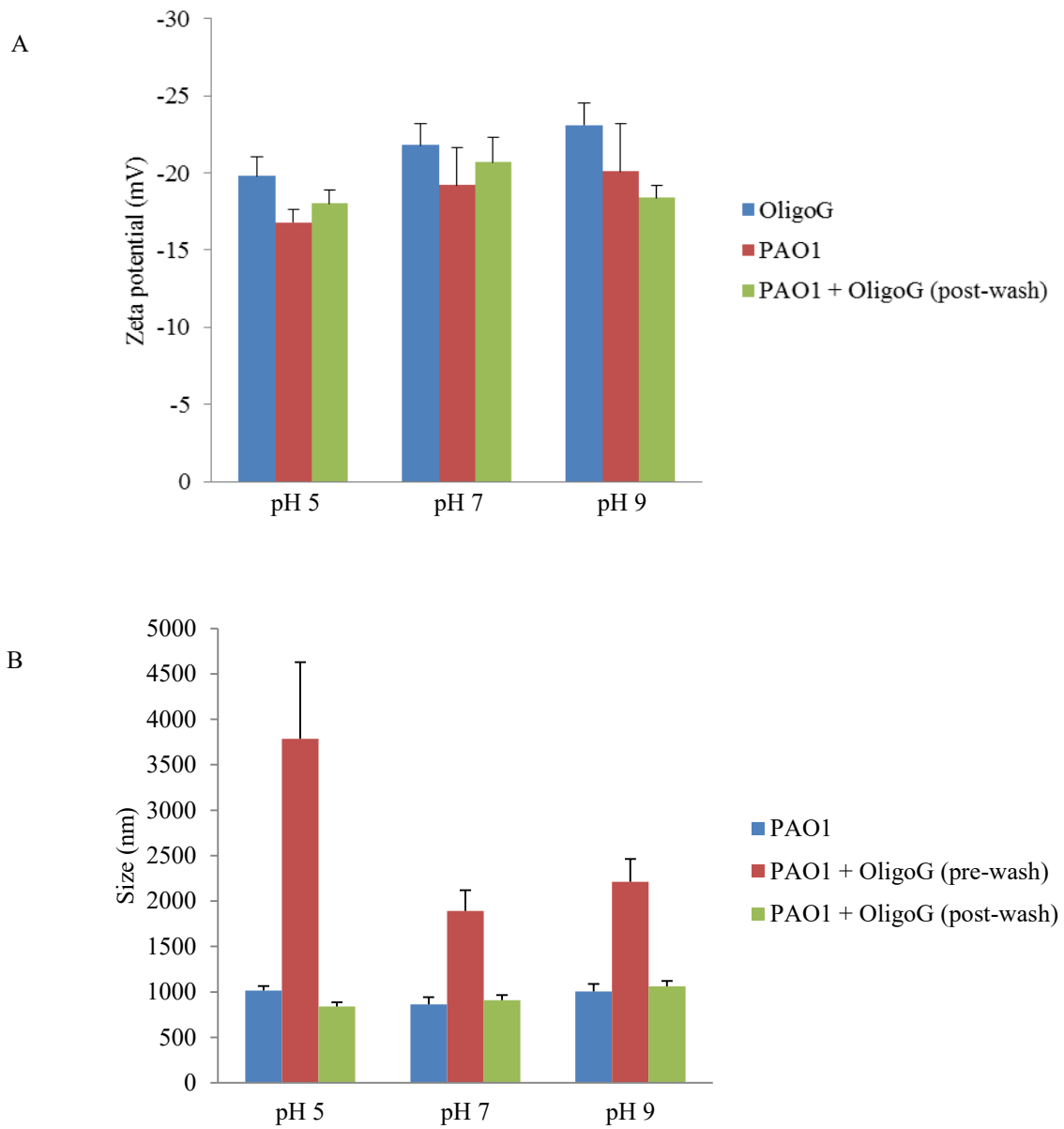


Fig 1.i: A) Mean zeta potential values for 10% OligoG, untreated PAO1 and PAO1 treated with 10% OligoG (post-wash) at various pH values in 0.1 M NaCl. B) Cell size analysis of PAO1, PAO1 treated with 10% OligoG (pre-wash) and PAO1 treated with 10% OligoG (post-wash) in 0.1 M NaCl.

Table I.i: Effect of a hydrodynamic shear test at 3,300 g for 3 mins on OligoG treated cells tested in 0.01 M NaCl, pH 5; mean zeta potential values (mV) and mean sizing values (nm).

	No wash	1st wash	2nd wash
	Mean Zeta Potential (mV)		
PAO1	-30.7 ±1.0	-30.6 ±0.7	-29.9 ±1.1
PAO1 + OligoG	-36.5 ±1.2	-33.4 ±1.2	-32.1 ±1.1
	Mean Sizing (nm)		
PAO1	947 ±77	934 ±142	984 ±67
PAO1 + OligoG	1564 ±722	1684 ±559	1530 ±439

Appendix II:
FTIR patient samples

Table II.i Patient data for FTIR, including antibiotic and rhDNase I (if applicable) regimen at time of sampling.

Patient	Sex	Age (Yrs. months)	Taking rhDNase I	Immunised against <i>Influenzae</i>	Receiving antibiotics	Sputum induced	Microbiology	FEV ₁ (L)
1	M	28.8	Yes	Yes	Yes	No	<i>P. aeruginosa</i>	1.93
2	F	37.10	Yes	Yes	Yes	No	<i>P. aeruginosa</i>	0.65
3	M	31.1	No	Yes	Yes	No	<i>P. aeruginosa</i>	1.15
4	M	39.5	Yes	Yes	Yes	No	<i>P. aeruginosa</i> <i>S. aureus</i>	1.99
5	F	17	Yes	Yes	Yes	No	<i>P. aeruginosa</i>	*
6	M	13	Yes	Yes	Yes	No	<i>Atypical myobacterium</i>	*
7	F	22.1	Yes	Yes	Yes	No	<i>P. aeruginosa</i> <i>C. albicans</i>	1.1
8	F	39.2	No	Yes	Yes	No	Normal flora#	2.13
9	M	25.8	No	*	Yes	No	<i>S. aureus</i>	4.05

Patient recently had bilateral lung transplant

* Unknown

FEV₁ Forced expiratory volume in 1 second

P. aeruginosa, *Pseudomonas aeruginosa*; *S. aureus*, *Staphylococcus aureus*; *C. albicans*, *Candida albicans*.

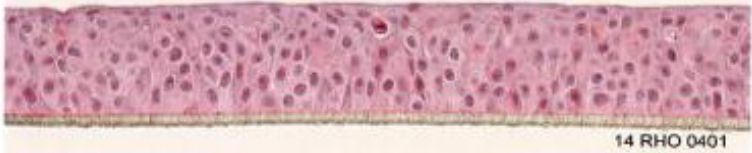
Appendix III:
Preliminary fungal experiments

Table III.i: MICs ($\mu\text{g/ml}$) of antifungals alone and with increasing concentrations of OligoG (2, 6, 10%) for a range of *Candida* species (Department of Bioprocess Technology, SINTEF Materials and Chemistry, Trondheim, Norway)

% OligoG	Nystatin				Fluconazole				Terbinafine			
	0	2%	6%	10%	0	2%	6%	10%	0	2%	6%	10%
<i>C. albicans</i> CCUG 39343	8	8	4	2	16	16	8	4	>32	>32	>32	>32
<i>C. parapsilosis</i> ATCC 22019T	8	4	1	0.5	2	2	0.5	0.25	2	2	2	2
<i>C. krusei</i> 141/03	8	4	2	2	128	64	64	64	>32	>32	>32	>32
<i>C. krusei</i> 249/03(2)	8	8	8	4	8	4	2	1	4	4	8	4
<i>C. lusitanae</i> 994/01(2)	8	8	2	1	0.5	0.25	<0.13	<0.13	8	4	4	2
<i>C. tropicalis</i> 12	8	8	4	4	1	1	<0.13	<0.13	>32	16	>32	32
<i>C. tropicalis</i> 75	8	8	8	2	2	1	0.5	0.25	>32	>32	>32	>32
<i>C. tropicalis</i> 519468	16	8	4	2	128	1	0.5	0.25	>32	>32	>32	>32
<i>C. tropicalis</i> 544123	8	8	2	2	1	1	0.5	0.25	>32	>32	>32	>32
<i>C. tropicalis</i> 250/03	8	4	2	1	8	4	2	2	>32	>32	>32	>32
<i>C. tropicalis</i> AG1	8	8	4	2	128	>128	0.5	<0.13	>32	32	>32	>32
<i>C. tropicalis</i> T2.2	8	8	4	2	>128	0.5	0.25	<0.13	>32	>32	>32	32

SkinEthic Laboratories

TECHNICAL DATA, SAFETY SHEET AND CERTIFICATE OF ANALYSIS OF RECONSTRUCTED HUMAN EPITHELIA

Description:	SkinEthic RHO / S / 5 0,5 cm ² epithelium reconstituted by airlifted culture of transformed human keratinocytes for 5 days in chemically defined medium on inert polycarbonate filters.		
Thickness at day 5:	75 µm (indicate value)		
Usage:	FOR SCIENTIFIC USE ONLY - PRODUCT OF HUMAN ORIGIN		
Storage:	This product was prepared and packaged using aseptic techniques, Store in an incubator at 37° C, 5% CO ₂ with saturated humidity.		
Batch N°:	14 RHO 0401		
Origin:	TR146 Squamous cell carcinoma derived cell line.		
Histology:			
Quality Controls:	Test	Acceptance criteria	Result
	Immersed parallel culture at 5 days	cell growth and sterility	Conform
	Histological observation at day 5 <i>(HES stained vertical paraffin sections)</i>	At least 4 viable cell layers are present. Absence of significant histological abnormalities.	Conform Indicative value : 5/6 cell layers
	Cell viability at day 5 <i>(MTT test, n= 2)</i>	O.D. > 0.8	O.D. = 1,163 ± 0,041
Biological safety:	On this cell line, we have verified : . Absence of HIV-1 and HIV-2 . Absence of hepatitis C . Absence of hepatitis B On cell supernatant, we have verified : . Absence of mycoplasma		
Expiration date:	April 14, 2014 ; day 12 of airlifted culture		
<small>*The use of this epithelial tissue is strictly limited to in vitro testing provided such testing does not include extraction of the cells constitutive of the tissue for maintenance and use for culture, which is strictly prohibited. Furthermore, it excludes any diagnostic or therapeutic use and any use in human subjects.*</small>			

Lyon, April 7, 2014

Certified and released by
Anne Sophie Rigaudeau



Data validation
Delphine Guillot



CERTIFIEE ISO 9001
 4, rue Alexander Fleming - 69006 Lyon Cedex 07 - France - Tél. (33) 04 37 28 22 00 - Fax. (33) 04 37 28 22 01
 au capital de 13 608 807 € - 412 127 565 R.C.S. Lyon - N° TVA intracommunautaire FR 46 412 127 566
 Email : sales@skinethic.com



Fig III.i: Reconstituted Human Oral Epithelial Cells Documentation

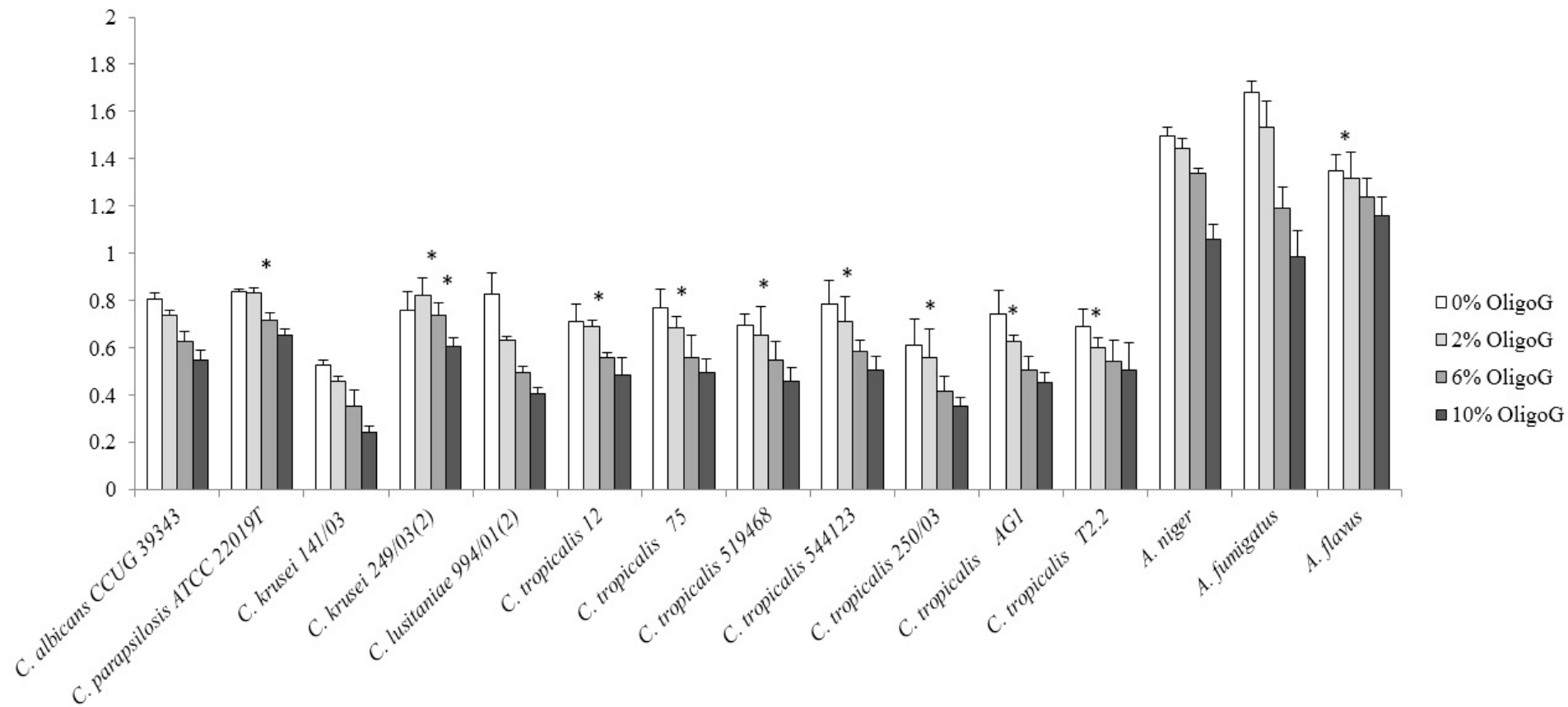


Fig III.ii: Effect of increasing concentrations of OligoG (0%, 2%, 6%, and 10%) on cell densities after cultivation in MH broth for 48 h at 34°C for various *Candida* and *Aspergillus* species. Error bars represent standard deviation from the mean (n≥4). (*, data not significantly different from control results; P>0.05). Work carried out by the Department of Bioprocess Technology, SINTEF Materials and Chemistry, N-7465 Trondheim, Norway.

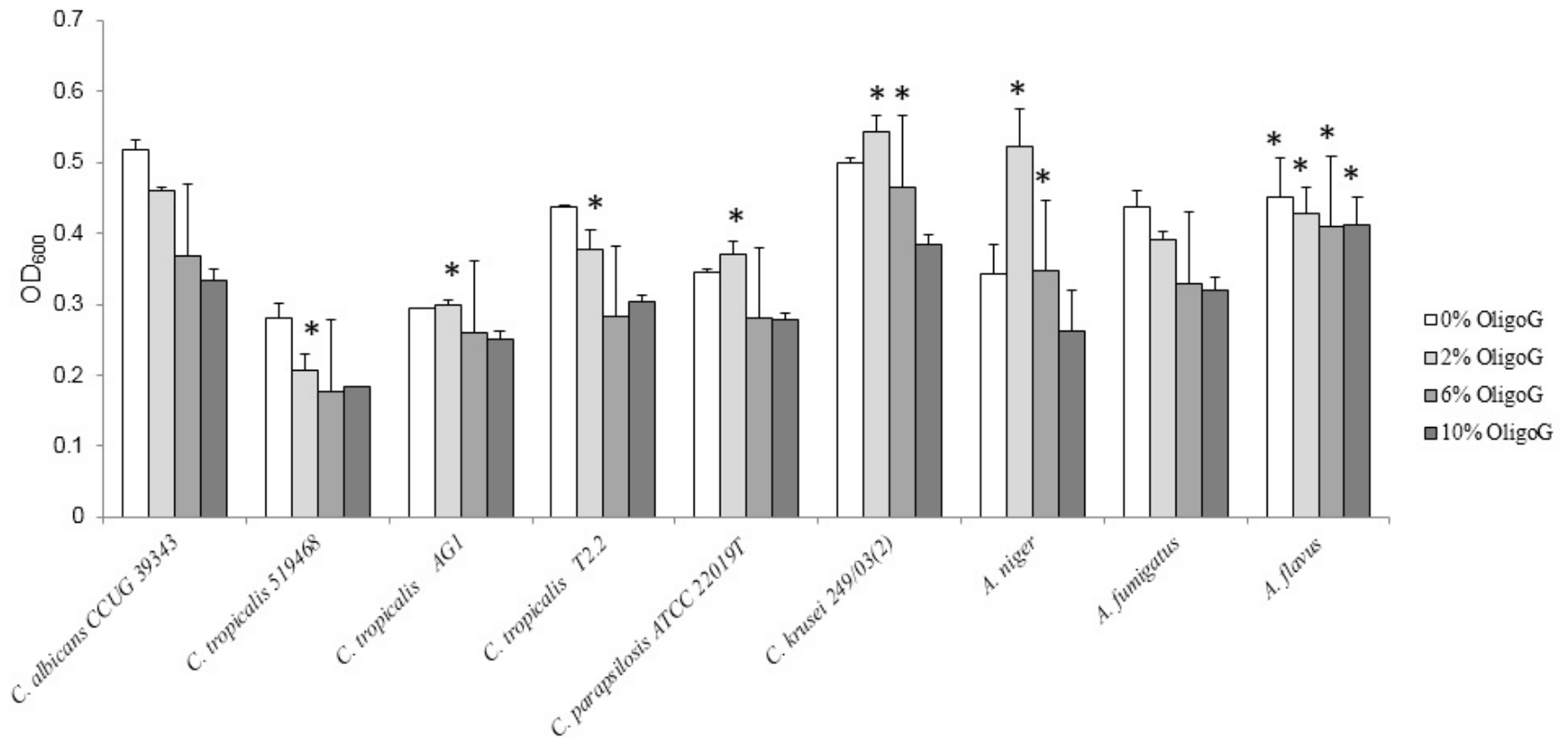


Fig III.iii: Effect of increasing concentrations of OligoG (0%, 2%, 6%, and 10%) on cell densities after cultivation in RPMI broth for 48 h at 34 °C for various *Candida* and *Aspergillus* species Error bars represent standard deviation from the mean (n≥4). (*, data not significantly different from control results; P>0.05). Work carried out by the Department of Bioprocess Technology, SINTEF Materials and Chemistry, N-7465 Trondheim, Norway.

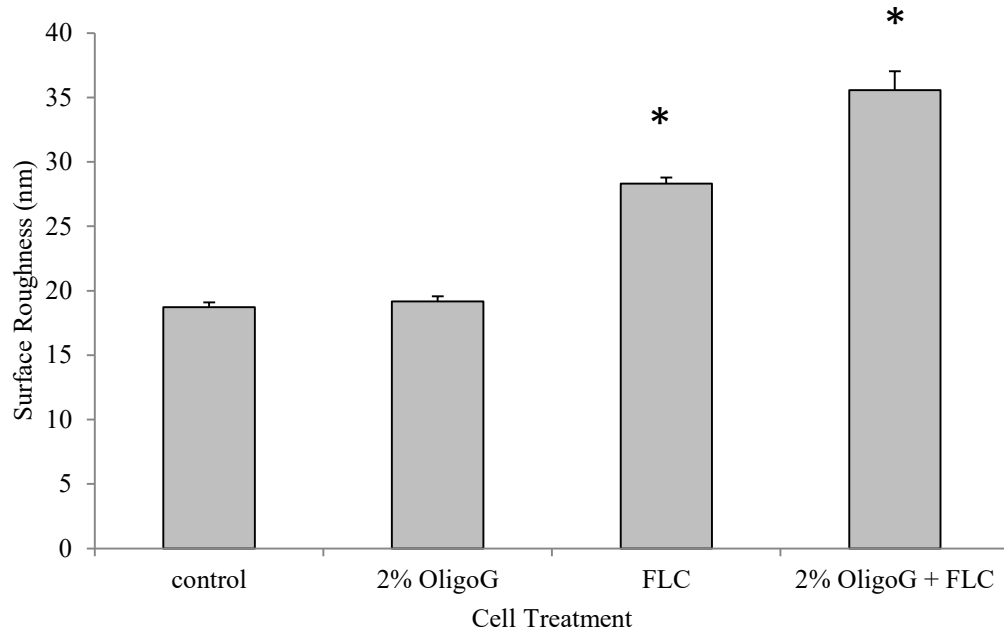


Fig II.iv: Mean surface roughness expressed as (Ra) \pm standard error. *indicates significantly different from the control. FLC, fluconazole. Work carried out by Mr K. Craine.

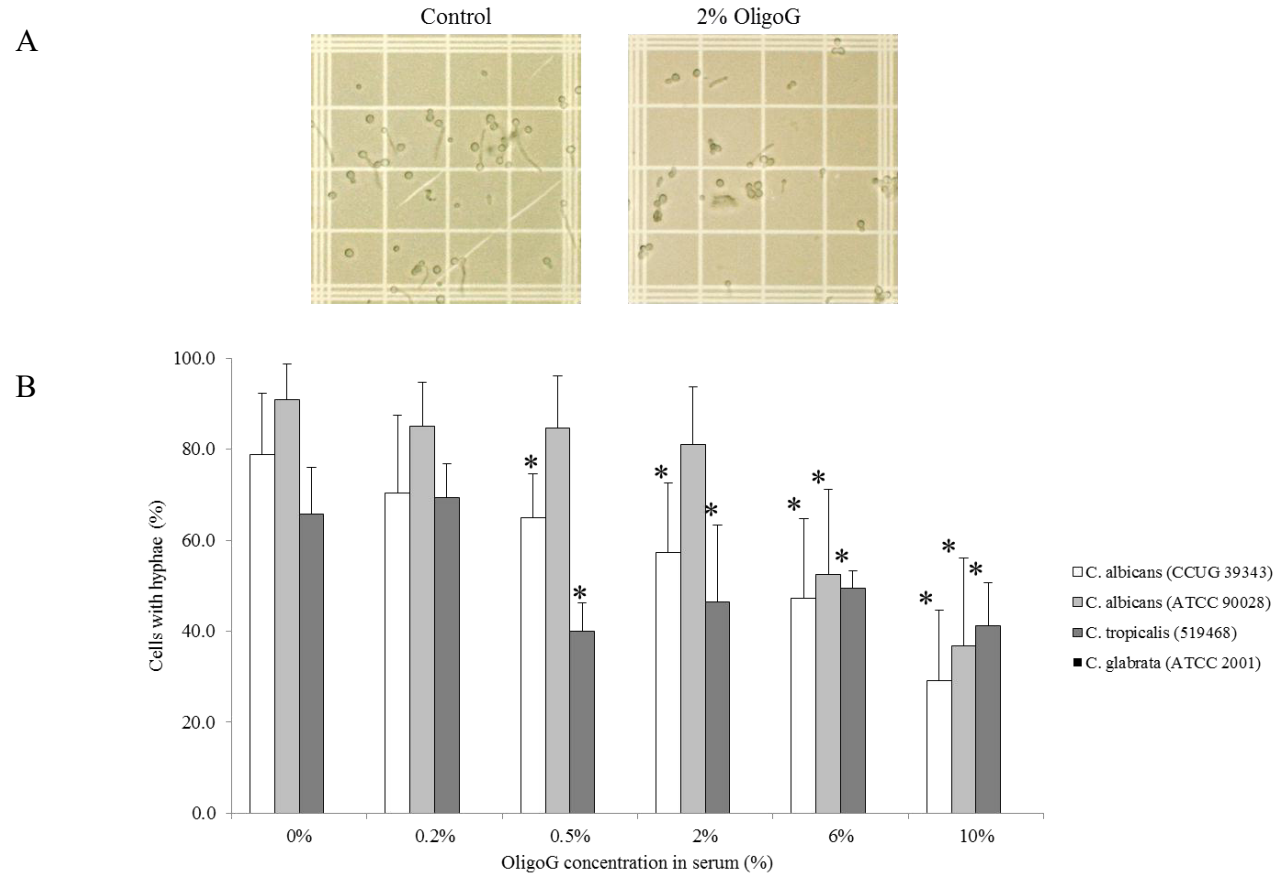
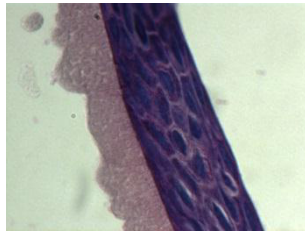


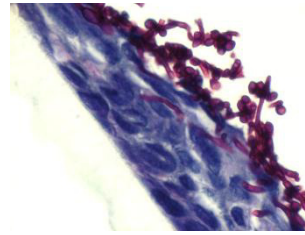
Fig III.v: Germ tube assay showing; A) light microscopy images of *Candida albicans* (CCUG 39343) cells grown with/without the presence of OligoG, (Scale bar is 100 μ m). B) Percentage of *Candida* cells producing hyphae for four different strains grown for 2 hours in the presence of OligoG (0, 0.2, 0.5, 2, 6 and 10%). *C. glabrata* as a non-hyphae producer was the negative control. * indicates significantly different from the control, ($P < 0.05$). Work carried out by Dr C. Emanuel.

A

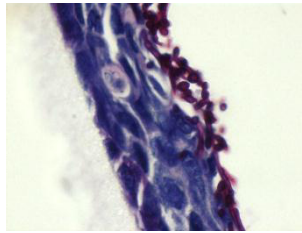
HEALTHY CONTROL



INFECTED CONTROL



0.2% OLIGOG TREATED



B

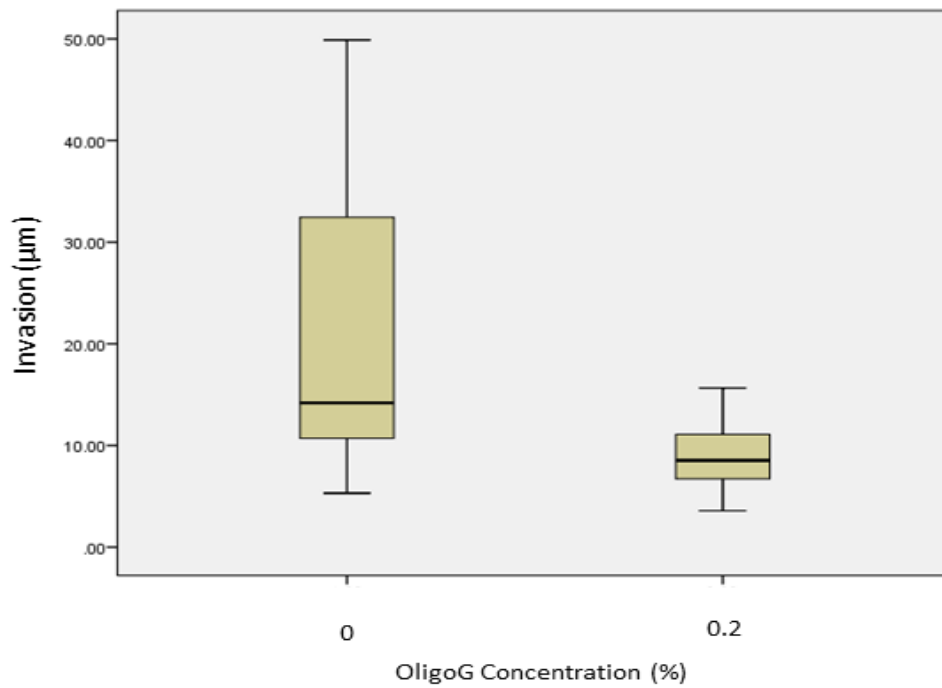


Fig III.vi: Periodic-acid Schiff (PAS) of control, infected and 0.2% OligoG treated RHE samples showing; A) imaging B) box plot of hyphal invasion measurements (n=64; P<0.05). Work carried out by Dr A. Jack.

Appendix IV:
**Animal and human studies into the
safety and tolerability of OligoG for
inhalational delivery**

Animal clinical trials of the alginate oligosaccharide OligoG (CF-5/20)

Inhalation studies were carried out with OligoG in experimental animals: single dose and multiple doses at variable exposure times, as well as single oral or intravenous administration of tritium-labelled OligoG (for details see **Table IV.i-iii**).

No clinical changes were evident with the single- or repeated nebulised administration of OligoG for up to 28 days for 4 hours/day. The only OligoG related necropsy finding was bronchial lymph node enlargement in 8/15 animals treated with OligoG for 4 hours/day. There was a (histologically-scored) minimal-mild alveolar foamy macrophage accumulation in the lung of all animals from the 28-day groups, which reflected normal clearance mechanisms of the rat lung and was not considered to be a toxicological effect of administration of 6% OligoG. All other histology and clinical tests including blood and urine analysis displayed normal parameters.

For the ³H-labelled OligoG oral dose, mean plasma levels reached a peak at 2 hours post-dosing and decreased to background levels within 12 hours. For the ³H-labelled OligoG intravenous dose, mean plasma radioactivity levels reached a peak 5 mins after injection and decreased to background levels within 24 hours. After oral dosing, the major elimination route was via the faeces and urine (82.6% and 8.5% respectively within 24 hours). The remainder was recovered over the following 168 hours, with minute amounts ($\leq 2.4\%$) also recovered in expired air at 48 hours post dose. After intravenous administration, the major route of elimination was via the urine (73.1% within 6 hours of dosing). These data show that whilst OligoG is rapidly absorbed, it also rapidly excreted which are standard drug-like properties.

Human clinical trials of the alginate oligosaccharide OligoG (CF-5/20)

A Phase I, randomised, double-blinded, placebo-controlled, dose-escalated trial was carried out to investigate the safety and tolerability of inhaled aerosolised OligoG in healthy volunteers (EudraCT number: 2009-009330-33, <http://www.clinicaltrials.gov> identifier NCT00970346). The product was found to be well tolerated with mild and transient adverse effects, which occurred equally in the placebo group. No serious adverse events occurred and no clinically significant

changes in laboratory analysis of vital signs, ECG or spirometry were recorded. No systemic absorption was seen above the level of quantification in the pharmacokinetic data (AlgiPharma, 2014). From this study, the initial working concentrations between 2-10% OligoG were selected as it was confirmed safe for clinical use (Khan et al., 2012).

A Phase IIa double-blind, randomised, placebo-controlled, cross-over study has also been completed to evaluate the safety, tolerability and preliminary efficacy of OligoG when administered for 28 days in CF patients, chronically colonised with *P. aeruginosa* (EudraCT number:2010-023090-19, <http://www.clinicaltrials.gov> identifier NCT01465529). The results have not yet been published.

Another Phase IIa clinical trial is currently recruiting patients employing an open label, randomised, two-way crossover scintigraphic study to investigate the lung deposition of radiolabelled OligoG, when delivered as a dry powder and as a nebulised solution in CF patients ((EudraCT number: 2013-003774-27, <http://www.clinicaltrials.gov> identifier NCT01991028). These results will aid our understanding of the clinically relevant dose to use for maximum efficacy of the therapeutic.

A further Phase IIb double-blind, randomised, placebo-controlled cross-over study is planned to start analysing efficacy and safety of inhalation of OligoG administered for 28 days in CF patients (<http://www.clinicaltrials.gov> identifier NCT02157922).

Table IV.i: Summary of dosing for inhalation studies with OligoG in experimental animals (experiment I).

Experiment	Phase of study	Dose group/ treatment[#]	Mean aerosol OligoG conc.	Respiratory minute volume (L min⁻¹)	Dose duration (min)	Body weight (kg)	Estimated achieved dose (mg/kg)
I	Single dose, variable OligoG conc.	1.Vehicle control	0.007	0.159	240	0.248	1.08
		2.Low dose	1.07	0.164	240	0.258	163.2
		3.Intermediate dose	1.14	0.160	240	0.249	175.8
		4.High dose	2.19	0.169	241*	0.270	330.4

[#]N=5 male rats; *High dose animals overdosed by 1 min in error.

Table IV.ii: Summary of dosing for inhalation studies with OligoG in experimental animals (experiments II and III).

Experiment	Phase of study	Dose group/ Treatment [#]	Daily exposure duration (min)	OligoG formulation in mg ⁻¹ kg ⁻¹ day ⁻¹	Non-aqueous component mg ⁻¹ kg ⁻¹ day ⁻¹
II	Single dose, variable exposure times	1.6% OligoG	60	500.0	75.6
		2.6% OligoG	120	997.6	150.8
		3.6% OligoG	240	1999.8	301.9
III	Single dose	6% OligoG	60	500.0	75.6
		6% OligoG	120	997.5	150.8
		6% OligoG	240	1999.8	301.9
	7 days dosing	6% OligoG	60	511.4	71.0
		6% OligoG	240	2034.4	282.4
	14 days dosing	6% OligoG	60	498.5	71.6
		6% OligoG	240	1984.3	284.8
	28 days dosing	Vehicle only	240	1916.7	0
		6% OligoG	120	494.4	71.6
		6% OligoG	240	1988.2	288.0

[#](n=10; 5 female, 5 male rats)

Table IV.iii: Summary of sampling for inhalation studies with ^3H OligoG in experimental animals (experiment IV).

Experiment	Dose group/ Treatment[#]	Samples	Additional samples	Additional samples from selected animals
IV	IV (n=4)	Blood, plasma	Blood, plasma, selected tissues/organs, carcass	Expired air (n=2)
	OD (n=4)			
	IV (n=4)	Urine/feces		
	OD (n=4)			
	IV (n=18)	Tissues and organs		

All animals received a dose of 5 mg/kg tritium-labelled OligoG; IV, intravenous; OD, oral dose.